Synthesis, Characterization and Evaluation of Tin-containing Silicates for Biomass Conversion

Tolborg, Søren

Publication date:
2016

Document Version
Publisher's PDF, also known as Version of record

Synthesis, Characterization and Evaluation of Tin-containing Silicates for Biomass Conversion

Ph.D. dissertation by Søren Tolborg

Technical University of Denmark

Supervisors
Professor Anders Riisager
Research Scientist Irantzu Sádaba

December 2016

Preface

This dissertation describes the work performed during my Ph.D. studies in the period September 2013 to December 2016 at the Technical University of Denmark (DTU). The work was done as part of the Bio-Value platform funded under the SPIR initiative by the Danish Council for Strategic Research and The Danish Council for Technology and Innovation. The project was done in collaboration with Haldor Topsøe A/S (HTAS), and the experimental work presented have either been completed at the Department of Chemistry (DTU) or in the New Business R&D department (HTAS). The project was initially supervised by Assoc. Prof. Peter Fristrup (DTU) and co-supervised by Research Scientist Martin S. Holm (HTAS). Both supervisors ended up leaving for other challenges and instead Research Scientist Irantzu Sádaba (July 2014, HTAS) and Prof. Anders Riisager (August 2016, DTU) took over.

The thesis is divided into 7 chapters. **Chapter 1** presents the motivation and introduces the field and state of the art of carbohydrate conversion using stannosilicates. **Chapter 2** details the experimental procedures used to synthesize, characterize and test the catalysts. **Chapters 3 to 6** present the main results obtained including a brief introduction at the beginning of each chapter and concluding remarks at the end. **Chapter 3** describes the effect of tin on the hydrothermal synthesis of Sn-Beta. **Chapter 4** details the optimization of methyl lactate using an alkali cosolute. **Chapter 5** investigates the pathways involved in the conversion of carbohydrates. **Chapter 6** describes the use of shape selectivity to convert glycolaldehyde into valuable products. **Chapter 7** provides an overarching conclusion across all chapters. Unless otherwise stated, all tables, figures and schemes have been prepared by me.

A detailed list of abbreviations used throughout the dissertation can be found in Tables A.6 and A.7 on p. 163 and 166, respectively.

The thesis is the culmination of many years of studies (and hard work), and I hope you will enjoy the read!

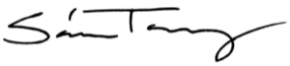

Søren Tolborg
Kgs. Lyngby, Denmark
December 2016

Acknowledgements

There are so many people I would like to thank for making my three years of studies a great and fun experience. People who have taken part in the work done, have supported me or have been there to make the hours in the lab more enjoyable. Over the three years of studies I have come into contact with a good many people, too many to mentioned them all here, but their assistance, help and support is no less appreciated.

First and foremost, I would like to extend my gratitude to all the supervisors I have had over the years. Peter Fristrup and Martin S. Holm for supporting me in getting started, giving feedback and always being ready for discussions or for a quick meeting. I would also like to thank Anders Riisager who stepped in late in the project as main supervisor, helping in the more practical parts of finalizing my studies. I would like to especially thank Irantzu Sádaba, who took over as co-supervisor in 2014. Her insight, overview, positive attitude and willingness to discuss the newest results has meant a lot to me and helped me get this far. I would furthermore like to extend my sincere gratitude to Esben Taarning and Martin S. Holm for giving me the opportunity to do first my Master's thesis at Haldor Topsøe A/S and later were instrumental in finding funding for my Ph.D. I would especially like to thank Esben for letting me be the one to realize some of his countless ideas in the lab. Also Christian M. Osmundsen deserves my appreciation both for the many discussions we have had over the years but also for the influence he has had on the direction of my work. The rest of the Sustainable Chemicals group likewise deserves my gratitude for putting up with me in the lab and for all the great times we have had.

I would also like to thank those who have been instrumental in the success of the projects undertaken during my studies. Sebastian Meier deserves a thanks for taking us another few steps forward using his extensive knowledge within NMR spectroscopy. Who knew working with beer for a decade could be such an advantage for the future of the biorefinery sector. Also all the many competent people, I have come into contact with at Haldor Topsøe A/S. All with an eagerness to help with analysis or with a question or two despite busy schedules. Thanks to Lars F. Lundegaard, Anna Katerinopoulou, Henrik Fordsman, Lars F. Østergaard and Hale Yasin to just name a few. In general, the entire analysis department at Haldor Topsøe A/S deserves my gratitude.

I would also like to thank Irina I. Ivanova and her group at Moscow State University for all the fruitful discussions and for her hospitality during our visits to Russia. It has been a privilege to collaborate with such a dedicated group of people and it has been impressive to follow the work done in her laboratory. In this regards I would also like to extend my gratitude to Peter N. R. Vennestrøm for letting me be part of this collaboration.

Finally, I would like to thank my family; my parents for always believing in me and what I could achieve, and most importantly my wonderful wife Gerit, who has supported me during the emotional rollercoaster that research can also be sometimes. You have stood by me for years now, moved the place you call home to a foreign country and given me the most wonderful son. You have listened when I babble chemistry, and you have motivated me, when things weren't going my way. At the end of every day, I still *just want to hurry home to you*.

Abstract

The transition to renewable carbon sources such as biomass will require entirely new catalytic processes and result in completely new products. An entire industry is built up around the chemicals that are available from fossil resources but will be unfeasible to prepare from other carbon sources. This dissertation describes the preparation and use of several important stannosilicate materials, known to transform carbohydrates into different valuable products. Several aspects of the tin-containing catalysts are investigated and discussed and new insight into the conversion of sugars is provided.

The catalyst Sn-Beta is an important and highly active catalyst in a number of reactions. By carefully investigating the fluoride-route synthesis, the active component tin was discovered to influence the crystal morphology by changing the growth of the crystals. Even a small increase in tin content lead to much longer crystallization times (up to 60 days). Tin was furthermore not evenly distributed within the crystals, but instead found as an enriched outer shell. Small amounts of alkali were found to limit the growth retardation, enabling the preparations of Sn-Beta materials with high tin content.

For the catalytic conversion of sugars, the addition of alkali to the reaction media was also found to have a large effect on the product distribution. Having small concentrations of alkali present modified Sn-Beta to favor retro-aldol/aldol condensation reactions resulting in up to 75% methyl lactate from sucrose at optimized conditions. The effect of alkali was found to transcend to a variety of sugars, solvents and other stannosilicates such as Sn-MCM-41 or Sn-Beta prepared by a post-synthesis methodology. The latter makes it possible to use industrially relevant tin-containing catalysts to achieved high yields of methyl lactate simply by optimizing the amount of cosolute.

In the absence of alkali, instead of retro-aldol reaction, hexoses and pentoses were found to undergo β-dehydration leading to several new and highly functional products. These include the *trans*-2,5,6-trihydroxy-3-hexenoic acid methyl ester (from hexoses) or *trans*-2,5-dihydroxy-3-pentenoic acid methyl ester (from pentoses) in acceptable yields (18-33%). Several additional products and intermediates were identified and quantified, providing a better understanding of the transformation of sugars catalyzed by tin.

By using a zeolite with narrow channels (Sn-MFI), shape selectivity could be exploited for the valorization of small sugars. Glycolaldehyde (GA) could

selectively undergo aldol condensation to give high yields of the rare tetroses (74%). With larger pore systems and channels either substantial yields of hexoses were formed from subsequent condensation reactions (Sn-MCM-41 and Sn-Beta): In the particular case of Sn-MFI and Sn-Beta, additional conversion of the tetroses lead to vinyl glycolic acid and α-hydroxy-γ-butyrolactone (HBL). Changing the conditions, it was possible to form up to 44% of VGA directly from GA using Sn-MFI.

An important part of making the transition to more renewable resources is to have attractive alternatives to switch to. This means new, interesting chemicals easily obtainable from the most abundant biomass-derived sugars need to be found. The findings and processes investigated and discussed here should be a move in this direction.

Resumé

Skiftet til fornybare kulstofkilder såsom biomasse vil kræve helt nye katalytiske processer og resultere i fuldstændig nye produkter og kemikalier. En hel industri er bygget op omkring de kemikalier, der er tilgængelige fra fossile ressourcer. Kemikalier det ikke vil være muligt at fremstille fra andre kulstofkilder. Denne afhandling med titlen "Syntese, karakterisering og evaluering af tin-holdige silikater til omdannelse af biomasse" beskriver fremstillingen og brugen af adskillige, vigtige stannosilikat-materialer, der er kendte for deres brug inden for netop omdannelsen af kulhydrater til forskellige værdifulde produkter. Adskillige aspekter af de tinholdige katalysatorer bliver belyst og diskuteret, og der bliver givet ny indsigt i den katalytiske omdannelse af sukker.

Zeotypen Sn-Beta er en vigtig og meget aktiv katalysator i en række reaktioner. Ved omhyggeligt at undersøge fluorid-rute syntesen blev det opdaget, at den aktive komponent tin har stor indflydelse på krystalmorfologien ved at ændre på, hvordan krystallerne vokser. Selv ved en lille forøgelse af mængden af tin blev den nødvendige krystallisationstid betydeligt længere (op til 60 dage). Derudover blev det opdaget, at tin ikke indsættes ligeligt inden i krystallen, men i stedet blev fundet som en beriget ydre skal. Små mængder af alkali kunne begrænse vækst-retardation, hvilket gjorde det muligt at fremstille Sn-Beta materialer med meget højt tin-indhold.

For den katalytiske omdannelse af sukker blev det konstateret, at tilsætningen af alkali direkte til reaktionsblandingen havde en stor effekt på sammensætningen af de dannede produkter. Små mængder af alkali ændrede Sn-Beta katalysatoren til i højere grad at favorisere retro-aldol/aldol kondensation reaktioner, hvilket resulterede i op til 75% methyllaktat fra sukrose under optimerede forsøgsbetingelser. Det blev ydermere opdaget, at alkalieffekten også var tilstede ved omdannelse af andre sukre og i andre solventer. Effekten blev ligeledes observeret ved brug af helt andre stannosilikater såsom Sn-MCM-41 eller Sn-Beta fremstillet ved post-syntese. Dette gør det muligt at bruge industrielt relevante tinholdige katalysatorer til at opnå høje udbytter af metyllaktat ved blot at optimere mængden af additiv.

Når alkali i stedet blev undgået blev en anden reaktionsvej favoriseret. I stedet for retro-aldol reaktioner, så blev både pentose- og hexose-sukrene omdannet via en β-dehydrerings reaktion, som førte til adskillige nye og meget funktionelle produkter. Disse produkter inkluderer blandt andet *trans*-2,5,6-trihydroxy-3-

hexensyremethylester (fra hexose-sukre) og *trans*-2,5-dihydroxy-3-pentensyre-methylester (fra pentose-sukre) i acceptable udbytter (18-33%). Adskillige yderligere produkter og intermediater blev identificeret og kvantificeret, hvilket gav en bedre forståelse af de transformationer, som sukre kan gennemgå katalyseret af tin.

Ved at bruge zeolitter med smalle porekanaler (Sn-MFI) var det muligt at udnytte "form selektivitet" til at valorisere små sukre. Den selektive aldol kondensation af glykolaldehyd (GA) førte til høje udbytter af de sjældne tetrose sukre (74%). Med større poresystemer og porekanaler blev betydelige mængder hexose sukre dannet (Sn-MCM-41 og Sn-Beta). I det særlige tilfælde for Sn-MFI og Sn-Beta førte den efterfølgende omdannelse af de dannede tetrose sukre til dannelsen af vinylglykolsyre (VGA) og α-hydroxy-γ-butyrolakton (HBL). Ved at ændre forsøgsbetingelserne var det muligt at opnå op til 44% VGA direkte fra GA ved brug af Sn-MFI.

En vigtig del af at lave skiftet til mere vedvarende ressourcer er at have attraktive alternativer at skifte til. Dette kræver nye, interessante kemikalier, som nemt kan fremstilles fra de mest tilgængelige sukre, der kan fås fra biomasse. Opdagelserne gjort til denne afhandling og de undersøgte og diskuterede processer er forhåbentligt et lille skridt i den retning.

Contents

1
Introduction*

Material science has greatly contributed to many of the scientific advances that have led to the development status of the 21st century. The most obvious innovations are found in the things that surrounds on a daily basis. Phones and computers have increased in complexity and speed thanks to flash memory and faster processors, and solar panels on houses and battery-fueled cars are becoming an increasingly common sight. Another area of material science has however had an even greater impact on the world that surrounds us. The use of catalysts has had an immense influence on all aspects of society over the last 100 years from providing the ability to feed the growing population to cleaning the off gas from chemical plants for cleaner air. From synthetic fertilizer, over fuels, to the chemicals involved in everything from plastics to fine chemical pharmaceuticals, almost all are at some point in their manufacture dependent on the use of catalysts. It is estimated that 90% of chemicals produced in the word involve at least one catalytic step.[1] In this sense, catalysis has paramount importance in almost everything man-made that we come into contact with including the phones and cars mentioned above. The majority of the chemicals produced are currently obtained from fossil resources such as natural gas or oil. As we slowly transition from these finite sources of carbon for the production of chemicals to more renewable resources, new catalysts and catalytic systems will be needed.[2] Biomass, one of the most readily available carbon sources, is so different in its chemical structure from oil that many existing technologies will not be usable for this new feedstock. Not only will new catalysts and processes have to be

* Parts have been adapted from Tolborg *et al.* The Catalyst Review 2013, 26 (11), 6-12.

developed, entirely new chemicals will be the result of this change derived from the more oxygen-rich sugars obtained from biomass.[3] As a result, not only will the chemical industry have to change with this transition, but the off-takers; the polymer producers, the chemical companies will likewise have to evolve and adapt. This can be done either by incorporating these new chemicals into their current portfolio, if possible, or for the production of an entirely new biomass-specific portfolio of products.

This dissertation covers the preparation and evaluation of a specific type of catalyst for the conversion of sugars substrates into chemicals of high value. These catalysts are reliant on tin as their active site, previously shown to possess excellent properties in many different reactions involving sugars. The aim of the introduction is to provide insights into the nature of the different types of available stannosilicates and their use for carbohydrate conversion. This entails a brief introduction to zeolites and zeotypes, the preparation and active site of Sn-Beta and the use of this type of material in the conversion of sugars of all sizes.

1.1 Zeolites and zeotypes

Zeolites are well-known in industrial chemistry due to great potential as catalyst in many wide-spread applications, for instance in fluid catalytic cracking and as a hydrocracking catalyst.[4, 5] These crystalline microporous aluminosilicates are widely used in industrial processes employing solid acid-base catalysts, for instance dehydration/condensation, isomerization, alkylation and cracking.[6] Although many naturally occurring zeolites exists, hundreds of different zeolite frameworks have been prepared synthetically. Framework structures are denoted using a 3-letter code, and the Structure Commission of the International Zeolite Association covers 232 different framework topologies. Out of these only a few have been widely used as catalysts in industry with an approximate consumption of ~250.000 metric tons (anhydrous) per year.[7] A particular example of common zeolite is ZSM-5, with the MFI framework, is extensively used. Zeolites possess distinct active sites and a framework with well-defined pore dimensions, allowing for the discrimination of products and reactants based on size and shape.[8, 9] The channel systems can protrude the structure in one, two or three dimensions with the channel in the Ångstrøm-scale *i.e.* similar in size to many chemicals. The fact that the pores have very specific and uniform sizes makes these material excellent at shape selectivity. They are also called molecular sieves, since they can separate molecules based on their size. The most common types of shape selectivity are shown in Figure 1.1. These different types of selectivity involve restricting the access of certain reactants into the pore

channels (reactant selectivity), allowing only the release of one type of product (product selectivity) or hindering the formation of more than one product around the active site (transition-state selectivity).[9] The types of selectivities are similar to what is achieved using enzymes, affording zeolites the nickname metalloenzymes.[4, 10]

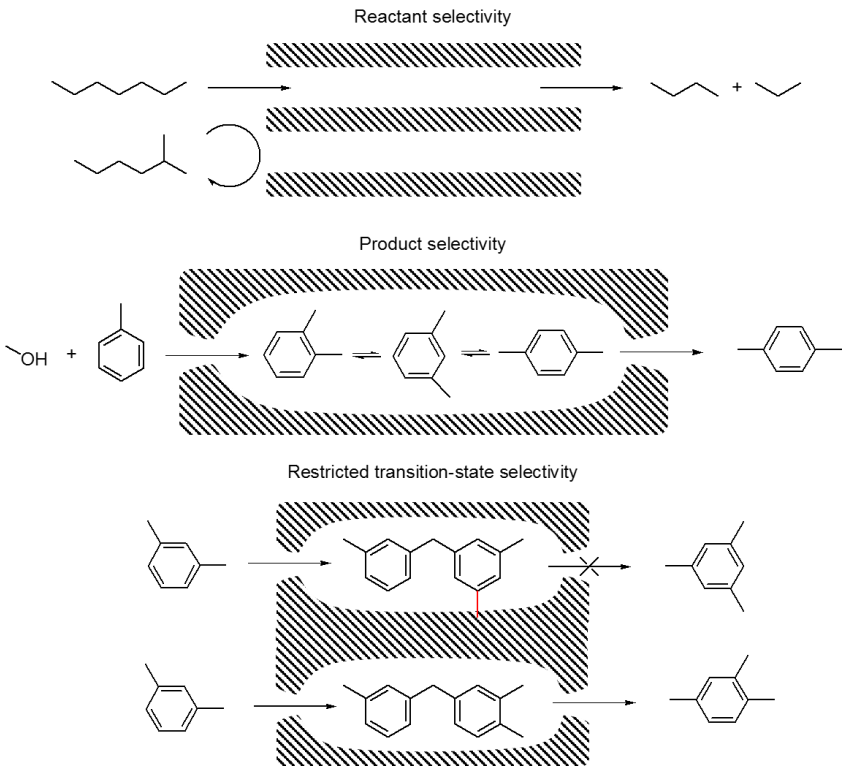

Figure 1.1. Reactant, product and transition-state shape selectivity.[9]

In conventional zeolites, connected tetrahedra of SiO_4 and $[AlO_4]^-$ impose a charge imbalance in the crystalline framework, which is compensated for by external cations present in the material such as protons or alkali/alkaline earth metals. This inequity in charge is what gives zeolites its useful properties as a solid Brønsted acid or for ion-exchange purposes.

A zeolite is defined as a porous, crystalline aluminosilicates. In either the absence of alumina or silicon or when additional elements are introduced, the material is instead denoted a zeotype material. A zeotype is thus structurally identical to a zeolite. Although many different types of zeotypes exist, this dissertation will focus on the introduction of Lewis acidic elements into the zeolite

framework while excluding aluminum entirely. By inserting elements such as tin, titanium or zirconium into the crystal lattice of the material, Lewis acidity is introduced, making sites available in the material capable of attracting and accepting electrons. This is vastly different from the conventional Brønsted acidic zeolites instead able to donate a proton. As a result, the solid Lewis acids possess completely altered catalytic properties. In the work done here the focus will primarily be on zeotypes where tin is introduced as the active metal, the so-called stannosilicates. This group of catalysts have shown exceptional properties for the conversion of biomass-derived sugars, something that will be discussed in more details later.[11-13] Although in general only little tin can be incorporated in the zeolite structure, often as low as one tin atom per hundreds of atoms of silica, the atomic distribution in the structure makes for an ideal single-site heterogeneous catalyst, creating a catalyst in which every single embedded metal can be an active site.

The stannosilicate Sn-Beta is one such zeotype consisting exclusively of silicon, tin and oxygen and has the *BEA zeolite framework. Sn-Beta has continuously been shown to possess high catalytic activity and selectivity in a number of industrially relevant reactions including in Baeyer-Villiger (BV) oxidation and in Meerwein-Ponndorf-Verley-Oppenauer (MPVO) redox reactions.[14, 15] For the work here, it is the role for Sn-Beta for the conversion of carbohydrates that makes the catalyst of high interest. This catalyst has been shown to possess high activity both in the isomerization of sugars as well as in the conversion of sugars to the biomonomer methyl lactate (ML) in high yields.[16-18] To better understand the exceptional properties of Sn-Beta and its uses as well as to introduce some of the different zeotypes used throughout this dissertation, I will here briefly introduce key discoveries within this group of Lewis acidic zeotypes.

The discovery of titanium silicate-1 (TS-1) was made around 30 years ago by the group of Taramasso by substituting a small but significant percentage of the silicon atoms in the zeolite with titanium.[19] TS-1 has the MFI crystal structure, making it isomorphous to industrially important zeolite ZSM-5 mentioned earlier. The solid Lewis acid possessed exceptional catalytic properties in the epoxidation of olefins and the oxidation of alcohols to aldehydes and ketones, leading to rapid industrialization in the production of diphenyls (catechol and hydroquinone), cyclohexanone oxime, and propylene oxide.[20] Cyclohexanone oxime is an important intermediate in the production of Nylon-6, and propylene oxide is used in the production of polyurethane plastics and propylene glycol. The discovery of Ti-Beta (isostructural to Sn-Beta) occurred in 1992, when the group of Camblor

prepared a titanoaluminosilicate with the *BEA framework structure.[21] It was later prepared without aluminum in the structure using fluoride ions instead of hydroxide ions as the mineralizing agent during synthesis.[22] Fluoride ions change the supersaturation during synthesis enabling the preparation of materials otherwise difficult to synthesis. It however also often, as in the case of Ti-Beta (and later Sn-Beta) involves the use of hydrofluoric acid (HF) making direct industrial upscaling difficult.

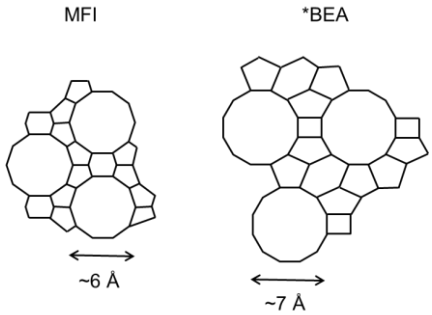

Figure 1.2: Graphic visualization of the respective frameworks of the pore systems in the crystalline MFI and *BEA zeotypes.[23]

One of the main advantages of introducing the Lewis acidic metal into the *BEA framework as compared to that of MFI was the slightly larger pore size as shown in Figure 1.2. MFI is made up of 10-membered ring pore openings (diameter of ~6 Å) whereas the ones in *BEA are 12-membered (diameter of ~7 Å). Since most of the active sites are present within the pore system of the zeolite, the size of the channels can both be a benefit resulting in some of the shape selective properties shown in Figure 1.1 on p. 3, or unfortunate limitations in the size of the molecules that can be converted using the porous catalyst. For TS-1 the narrow channels restricted the choice of substrate to relatively small sizes. Although the difference in size of the pore opening is modest, it had tremendous effect on reactivity and selectivity in a number of reactions when comparing the two titanium-containing materials. TS-1 was for instance able to selectively convert 1-hexene to the corresponding epoxide, whereas the use of Ti-Beta resulted in the formation of primarily byproducts (Figure 1.3a).[24] When a bulkier product was targeted such as the epoxide of norbonene (Figure 1.3b), no reaction was observed with TS-1, whereas Ti-Beta could successfully form the epoxide.[25]

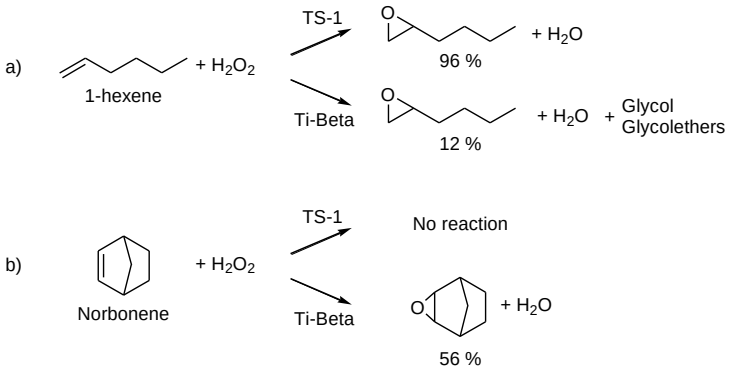

Figure 1.3: Epoxidation of a) 1-hexene and b) norbonene with TS-1 and Ti-Beta.[24, 25]

Despite the rapid industrial success of the TS-1 catalyst, the tin-containing equivalent Sn-MFI was synthesized approximately 10 years later but has received little attention over the years.[26-29] Sn-MFI showed promising results in the oxidation of ethylbenzene to acetophenone, yielding better results than TS-1 at similar conditions (Figure 1.4a).[30]

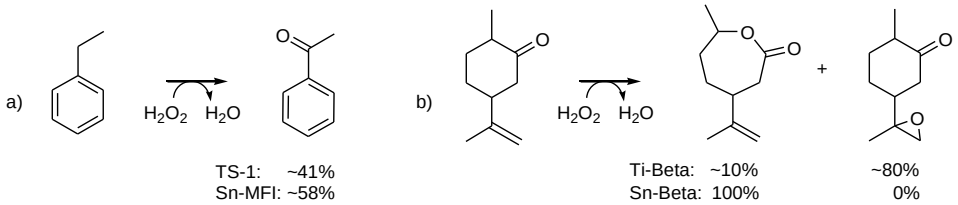

Figure 1.4. a) Oxidation of ethylbenzene to acetophenone over TS-1 and Sn-MFI.[30] b) Oxidation of dihydrocarvone catalyzed by Sn-Beta and Ti-Beta.[31]

The benefit of having tin as the active metal instead of titanium became apparent as Sn-Beta was introduced, initially by the group of Ramaswamy (1997) and then by Corma *et al.* (2001).[14, 32] The latter showed the excellent selectivities of this zeotype for the BV oxidation of cyclohexanone to ε-caprolactone (Figure 1.5a), an important chemical in polymer production.[14] Sn-Beta was likewise found to selective catalyze the MPVO redox reaction for the conversion of cyclohexanone to cyclohexanol (Figure 1.5b), and the C-C bond formation for the conversion of citronellal to isopulegol, a chemical used for the preparation of menthol (Figure 1.5c).[15, 33] In all cases the use of Sn-Beta had significant advantages over the existing system either by replacing expensive peracids with hydrogen peroxide (for BV) or homogeneous metal alkoxides (for MPVO) or by offering higher selectivities to the desired products.

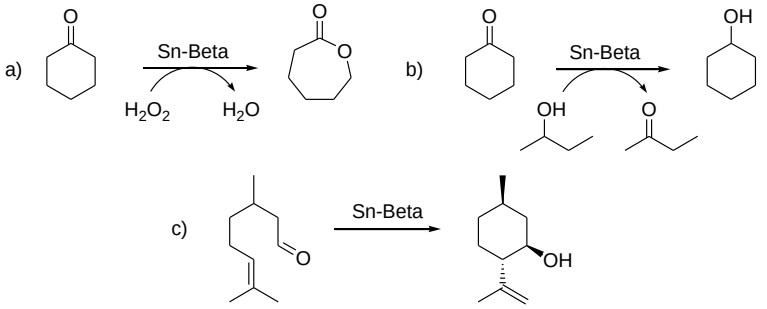

Figure 1.5. a) Baeyer-Villiger Oxidation reaction of cyclohexanone to ε-caprolactone, b) Meerwein-Ponndorf-Verley-Oppenauer redox reaction of cyclohexanone to cyclohexanol, and c) conversion of citronellal to isopulegol by oxo-ene reaction.[14, 15, 33]

Similar to Sn-MFI and TS-1, Sn-Beta was found to catalyze the same type of reactions as Ti-Beta but with significantly higher activity.[15] Distinct differences in the catalytic properties of the two incorporated metals have however also been reported. Ti-Beta was found to be almost inactive in the aforementioned oxidation and redox reactions of cyclohexanone (Figure 1.5a and b, respectively) but were active in the epoxidation of octene, the exact opposite activities were found for Sn-Beta.[34] Moreover, when converting a substrate that could be oxidized to yield either the corresponding epoxide or lactone, Ti-Beta was found to primarily yield the epoxide and Sn-Beta the lactone, see Figure 1.4b, showing the complementary selectivities of these catalysts.[31] Similar changes in reactivity was found when zirconium was introduced in the framework. Zr-Beta was found capable of catalyzing many of the same oxidation reactions as mentioned above, but was likewise able to catalyze the MPV reduction of cinnamaldehyde, where both Sn- and Ti-Beta showed no activity. [35-38] This shows the versatility in and importance of choosing the right metal to impart Lewis acidity onto the catalyst. Although a difference in Lewis acid strength has been provided as explanation for this difference in reactivity, there are fundamental differences between the different incorporated metal aside from the acid strength.[14]

1.2 **Ordered mesoporous stannosilicates**

Apart from the zeotypes, an entirely different type of Lewis acidic metallosilicates exist. These materials are made up of a mesoporous hexagonally-ordered pore system with the walls of the structure consisting of amorphous silica, see Figure 1.6.[39] In a similar manner as for the zeotypes, different Lewis acidic elements can be implemented into the structure. Due to the amorphous nature of

the material, however, sites are distributed randomly in the material, thereby differing substantially from the somewhat well-defined incorporating in a crystalline framework. Of these materials especially the Mobil Composition of Matter No. 41 (MCM-41) and the Santa Barbara Amorphous-15 (SBA-15) materials have been extensively studied both as catalysts and as catalyst supports.[13, 23, 36, 40, 41]

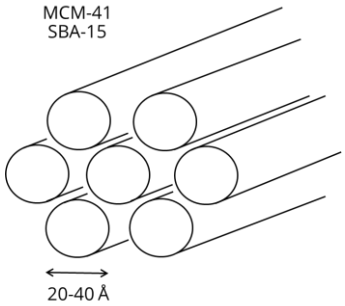

Figure 1.6. Graphic visualization of the hexagonally-ordered structures found in MCM-41 and SBA-15.

The main differences between the two materials are the slightly higher surface area and larger wall thickness of SBA-15 as well as the presence of some microporosity in this material. Although these materials have generally been shown to possess a lower intrinsic activity than the zeotypes, a benefit can be found in their large surface area (>900 m^2/g), the possibility of preparing them with high metal content, and the much larger pores.[13, 27, 40, 41] These catalyst allow for the conversion of even bulkier substrates than what is possible with Sn-Beta. [40, 42]

1.3 **Preparation of stannosilicates**

For this dissertation a variety of catalysts were prepared to investigate and evaluate their use in reactions involving different carbohydrates. The stannosilicates include; the medium-sized pore zeotype Sn-MFI, the large-pore zeotype Sn-Beta and the two ordered mesoporous stannosilicates Sn-MCM-41 and Sn-SBA-15.

Most of the zeotypes are prepared by hydrothermal synthesis. This involves mixing a silica and tin sources with a structure directing agent (SDA) and treating the mixture at elevated temperatures under autogenous pressure. The role of the SDA is to guide which zeolite framework is formed. A number of approaches have been followed for the preparation of these silicate materials containing Lewis

acidic elements. For the preparation of Sn-Beta, an overview of some of the synthesis protocols is shown in Table 1.1 including brief descriptions of the procedures.

Table 1.1. Different synthesis protocol used for the preparation of tin-containing Beta zeotypes.

Method	Brief description	Ref.
Hydrothermal synthesis	Fluoride route: 1) TEOS and are mixed with the structure-directing agent, TEAOH. 2) Hydrolysis of the silica source releases ethanol leading to formation of viscous gel. 3) HF is added, solidifying the gel. 4) (Optional) Seeds made from a dealuminated commercial Beta zeolite are added. 5) Gel is hated to 140-160 °C (2-60 days).	[14, 17, 43-46]
	Steam-assisted conversion (fluoride): 1) $SnCl_4 \cdot 5H_2O$, fumed silica, NH_4F and TEAOH are mixed, stirred and finally dried at 60 °C. 2) The gel is heated to 180 °C (6 h) in the presence of water vapor.	[47, 48]
	Dry gel conversion (fluoride free): 1) NaOH, TEAOH and fumed silica is dissolved in an excess of water, followed by addition of tin *tert*-butoxide and H_2O_2. 2) Seeds made from dealuminated commercial Beta zeolite are added. 3) Solvent allowed to evaporated by heating for 24 h at 80 °C. 4) The gel is placed at 140 °C (5 days) in the presence of water vapor.	[49]
Post-synthesis	Grafting: 1) A commercial source of Beta zeolite is dealuminated using HNO_3 at 80 °C for 8 h. 2) A flow of nitrogen was first passed through an anhydrous $SnCl_4$ liquid then exposed to the dealuminated sample.	[50-52]
	Solid state ion exchange: 1) A commercial source of Beta zeolite is dealuminated using HNO_3 at 100 °C for 20 h. 2) The dealuminated sample is then ground mechanically with a tin salt.	[37, 51, 53, 54]

Post-synthesis	Wet impregnation: 1) A commercial source of Beta zeolite is dealuminated using HNO_3 at 80 °C. 2) Tin is impregnated onto the sample by adding tin salt dissolved in a volume of water matching the internal volume of the zeolite.	[51, 55, 56]
	Reflux impregnation: 1) A commercial source of Beta zeolite is dealuminated using HNO_3 at 80 °C overnight. 2) A dried sample is refluxed under N_2 atmosphere in isopropanol containing the tin salt.	[51, 57]

The conventional synthesis method (fluoride route), developed by Corma *et al.* (Figure 1.7) involves mixing tetraethyl orthosilicate (TEOS) with tin(IV)chloride and the SDA tetraethylammonium hydroxide (TEAOH) yielding a thick gel. The synthesis is finalized by adding HF to exchange the hydroxide ions from the SDA with fluoride ions transforming the gel into a solid. This material is then placed under hydrothermal conditions (140 °C, autogenous pressure) for several days. The benefit of this approach is the highly defect-free crystals formed, creating a hydrophobic, crystalline material consisting entirely of silicon, tin and oxygen. This preparation route has certain shortcomings, however, in terms of long crystallization times, large crystal sizes (>1 μm) and the use of hydrofluoric acid. A thorough investigation of this synthesis method and the effect of incorporating tin is the focus of **Chapter 3**. This type of Sn-Beta material is furthermore used extensively for the conversion of different sugars in **Chapters 4 to 6**.

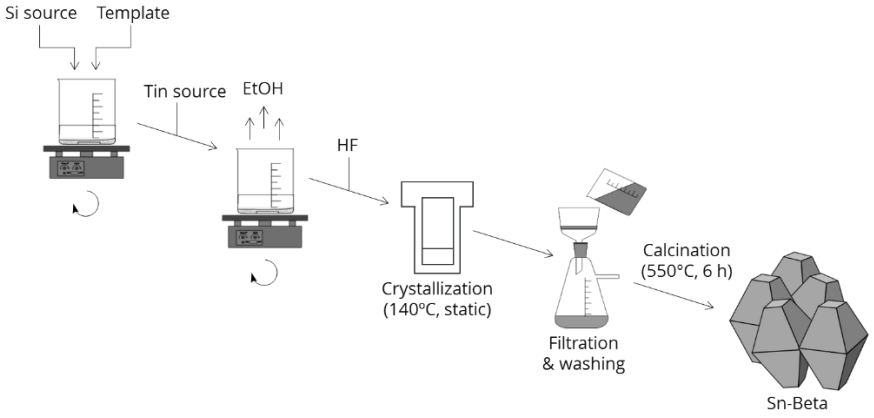

Figure 1.7. Overview of the different steps involved in the fluoride-route synthesis of Sn-Beta.

As a consequence of the drawbacks of the fluoride route synthesis, several alternative approaches have been investigated to ease preparation. These focus either on improving or modifying the existing synthesis or on a post-synthesis protocol. For the hydrothermal synthesis it has been shown that extensive seeding can lead to a significant decrease in required crystallization time.[43] Seeding involves adding already crystalline zeolite to the synthesis to ease the initial nucleation. A significant reduction in synthesis time was also achieved by using a 'steam-assisted conversion' approach where water vapor is present during crystallization.[48, 55] Interestingly, decreasing the amount of water present during synthesis was likewise found to lead to faster crystallization either by reducing water content partially,[45] or to the state of having a dry gel with as little water as possible.[49] The latter dry-gel conversion approach led to the first successful fluoride-free preparation of Sn-Beta.

Sn-Beta can also be prepared by a post-synthesis approach. By modifying an already crystalline zeolite it is possible to create vacancies in the framework in which tin can be incorporated. For the preparation of Sn-Beta, a commercial aluminum-containing Beta zeolite is often used. By first treating the zeolite in concentrated nitric acid, aluminum is removed from the framework, creating hydroxyl nest vacancies. Tin can then be introduced into these created sites in a variety of ways including gas-phase grafting, [50-52] solid-state ion exchange,[51, 53, 54] simple wet impregnation,[51, 55, 56] or reflux impregnation in an alcohol solvent.[51, 57] Using either of these preparation methods it is possible with relative ease to prepare Sn-Beta with a small crystal size (<0.5 μm) and with the potential inclusion of large amounts of tin.[58-60] It does however also lead to a much more hydrophilic material due to the presence of defects in the framework and residual aluminum.[58] The group of Hammond has furthermore shown that not all tin is necessarily introduced into the created vacancies resulting instead in tin oxide species upon calcination.[60] This could however be related to the chosen impregnation technique or potentially avoided by removing excess tin species before calcination.[52] Most important of all, this preparation method is simple, scalable and as a result more likely to be successfully prepared on industrial scale. For the work done for this dissertation, a wet impregnation methodology was chosen and used extensively for the conversion of carbohydrates in **Chapters 4 and 5**.

For Sn-MFI the hydrothermal synthesis was to a large extent pioneered by the group of Ramaswamy with preparation methods available involving both the use of fluoride and hydroxide ions as mineralizing agents.[26, 30, 61] Several of these protocols are still forming the basis of the preparation used today with the

materials prepared for this dissertation being no exception. For **Chapter 6**, Sn-MFI was both prepared using both a hydroxide and a fluoride route protocol. Similar to the work done to produce Sn-Beta through a post-synthesis procedure, the group of Perez-Ramirez prepared Sn-MFI following a top-down approach.[28] Instead of an initial dealumination step, however, the parent zeolite was desilicated using alkaline media to create defects in the framework in which tin could be incorporated. Some issues with stability during reaction of these materials were however found.[62]

For the mesoporous stannosilicates, Sn-MCM-41 and Sn-SBA-15, the preparation involves mixing different surfactants that align to form micelles that then again arrange into a hexagonal array. It is around this ordered organic network that silica and tin can connect to form the ordered amorphous structure.[13]

1.4 The active site of Sn-Beta

There has been much speculation to the nature of the active site in Sn-Beta, since its discovery 15 years ago. There are still many unknowns regarding the active site and the high activity of this zeotype materials. The main focus over the years has been to find a correlation between the nature of the tin site and the catalytic performance of the material, the so-called structure-activity relation.[13]

A multitude of spectroscopic techniques has been employed to investigate the exact configuration of tin in the catalyst including ultraviolet-visible (UV-Vis),[52, 63] infrared (FTIR),[46, 64, 65] and nuclear magnetic resonance (NMR).[31, 66-68] These techniques have often combined with density functional theory (DFT) to aid in the interpretation of the acquired results.[59, 64, 69, 70] Additionally, several of the techniques have also been combined with the use of probe molecules such pyridine, ammonia or acetonitrile have likewise been used to 'interrogate' the active site.[71-74]

It is generally well-established that the active sites found within Sn-Beta does not simply exists as a uniform environment imbedded in the zeolite framework. Over the years it has become clear that tin can be found in at least two different coordinating environments, however the nature of these sites are currently being debated. An 'open' and 'closed' site was introduced by the group of Corma in which tin is either isomorphously substituted within the zeolite framework (Site A, Figure 1.8) or partially inserted leading to the partly hydrolyzed site (Site B, Figure 1.8), respectively.[64] To again draw upon the history of the zeotype materials, the presence of two distinct active sites was previously found to be present in TS-1 by the group of Millini and in Ti-Beta by the group of

Matsukata.[75, 76] For these titanium-containing zeotypes, the hydrolyzed sites were generally found to have detrimental effects on catalysis. Removal of the hydrolyzed site (Site B, Figure 1.8) in Ti-Beta by ion-exchange for instance increased activity in the epoxidation of cyclohexene.[76, 77] Conversely, for Sn-Beta this site has generally been considered the most active due to its higher Lewis acid strength (found from FTIR).[34, 64]

One of the main arguments supporting the existence of these two sites in Sn-Beta has been the use results obtained from the combination of DFT combined with either FTIR or NMR. For FTIR the presence of the two tin sites was shown by adsorbing volumes of a probe molecule such as acetonitrile (as is the case on Figure 1.8) over a dehydrated Sn-Beta sample. From the interaction between the tin and the adsorbate, two distinct bands at 2308 and 2317 cm^{-1} appear. Using DFT calculations, these two bands could then be correlated to the two sites shown in Figure 1.8. The sample had to be dehydrated as the tin site can coordinate to up to two water molecules thereby hindering true interaction with the probe molecule.[14, 64] Using solid state NMR spectroscopy on similar dehydrated samples, likewise yielded what appeared to be two distinct peaks at -420 and -443 ppm again leading to the interpretation that two discrete tin sites exist in the material.[10, 14] The peak with the highest chemical shift (-420 ppm) was even observed to be in the presence of a hydrogen in the close environment using cross-polarization (CP) in agreement with one hydroxyl group present on the 'open' site of tin.[10]

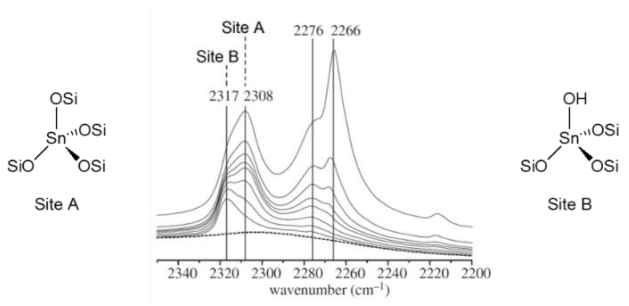

Figure 1.8: Probe-molecule infrared spectroscopy of Sn-Beta using deuterated acetonitrile showing the presence of two distinct bands and the tin sites believed to cause them. All silicon shown are further connected to the zeolite framework through three oxygen atoms. Adapted from ref. [13].

Recently, however, it is slowly being shown that the nature of tin incorporated within Sn-Beta is even more complex and exists in many more configuration than previously assumed. These differences include the likely presence of a defect in the near vicinity of the tin site, the interaction of the site with water at ambient

temperatures as well as the distribution of tin within the framework.[59, 73, 74, 78] The *BEA framework consists of 9 distinct so-called T-sites in which tin can be placed, recent work performed by the group of Hermans and Coperét shows that it is not straight forward to elucidate which (if any) of these potential sites are favored for the incorporation of tin.[59] It was recently shown by Otomo *et al.* that ion exchanging Sn-Beta with different cations affected what was assumed to be both the 'open' and 'closed' site in FTIR.[46] Since the 'closed' site should be unaffected by cations, this indicates that the initial interpretation could be too simplified. Furthermore, tin present in the zeolite appears able to interact with water to form hydrated open sites already at room temperature, meaning that the site could be more dynamic under reaction conditions at higher temperatures as well.[65, 74] The group of Corma showed that the catalytic properties of Sn-Beta samples was affected by being aged under ambient conditions.[79] It was furthermore shown by the group of Ivanova that even the coordination of the active site with different substrate and solvent molecules is not straight forward.[74] These recent findings underline the complexity of the behavior of the tin site in reaction.

Recent advances within solid state NMR of tin-containing materials have made investigating the environment of tin more reliable by significantly increasing the sensitivity of the technique affording much higher resolution of the spectra.[66-68] NMR has received much focus as the information gained by investigating a sample gives direct information about the environment of the measured nucleus. Previous techniques relied heavily on indirect measurements to yield information of the tin site for instance the aforementioned use of acetonitrile where the interaction with the tin would affect the C≡N bond length, detectable by FTIR. By studying tin using NMR techniques, it is possible to investigate the environment of the active site and ideally to relatable this to the activity of the material. The low natural abundance of ^{119}Sn (of 8.6%) visible by NMR coupled with a high relaxation time of the isotope makes it difficult to increase sensitivity by conventional means (*e.g.* increasing number of scans). One way of overcoming this problem has been to investigate enriched Sn-Beta samples prepared using the tin isotope (^{119}Sn) as the metal source. This is however both an expensive approach and one that distances the technique from being used on 'real' catalysts.[10, 14, 80] Instead, two new approaches of obtaining NMR measurements have been developed within the last few years. One approach involves transferring polarization of electron spin of an external radical to the nuclear spin of tin by way of microwave irradiation. The technique coined 'dynamic nuclear polarization' (DNP) NMR was developed simultaneously by the

group of Román-Leshkov and the groups of Coperét and Hermans.[66, 67] A different approach based on the application of Carr−Purcell−Meiboom−Gill (CPMG) echo-train acquisition was developed by the group of Ivanova. This technique utilizes a series of refocusing pulses in order to measure the response of tin without having to let the nuclei fully relax.[68] Both approaches significantly reduces the measuring time (from several days to hours) while simultaneously reducing the signal-to-noise ratio. This has allowed studies showing large heterogeneities in the environment of tin within Sn-Beta depending on the synthesis approach,[59, 81] but more importantly have led to spectra resolution making it clear that the aforementioned two bands observed with conventional solid state NMR (at -420 ppm and -443 ppm) are in fact a collection of several peaks in the region from -420 to -445 ppm (Figure 1.9).[68]

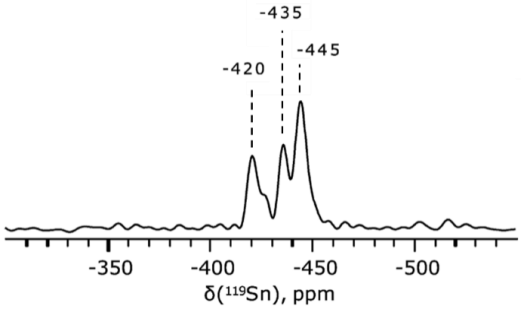

Figure 1.9. ^{119}Sn DP/CPMG MAS NMR of dehydrated Sn-Beta showing the occurrence of additional peaks in the range of -400 to -470 ppm. Adapted from ref. [68].

Furthermore, in the study by the group of Ivanova it was found that the cross-polarization with ^{1}H observed for the highest shift, originally proving the presence of an 'open' hydrolyzed tin site, disappeared upon dehydration of the sample at temperatures above 150 °C.[74] These findings in truth show that the interpretation of two static tin sites is much too simplified to describe the interior of the Sn-Beta zeolite. Very recent work done by the group of Ivanova using a combination of NMR utilizing CPMG and various probe molecules have however confirmed the existence of at least a strong and a weak Lewis acidic interaction between tin present in Sn-Beta and different adsorbates.[74]

The technological improvements within computing over the last decade, has made it possible to model large complex structures such as zeolites with much larger parts of the framework represented in the calculations.[59] Combined with the improvements within NMR this has made it possible to make some careful interpretations into the actual placement of tin within the framework showing a

multitude of possible configurations of the sites. As is often the case, introduction of new more advanced techniques presents several more questions. For Sn-Beta it appears that the unknowns surrounding the active site have only increased in complexity as a result.

1.4.1 Modification of Sn-Beta

For all its complexity, the tin sites have likewise been shown sensitive to the presence of impurities present during synthesis or added during reaction. The zeotypes (TS-1, Sn-MFI, Ti-Beta) have generally been shown to be difficult to prepare with alkali or alkaline earth metals present during synthesis.[21, 82-84] A major source of these impurities is found in the variety of templates used to direct the zeolite growth. The presence of alkali has likewise been shown to modify the active site of the material, presumably by exchanging onto hydroxyl sites present in the framework. These sites could either be present as defects near the tin site or some variant of the 'open' site mentioned earlier. For TS-1 it was found that any alkali or alkaline earth metals had to be avoided during synthesis but had a beneficial effect on the epoxidation of allyl alcohol and the oxidation of cyclohexene and styrene when added in the appropriate amounts.[83, 85] In most studies, however, alkali was found to have detrimental effects on the catalytic properties, often explained by the increased polarity of the tin site with alkali exchanged onto the hydroxyl.[86-88] As a result of this negative effect, several groups have studied the post-synthetic removal of these impurities from the zeotype, either by ion exchange or acidic treatment.[76, 86, 88, 89] Recently, the effect of having alkali present during the catalytic conversion of sugars using Sn-Beta was shown to influence product selectivity.[46, 90, 91] This will be investigated and discussed in more detail in **Chapters 4 and 5**.

1.5 Stannosilicates for biomass conversion

Glucose and xylose are the most abundantly available sugars from lignocellulosic biomass, making up an average 70% of the total carbon.[92] Products derived from these substrates have a high potential for industrial implementation.[3, 93] Although fermentative and enzymatic processes are already implemented industrially for the production of a range of chemicals from sugars, inorganic systems have many potential advantages in terms of scalability, tolerance to a broad range of reaction conditions and several options for continuous conversion. Currently, direct industrial conversion from glucose using inorganic catalysis has only been applied in the production of sorbitol and

gluconic acid. Several promising chemicals have however been shown to be accessible from both the hexoses and pentoses including ethylene- and propylene glycol and a variety of furanic and lactic acid derivatives.[16, 17, 94-98] Several of these compounds are interesting for their use as polyester building blocks.

In recent years several potential uses of stannosilicates have been explored for the emerging area of biomass conversion.[13, 16, 17] For carbohydrate conversion, especially Sn-Beta has been shown to catalyze a number of interesting reactions taking advantage of the strong Lewis acidity of the material. One of the important reactions, Sn-Beta was found to efficiently catalyze, was isomerization of glucose to fructose and mannose in water, see Scheme 1.1.[10, 13, 17, 18, 99, 100]

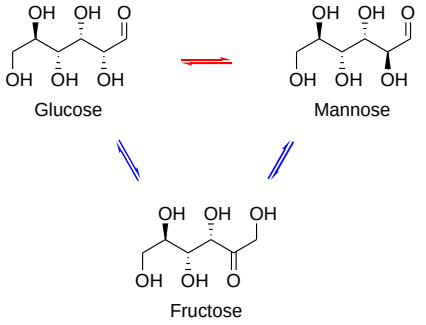

Scheme 1.1. Reaction scheme for the isomerization (blue) and epimerization (red) of glucose to either fructose or mannose, respectively.

High-fructose-corn-syrup is still used extensively in the United States, and the potential of catalytically converting glucose to the much sweeter fructose has spiked interest in the field. Similar to the Meerwein-Ponndorf-Verley-Oppenauer (MPVO) redox reaction mentioned earlier, the isomerization likewise involves the simultaneous oxidation and reduction of the carbonyl and alcohol group of the sugar. The mechanism of the isomerization step is believed to consist of a 1,2-hydrideshift similar to what takes place in the MPVO redox reaction. Through coordination of tin with the ketone and hydroxyl group of the sugar a hydrogen is moved, facilitating the reduction of the aldehyde and subsequent oxidation of the secondary alcohol (Scheme 1.2).[70, 101, 102]

This reaction was furthermore found to be influenced by the presence of alkali metals during reaction. It was discovered by the groups of Román-Leshkov and Davis that the addition of a cosolute in the shape of either sodium borate or sodium chloride could modify the reaction pathway when Sn-Beta was used to convert glucose.[90, 91] Both groups showed that the direct epimerization of glucose to mannose (Scheme 1.1) could be done under these modified conditions.

This effect was found to also apply to the pentose sugars.[103] Both the isomerization and epimerization reaction has later been extensively studied both to obtain the isomers and epimers themselves, but also combined with other homogeneous or heterogeneous catalysts to yield products easier to obtain from the fructose isomer such as for instance 5-(hydroxymethyl)furfural (HMF).[29, 90, 91, 96, 104] In a similar way, Sn-Beta was recently combined with a nickel catalyst for the one-pot conversion of lignin-derived alkylquaiacols to caprolactone derivatives exploiting the activity of Sn-Beta in BV.[105]

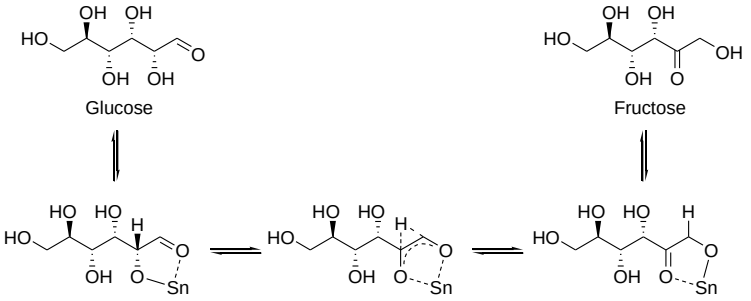

Scheme 1.2. Schematic representation of the tin-catalyzed isomerization of glucose to fructose.[101]

The catalytic synthesis of lactates from sugars is another example where Sn-Beta has been found to be a highly active and selective catalyst.[16, 18, 99, 106] Methyl lactate (ML) is an ester of lactic acid, which can be used in the production of poly(lactic acid) (PLA); a compostable bio-plastic.[107] The production of this biodegradable monomer is otherwise restricted to base catalyzed conversion of sugars and fermentation and is currently produced on an industrial scale using fermentative processes.[108-112] Sn-Beta was initially found to selectively convert the triose sugars (1,3-dihydroxyacetone and glyceraldehyde) to methyl lactate even at low temperatures.[99] With the larger pentose and hexose sugars such as glucose and xylose, Sn-Beta was likewise capable of forming ML through a retro-aldol fragmentation of the sugars though less selectively leading to lower obtained yields (~42% for pentoses and ~54% for hexoses). The lower yields are due to the increased complexity of these larger sugars leading to the formation of additional products.[16, 56] Some of these additional products will be touched upon later, others are investigated in more detail in **Chapter 5**.

As Sn-Beta is capable of catalyzing the isomerization of the hexose and pentose sugars, similar yields of methyl lactate are obtained when reacting different isomers of the monosaccharaides.[10, 18, 43, 99, 100] This alleviates the need to use a specific sugar substrate, which is often a limitation in enzymatic

reactions. Interestingly, sucrose, the disaccharide combination of glucose and fructose, was found to afford the highest yields of ML using Sn-Beta (68%),[16] assumed to result from the higher thermostability and slow release of glucose and fructose upon hydrolysis.[113] Similar to the 1,2-hydrideshift taking place in the isomerization (Scheme 1.2), the mechanism of the retro-aldol reaction is likewise believed to involve coordination of the tin site with the carbonyl and alcohol moiety of the sugar, facilitating the bond breaking reaction, see Scheme 1.3.[13]

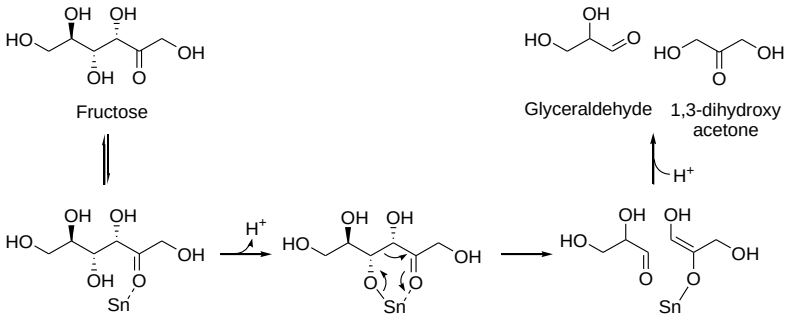

Scheme 1.3. Schematic representation of the tin-catalyzed retro-aldol reaction of fructose leading to the formation of the triose sugars; glyceraldehyde and 1,3-dihydroxyacetone.[13]

The many sequential reactions involved in the conversion of sucrose to ML can be seen in Scheme 1.4. Initially, sucrose is hydrolyzed to yield equimolar amounts of glucose and fructose. Both the aldohexoses (glucose and mannose) and the ketohexose (fructose) can undergo retro-aldol reaction, the resulting products are directly affected by which sugar is cleaved. If fructose undergoes retro-aldol reaction (Scheme 1.4, green path), the primary product is ML. From the retro-aldol of fructose, the two triose sugars, glyceraldehyde (GLA) and 1,3-dihydroxyacetone (DHA), are formed. These smaller sugar fragments then undergo first β-dehydration to yield the 1,2-dione intermediate pyruvaldehyde (Scheme 1.5). This is a very reactive intermediate that upon reaction with the alcohol solvent yields the corresponding hemiacetal and undergoes an additional 1,2-hydrideshift to yield ML.[114, 115]

Alternatively, if glucose undergoes retro-aldol reaction (Scheme 1.4, blue path), none of the formed sugar fragments convert directly into ML. This bond cleavage instead leads to other, interesting potential high-value products. The C-C bond breaking of the aldohexose leads to the formation of an aldotetrose (erythrose or threose) and glycolaldehyde. The latter can either react with the alcohol solvent forming glycolaldehyde dimethyl acetal or undergo aldol condensation by reacting with another sugar molecule.[18, 116, 117] From the

tetrose sugars the subsequent cascade of reactions are similar to those explained for the trioses to methyl lactate instead involving the formation of the 1,2-dione intermediate 3-deoxytetrosone (3DT). The formation of this intermediate is believed to follow a similar mechanism as the one shown for the trioses in Scheme 1.5 on p. 21.

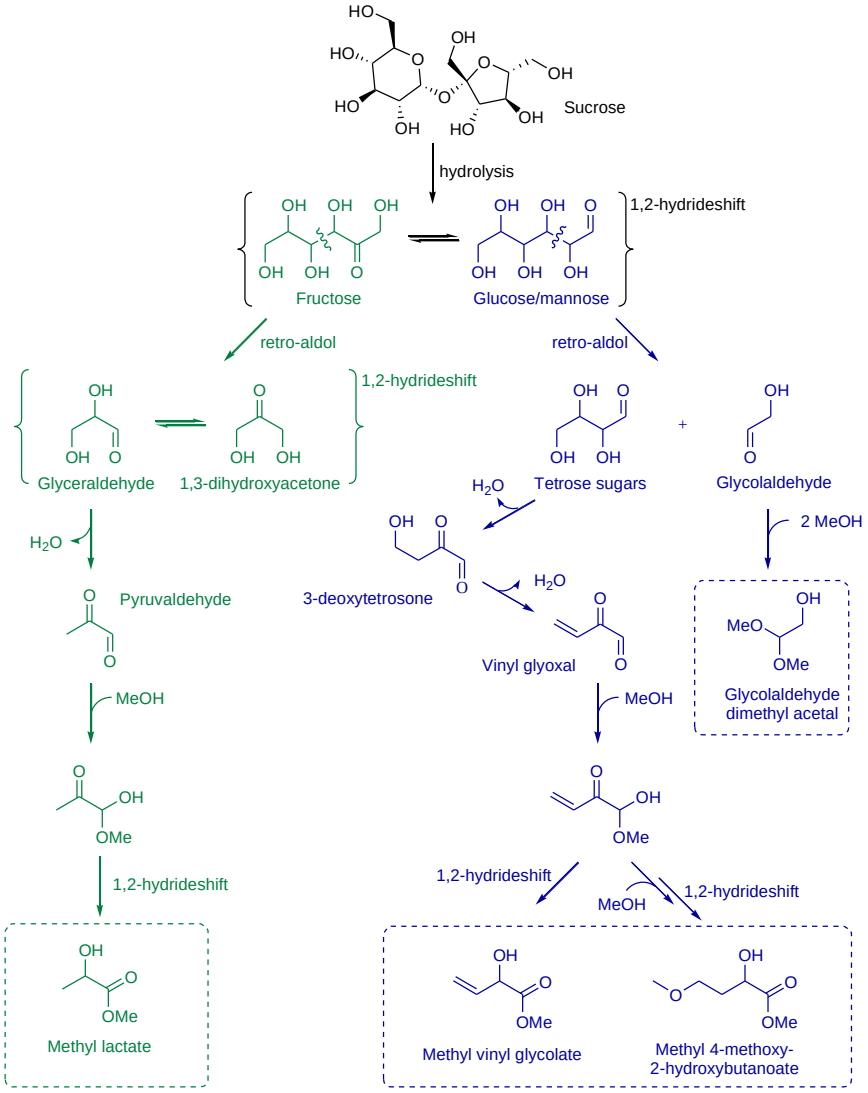

Scheme 1.4. Reaction scheme for the conversion of sucrose to methyl lactate through the retro-aldol reaction of fructose (shown in green) and to methyl vinyl glycolate and co-products from the retro-aldol reaction of glucose (shown in blue).[16, 99, 118]

3DT can undergo an additional β-dehydration leading to the second intermediate vinyl glyoxal (Scheme 1.4).[118, 119] From the hemiacetal of this intermediate either methyl vinyl glycolate (MVG) is obtained or through addition of methanol to the vinyl group; methyl-5-methoxy-2-hydroxybutanoate (MMHB).[16, 18] Especially MVG has been shown to possess interesting properties for both further conversion to high value products or for the direct use as building block for polymer production.[23, 116, 118, 120-122]

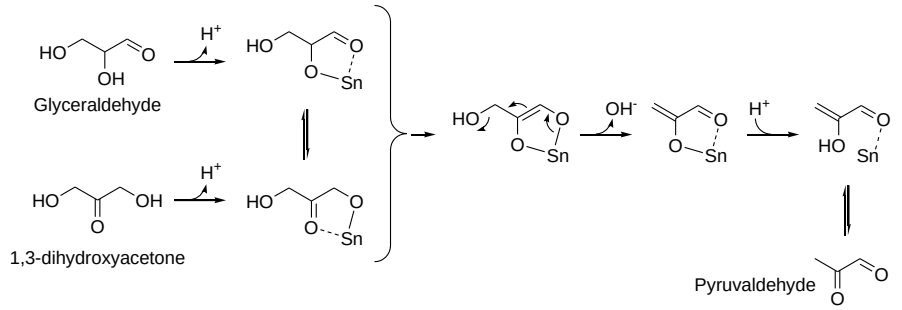

Scheme 1.5. Proposed mechanism for the β-dehydration of glyceraldehyde to the 1,2-dione intermediate pyruvaldehyde.[119]

Sn-Beta is thus capable of sequentially catalyzing a cascade of reactions resulting in modest to very high yields of methyl lactate depending on the complexity of the starting carbohydrate substrate. This versatility in choice of substrate could prove to be an important advantage over the much more substrate specific enzymatic systems. This will be exploited in the different chapters of this dissertation. In **Chapter 3** the selective conversion of the triose DHA to ML will be used at low temperatures (75 °C) to probe the activity of the synthesized Sn-Beta materials. In **Chapter 4**, the conversion of glucose at moderate temperatures (120 °C) and sucrose at high temperatures (170 °C) will be used for the optimization of the ML yield from more complex sugars. The catalytic system and reaction pathways involved are investigated in more detail starting from both the pentose and hexose sugars in **Chapter 5**.

Sn-MFI has also received some attention for the conversion of carbohydrates especially for the isomerization of sugars, although the smaller channel openings in zeotype has limited its application compared with Sn-Beta.[13, 27, 28] Sn-MFI has been shown to efficiently isomerize both triose and tetrose sugars, but for larger sugars conversion is hindered. Where the isomerization of the pentoses occur albeit slowly, the hexose sugars are barely converted.[100] For isomerization this naturally restricts the use of Sn-MFI, but embracing the size limitations of Sn-MFI opens up other interesting options for the selective condensation of smaller sugar substrates.[117] This will be discussed further in **Chapter 6**. In a similar

manner, the amorphous stannosilicates such as Sn-MCM-41 can also be exploited for their large pore system with no limitations in diffusion. In a study by Osmundsen *et al.*, Sn-MCM-41 was shown to retain a higher carbon balance in the isomerization of sugar, presumably due to its lower intrinsic activity compared with Sn-Beta.[13] Sn-MCM-41 was able to catalyze the isomerization but less active in any further conversion leading to a higher overall yield of sugars left after reaction.

In conclusion, tin-containing silicates have proven to be excellent catalysts for the conversion of sugars to value-added products. By keeping within the philosophy of retaining as much of the functionality found in carbohydrates, the ability of Lewis acids to efficiently catalyze the movement of hydrogen within the structure through a 1,2-hydrideshift, opens up a vast portfolio of products depending on the chosen reaction conditions. Temperature, solvent, cosolutes are key factors in directing the reaction to either undergo a simple hydride shift of glucose to fructose (at moderate temperatures) or facilitate a retro-aldol cleavage and subsequent hydride shift of glucose to methyl lactate (at higher temperatures). The outcome of the reaction becomes transparent with the understanding of these principles, leading to a range of similarities in the way tin catalyzes the conversion of small sugars such as glycolaldehyde (**Chapter 6**) or trioses (**Chapter 3**) to the larger carbohydrates xylose and glucose (**Chapters 4 and 5**).

1.6 Aim and outline of the study

The aim of the project is to prepare and investigate the use of stannosilicate catalysts for the conversion of carbohydrates to value-added chemicals. Preparation and analysis of the different Lewis acidic catalysts has been a key focus point as well as investigating the reactivity of the materials towards the desired products. As a result, **Chapter 3** details a thorough investigation of the synthesis and modification of Sn-Beta, and **Chapters 4 to 6** investigate the use of different stannosilicates for the conversion of a variety of sugars and how to control and improve selectivity of these materials. Throughout the project it has been a prerequisite that reactions involving the conversion of carbohydrates be performed at moderate temperatures and in 'green' solvents such as water and methanol when possible.[123]

I hope throughout this dissertation to show both the versatility of the tin-containing silicates and the importance of directing the catalytic outcome by choosing the appropriate catalyst and conditions.

All experimental procedures for **Chapters 3 to 6** are collected and included in **Chapter 2**. This chapter details the synthesis and preparation of the

investigated stannosilicate materials as well as their characterization. In the chapters is also included the catalytic evaluation and subsequent analysis of the reaction mixtures as well as the external work done to polymerize one of the new products described in this dissertation.

Chapter 3 focuses primarily on the preparation and characterization of Sn-Beta by the fluoride-route. In the chapter the influence of tin on the synthesis and resulting materials is investigated using a variety of techniques, bringing light to both the extensive retardation of the crystal growth, the resulting influence on crystal morphology and the distribution of tin within the zeolite crystal. Additionally, the effect of alkali salts on these parameters will be discussed. The chapter is to a large part based on the work published as; Tolborg *et al. J. Mater. Chem. A* 2014, 2, 20252-20262.

Chapter 4 will be used to describe the significant effect of having a cosolute present alongside Sn-Beta during catalytic conversion of sugars for the formation of methyl lactate. The effect is studied both when added during synthesis and when added directly to the reaction media. Additionally, the effect is shown to both apply to a variety of sugar substrates and stannosilicate materials, making the effect widely applicable for this system. The chapter is to a large part based on the work published as Tolborg *et al. ChemSusChem* 2015, 8, 613-617.

Chapter 5 can be considered a direct follow-up for the effects observed in **Chapter 4**. By employing advanced characterization of the reaction mixtures, it is shown that at least two different reaction pathways exist when converting carbohydrates using Sn-Beta. The influence of alkali on these pathways are investigated. Previously unreported α-hydroxy acids and lactones are found and shown to be able to undergo co-polymerization. The chapter is based on results published as Tolborg *et al. Green. Chem.*, 2016, 18, 3360-3369 and submitted as Elliot *et al. RSC Adv.,* 2016, *in press*.

Chapter 6 describes the importance of choosing the appropriate stannosilicate framework for the conversion of small sugars. Due to the smaller pore openings of Sn-MFI, this catalyst is shown to selectively form tetrose sugars from glycolaldehyde. Using stannosilicates with larger pores (such as Sn-Beta, Sn-MCM-41 and Sn-SBA-15) are found to form or further convert the formed sugars. Additionally, the presence of alkali metal salts is shown to influence the selectivity of the reaction. The chapter is to a large part based on the work published as Tolborg *et al. ChemSusChem*, 2016, *9*, 3054-3061.

Concluding remarks and key findings across all chapters are included as **Chapter 7**.

At the end of the dissertation can be found; additional information (Figures, Tables, Schemes) used in the individual chapters (**Appendix A**), a detailed list of publications including first pages of the published articles (**Appendix B**), the front cover prepared for ChemSusChem (issue 21/2016) (**Appendix C**), conference contributions (**Appendix D**), Curriculum Vitae (**Appendix E**) and the Ph.D. Student award received at the EuropaCat XII conference (**Appendix F**). A detailed list of abbreviations used throughout the dissertation can be found in Table A.6 (chemicals) on p. 163 and Table A.7 (general) on p. 166.

2
Experimental

The conversion of biomass using heterogeneous catalysts embraces several very different disciplines within chemistry in order to fully understand the reactions taking place and how to improve them. The disciplines range from preparation and characterization of the chosen catalysts to investigating the use of these catalytically as well as analysis of the formed products. In depth knowledge of all aspects of the catalytic system ideally leads to better control of the entire process. This chapter collects the detailed descriptions of the experimental methods and techniques used in **Chapters 3 to 6**.

Few dissertations are made without the collaboration of others and the work done here is no exception. Several very skilled researchers and specialists have aided me with analyses and in the interpretation of these, enabling the acquisition of the data presented here. The different collaborators will be mentioned for the individual methods.

2.1 **Material preparation**

The synthesis and preparation of Sn-Beta can, as mentioned in **Chapter 1**, be divided into two different strategies; 1) a direct hydrothermal approach involving the mixing of a source of silica and tin as well as a structure directing agent followed by incubation in an autoclave at elevated temperatures, and 2) a post-synthesis route involving the removal of aluminum from an already commercially available Beta zeolites followed by insertion of tin in the created vacancies. Here, Sn-Beta was prepared using both methodologies. Samples prepared by the hydrothermal route will be denoted Sn-Beta (*X*, HT) throughout the report, where *X* is the nominal Si/Sn ratio of the synthesis gel. Samples prepared by the

post-treatment route will be denoted Sn-Beta (*X*, PT). This notation will be used for all metallosilicates presented in this dissertation thus representing incorporated metal, type of material, metal content and preparation method *e.g.* Zr-Beta (200, HT) is likewise a zirconium-containing zeotype with the *BEA framework prepared by hydrothermal synthesis with a Si/Zr ratio of 200. Only Sn-MFI will deviate slightly from this notation as two different hydrothermal synthesis approaches were used based on either fluoride (F^-) or hydroxide (OH^-). To differentiate the two materials these are denoted Sn-MFI (*X*, *Y*) where *X* again is the nominal metal content and *Y* is whether the synthesis was based on fluoride (F^-) or hydroxide ions (OH^-), *i.e.* Sn-MFI (100, OH^-).

It is common to refer to the concentration of active sites in the silicate material as a ratio of silicon per metal atom (Si/*M*) as used above. This fraction gives an indication of the distribution of the metal in the material and is independent of the weight of the chosen element (Sn, Zr, Ti or Al). The correlation between this ratio and the estimated weight percent theoretically present in the finished material can be seen in Table 2.1.

Table 2.1. Correlation between the nominal Si/Sn ratio and the theoretical tin content in the finished silicate material.

Nominal Si/Sn ratio (*X*)	Tin wt%
800	0.25
400	0.49
200	0.99
150	1.3
125	1.6
100	2.0
75	2.6

For all materials prepared by hydrothermal synthesis the same calcination procedure was used for the removal of carbonaceous species left from the template. Upon recovery, all samples were removed from the Teflon liner and washed with ample demineralized water, followed by drying at 80 °C overnight. To finalize the material, any residual organic template still retained within the material was removed thermally by heating the sample at 2 °C/min to 550 °C and

held at this temperature for 6 hours. All samples were stored under ambient conditions.

2.1.1 Sn-Beta by hydrothermal synthesis

The tin-containing silicate Sn-Beta is used throughout the dissertation (**Chapters 3 to 6**). The preparation of Sn-Beta (and similar materials) were done by modifying and adapting the synthesis procedure described by Corma *et al.*[14] The use of seeds in original preparation method was omitted entirely from the synthesis as the addition makes any investigation of crystal morphology difficult (an important part of **Chapter 3**). A few of the used Sn-Beta materials in **Chapter 3** were prepared by Ph.D. Student Derek D. Falcone (University of Virginia) and in **Chapter 4** by Research Scientist Christian M. Osmundsen (Haldor Topsøe A/S).

In a typical synthesis of Sn-Beta (*X,* HT), 30.6 g of tetraethyl orthosilicate (TEOS, Aldrich, 98%) was combined with 33.1 g of tetraethylammonium hydroxide (TEAOH, Sigma-Aldrich, 35% in water) under stirring for approximately 60 min, or until a single phase system was formed. The appropriate amount of tin source was dissolved in 2 mL of demineralized water and added dropwise to the solution. The tin source most often used was tin(IV) chloride pentahydrate ($SnCl_4 \cdot H_2O$, Aldrich, 98%). The mixture was then left under increasingly fasters stirring to allow evaporation of the ethanol formed from the hydrolysis of the silica source, leading to the formation of a thick, rigid gel. To conclude the synthesis, 3.1 g of hydrofluoric acid (HF, Fluka, 47-51%) diluted with 1.6 g of demineralized water was added to the gel, resulting in the immediate formation of a brittle solid. At this point the approximate gel composition was; $1.0Si{:}x Sn{:}4x Cl^-{:}0.55TEA^+{:}0.55F^-{:}7.5H_2O$ with x ranging from 0.0025 to 0.01. Using mechanical force, the sample was reduced to a homogeneous granulate powder and transferred to a Teflon liner. This liner was then sealed and placed within a stainless steel autoclave and placed at 140 °C for between 2 and 60 days, depending on the tin content.

In **Chapter 3**, replacing the conventional tin source tin(IV) chloride pentahydrate in the synthesis of Sn-Beta with alternatives was investigated. In two out of three cases this involved directly replacing the conventional tin source with either tin oxide nanoparticles (SnO_2, Aldrich, <100 nm particle size) or tin(IV) acetate ($Sn(CH_3CO_2)_4$, Aldrich). For the third alternative tin source tetraethylammonium hexafluorostannate, $(TEA)_2SnF_6$, a preparation procedure was adapted from the work by Larlus *et al.*[124] Prior to synthesis, the desired amount of tin source in the form of ammonium stannifluoride, $((NH)_4SnF_6$,

Aldrich, 99.999%) was added directly to the 33.1 g of tetraethylammonium hydroxide later used as template for the synthesis. This solution was then placed under rotation at 0.2 bar for 20 min at room temperature in a rotary evaporator to ensure the evaporation of ammonia in order for the desired tin source to form. This mixture of tin source and template was then used during synthesis with no additional tin source added. For samples prepared with small amounts of added alkali, KOH (Sigma-Aldrich, ≥85%) in the appropriate amount was dissolved in the template (TEAOH) prior to use. This template was then used following the standard protocol. Purely siliceous Beta (Si-Beta) was prepared by omitting the addition of a metal source entirely during synthesis.

In **Chapter 4 and 5** the impact of adding alkali metal salts to the structure directing agent was investigated. These alkali- and alkaline-earth containing Sn-Beta zeolites were prepared by dissolving the hydroxide of the chosen metal salt directly in the 33.1 g of tetraethylammonium hydroxide used as structure directing agent during the synthesis. The sources used were the hydroxides of lithium (LiOH, Sigma-Aldrich, ≥98%), sodium (NaOH, Sigma-Aldrich, ≥98%), potassium (KOH, Sigma-Aldrich, ≥85%), rubidium (RbOH, Aldrich, 50 wt% in water, 99.9%) and cesium (CsOH, Aldrich, 50 wt% in water, 99.9%) as well as the hydroxides of calcium ($Ca(OH)_2$, Sigma-Aldrich, ≥96%), strontium ($Sr(OH)_2 \cdot 8H_2O$, Aldrich, 95%) and barium ($Ba(OH)_2 \cdot 8H_2O$, Sigma-Aldrich, ≥98%).

For **Chapter 4 and 5**, Beta zeolites were prepared with other Lewis and Brønsted acidic elements (Al, Ti, Zr) in the materials by merely replacing the tin source with a source of other metals. For Zr-Beta and Al-Beta this was done by adding zirconyl(IV) chloride octahydrate ($ZrOCl_2 \cdot 8H_2O$, Sigma-Aldrich, 98%) or aluminum(III) chloride hexahydrate ($AlCl_3 \cdot 6H_2O$, Fluka, ≥99%) at the appropriate time during synthesis. For Ti-Beta, tetraethyl orthotitanate ($(CH_3CH_2O)_4Ti$, Aldrich) was used. This metal source first required dissolution in a mixture of hydrogen peroxide and water before being employed as metal source.

2.1.2 Sn-MFI

In **Chapter 5 and 6**, the tin-containing zeotype Sn-MFI was used. Sn-MFI was prepared following two different synthesis routes both described by Mal *et al.*[61] One involving the use of hydroxide ions as the mineralizing agent denoted Sn-MFI (OH^-) and one using fluoride ions, denoted Sn-MFI (F^-).[61] Sn-MFI (OH^-) was used in both **Chapter 5 and 6** whereas Sn-MFI (F^-) was only introduced in **Chapter 6**.

For the preparation of Sn-MFI (100, OH^-), the appropriate amount of tin(IV) chloride pentahydrate was dissolved in 5 g of demineralized water and added to 15.6 g of tetraethyl orthosilicate under stirring. After approximately 30 min, 13.4 g of tetrapropylammonium hydroxide (TPAOH, 40%, AppliChem) diluted using 13.4 g of demineralized water was added to the mixture and stirred for 1 hour. Following this, an additional 60 g of demineralized water was added to the solution and left to stir for approximately 20 h, yielding a gel with the composition; $1.0Si:0.01Sn:0.44TPA^+:0.44OH^-:34H_2O$. After completion, the solution was added to a Teflon liner, placed in an autoclave and synthesized at 160 °C for 2 days under static conditions. For the preparation of Sn-MFI (400, F^-), 5.35 g of ammonium fluoride (NH_4F, Sigma-Aldrich) was dissolved in 25 g of demineralized water. The tin source tin(IV)chloride pentahydrate was dissolved in demineralized water and added under rapid stirring. To this solution, 9.8 g of tetrapropylammonium bromide (TPABr, Sigma-Aldrich) dissolved in 56 g of demineralized water was added slowly followed by 8.6 g of fumed silica. The latter was added slowly and under vigorous stirring for 3 hours to prevent agglomeration of the silica instead of dispersion. The resulting gel composition was; $1.0Si:0.0025Sn:0.26TPA^+:1.0F^-:35H_2O$. After completion, the finalized gel was transferred to a Teflon-lined autoclave and heated to 200 ºC for 6 days.

2.1.3 Sn-MCM-41 and Sn-SBA-15

Mesoporous stannosilicates including Sn-MCM-41 and Sn-SBA-15 were likewise prepared and tested alongside the aforementioned catalysts in **Chapters 4 to 6**.

Sn-MCM-41 (*X*, HT) was synthesis following the method described by Li *et al.*[41] In a typical synthesis, 26.4 g of tetraethylammonium silicate (TMAS, Aldrich, 15-20 wt% in water, ≥99.99%) was added slowly to a premade solution of 13.0 g of hexadecyltrimethylammonium bromide (CTABr, Sigma, ≥99.0%) dissolved in 38.0 g of demineralized water. This mixture was allowed to stir for 1 h, followed by the dropwise addition of a mixture of tin(IV) chloride pentahydrate and hydrochloric acid (HCl, Sigma-Aldrich, min. 37%) in 2.1 g of water. The solution was then stirred for 1.5 hours, followed by the addition of 12.2 g of tetraethyl orthosilicate and stirring for 3 hours. This gave a gel solution with the approximate composition of $1.0Si:xSn:0.44CTABr:0.27TMA:0.08Cl^-:46H_2O$ with *x* varying between 0.005 and 0.02. The finished gel solution was then transferred to a Teflon-lined container in a stainless steel autoclave and placed in a pre-heated oven at 140 °C for 15 h.

Sn-SBA-15 (*X*, HT) was prepared following the synthesis route described by Ramaswamy *et al.*[125] In a typical synthesis, 1.0 g of hydrochloric acid (HCl, 37 wt%) in 140 g of demineralized water was added to a solution of 8.0 g of Pluronic P-123 (PEG-PPG-PEG polymer, Aldrich, M_w = ~5,800 g/mol) in 60 g of demineralized water. The solution was then stirred for 2 h. To the synthesis mixture 18.0 g of TEOS (98%, Aldrich) was added followed by tin(IV) chloride pentahydrate dissolved in 2.0 g of demineralized water. This gave a gel with the molar composition: 1.0Si:*x*Sn:0.016P123:(0.12+*x*)Cl^-:134H_2O with *x* varying from 0.005 to 0.0067. The mixture was then stirred for 24 hours at 40 °C and then transferred to a Teflon-lined autoclave and heated to 100 °C for 24 hours. The solid was recovered by filtration, washed with ample water and then calcined at 550 °C for 6 hours.

2.1.4 **Sn-Beta prepared by post-synthesis**

Sn-Beta prepared by the post-treatment methodology denoted Sn-Beta (PT) was used alongside Sn-Beta in **Chapters 4 and 5**. In both chapters the materials were prepared by either Research Scientist Irantzu Sádaba (Haldor Topsøe A/S) or Research Technician Mette Rams (Haldor Topsøe A/S). Sn-Beta (*X*, PT) was prepared by the post-synthesis methodology was made by modifying the procedure described by Hammond *et al.*[53] In a typical preparation, a commercial Beta zeolite (Zeolyst, Si/Al = 12.5, NH_4^+-form) was calcined at 550 °C for 6 hours to remove the ammonia counter ion and instead give the H^+-form. This sample then underwent dealumination at 80 °C for 12 hours by exposing it to concentrated nitric acid (HNO_3, Sigma-Aldrich, ≥65%) in quantities of 10 g of acid per gram of zeolite powder. The dealuminated solid was recovered, washed with ample water and calcined at similar conditions just described for the samples prepared by hydrothermal synthesis. Following calcination, the prepared sample was then impregnated by incipient wetness methodology with a Si/Sn ratio of 125. For this purpose, tin(II) chloride (0.128 g, Sigma-Aldrich, 98%) was dissolved in demineralized water (5.75 mL) and added to 5 g of the solid. After the impregnation process, the sample was dried at 110 °C for 12 h and calcined again at the conditions mentioned previously.

2.2 Materials characterization

2.2.1 Powder X-ray diffraction

Powder X-ray diffraction (XRD) is a fast analysis method with which information regarding bulk sample composition, crystallinity and purity can be investigated. By measuring the sample using a beam of known wavelength at different angles, a pattern can be produced which can either be compared to the library of already known compounds or can undergo Rietveld refinement. The latter can both be used to identify previously unknown crystal structures but was here used especially for the evaluation of crystallinity. This was done in particular for **Chapter 3** and was performed by Principal Research Scientist Lars F. Lundegaard (Haldor Topsøe A/S). For the measurement for this dissertation, XRD patterns of the calcined samples were done on an X'Pert diffractometer (Philips) using Cu-Kα radiation (5°-70° 2θ). The estimated crystallinities of the prepared samples were calculated using the TOPAS software following the 'Partial or no known crystal structure' method (PONCKS) described by Scarlett and Madsen.[126] This approach used to evaluate the crystallinity of the samples involves the Rietveld refining both the crystalline and the amorphous contribution in the sample, leading to a fully resolved X-ray diffractogram. Comparing the obtained ratio against mixtures of crystalline and amorphous samples, it is then possible to relate the individual contributions as an evaluation of percentwise crystallinity. For non-crystalline samples such as the ordered amorphous stannosilicates, low-angle XRD was performed. For these materials, diffraction occurs not from the crystal lattices but instead from the hexagonal ordering of the material, but requires the incident X-ray radiation to be done a low incident angles (0°-5° 2θ).

2.2.2 Elemental analysis

In this dissertation, small amounts of metals are either introduced into silicate materials as the active component (*e.g.* tin, zirconium, titanium) or added to the material to aid crystallization or promote activity (*e.g.* potassium, sodium). In both cases, the information of whether these elements are successfully introduced into the material is valuable to evaluate any resulting catalytic results obtained with these samples. Although it is not possible to distinguish between framework or extraframework species using inductively coupled plasma optical emission spectroscopy (ICP-OES), the technique still allows for the quantification of elements in the bulk material. The analyses were done in collaboration with

Principal Research Scientist Lars F. Østergaard (Haldor Topsøe A/S). By dissolving the solid in a mixture of acids, the resulting liquid can be nebulized and vaporized as it is introduced into an inductively coupled argon plasma reaching temperatures of around 9,000 K. These high temperatures cause the immediate reduction of the sample into atoms and ions, detectable and quantifiable by spectroscopy measuring the element specific wavelength and the intensity of these. In a typical analysis, the silicate materials were first dissolved in a mixture of HF, HCl, HNO_3 and H_3PO_4. Due to the use of HF to ensure dissolution of the silica framework, $B(OH)_3$ is added to neutralize any excess of the highly corrosive acid. The resulting solution was then measured on a Perkin Elmer model Optima 3000 (Varian Vista) and the resulting spectra were compared against calibrations of the investigated elements.

2.2.3 Pore and surface measurements

Adsorption/desorption isotherms are used extensively to investigate the physical properties such as surface area and pore volume of porous materials. The technique takes advantage of the interaction between a well-defined sorbate such as nitrogen or argon and the internal volume of the measured sample. Surface area and pore volume measurements were here performed in collaboration with Laboratory Technician Hale Yasin using multipoint N_2 adsorption/desorption on an Autosorb automatic surface area and pore size analyzer (Quantachrome Instruments). Typically, around 10-15 mg of sample was placed in the cylindrical glass vessel, degassed overnight and exposed to nitrogen at 77 K. The total surface area of the samples was obtained using the Brunauer–Emmett–Teller (BET) method and the micropore volume was calculated by the *t*-plot method using the Autosorb3 software.

2.2.4 Electron microscopy

Electron microscopy is an analytical technique that takes advantage of the physical interaction between an accelerated beam of electrons that is directed onto a specimen. Upon interaction with the sample, the electrons undergo either elastic or inelastic scattering resulting in a variety of signals that can be used for analysis of different aspects of the sample. These include backscattered, secondary and Auger electrons as well as element specific X-rays to name a few. The different types of signals can be used to obtain either detailed information about the morphology of the materials through imaging or composition of the sample by analyzing the emitted radiation. Electron microscopy was used extensively in

Chapter 3 to investigate the prepared sample. These measurements were performed in collaboration with Research Scientist Anna Katerinopoulou (Haldor Topsøe A/S). Preparation of transections of Sn-Beta (HT) was done by former Research Technician Anne-Mette Heie Kjær (Haldor Topsøe A/S). Secondary electron (SE) and backscattered electron (BSE) images were analyzed on a XL30 field emission scanning electron microscope (FEI). Due to the nonconductive nature of the high silica samples used throughout this project, the samples were coated with Pt/Pd or Au to avoid charging effects. Element maps of cross sections of Sn-Beta (HT) were obtained using a JXA-8530F field emission electron probe micro analyzer (JEOL) operated at 10 kV and 7 nA. For these experiments, a sample of crystals were mounted in a drop of epoxy and polished to expose cross sections through the grains. The surface of the mounts was carbon coated prior to analysis. The elemental maps were composed by beam rastering across the transection of the crystal at low dwell times due to material instability under the electron beam. As a result, maps were collected using several accumulations and combined. Beam tracking was applied to avoid lateral drift, which would affect the spatial resolution. Characteristic X-rays were analyzed on a TAP crystal for silicon and PETH crystal for tin. The ZAF procedure was used as implemented in the JEOL software using SiO_2 and $CaSiO_3$ as primary and secondary standard for silicon, respectively, as well as metallic tin for occurrence of tin in the sample.

2.2.5 Ultraviolet–visible spectroscopy

Ultraviolet-visivle (UV-Vis) spectroscopy is often as a fast way to evaluate the nature of tin in the prepared stannosilicates as different absorption profiles have been shown for samples with tin primarily incorporated in the framework and material containing extra-framework species. For **Chapter 5** the UV-Vis reflectance spectroscopy was performed on a DH-2000-BAL balanced deuterium, halogen light source (Ocean Optics). The obtained measurements were converted using the Kubelka-Munk equation, where R is the absolute reflectance of the measured sample; $f(R)=(1-R)^2/(2R)$.

2.2.6 Thermogravimetric analysis

Information about carbonaceous residue left in the porous sample after catalytic reaction performed for **Chapter 6** was investigated using thermogravimetric analysis (TG/DSC). This analysis was performed on a TGA/DSC-1 (Mettler-Toledo) with an attached mass spectrometer. A small

quantity of sample (~50 mg) was heated first to 150 °C at 5 °C/min and held for 2 hours to allow confined water to evaporate from the porous sample. Following this initial weight loss, the sample was allowed to cool to 40 °C and then heated to 1000 °C at 5 °C/min, providing thermogravimetric (TG) and scanning differential calorimetric information about the sample. These measurements were performed in collaboration with Research Scientist Henrik Fordsman (Haldor Topsøe A/S).

2.3 Catalytic evaluation

A range of different reactions centered around the conversion of carbohydrates was used to either evaluate the activity of the prepared catalysts (**Chapter 3**), investigate the influence of cosolutes (**Chapter 4 and 5**) or study shape-selectivity (**Chapter 6**).

In **Chapter 3**, Sn-Beta samples of varying tin content are tested in the catalytic conversion of 1,3-dihydroxyacetone (DHA) to methyl lactate. Typically, 0.300 g (3.33 mmol) of DHA, 0.025 g of catalyst, and 6.5 mL of methanol were added to a 15 mL thick-walled glass reactor (ACE) and placed in a preheated oil bath at 75 °C. The vessel was then heated and vigorously stirred for 2 h, and subsequently quenched in cold water. After reaction, the resulting liquid was analyzed using a 7890A Series GC system (Agilent Technologies) with a SolGel-WAX column (Phenomenex) to quantify the ML yield.

Leaching experiments were carried out as follows; 0.025 g of Sn-Beta zeolite was treated in 6.5 mL of methanol at 75 °C for 2 h. After this time, the catalyst was filtered off and this methanol was used as the solvent for the reaction under the previous conditions.

In **Chapter 4**, catalytic conversion of sucrose to methyl lactate (ML) was performed in a 40 mL stainless steel pressure vessel (Swagelok). Typically, 0.450 g (1.3 mmol) of sucrose (Fluka, ≥99.0%), 0.150 g of catalyst, and 15 g of methanol (Sigma-Aldrich, ≥99.8%) were added to the container. The reactor was sealed and heated to 170 °C under stirring (~700 rpm) in a pre-heated oil bath. The temperature was chosen to reach an internal temperature of the vessel of 160 °C. Some experiments were instead performed in 50 mL autoclaves (Parr Instruments) using the reaction conditions and concentrations as described above, except due to internal temperature measurements, these experiments were set to 160 °C. In **Chapter 4** the experiments performed using the Parr autoclaves will state so in the figure caption. For both types of autoclaves, the reaction was quenched after 16 hours by submerging the reactor in cold water.

Reactions involving the catalytic conversion of glucose were done in exclusively in glass pressure vessels (ACE) using 0.250 g glucose, 0.100 g of catalyst and 5 g of solvent. For these experiments, the vessel was placed in a pre-heated oil bath at 120 °C and left for 19 hours under 500 rpm stirring. Upon completion, the experiments were quenched in cold water. In reactions involving alkali-containing solutions, a stock solution was made by dissolving the appropriate alkali metal salt directly in methanol. This stock solution was then used and diluted with additional methanol to achieve the desired concentration of alkali for the experiment. Alkali sources used for these experiments were lithium chloride (LiCl), cesium chloride (CsCl, Sigma-Aldrich, 99.9%) potassium acetate (CH_3COOK, Sigma-Aldrich, ≥99.0%), potassium bicarbonate ($KHCO_3$, Fluka, 99.7%), potassium bromide (KBr, Sigma-Aldrich, ≥99.0%), potassium carbonate (K_2CO_3, Sigma-Aldrich, ≥99.0%), potassium chloride (KCl, Sigma-Aldrich, 99.5-100.5%), potassium fluoride (KF, Sigma-Aldrich, ≥99.0%), potassium iodide (KI, Sigma-Aldrich, ≥99.5%) potassium lactate ($CH_3CH(OH)COOK$, Fluka, 60% in water), potassium nitrate (KNO_3, Riedel-de Haën, ≥99.%), rubidium chloride (RbCl, Aldrich, ≥99.0%) and sodium nitrate (NaCl, Sigma-Aldrich, ≥99.5%).

In **Chapter 5**, catalytic conversion of sugars was performed in a 5 mL glass microwave reaction vial (Biotage). Typically, 0.120 g (0.67 mmol) of glucose (Sigma-Aldrich, >99.0%), 0.060 g of catalyst, and 4.0 g of methanol (Sigma-Aldrich, >99.8%) were added to the reaction vial. The reactor was sealed and heated to 160 °C under stirring (600 rpm) in a microwave synthesizer (either a Biotage Initiator or a Biotage Initiator+). After 2 h, the reaction was cooled and aliquots were retrieved from the reactor vessel and filtered using a 0.22 μm syringe filter. In reactions involving alkali-containing solutions, the alkali metal source (K_2CO_3, Sigma-Aldrich, ≥99.0%) was dissolved in methanol to yield a stock solution, which was then used in combination with additional methanol to yield the desired concentration of alkali for the experiment.

In **Chapter 6**, catalytic conversion of glycolaldehyde (GA) was done by mixing 0.075 g catalyst, 0.125 g GA (dimer, Sigma-Aldrich) and 2.5 g demineralized water in a 15 mL glass pressure vial (ACE). The reaction mixture was then heated at 40-100 ºC under vigorous stirring (600 rpm) for between 10 min and 48 hours. After finishing, the reaction was quenched in cold water and filtered samples were retrieved for analysis. In reactions where alkali was added to the reaction, 0.2-1.0 g of KNO_3 (Riedel-de Haën, ≥99.%) was simply added alongside GA to the reaction vessel.

2.4 Reaction analysis

Over the course of the project, much insight has been gained into reaction pathways taking place and the products formed when converting different sugars using a Lewis acidic catalyst. This is among other things one of the main focus points of **Chapter 5**. As a consequence, the required analysis of the reaction media has grown increasingly more demanding over the years. In this section the analysis techniques used in each individual chapter will be described including high-performance liquid chromatography (HPLC), gas chromatography (GC) and nuclear magnetic resonance spectroscopy.

NMR spectroscopy was used extensively to identify and quantify products obtained from the conversion of sugars in **Chapters 5 and 6**. Measurements done for **Chapter 5 and 6** were performed and analyzed by Senior Research Scientist Sebastian Meier (Technical University of Denmark) with some parts involving analysis of xylose-derived products (**Chapter 5**) done by Ph.D. Student Samuel G. Elliot (Technical University of Denmark).

Several biomass-derived compounds obtained here using stannosilicates have already been provided with names by different research groups following varying naming conventions. In this dissertation, the names used for the different compounds will be those adopted in the research field and the corresponding abbreviations. This will be most obvious in **Chapter 5** where several old and new compounds are identified and named as they have been in their corresponding publications. A comprehensive list of relevant compounds and their corresponding abbreviations and IUPAC names is provided in Table A.6 on p. 163.

In **Chapter 3** the yield of methyl lactate (ML) was used to evaluate the activity of the prepared Sn-Beta material. The yield of ML was quantified using a 7890A Series GC system (Agilent Technologies) utilizing a SolGel-WAX column (Phenomenex) and a flame ionization detector (FID).

In **Chapter 4** a combination of HPLC and GC techniques were used to quantify the products from the conversion of a variety of sugars to methyl lactate (ML). After reaction the resulting liquid was filtered and analyzed using a 7890A Series GC system (Agilent Technologies) with a SolGel-WAX column (Phenomenex) to quantify the yields of ML. An Agilent 1200 series HPLC equipped with an Aminex HPX-87H (BioRad) column held at 65 °C equipped

with a refractive index (RI) detector was used with an eluent of 0.004 M H_2SO_4 at a flow of 0.6 mL/min to quantify unreacted sugars.

In **Chapter 5** reaction solutions were analyzed using a combination of NMR spectroscopy and chromatography. The yields of methyl lactate (ML), methyl vinyl glycolate (MVG), glycolaldehyde dimethyl acetal (GA-DMA) and methyl 4-methoxy-2-hydroxybutanoate (MMHB) were quantified using a 7890A Series GC system (Agilent Technologies) with a SolGel-WAX column (Phenomenex) and an FID. Since MMHB is not available commercially, the response factor for MVG was used to approximate the amount of the compound.

The α-hydroxy ester; *Trans*-2,5,6-trihydroxy-3-hexenoic acid methyl ester (THM) was identified and quantified using GC-MS on an Agilent 6890 with a Zebron ZB-5MS column (Phenomenex) equipped with an Agilent 5973 mass selective (MS) detector. *Trans*-2,5-dihydroxy-3-pentenoic acid methyl ester (DPM) was likewise identified using the same GC-MS system but was quantified using a GC-FID on an 7890A Series GC system (Agilent Technologies) utilizing a Zebron ZB-5 column (Phenomenex). For both compounds, no commercial sources were available. Quantification was done by purifying a sample of the product and using this for calibration. The purified sample of THM was prepared by Ph.D. Student Steffan K. Kristensen (Aarhus University) using flash column chromatography, whereas the purified sample of DPM was prepared by Ph.D. Student Samuel G. Elliot (Technical University of Denmark) using dry column vacuum chromatography with a mixture of ethyl acetate and heptane as eluent. For both samples, the purity (>90%) of the samples was evaluated by NMR spectroscopy.

For the quantification of furanic compounds, an Agilent 1200 series HPLC was used equipped with an Aminex HPX-87H (BioRad) column using an RI and diode array detector (DAD). The eluent used was a solution of 0.004 M H_2SO_4 run at 0.6 mL/min using a column temperature of 65 °C. During the reaction, any furanics present in the reaction mixture might undergo acetalization with the alcohol solvent to yield a range of furan derivatives. Under the acidic conditions of the eluent used for this column, the formed furanic acetals hydrolyze and are thus quantified as 5-(hydroxymethyl)furfural (HMF), 5-(methoxymethyl)furfural (5-MMF) and furfural (F) using standards provided by Sigma-Aldrich (HMF and F) and Manchester Organics (MMF).

Conversion of sugar as well as an estimation of formed methyl glycosides were quantified using a combination of NMR spectroscopy and HPLC analysis. For experiments involving hexoses, the remaining sugars and methyl glucosides (MG) were quantified on an Agilent 1200 series HPLC equipped with a

Carbohydrate (Zorbax) column using an eluent of 60 wt% acetonitrile/water run at 0.5 mL/min with a column temperature of 30 °C. The response factor used for the combined methylated sugar yield was based on an average of the three commercially available methyl sugars; methyl α-D-glucopyranoside (Sigma, ≥99%), methyl β-D-glucopyranoside (Sigma, ≥99%) and methyl α-D-mannopyranoside (Sigma, ≥99%). The calibration curve for the three compounds can be seen in Figure A.1. An overview of the different isomers of the methyl glycosides from glucose and mannose can be seen in Figure A.2.[127] The yield of MG was additionally verified by NMR of the reaction liquids.

For pentose sugars, 2-dimensional (2D) ^{1}H-^{13}C heteronuclear single quantum coherence (HSQC) spectra were used to quantify methyl glycosides and residual substrate. The quantification was done relative to DPM at natural ^{13}C isotopic abundance. The ^{1}H-^{13}C HSQC spectra had a ^{13}C carrier offset of 101 ppm and employed a spectra width of 22 ppm to sample the anomeric region of xylose and its methyl glycosides at high resolution and sensitivity. Samples were prepared by condensing 1 mL of the filtered reaction mixture using a SpeedVac vacuum concentrator and redissolving the resultant residue in deuterated methanol (Sigma-Aldrich, 99.96%). These spectra were recorded on a Bruker Avance III HD spectrometer equipped with a 9.4 T magnet and a Bruker CryoProbe Prodigy, sampling 1024 and 128 complex data points in the ^{1}H and ^{13}C spectral dimensions for acquisition times of 292 and 58 milliseconds, respectively. Spectra were processed with extensive zero filling in all dimensions and integrated in Topspin 3.5.

High-field NMR spectroscopy was conducted on a Bruker Avance II 800 MHz spectrometer equipped with a TCI Z-gradient CryoProbe and an 18.7 T magnet (Oxford Magnet Technology, Oxford, U.K.). Sufficiently ^{13}C resolved ^{1}H–^{13}C HSQC spectra were acquired by sampling 1024 complex data points in the direct (^{1}H) dimension and 1024 complex data points in the indirect (^{13}C) dimension during acquisition times of 143 and 93 milliseconds, respectively. All spectra were recorded at 37 °C.

For the discovery of chemicals formed in the stannosilicate-catalyzed conversion of glucose, high-field NMR spectroscopy was employed on a Bruker Avance II 800 MHz spectrometer equipped with a TCI Z-gradient CryoProbe and an 18.7 T magnet (Oxford Magnet Technology, Oxford, U.K.). For this purpose, 1 mL of reaction mixture was condensed and re-dissolved in deuterated methanol. Standard homonuclear 1-dimension (1D), 2D correlation spectroscopy (COSY) and 2D total correlation spectroscopy (TOCSY) were carried out on the sample in addition to heteronuclear ^{1}H-^{13}C heteronuclear multiple bond

correlation (HMBC) and highly ^{13}C resolved ^{1}H-^{13}C HSQC and ^{1}H-^{13}C HSQC-TOCSY spectra. All spectra were recorded at 30 °C.

The NMR quantification of identified compounds such as 3-deoxy-*γ*-lactones (DGL) in reaction mixtures was performed by addition of 10% deuterated methanol to 500 μL of reaction mixture and subsequent ^{13}C 1D NMR spectroscopy sampling 16384 complex data points during an acquisition time of 1.6 seconds and using a recycle delay of 58.4 seconds between 400 scans. One-dimensional ^{1}H NMR spectra were used to quantify 3-deoxy-γ-pentonolactones (DPL), 2,4,5-trihydroxypentanoic acid methyl ester (TPM) and 2,5-dihydroxy-4-methoxy pentanoic acid methyl ester (DMPM) relative to methyl lactate. Spectra were recorded directly on reaction mixtures in methanol after removal of catalyst and upon addition of 10% deuterated methanol. Spectra were recorded on a Bruker Avance III spectrometer equipped with a 9.4 T magnet and a BBO probe.

In **Chapter 6** filtered samples were analyzed on an Agilent 1200-series HPLC equipped with an Aminex HPX-87H (BioRad) column using an RI and DAD detector. The eluent used was a 0.004 M solution of H_2SO_4 run at 0.6 mL/min with temperature of the column held at 65 °C. Unconverted glycolaldehyde (GA), formed tetrose sugars; erythrose (ERY), threose (THR) and erythrulose (ERU) and larger hexose sugars were quantified using an RI detector. Standard solutions of the tetrose sugars were obtained from Omicron Biochemicals, Inc. The formation of larger hexose sugars was quantified using the response factor of the aldohexose; glucose and verified using NMR spectroscopy. Vinyl glycolic acid (VGA) was quantified using the DAD detector at a wavelength of 210 nm with a standard provided by Enamine (95%). α-Hydroxy-γ-butyrolactone (HBL) was tentatively quantified on HPLC using the RI detector and a standard provided by Aldrich. High-field NMR spectroscopy was conducted on a Bruker Avance II 800 MHz spectrometer equipped with a TCI Z-gradient CryoProbe and an 18.7 T magnet (Oxford Magnet Technology, Oxford, U.K.). Sufficiently ^{13}C resolved ^{1}H–^{13}C HSQC spectra were acquired by sampling 1024 complex data points in the direct (^{1}H) dimension and 1024 complex data points in the indirect (^{13}C) dimension during acquisition times of 143 and 93 ms, respectively. All spectra were recorded at 37 °C. Identification of compounds in the reaction mixture was performed by the use of pure reference standards for glycolaldehyde, tetroses and hexoses.

2.5 **Polymer preparation and characterization**

In **Chapter 5** the potential of using the *trans*-2,5-dihydroxy-3-pentenoic acid methyl ester (DPM) for polymerization. Polymer synthesis and characterization were done entirely at the Danish Polymer Center by Research Assistant Christian Andersen (DTU) and Associate Professor Anders E. Daugaard (DTU). Senior Researcher Sebastian Meier (DTU) assisted with NMR characterization of the resulting polymers. A brief description of the polymerization will be given here as well as an overview of the measurement techniques. Any further information will be found described in ref. [128].

For the co-polymerization, 0.40 g (3 mmol) of DPM, 2.0 g (13 mmol) of ethyl 6-hydroxyhexanoate (E6-HH, Sigma-Aldrich, 97%) and 0.24 g of *Candida arctica* Lipase B (CAL-B; N435, Novozymes) was added to a Schlenk tube. The mixture was placed in an oil bath under magnetic stirring at 60 °C and 200 mbar pressure for 2 hours, before being reduced to 5 mbar for another 70 h. The product was dissolved in tetrahydrofuran (Sigma-Aldrich, ≥99.9%) and filtered. The filtrate was evaporated, re-dissolved in tetrahydrofuran and precipitated in cold methanol. After refrigeration at 5 °C for 30 min and filtration, and orange solid sample of poly(E6-HH-co-DPM) was obtained.

NMR characterization of prepared polymers was performed on a 7 T Spectrospin-Bruker AC 300 MHz spectrometer at room temperature in $CDCl_3$. Assignments of NMR spectra were based on ^{1}H-^{1}H COSY and ^{1}H-^{13}C HSQC spectra. Glass transition temperatures (T_g) and melting temperatures (T_m) were obtained using a Discovery DSC (TA Instruments). Thermal analyses were performed by heating and cooling the sample from -100 to 150 °C at a rate of 10 °C/min. FTIR spectroscopy was conducted on an attenuated total reflection ATR-FTIR (Thermo iS50). Molecular weight (M_w) and dispersities (*Đ*) were determined using Size Exclusion Chromatography (SEC). SEC was performed in THF on a Viscotek GPCmax autosampler using a Viscotek TriSEC model 302 triple detector array including an RI detector, viscometer detector and light scattering detectors measuring at 90° and 7° as well as a Knauer K-2501 UV detector on two PLgel MIXED-D columns (Polymer Laboratories). The samples were run at a flow rate of 1 mL/min at 35 °C and molecular weights were determined from a PS calibration.

3
Impact of Tin on the Synthesis of Fluoride-route Sn-Beta†

Although Sn-Beta has received much attention since its discovery due to its high activity and selective in a number of important reactions, several fundamental aspects surrounding the hydrothermal synthesis of the material are still not fully understood. In the synthesis of other zeolite structures it is well-known that even small changes to the synthesis gel can result in large changes to the finished material. Changing basicity of the synthesis gel, choosing a different silica-source or structure directing agent (SDA), altering the content of water or using agitation affect zeolite crystallization behavior.[129-133] The traditional procedure for synthesizing Sn-Beta involves fluoride media at near neutral pH as described in **Chapter 1** and detailed in **Chapter 2**.[10, 14, 16, 32] The role of the mineralizing agent is to dissolve and transport silica species during the formation of the zeolite framework.[134] Since the interaction between fluor and the silica-species is strong, fluoride ions can advantageously be used as the mineralizing agent for materials difficult to prepare in basic media.[14, 22, 135] For Sn-Beta the preparation in a fluoride media results in the formation of highly defect-free materials. Since no charge imbalance is present in the zeolite when tin is introduced as mentioned in **Chapter 1**, this results in a very hydrophobic material. The fluoride route also leads to the formation of zeolites with a much larger crystal size often of several micrometers. Conversely, hydroxide route

† This chapter was adapted from Tolborg *et al. J. Mater. Chem. A* **2014**, *2*, 20252.

syntheses generally result in crystals of only a few hundred nanometers in diameter. The difference between the two syntheses is shown in **Chapter 6** where Sn-MFI is prepared by both routes. The larger crystals are formed due to the low degree of supersaturation obtained with fluoride. This limits nucleation in the preliminary steps of zeolite formation and results in the growth of fewer crystal that grow to larger sizes.[124] This also affects the crystallization time of the materials, as the time required to obtain a fully crystalline zeolite increases drastically. This can sometimes be countered by the addition of zeolite seeds to the synthesis to induce nucleation.[43, 136] This however also severely affects the crystal morphology of the sample, as the additional points of nucleation often results in intergrown zeolite crystals growing into larger agglomerates.[13] Since obtaining information about the morphological changes of Sn-Beta is part of this chapter, seeds were avoided here.

The aim of this fundamental study is to identify the effect of the presence of tin on the synthesis of Sn-Beta materials in terms of crystal morphology, crystallization time and distribution of tin in the individual crystals. Understanding the role of tin could help increase the amount of active sites which can be incorporated in the zeolite. The tin content of Sn-Beta is often kept low (Si/Sn>100) as it has been stated that incorporation retards crystallization, resulting in long crystallization times.[14, 16, 17] To investigate these parameters, the conventional fluoride-route synthesis described by Valencia *et al.* is used to obtain the larger crystals that can be analyzed by advanced spectroscopic techniques in the electron microscope.[137]

In this chapter, it is shown that the incorporation of tin during synthesis of Sn-Beta not only introduces Lewis acid sites in the zeolite material but also directly affects the growth kinetics and the morphology of the resulting crystals. Several of the reactions that Sn-Beta is known to catalyze are liquid phase reactions where diffusion limitations are expected to be an even more important factor than in gas phase reactions. The understanding and control of the crystal morphology as well as the accessibility to the active tin sites are therefore important for the activity of the catalyst. Furthermore, it will be shown that alkali ions can counter some of these effects resulting in significantly reduced crystallization times. Additionally, tin is shown to not incorporate evenly within the crystal particles, resulting in a localized tin-rich shell.

3.1 Results and discussion

3.1.1 Effect of tin on crystallization time

A series of Sn-Beta samples was prepared following the fluoride route synthesis, keeping all synthesis parameters unchanged apart from the content of tin added and the time of crystallization. Samples with varying Si/Sn ratios from 100 to 400 were synthesized and crystallized for between 2 and 60 days. The temperature during crystallization was kept constant for all samples at 140 °C. It was found initially that the use of higher temperatures favored the formation of the MFI zeolite framework. Crystallinity, amounts of tin and properties of the pore system can be seen in Table 3.1 for the samples prepared using a nominal Si/Sn ratio of 200 in the gel.

Table 3.1. Physical properties of Sn-Beta samples synthesized with a nominal Si/Sn ratio of 200.

Entry	Crystallization	Crystallinity[a]	Tin[b]	Si/Sn[b]	S_{BET}[c]	$V_{micropore}$[d]
	days	%	wt %		m^2/g	mL/g
1	2	8	0.93	211	395	0.10
2	4	52	0.90	219	422	0.14
3	5	60	0.91	217	437	0.16
4	7	>95	0.97	203	471	0.19
5	14	>95	0.96	204	473	0.19
6	30	>95	0.94	209	475	0.20

a. Determined by Rietveld refinement of XRD measurements using the PONCKS method. b. Determined by ICP analysis. c. BET surface area. d. Micropore volume, calculated using the *t*-plot method.

Crystallinity of the prepared samples was assessed using X-ray diffraction (XRD) by evaluating the obtained diffraction patterns using the 'Partial or no known crystal structure' method (PONCKS) for the Rietveld refinements.[126] This techniques evaluates both contributions from the crystalline and amorphous phase in the sample, leading to a fully resolved refinement. By comparing these contributions with fully crystalline and amorphous phases, it is possible to relate the calculated contributions as a percentage of crystalline material present in the sample.

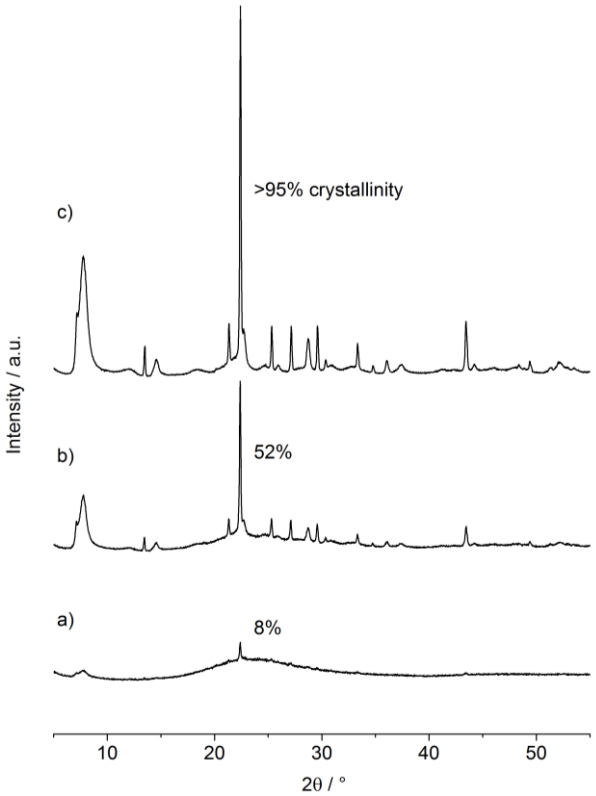

Figure 3.1. X-ray diffraction patterns of Sn-Beta samples with Si/Sn = 200 crystallized for a) 2, b) 4, and c) 7 days. The latter is representative of an X-ray diffraction pattern of a fully crystalline Sn-Beta material.

XRD diffractograms of some of the samples shown in Table 3.1 can be seen in Figure 3.1 for samples crystallized for 2, 4 and 7 days. A steady increase in crystallinity is clearly observed also seen from the calculated crystallinity increasing from 8 to >95%. A well-crystalline Sn-Beta sample is obtained after 7 days with little to no amorphous background present in the diffractogram (Figure 3.1c). Longer crystallization times (14 and 30 days) did not lead to any changes in the XRD diffractograms with the assessed crystallinity remained >95% (Table 3.1, entries 4-6). For all samples series aside from the presence of an amorphous component in the materials, no other crystalline phases were observed aside from that arising from the *BEA zeolite framework. Even at very long crystallization times and with large quantities of tin in the synthesis mixture, no formation of MFI framework structure was detected at the chosen conditions. MFI is often

found as a secondary phase when varying the synthesis conditions of Beta zeolites.[124]

The amount of tin that was recovered in the finished Sn-Beta samples was found to vary only from what was introduced during the synthesis with Si/Sn ratios ranging from 203 to 219 (Table 3.1). Almost all tin present in the gel is recovered in the finished solid. This was however also the case for samples of low crystallinity (Table 3.1, entries 1-3). In almost all samples, small tin oxide nanoparticles were visible on the surface of the zeolite crystals (Figure A.6.) The tin content in the samples is determined by elemental analysis of the zeolite dissolved in a mixture of acids. A consequence of this method is both tin successfully incorporated in the framework *and* the formed tin oxide particles counts towards the amount of recovered tin. More importantly, the presence of these particles on the surface also means that not all tin added to the synthesis gel can be assumed to be incorporated in the framework. Since tin oxide is found to be inactive in all reactions investigated in this dissertation, these particles also mean a lower number of active sites present in the catalyst. No contribution from tin oxide could be found in any of the diffractograms due to the small size of the particles. As a result, it was not possible to quantify the fraction of tin ending up as tin oxide for this study. It is likewise unknown at which stage of the synthesis these particles are formed. The particles could result from precipitated tin species that upon calcination are turned into the oxides, or the particles could simply form during the synthesis.

The properties of the pore system of the samples shown in Table 3.1 undergo similar changes as was observed from XRD. A typical Sn-Beta zeolite (200, HT) has a surface area (S_{BET}) and micropore volume ($V_{micropore}$) of 450-500 m^2/g and 0.20 mL/g, respectively.[13] These physical characteristics of Sn-Beta are caused by the channel and pore system of the zeotype material. Especially the micropore volume is only found in crystalline samples. These properties can therefore also be used as an indication of the achieved crystallinity of a samples.[45] For the mentioned Sn-Beta samples prepared with a Si/Sn ratio of 200, the total surface area increases from 395 to 471 m^2/g (Table 3.1, entries 1-4) with the increase in crystallinity from 8% to >95%. After full crystallinity is achieved, the surface area remains unchanged at ~475 m^2/g for longer crystallization times (Table 3.1, entries 4-6). The micropore volume likewise increases from 0.10 to 0.19 mL/g at the point of full crystallinity (>95%) and stay at ~0.20 mL/g beyond this point (Table 3.1, entries 1-6). The crystallinities determined by Rietveld refinement are thus supported by the surface area and pore volume measurements.

For samples with varying tin contents, the crystallinity values obtained from XRD results were plotted as a function of the crystallization time, see Figure 3.2. The hydrothermal synthesis time required to obtain Sn-Beta samples of high crystallinity (>95%) was found to vary greatly with the amount of tin added during synthesis. For samples prepared without or low amounts of tin (Si/Sn = 400), highly crystalline Beta samples could be obtained after only 4 days. When the amount of tin was increased to give a Si/Sn ratio of 200, the required crystallization time likewise increased slightly to 7 days. As a result, when the tin content was further increased to Si/Sn 150 and 100, the required synthesis time increased to 14 days and to 60 days, respectively. A similar retardation caused by the introduction of tin has previously been reported for the synthesis of Sn-MFI.[27]

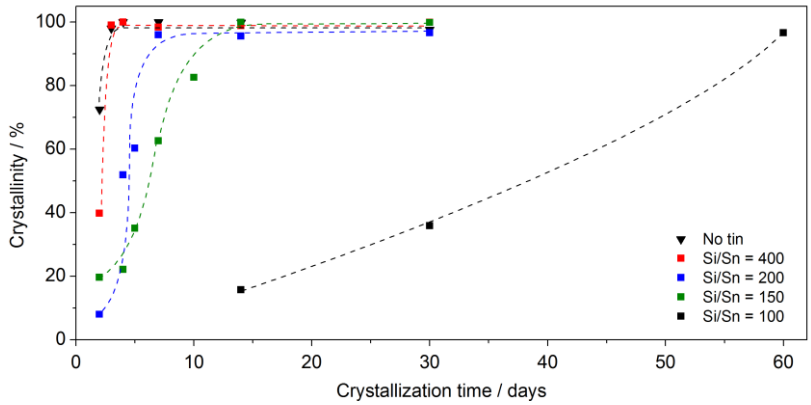

Figure 3.2. Crystallinity of Sn-Beta samples of varying hydrothermal synthesis times from 2-60 days and with Si/Sn ratios ranging from 100 to 400 and without tin. The lines are a guide to the eye.

The structural and material properties of the Sn-Beta samples at the point of high crystallinity (>95%) can be seen in Table 3.2 for the different Si/Sn ratios. Even the required crystallization time varies greatly in-between the different sample series, almost no differences in the physical properties are observed. Only the Sn-Beta sample prepared with a Si/Sn ratio of 100, synthesized for 60 days gave a slightly higher surface area than the other samples (508 m^2/g, Table 3.2, entry 5). The retardation in the synthesis caused by tin clearly shows the impracticality of preparing Sn-Beta catalysts with higher tin loadings (Si/Sn < 100) and the reason why high tin content is often avoided in this type of synthesis. The consequence of this practical limit in tin content is a lower number of active tin

sites that can be present in a Sn-Beta catalyst synthesized in a fluoride medium under these current conditions.

Table 3.2. Physical properties of Sn-Beta samples with varying tin content after obtaining full crystallinity (>95%).

Entry	Nominal Si/Sn[a]	Crystallization	Tin[b]	Si/Sn[b]	S_{BET}[c]	$V_{micropore}$[d]
		days	wt%		m^2/g	mL
1	-	4	-	-	459	0.19
2	400	4	0.42	468	464	0.19
3	200	7	0.97	202	471	0.19
4	150	14	1.24	157	470	0.20
5	100	60	1.81	107	508	0.20

a) Nominal Si/Sn ratio in the synthesis gel. b) Determined by elemental analysis (ICP). c) Total surface area of the material. d) Calculated using the *t*-plot method.

3.1.2 **Impact of tin on crystal morphology**

In order to investigate the influence of tin on the growth of the zeolite crystals and their morphology, samples of varying tin content and crystallinity was analyzed using electron microscopy. As expected for this type of material, all prepared Sn-Beta samples were found to possess the capped square bipyramidal (CSBP) morphology typical to Beta zeolites.[138] A graphical representation of this morphology can be seen in Figure 3.3f. The elongated CSBP crystal morphology of the purely siliceous Beta (Figure 3.3a) resemble what has been reported previously under comparable synthesis conditions.[139]

From the micrographs shown in Figure 3.3 of crystalline Sn-Beta samples of high crystallinity (Table 3.2), it is clear that tin has a pronounced effect on the shape and size of the morphology of the formed crystals. As the amount of tin is increased from a Si/Sn ratio of 400 to a ratio of 100 (Figure 3.3b to Figure 3.3e, respectively), the resulting morphology changes systematically. This is seen by a significant decrease in the height of the crystal and the expansion of the square base of the pyramidal morphology (Figure 3.3a-e).

The morphology of a zeolite crystal is directly determined by the relative growth rates of the different faces of the crystal.[138] If the outward growth of one of the faces is higher than the other(s), this will be witnessed as a

diminishment of this face in the crystal morphology, while the slower face of the crystal will be more pronounced. With the introduction of the tin source for the synthesis of Sn-Beta, the growth of the pyramidal (*h0l*) face relative to the pinacoidal (*00l*) face is significantly increased. This can be seen as the change from the morphology shown in Figure 3.4a to the one shown in Figure 3.4e. At very high tin content (Si/Sn = 100), the resulting crystals are almost plate-like, although the distinct shape of the CSBP morphology is still clearly visible.

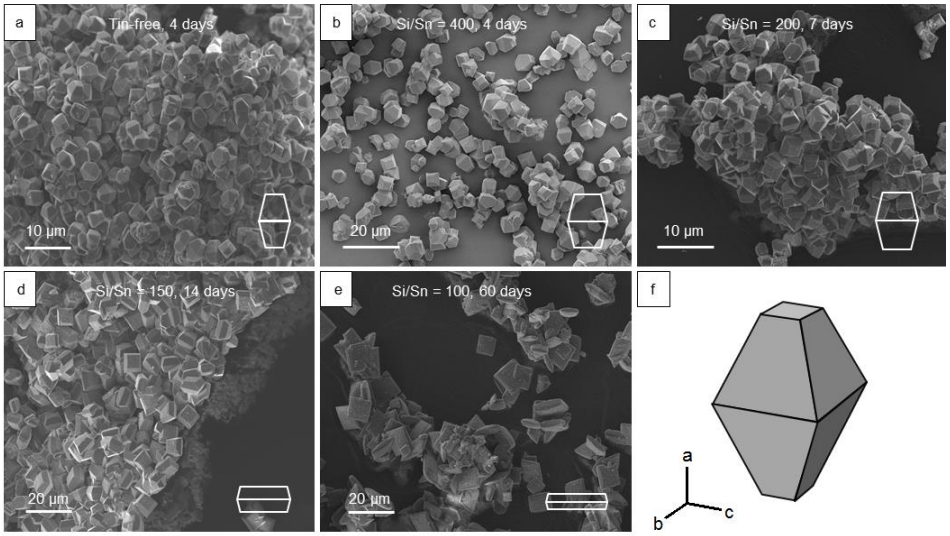

Figure 3.3. SEM imaging of Sn-Beta crystals synthesized with a Si/Sn ratio and crystallization time of a) tin-free, 4 days, b) 400, 4 days c) 200, 7 days d) 150, 14 days and e) 100, 60 days. In f) a representation of the capped bipyramidal morphology typical to Sn-Beta is shown with the a, b and c direction presented. Adapted from ref. [44].

The length of the pyramidal, *a*, and plateau, *b*, edges (represented on the crystal shown in Figure 3.5 on p. 50) has previously been used to track the changes in the morphology of crystals with the CSBP morphology.[138] Obtaining these two crystal parameters are, however, not straightforward using electron microscopy (Figure A.7). Measuring distances on images obtained from SEM can be difficult and requires the precise knowledge of the geometry between the orientation of the crystal and the detector. In the absence of this correlation and with no reference this makes measuring a height or width of a crystal inaccurate. However due to the parallelism of the two lengths *a* and *b* and their equal orientation relative to the detector, the ratio *a*/*b* of the investigated crystals can be determined far more precisely. In Table 3.3, the average approximate crystal size (as determined by electron microscopy as the length of *a*) and the ratio *a*/*b* of

the zeotype crystals are shown. Standard deviations have been included for the crystal size for reasons mentioned above and the size is primarily used to get an indication of the growth of the crystal. The sizes of the crystals were confirmed by transections used for SEM-WDS described later.

Table 3.3. Changes in the crystal size and aspect ratio (*a*/*b*) of the formed crystals. The crystal size is done as an average of a minimum of 10 crystals. Adapted from ref. [44].

Entry	Si/Sn	Crystallization	Crystal size[a]	*a*/*b*
		Days	μm	
1	-	4	3.4(7)	2.3
2	400	4	5(1)	1.7
3	200	7	4.0(7)	1.6
4	200	14	7(1)	1.5
5	200	30	11.8(9)	1.5
6	150	14	7(1)	1.4
7	100	60	8(3)	1.1

a. Crystal size measured from SEM as the length across the pyramidal base (*a*) as shown from the representation of Sn-Beta in Figure 3.5. The numbers in parentheses show the standard deviation of the measurement.

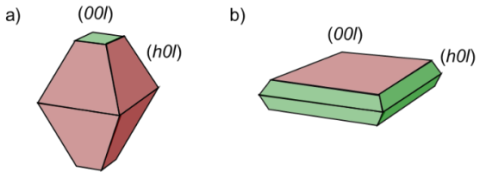

Figure 3.4. Representation of the effect of the growth rates of the individual faces on the resulting morphology shown for dominant a) pinacoidal and b) pyramidal growth rates. High growth rate is marked in green, low rate in red.

From purely siliceous Beta (Table 3.3, entry 1) to samples with a Si/Sn ratio of 100 (Table 3.3, entry 7), a steady decrease in the *a*/*b* ratio from 2.3 to 1.1 is found, see Figure 3.5. This trend suggests that there is a direct correlation between the amount of tin added during synthesis and resulting change in the morphology. Interestingly, a similar (albeit not as pronounced) change in morphology of purely siliceous Beta was found by Larlus and Valtchev in a two-step synthesis procedure involving first nucleation of the zeolite in fluoride media followed by aging in basic media.[138] It that study, they found a clear correlation between increasing

the amount of alkaline template used in the second step of the preparation and the increase in pyramidal growth. The correlation was later confirmed in a one-step synthesis similar to the one used in the current study.[140] The dependence on basicity in the system could help explain the drastic change in morphology and will discussed in more detail later.

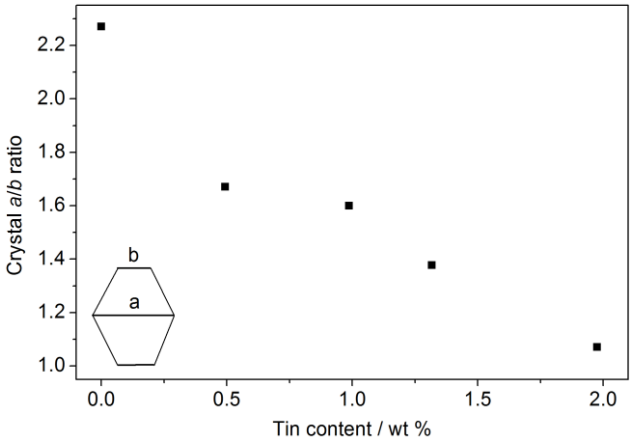

Figure 3.5. The *a*/*b* aspect ratio measured for samples of varying tin content after full crystallization (>95% crystallinity). Adapted from ref. [44].

As mentioned previously, growth rates of the individual crystal faces determine the resulting morphology of the formed crystals (as shown in Figure 3.4).[124] This suggests that the addition of tin to the synthesis mixture changes the growth of the pyramidal and pinacoidal faces, making the plateau of the crystal the dominant feature with higher tin loadings. This change in morphology could have an effect on the resulting catalytic properties as it would mean that different parts of the channel would be represented in the crystal and thus available for reactants. Any changes to the activity or selectivity of the materials caused by this effect were however not possible to separate from the additional active tin sites present when increasing tin content.

It is important to note that although no change is observed for the physical properties of the zeolite samples after full crystallinity is reached, the crystals were found to undergo Ostwald ripening. In this process smaller crystals are continuously during synthesis dissolved and redeposited onto larger ones, resulting in an overall increase in the average crystal size of the sample.[141, 142] Ostwald ripening can occur even after a fully crystalline material has been obtained and was also observed here for Sn-Beta. In Table 3.3 entries 3-5, the Ostwald ripening effect can be seen from the increase in crystal size observed for samples with a Si/Sn ratio of 200. After 7 days samples prepared with this amount

of tin are fully crystalline and have an average crystal size of ~4 μm (Table 3.3, entry 3). Upon further crystallization for up to 14 and 30 days, the size of the particles increased to ~7 μm and then to ~12 μm, respectively (Table 3.3, entries 4-5). This restructuring could have an impact on the catalytic activity of the material, not only due to diffusion limitations introduced with larger crystals but also caused by changes in the environment of tin. One consequence of this continued crystal growth could be an increased formation of inactive tin oxide species, although this was not confirmed in this study. Although the crystals increased roughly three-fold in size for the samples shown in Table 3.3, the measured *a*/*b* ratio of the formed crystals remained constant at ~1.6. This shows that although crystal growth continues with longer synthesis time, ripening does not affect the morphology. The morphology is thus dictated by the tin content and not the time of crystallization.

3.1.3 Internal crystal composition

The morphology of the samples is very important with respect to catalyst activity,[143] but the distribution of tin in the zeolite crystal could have an even greater importance. To investigate the incorporation of tin in the crystals, transverse cuts of the samples of various tin contents and synthesis times were prepared and investigated by SEM with a wavelength-dispersive spectrometer (SEM-WDS). Interestingly, for a number of transverse cuts of the array of Sn-Beta crystals, lines protruding from the center towards the corners were observed, see Figure 3.6a. This is known as the '*hourglass phenomenon*' and is believed to be caused by the continuous incorporation of defects during the crystal growth, where the crystal faces meet found for several other types of zeolite.[144, 145]

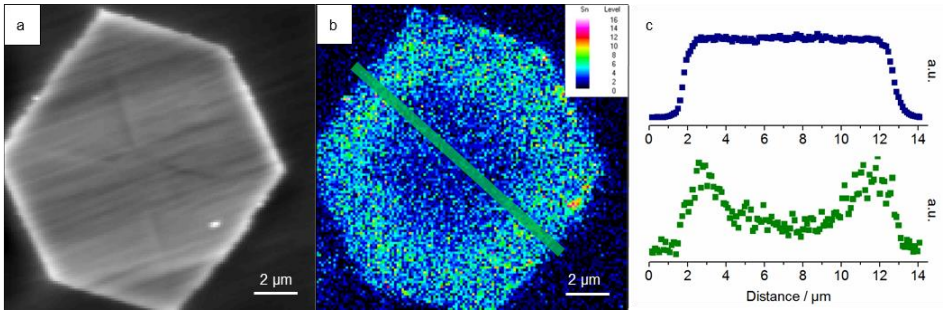

Figure 3.6. WDS analysis of a Sn-Beta sample (Si/Sn = 200) crystallized for 30 days showing a) SE image of the investigated crystal, b) Sn X-ray intensity, and c) X-ray intensities for Si (*blue*) and Sn (*green*). The data for c) were extracted from the map at

the area indicated by the green outline on b) and averaged across the thickness of the line. Adapted from ref. [44].

Using SEM-WDS, it was possible to select and accurately map the elemental composition of the chosen crystal transections. In all cases where the CSBP morphology was clearly visible as a symmetrical hexagonal geometry (Figure 3.6a), a clear gradient was observed in the distribution of tin in the zeolite crystal. In Figure 3.6 this is shown for a sample crystallized for 30 days with a Si/Sn ratio of 200 showing both the tin gradient (Figure 3.6b) and a plot of the X-ray intensity acquired for Si and Sn across the transection (Figure 3.6c). For silicon the latter shows a constant concentration throughout the crystal, but for tin a clear decrease in metal content can be seen towards the center of the crystal. After acquisition of the maps, the signal on each pixel was processed. A fixed background was subtracted and full ZAF standard-based correction routine was applied. The latter procedure involves correlating the measured 'counts' of silicon and tin in the sample computationally against reference sample containing these elements in known amounts, correction for atomic number (Z), absorbance (A) and fluorescence (F), leading to quantitative results. Due to the large difference between the acquisition time of calibration intensities and the dwell time of mapping, the quantitative results can only show a relative difference in concentrations rather than absolute mass concentrations. Applying this technique to the measurement shown in Figure 3.6b, it was found that the rim contained approximately twice as much tin compared to the center.

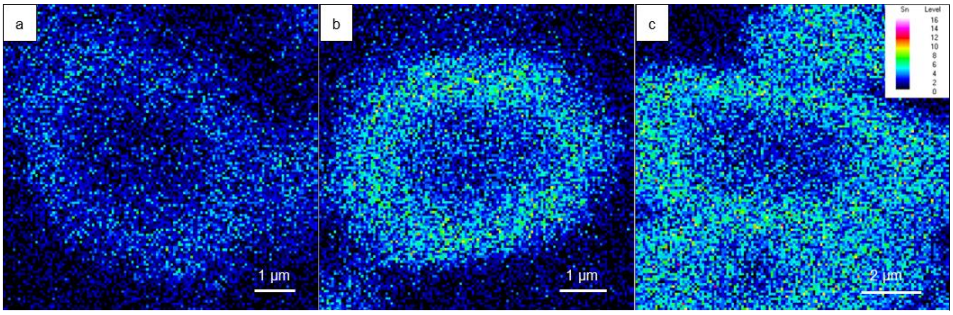

Figure 3.7. SEM-WDS measurements showing the tin distribution in transverse sections of Sn-Beta zeolites with Si/Sn ratios of a) 400 (crystallized for 4 days), b) 200 (7 days) and c) 100 (60 days). Adapted from ref. [44].

The enriched outer shell of tin was found for all prepared Sn-Beta materials with varying tin content, irrespective of the resulting morphological changes and the size of the formed crystals. Figure 3.7 shows the tin distribution in Sn-Beta crystals with Si/Sn ratios of 400, 200, and 100, respectively. All analyses show the

same decrease in tin concentration towards the center of the zeolite crystal with a thickness of the shell varying from 1-2 μm. This shows that tin is primarily found as a shell with a thickness corresponding to roughly half the distance along the center of the crystal independent of the amount of tin incorporated in the material. The tin distribution was also found in transection before and after calcination showing that it is not caused by a thermal redistribution (Figure A.8). The occurrence of zoning of aluminum within synthesized crystals of ZSM-5 (with the MFI framework) is a well-known phenomenon.[146-148] Despite being shown for the first time in 1981, the occurrence is still not fully understood with explanations ranging the redistribution of aluminum during synthesis to deposition of aluminum during cooling.[148] The gradient in the tin distribution within the bulk crystal has to our knowledge not previously been observed for tin-containing zeolites.

3.1.4 **Ostwald ripening effects**

Since a continued growth of the zeolite crystals was observed with longer synthesis times, presumably due to Ostwald ripening effects, it was important to investigate the evolution of this outer layer of tin within the crystal over time. Samples of different crystallization times from 4 to 30 days and Si/Sn = 200 (Table 3.3, entries 3-6 on p. 49) were investigated. As described earlier, a significant difference in crystal size was measured for this sample series with crystal size increasing from 4 to 12 μm over time. Investigating these samples using SEM-WDS, it was discovered that the enriched tin layer described above likewise changes in thickness as the crystals grow. This is especially clear from the two transections shown in Figure 3.8 crystallized for 7 and 30 days. After 7 days the crystal size is 4 μm with the enriched tin shell having a thickness of roughly 1-2 μm (Figure 3.8a), thus corresponding to roughly half the crystal radius. For the very large crystals (12 μm) obtained after 30 days the shell was found to have a shell thickness of 3-3.5 μm (Figure 3.8b). Although this crystal has increased substantially in size with the increased crystallization time, the tin shell is still found to correspond to roughly half the radial distance. This means that the internal void with low tin concentration likewise must have grown in size as the zeolite grew. A consequence of these findings is that tin to some extent must have redistributed during crystallization. This is corroborated by the fact that the tin shell was found in all samples, and the shell was also observed in samples of low crystallinity containing only semi-crystalline crystal shapes. This shows that the tin gradient is already present in the crystal at the earliest stages of the synthesis. This is surprising as one would expect growth from nucleation to crystal formation to

occur radially. The difference in tin concentration in the crystal would then be a result of a late incorporation of tin during the synthesis. The fact that tin is already incorporated in what later becomes the catalyst crystals at such early stages, hints that tin is incorporated as part of the '*solid-phase transformation process*', where the T-O-T bonds within the solid are continuously formed and broken initially to form the crystalline solid from the amorphous phase and later to mediate the further growth brought on by Ostwald ripening between crystals.[149]

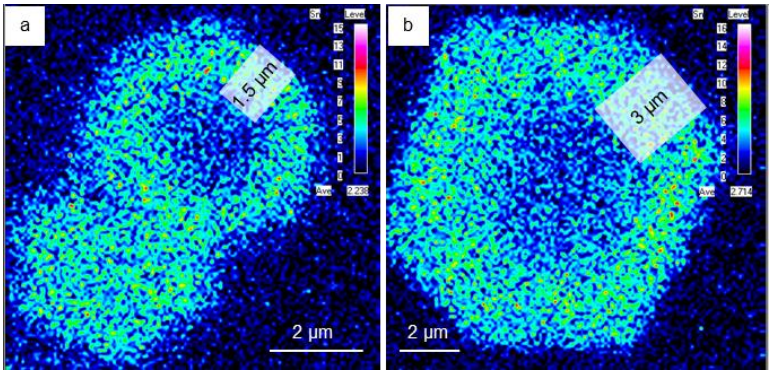

Figure 3.8. SEM-WDS measurements showing the tin X-ray intensity in transverse sections of Sn-Beta (200, HT) samples synthesized for a) 7 days and b) 30 days. The approximate thickness of the enriched outer shell has been overlaid in white.

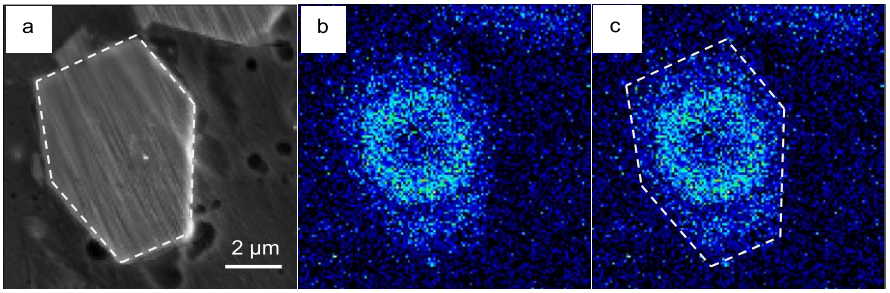

Figure 3.9. SEM and SEM-WDS measurements showing a) micrograph, b) tin X-ray intensity, c) Sn X-ray intensity with an overlay of the size and shape of the crystal from (a) of transverse sections of a zeolite synthesized by regrowing a sample of uncalcined Sn-Beta (200, HT) in a purely siliceous gel.

To further investigate the occurrence of redistribution of tin during the hydrothermal synthesis, a Sn-Beta sample with a Si/Sn ratio of 200 was prepared and allowed to crystallize for 7 days, producing fully crystalline Sn-Beta crystals with a diameter of ~4 µm (Table 3.3, entry 3). Upon recovery of the finished crystals, the sample was washed thoroughly but not calcined. This sample was then used as seeds (50% of the total silica content of the synthesis) in an otherwise

purely siliceous gel and crystallized for another 7 days to ensure high crystallinity. Figure 3.9 shows the SEM-WDS results obtained for the finished material. The Sn-Beta crystals used as seeds have a crystal size of ~4 μm, identical to those described in Table 3.3, entry 3. As it can be seen from the micrograph in Figure 3.9a, the seeds have clearly continued to grow in the siliceous gel, leading to the formation of larger crystals (diameter of 7-8 μm). Additionally, looking at the distribution of tin within the crystal, it can be seen that not only has the crystal continued to grow, it appears to also have fully incorporated the initial Sn-Beta seed within its core. As a result, the zoning of tin is still clearly visible in the center of the crystal, but now the majority of the tin concentration can be found a distance of 1-2 μm within the crystal (Figure 3.9b). Interestingly, although the second synthesis step was done using a purely siliceous gel, the hexagonal morphology of the resulting crystal can still be discerned from the Sn map alone (an overlay of the shape and size of the investigated crystal can be seen on Figure 3.9a and c). This indicates that some tin from the initial seed has indeed been dissolved and reinserted under hydrothermal conditions leading to a redistribution of tin as the larger zeolite crystals are formed. Compared with the initial shell, the amount of tin found in the outer layer is small and more experiments are required to conclude whether extensive redistribution of tin occurs.

3.1.5 Other synthesis parameters

The basicity of the synthesis mixture has as mentioned earlier been shown to result in similar changes to the morphology of Si-Beta under conditions similar to the ones used here as mentioned previously.[138, 140, 150] The change was introduced primarily by increasing the template content relative to the silica source. In an analogous manner, it was investigated whether the synthesis used in this study was influenced by the same parameters. Two purely siliceous Beta samples were prepared by changing the ratio of template to silicon (TEA/SiO_2) source from 0.55 to 0.44, 0.61 and 0.71, letting the samples crystallize for 7 days (micrographs are available in Figure A.9). Although both samples prepared with increased template content (TEA/SiO_2 = 0.61-0.71) largely led to a partly amorphous sample, the formed crystals did appear to undergo a similar change in morphology as seen for Sn-Beta. Lowering the template content (TEA/SiO_2 = 0.44) resulted in a fully crystalline sample, but with a much larger perceived size distribution of the sample but with no discernible change in morphology. In the case of Sn-Beta, the change in morphology occurring is induced by introducing an acidic component; tin(IV) chloride pentahydrate, thereby lowering the basicity of the system slightly. In order to prove that the reason for the change in

morphology was not due to formation of HCl from using $SnCl_4 \cdot 5H_2O$ as the tin source, HCl was added instead of the tin source in amounts equivalent to what would form *in-situ* from hydrolysis of the salt.[116] Again, no obvious change in morphology was found. Interestingly, when adding the tin source during synthesis a white precipitate is often observed slowly dissolving under stirring after several hours. This was assumed to be the precipitation of tin species formed upon reaction with the gel caused by its low solubility, but the same effect was observed from adding hydrochloric acid, making it clear that the *in-situ* formation of HCl from the tin source briefly solidifies parts of the gel upon addition.

Table 3.4. Sn-Beta samples (Si/Sn = 150) prepared with different tin sources synthesized at hydrothermal conditions for 14 days.

Entry	Tin source	Si/Sn[a]	S_{BET}[b]	$V_{micropore}$[c]	Crystal size[d]	*a*/*b*
			m^2/g	mL/g	μm	
1	$SnCl_4 \cdot 5H_2O$	159	470	0.20	7(1)	1.4
2	$Sn(CH_3CO_2)_4$	295	468	0.18	8(2)	1.3
3	$(TEA)_2SnF_6$[e]	165	478	0.19	10(2)	1.4
4	SnO_2[f]	177	456	0.19	6.6(9)	1.6

a) Determined by elemental analysis. b) Total surface area. c) micropore volume calculated using the *t*-plot method. d) Crystal size measured from SEM as the length across the pyramidal base. e) Prepared by adding $(NH_4)_2SnF_6$ to TEAOH under stirring allowing NH_3 to evaporate. f) SnO_2 particles < 100 nm.

To further investigate the impact of the tin salt on the resulting materials, Sn-Beta samples with a Si/Sn ratio of 150 were prepared using different tin sources and crystallized for 14 days. The metal sources used were tin(IV) oxide nanoparticles (SnO_2, <100 nm), tin(IV) acetate ($Sn(CH_3CO_2)_4$) and tetraethylammonium hexafluorostannate ($(TEA)_2SnF_6$). The latter was prepared from commercially available $(NH_4)_2SnF_6$ following a similar procedure described by Larlus *et al.* for the preparation of $(TEA)_2SiF_6$.[124] Tin(IV) oxide is insoluble in the synthesis gel creating instead a suspension of nanoparticles, tin(IV) acetate eliminates the presence of chloride ions, and the use of $(TEA)_2SnF_6$ allows the synthesis to proceed without introducing any additional anions. Aside from changing the tin source, all other parameters were kept constant. Micrographs and physical properties for these samples can be found in Table 3.4 and Figure 3.10.

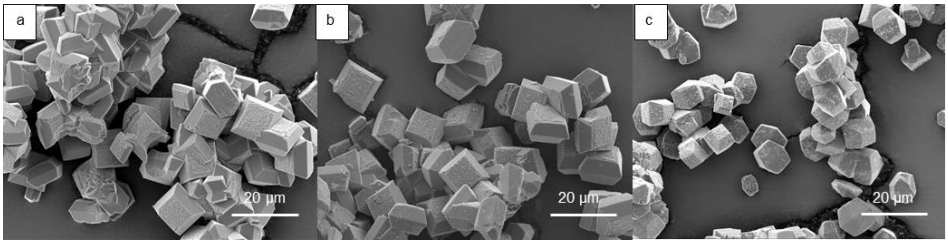

Figure 3.10. SEM images of Sn-Beta samples crystallized for 14 days using a) tin(IV) acetate, b) $(TEA)_2SnF_6$ and c) SnO_2 (<100 nm) as the tin source. Adapted from ref. [44].

When SnO_2 nanoparticles were used as tin source, the resulting crystals portrayed the more elongated morphology (Figure 3.10c), leading to an a/b ratio of 1.6 (Table 3.4, entry 4), comparable in appearance to samples prepared in absence of tin (Figure 3.3a). For this sample, we believe that no tin is incorporated in the zeolite framework due to the insolubility of the tin source. From the elemental map shown of a transection of this sample in Figure 3.11, very little tin is found to be contained within the crystal (Figure 3.11c). Instead highly localized tin concentrations were found on the surface of the crystals (Figure 3.11a and c). The surface of the crystals from this sample was covered with small particles found to be SnO_2. As a result, when tin is not incorporated in the framework, no enriched tin shell or change in morphology are observed.

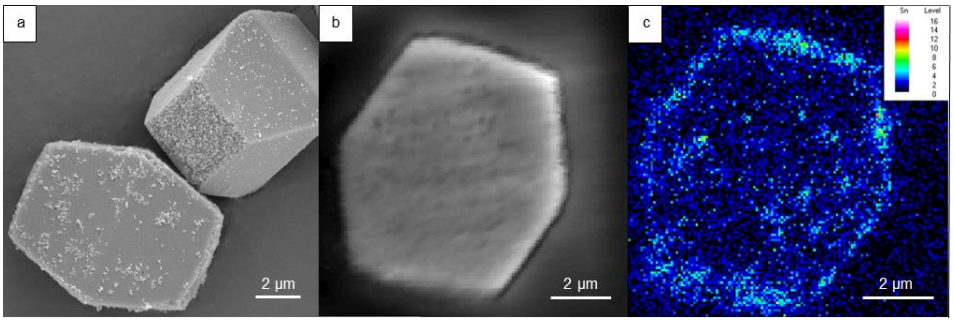

Figure 3.11. a) SEM image of Sn-Beta crystals prepared using SnO_2 as tin source, b) SE image of the transected SnO_2-Beta crystal and c) the X-ray intensities of tin of b). Adapted from ref. [44].

Using both tin(IV) acetate and $(TEA)_2SnF_6$ (Figure 3.10a-b) as the tin source yielded highly crystalline, truncated crystals with very similar morphological appearance (a/b ~ 1.4) to a comparable sample prepared using tin(IV) chloride (Table 3.4, entries 1-3). As a result, it can be ruled out that the change in morphology is related to the anion of the alkali source used. Although tin

gradients could be found both for Sn-Beta samples prepared using tin(IV) acetate (Figure 3.12a) and $(TEA)_2SnF_6$ (Figure 3.12b), it is clear that using the former lead to an even greater heterogeneity in the distribution of tin with much of the tin found near the surface of the crystal. This could indicate large amounts of formed tin oxide deposited on the surface of the crystals, comparable to the what was observed for SnO_2-Beta (Figure 3.11c). However, unlike SnO_2-Beta where the tin oxide nanoparticles were clearly visible in micrographs of the crystals (Figure 3.11c), no visible particles were found in Sn-Beta prepared using tin(IV) acetate (Figure 3.10a) aside from the small amounts found for all samples. Whether this then means that the tin is then instead incorporated in the zeolite framework within the first micrometer requires more investigation.

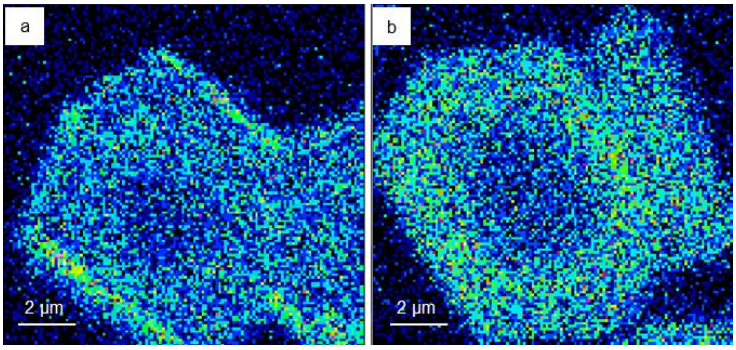

Figure 3.12. SEM-WDS measurements showing the tin X-ray intensity of transections of Sn-Beta (150, HT) samples prepared using a) tin(IV) acetate and b) $(TEA)_2SnF_6$ as the source of tin.

It is important to note that albeit the physical properties (surface area, micropore volume, crystal size and morphology, Table 3.4, entries 1-3) are comparable for all three samples, the amount of tin found confined within the zeolites varied greatly in the finished materials (Si/Sn = 159-295). This could indicate that the morphological change is caused by the presence of soluble tin ions in the synthesis gel, changing conditions of the growth of the zeolite, and not the incorporation of tin itself as more metal is added. Changes in the synthesis conditions can have a large impact on the resulting crystals; the aforementioned heterogeneous distribution of aluminum in ZSM-5 was for instance less pronounced when a different template was used.[146, 151]

3.1.6 **Countering retardation by addition of cosolutes**

The morphological change from elongated CSBP to plate-like particles appears to be related to the tin species present in the gel during the growth of the

zeolite, a synthesis component difficult to omit in the preparation of Sn-Beta. An alternative approach could be to post-functionalize tin into sites prepared by dealumination of an aluminum-containing zeolite, an approach being utilized by several groups (including our own) as an alternative synthesis method for Sn-Beta.[37, 50, 51, 56, 59] For the current study an alternative approach was used, attempting to counter the retardation and morphology changes caused by tin.

Alkali ions are known to be of great importance in the preparation of a variety of zeolites. As mentioned in **Chapter 1**, general consensus is that alkali metal ions must be avoided when synthesizing Ti- and Sn-containing zeotype materials, due to the formation of highly charged octahedral species, $[M^{4+}O_{6/2}]^{2-}$, essentially unable to incorporate within the zeolite framework unlike the tetrahedral equivalents, $[M^{4+}O_{4/2}]^{0}$.[152] As a result, when TS-1, Ti-Beta and Sn-MFI zeotype materials were synthesized in the presence of alkali metal ions both crystallization,[21, 82-84] and the catalytic activity were negatively influenced.[86-88] The addition of small amounts of alkali hydroxide (Na, K, Li) has however recently been shown to be a pre-requisite in the fluoride-free synthesis procedure develop by the group of Fan.[49] Similarly, we early got indications from samples prepared with small amounts of alkali metal impurities that the picture was more nuanced for Sn-Beta and positive effects could be achieved by stringent control of the alkali content.

In order to study, the impact of alkali metal salts on the crystallization of Sn-Beta, small amounts of alkali (here primarily KOH) was dissolved directly in the template solution and used for the synthesis of Sn-Beta. The base was added relative to the tin content in a molar ratio (M/Sn) ranging from 1 to 8. As it was described above, Sn-Beta with a Si/Sn ratio of 150 required ~14 days to obtain full crystallinity (Figure 3.13a-b). It was found that by adding small amounts of alkali during synthesis (M/Sn ~ 6) it was possible to reduce the crystallization time and obtain samples with comparable crystallinity after only 2 days (Figure 3.13c).

In a similar manner, a sample with a nominal Si/Sn ratio of 100 could be obtained after only 10 days (not shown), down from 60 days. Since the limitation in going beyond a tin content of ~2 wt% (Si/Sn = 100) is mainly due to the long crystallization times, we saw the introduction of alkali as a possibility for the synthesis of Sn-Beta samples with even higher levels of tin. With a Si/Sn ratio of 75, equivalent to 2.6 wt% tin in the materials, a theoretical synthesis time with the conditions used previously would be >150 days (assuming exponential increase in crystallization with tin content). A series of samples with nominal Si/Sn ratio of 75 was synthesized for only 7 days, varying the M/Sn ratio from 1 to 5.

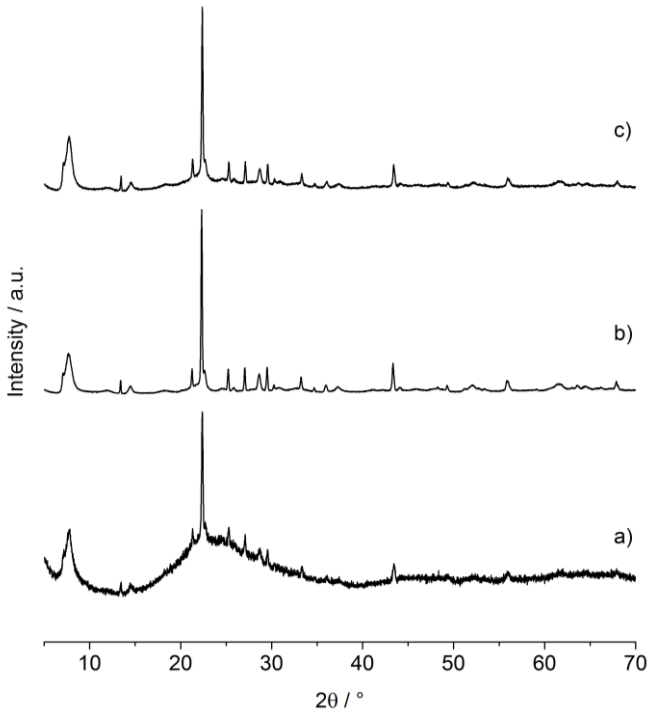

Figure 3.13. X-ray diffraction patterns of Sn-Beta zeolites prepared without (a-b) and with (c-d) alkali added during synthesis. The samples were Si/Sn ratio and synthesis time of the samples were a) 150, 2 days, b) 150, 14 days, and c) 150, 2 days with alkali added K/Sn ~ 6.

Figure 3.14 shows the crystallinity of the obtained samples versus the added alkali as well as a micrograph of the sample prepared with a *M*/Sn ratio of 2. It is quite clear that a large increase in crystallinity after 7 days is achieved by increasing the *M*/Sn ratio in the gel from 1 to 2, for higher *M*/Sn ratios, samples appear largely unaffected (according to XRD, Figure 3.14). For all crystalline samples irrespective of the tin loading, crystallinity higher than ~80% could not be achieved, presumably caused by the more alkaline conditions leading to desilication of the formed crystals (visible on Figure 3.15a).[153] This was also observed visually as the formed crystals were often etched across the surface and in some cases higher tin content was measured in the obtained solid than was present in the gel. This effect grew more pronounced with longer crystallization times (Figure 3.15a).

From both Figure 3.14 and Figure 3.15a it can be seen that the morphology of the samples likewise changed with the introduction of alkali. The Sn-Beta sample shown in Figure 3.15 synthesized for 21 days using a Si/Sn ratio of 75 and

a K/Sn ratio of 3 was found to be yield morphology with a/b = 1.4. Instead of obtaining plate-like crystals (a/b = 1.1) obtained for samples with Si/Sn = 100, the morphology more resembled samples synthesized with nominal Si/Sn ratios of 200 or 150 (a/b ~ 1.5). In earlier studies with purely siliceous Beta, Larlus *et al.* found that although an increase in amount of alkaline template used during synthesis resulted in changes to the morphology, adding similar amounts of NaOH only resulting in the formation of larger crystals.[138] For the synthesis of TS-1 (titanium-containing MFI zeotype) ammonium salts however had a large impact on the resulting morphology.[154]

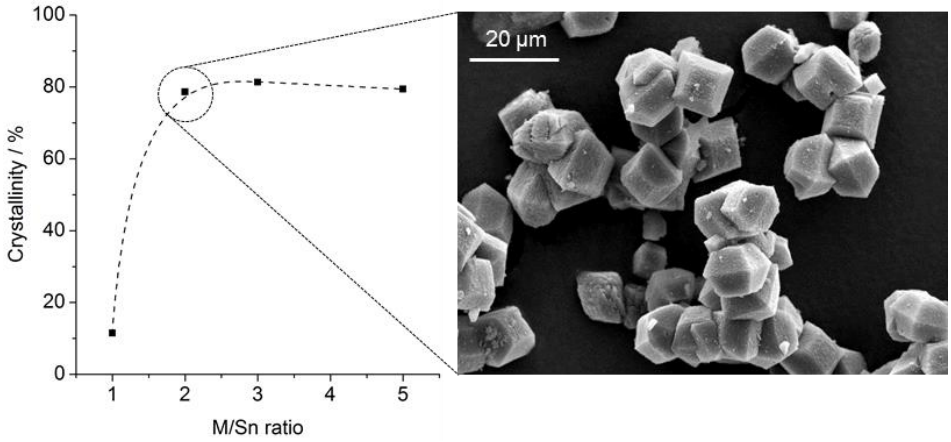

Figure 3.14. Sn-Beta (75, HT) prepared using different amounts of KOH added to the synthesis gel and crystallized for 7 days at 140 °C. A electron microscopy image has been included for the sample of ~80% crystallinity synthesized with K/Sn = 2.

This seems to indicate that the improvement in crystallization time is not related to the alkalinity of the system, but instead from the salts hindering the retarding effects caused by tin species, perhaps by forming a stable transition phase not interfering with the crystal growth. No change in the internal composition of the formed Sn-Beta particles were seen (Figure 3.15c) as the enriched outer shell of tin was also present of these samples. This likewise shows that the retardation in crystallization and the differences in morphology caused by preferred growth of the faces are indeed correlated; one a result of the other. Using the appropriate amount of alkali appears to allow for some degree of morphology control. This control could have an effect on the resulting catalytic properties of the materials, as the number of contribution of the pore openings of the different faces will change with the morphology. As mention earlier the introduction of alkali is however also known to influence the catalytic properties

of similar materials (often negatively). The catalytic activity of these types of modified Sn-Beta samples will briefly be mentioned in the next section, but will be described in more details in **Chapters 4**.

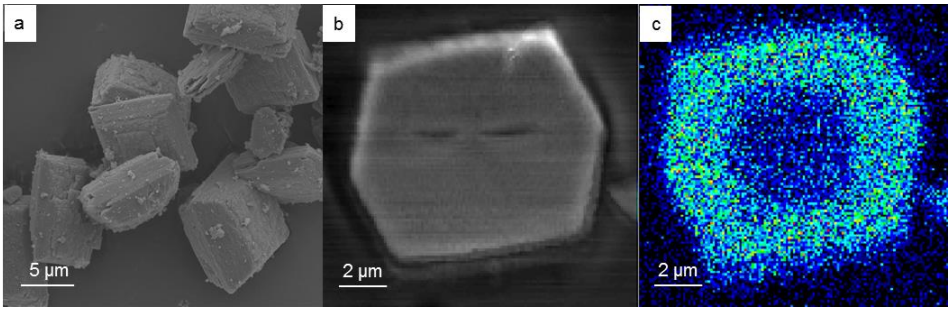

Figure 3.15. SEM-WDS analysis of Sn-Beta (75, HT) prepared with K/Sn ratio of 3 and synthesized for 21 days showing a) electron microscope image, b) image of the transected crystal and c) the X-ray intensities of tin of b).

3.1.7 **Catalytic activity**

To investigate the catalytic activity of the Sn-Beta materials for the conversion of sugars, a model reaction was used. The conversion of the trioses is well-known to undergo a cascade of reactions catalyzed by Sn-Beta, leading to the selective formation of methyl lactate (ML). [99] The number of steps involved in the reaction (involving both several 1,2-hydrideshift and dehydration reactions, see Scheme 1.4 on p. 20) makes it possible to probe the activity of the different materials prepared here. For the experiment, 1,3-dihydroxyacetone (DHA) was converted in methanol. To ensure moderate conversion, the reaction was at 75 °C for 2 hours, using a large excess of sugar compared with the amount of catalyst, m(DHA)/m(Sn-Beta) = 12. By keeping the conversion low, it was possible to compare the activity of the different Sn-Beta samples with both varying tin content and crystallinity.

Due to the inhomogeneous incorporation of tin and the large differences in morphology of the differences samples, this approach was chosen as opposed to comparing the samples based on tin content. Moreover, as mentioned previously, almost all samples prepared in this study contained small amounts of visible tin oxide particles on the surface of the crystals, a variant of tin known to be inactive in the conversion of sugars to methyl lactate. Although by visual inspection the amount of tin oxide particles appeared to increase with an increase in tin content, it was not possible to quantify how much of the tin ended up as inactive species.

Any contribution from leached tin species from the Sn-Beta zeolites under reaction conditions was found to be negligible (Figure 3.16).

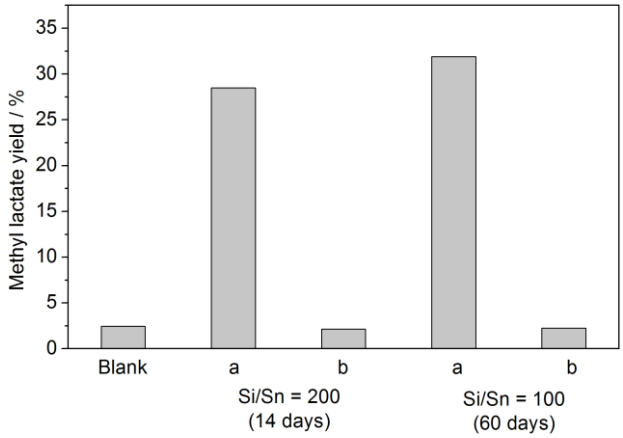

Figure 3.16. Comparison of the yield of methyl lactate obtained from 1,3-dihydroxyacetone using a) the Sn-Beta catalyst and b) from any leached species. The latter was done by initially treating the Sn-Beta sample in 6.5 mL of methanol at 75 °C for 2 hours, filtering off the catalyst and using this methanol as the solvent for the reaction. Reaction conditions: 0.025 g catalyst, 0.30 g DHA, 6.5 mL methanol, 600 rpm, 75 °C, 2 hours.

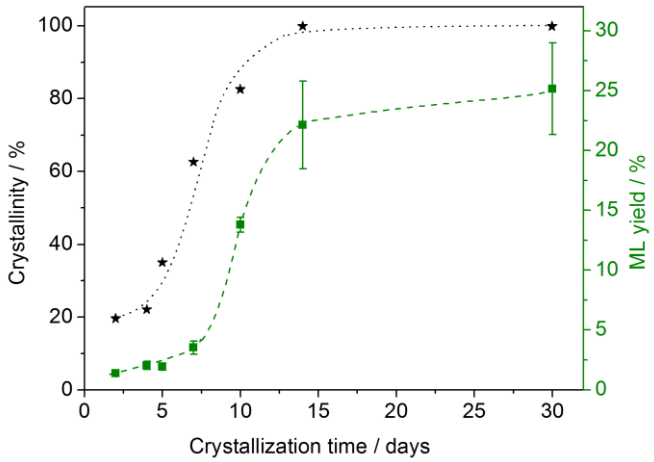

Figure 3.17. Crystallinity of and methyl lactate yield obtained with Sn-Beta samples (150, HT) prepared at varying hydrothermal synthesis times. Reaction conditions: 0.025 g catalyst, 0.300 g DHA, 6.5 mL methanol, 600 rpm, 75 °C, 2 hours. Each experiment was performed a minimum of 3 times.

Figure 3.17 shows the obtained ML yield for a sample with a Si/Sn = 150 as a function of crystallization time along with crystallinity of the sample. As the crystallinity increased from 20% to 63% (after 7 days), the ML yield remained below 5%. This is comparable to the yield of a blank experiment (~4%). An onset in activity is observed after 10 days of crystallization (83% crystallinity) with an obtained yield of ML of 14% increasing after 14 days (>95% crystallinity) to 22%. The Sn-Beta catalyst is relatively inactive until late in the crystallization. Simple pore blocking by amorphous material in the partial crystalline samples could explain this observation.

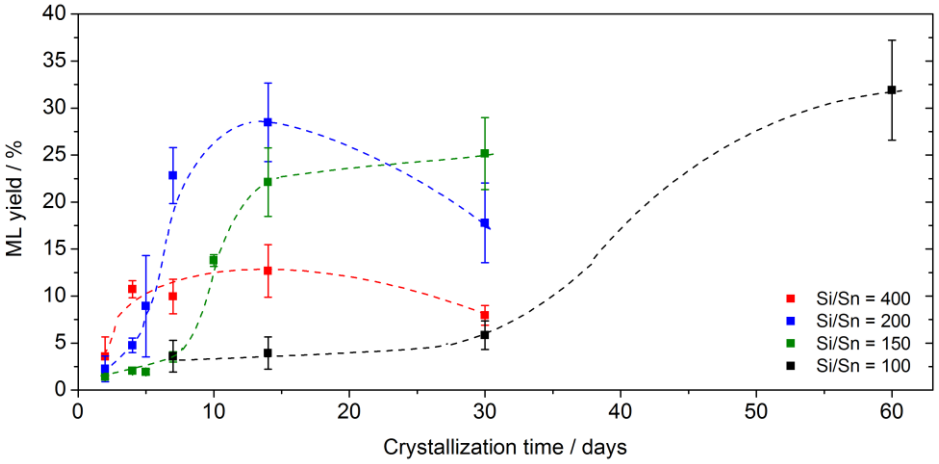

Figure 3.18. Yield of methyl lactate obtained using Sn-Beta samples crystallized for a varying amount of days and different tin content (Si/Sn ratios from 100 to 400). Reaction conditions: 0.025 g catalyst, 0.300 g DHA, 6.5 mL methanol, 600 rpm, 75 °C, 2 hours. Each experiment was performed a minimum of 3 times.

Expanding the catalytic results to the rest of the Sn-Beta series of varying tin content (Figure 3.18), it is evident that a large increase in yield of ML coincides with the point of full crystallization (>95% crystallinity). A ML yield of 11% (4 days) was obtained for a Si/Sn ratio of 400 whereas for Si/Sn ratios of 200 and 100, ML yields of 23% (7 days) and 32% (60 days) were obtained, respectively. Although Sn-Beta is active with low tin content for this reaction, it is clear that the bulk activity can be improved by incorporation of increasing amounts of tin. However, in all the cases the crystallinity needs to be above 80% to reach maximum activity. For two of the series (Si/Sn = 200 and Si/Sn = 400), a decrease in catalytic activity is observed for samples crystallized longer than what is required to obtain a crystalline sample. For a Si/Sn ratio of 200, the obtained ML yield decreases from 27% (14 days) to 18% (30 days). The observation that the

catalyst activity decreases for excessive synthesis times is very important when preparing the material for catalytic use. As explained in the previous section, Ostwald ripening phenomenon has been identified in the samples.

The catalytic activity was likewise measured for samples prepared with alternative tin sources (Figure 3.19) and samples where potassium was introduced. Both Sn-Beta prepared using tin(IV) acetate and $(TEA)_2SnF_6$ were found to be active in the conversion of DHA. Surprisingly, despite the poor incorporation of tin (Si/Sn = 295) and the large heterogeneity of tin found in samples prepared using tin(IV) acetate, this catalyst gave comparable or slightly higher yields (~27%) than when tin(IV) chloride (22% ML) was used. Although more thorough analysis of this catalyst is required to fully understand the incorporation of tin here, the catalytic activity of this material must mean that a high number of active, accessible tin sites are present in this catalyst. This seems to indicate that the high tin concentration found at the surface of the crystals are indeed active, incorporated tin sites and not tin oxide as earlier speculated.

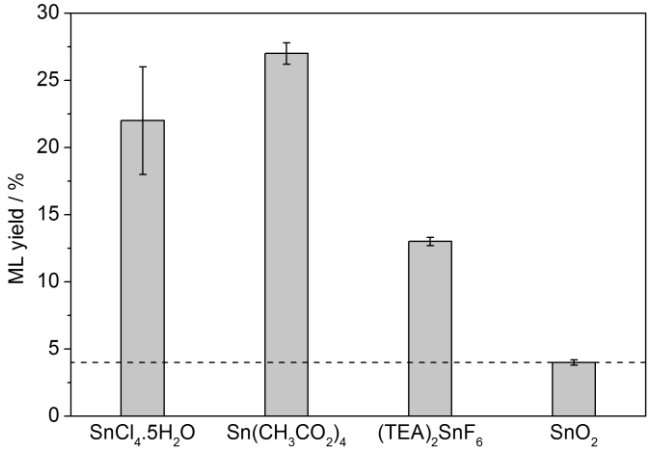

Figure 3.19. ML yield obtained with Sn-Beta prepared using different tin sources. The dashed line shows the yield when no catalyst is present. Reaction conditions: 0.025 g catalyst, 0.300 g DHA, 6.5 mL methanol, 600 rpm, 75 °C, 2 hours. Adapted from ref. [44].

For the Sn-Beta sample prepared using $(TEA)_2SnF_6$ a yield of 13% was obtained, lower than for the conventional Sn-Beta. Sn-Beta (75, HT) prepared in the presence of potassium (K/Sn = 3) was likewise found to be active in the conversion of the trioses resulting in a ML yield of 35%. Although only slightly higher than the yield achieved using a Sn-Beta catalyst with one third the amount of tin (Si/Sn = 200, 27% ML), this result shows that active Sn-Beta materials can

indeed be prepared in the presence of alkali metals. **Chapters 4 and 5** will describe the catalytic conversion of carbohydrates using alkali containing catalysts in more detail. It is important to note that the samples synthesized here using different tin sources or with the addition of alkali during synthesis were used primarily to investigate changes in crystal growth and composition and were not optimized for catalytic conversion of sugars. The lower or slightly higher yields achieved with the alternative tin sources could be a reflection of a number of the aforementioned factors (tin incorporation, crystallinity, etc.) which would likely improve upon proper optimization of the synthesis procedure.

When insoluble tin oxide nanoparticles were used as a source of tin, the material was inactive. These results illustrate that framework Sn sites are the active sites in the reaction and that the morphology changes are a consequence of the incorporation of tin in the framework.

3.2 Conclusions

In this chapter, I have shown that the addition of tin during near-neutral conditions in a fluoride medium severely retards the crystallization and changes the preferred growth of the crystal faces. A clear correlation was found between the tin content present during synthesis and the change in the capped square bipyramidal morphology. This was observed as a change from highly elongated crystals with low tin contents to highly truncated, almost plate-like, crystal at high tin contents. This retardation could be countered by adding the appropriate amount of alkali salt to the synthesis, resulting in the successful preparation of Sn-Beta with high tin content (Si/Sn = 75).

Furthermore, tin was found to be unevenly distributed within the bulk of the crystal. Regardless of tin content and resulting morphology, a clear gradient in the distribution of tin within the bulk crystal was observed using SEM-WDS for all samples. The tin enriched shell was observed to extend roughly half the crystal radius and contain approximately twice the amount of tin as the depleted core. This feature was found to exist in samples even before being fully crystalline in appearance and was surprisingly found in crystals that continuously increased in size from Ostwald ripening. Tin was additionally found in small amounts present as nanosized tin oxide particles on the surface of the crystals.

The catalytic activity of the prepared Sn-Beta materials for the conversion of the triose sugar 1,3-dihydroxyacetone to methyl lactate was likewise found to depend on the tin content with increasing activity following increasing tin incorporation. The activity was found to not directly follow the crystallization of the materials. Instead any activity of the material appeared to be introduced in the

very late stages of the crystal growth. Even though the physical properties such as degree of crystallinity, pore volume etc. were unchanged at prolonged synthesis times, we observed a decrease in the catalytic activity of the material as a function of prolonged synthesis time indicating that thorough control of the crystallization of Sn-Beta is required in order to make a good catalyst, also indicating that optimizing the catalyst could be done by reducing the crystal size. Furthermore, Sn-Beta was successfully prepared using a variety of tin sources including tin(IV) chloride, tin(IV) acetate and tetraethylammonium hexafluorostannate yielding active catalysts for the conversion of 1,3-dihydroxyacetone to methyl lactate and all having similar slightly truncated morphologies. A high density of tin was found at the surface of the catalyst when tin(IV) acetate was used as the tin source resulting in exceptional activities for this catalyst, indicating that the synthesis conditions could change the internal distribution of tin towards materials of higher activity. When using tin(IV) oxide particles as the tin source no activity was obtained and the crystals resembled purely siliceous Beta crystals by being highly elongated with a distribution of SnO_2 particles on the surface of the crystals.

These findings point out that careful control of the synthesis parameters is required in order to optimize the catalytic activity of the Sn-Beta when prepared in a fluoride medium. In addition, direct turnover number comparisons for different Sn-Beta materials, based on the amount of tin in the samples is likely to give an over-simplified picture of the number of accessible active sites, as the tin gradient distribution, crystal morphology and Ostwald ripening will distort such an analysis, and a varying degree of active site accessibility may result for different samples.

4
Effect of Alkali on Methyl Lactate Formation‡

The conversion of sugars to lactic acid is currently done by fermentation in processes that yields up to 95%. Although several benefits exist when using heterogeneous catalysts in terms of throughput, cost and efficiency, it is important to improve selectivity if this process is to be able to compete.[155] Homogeneous systems have been developed often using expensive lanthanide catalysts such as erbium triflate or chloride, yielding very high amounts of lactates (~90%) from cellulose.[156, 157] Less expensive systems have been described recently however using stoichiometric amounts of $Ba(OH)_2$ resulting in high yields from glucose.[112] However, utilizing inexpensive catalysts also easy to recover and recycle is essential for an industrial process for methyl lactate (ML) in order to keep costs low.

Alkali ions are known to be of great importance in the preparation of a variety of conventional zeolites. As mentioned in the previous chapters, alkali ions present in zeotype materials such as TS-1, Ti-Beta and Sn-MFI can have negative impacts on both crystal growth[21, 82-84] and activity of the prepared materials.[86-88] Several research groups have studied the post-synthetic removal of alkali metal impurities to obtain catalytically active materials.[76, 86-89] Small amounts of alkali metal ions have however also been reported to improve the activity of titanium-containing silicates for some epoxidation and oxidation reactions.[46, 83, 85] Recent studies have shown that, alkaline conditions and the presence of salts can also affect the catalytic conversion of monosaccharides.[90,

‡ This chapter was adapted from Tolborg *et al.* ChemSusChem, **2015**, *8*, 613.

91, 103] As mentioned in **Chapter 1**, alkali added either as sodium borate or chloride had a pronounced effect on the conversion of sugar in water using Sn-Beta. In the presence of alkali ions, glucose underwent epimerization to mannose, instead of isomerization to fructose.[17, 90, 91] The effect of alkali was also found in homogeneous systems. In the presence of either alkali using tin(IV) chloride, the yield of ML obtained from glucose increased from 25% to 45% when tin(IV) chloride was used as catalyst in the formation of ML from glucose.[158, 159]

The focus of this chapter is on the optimization of the catalyst synthesis and reaction conditions in order to increase the selectivity for ML from sugars. The effect of alkali on the catalytic conversion of sugars using stannosilicates will be investigated in both **Chapters 4 and 5**. **Chapter 5** will investigate the different pathways accessible catalytically from sugar by the stannosilicates and how these are affect by the presence of alkali metal salts. In this current chapter, the focus will be the investigation and optimization of the yield of methyl lactate using alkali. It will be shown that the addition of small amounts of alkali salts can significantly improve the yield of ML if added either directly to the Sn-Beta catalyst during synthesis or added directly to the reaction medium. After optimization, ML yields of up to 75% were obtained from sucrose, whereas in the absence of alkali, the ML yield was only 30%. Additionally, it is shown that this effect is not exclusive to traditional Sn-Beta synthesized in a fluoride media. Comparable yields of ML are achieved with optimized addition of alkali during reaction using Sn-Beta prepared by the post-synthesis method and at slightly lower yields using Sn-MCM-41 and Sn-SBA-15.

4.1 Results and discussion

4.1.1 Alkali- and alkaline earth-containing Sn-Beta

With the aim of investigating the influence of alkali metal ions on the catalytic conversion of sugars, a series of alkali or alkaline earth modified Sn-Beta samples were prepared. Alkali-free Sn-Beta (simply denoted Sn-Beta) was prepared similar to what was described in **Chapter 3** using a Si/Sn ratio of 200 and a crystallization time of 14 days. In the synthesis of these materials, however, dealuminated Beta seeds were added as described in the original synthesis protocol.[137] The modified Sn-Beta materials were prepared following the same synthesis procedure, but dissolving the source of alkali source in the structure directing agent (SDA) and using this mixture in the synthesis. Additionally, Sn-Beta materials were also prepared with alkaline earth metals in a similar manner. This yielded Sn-Beta samples containing mono- or divalent metals in addition to tin

ranging from lithium to cesium and from calcium to barium, see Table 4.1. In this chapter, modified Sn-Beta samples are denoted *M*-Sn-Beta with *M* being the added alkali or alkaline earth metal. The alkali metals were added to give a nominal *M*/Sn ratio of 8 in the gel. For the alkaline earth metals, it was not possible to obtain highly crystalline samples using this ratio, instead this ratio was reduced to 4. The metals are thus added in equivalent instead of equimolar amounts.

All syntheses produced high solid yields from the gel (≥89%) of highly crystalline Sn-Beta materials, see Table 4.1. Although all samples were found to have high pore surface area (≥400 m^2/g) and micropore volumes (0.16-0.20 mL/g), the physical characteristics were (apart from Li-Sn-Beta) slightly lower than what is normally found for Sn-Beta samples synthesized in the absence of alkali metal ions (Table 4.1, entry 1).[44, 45] Regarding the composition, the tin content was found to vary moderately between samples with Si/Sn ratios ranging from 202 to 238, resulting in a tin recovery in the finished catalyst of 81-98% (Table 4.1). UV-Vis measurements for samples synthesized in the presence of alkali metals (Figure A.10) showed the characteristic bands for tin incorporated in the zeolite framework (220-260 nm) for all samples. The samples Na-Sn-Beta and K-Sn-Beta deviated from the other samples, however, showing an additional band at 280-320 nm often. This band is often ascribed to the presence of extra-framework tin species.[17, 43, 47, 101] These two samples also showed the lowest micropore volume (0.16-0.17 mL/g) of the prepared samples. As mentioned earlier, alkali metal ions have pronounced effect on crystallization (as was also shown in **Chapter 3**) and both potassium and sodium are known to act as structure directing agents for zeolite synthesis.[132, 160, 161] This could indicate that although both samples were highly crystalline samples, the nature of tin and the pore system could be affected by having potassium or sodium present during synthesis. In **Chapter 3** it however did not appear to have any influence on the internal composition of the prepared materials (Section 3.1.6).

Despite being added with a nominal *M*/Sn ratio of either 4 or 8 to the synthesis gel, the recovered metal in the catalyst was significantly lower. Only Ca-Sn-Beta (*M*/Sn ~ 3) appeared to contain most of the metal introduced during synthesis (*M*/Sn = 4). For all other samples, the final *M*/Sn atomic ratios ranged from 0.18 to 0.79 (Table 4.1, entries 2-6 and 8-9) *i.e.* in the order of magnitude of the amount of tin found distributed in the material. A similar correlation between potassium and titanium was found for TS-1 by Tatsumi *et al.*[86] To investigate the inclusion of alkali metals, a series of Sn-Beta samples (Si/Sn = 200) was prepared by varying the amount of potassium hydroxide added to the template during the synthesis. This addition was done relative to tin to give a series with

K/Sn ratios varying from 0.3 to 11. The introduction of potassium in these levels were found to have no effect on the physical properties of the finished materials with all samples having high crystallinity and solid yields of >90%. From elemental analysis of the calcined samples, the K/Sn ratio found in the finished material could be compared with the nominal ratio (Figure 4.1).

Table 4.1. Properties of the *M*-Sn-Beta (200, HT) series: Composition in the synthesis gel and characterization of the final zeolite material.

Entry	*M*-Sn-Beta	Synthesis gel		Zeolite					
		Si/Sn	*M*/Sn	Sn[b]	Si/Sn[b]	*M*[b]	*M*/Sn[b]	S_{BET}[d]	V_{micro}[e]
		-	-	wt%	-	ppm	-	m^2/g	mL/g
1	-	201	-	0.80	237	-	-	477	0.20
2	Li	200	8	0.92	202	300	0.56	474	0.20
3	Na	211	7	0.90	202	310	0.18	403	0.16
4	K	204	8	0.91	212	780	0.26	435	0.17
5	Rb	200	8	0.84	222	3,580	0.60	447	0.18
6	Cs	200	8	0.83	220	7,220	0.78	448	0.18
7	Ca	200	4	0.93	199	10,330	3.16	469	0.19
8	Sr	200	4	0.94	199	4,060	0.60	460	0.18
9	Ba	200	4	0.93	197	7,070	0.65	464	0.18

a) The ratio of zeolite material obtained after calcination to the theoretical yield of silicon and tin in the synthesis mixture. b) Determined by elemental analysis. c) The ratio of tin detected by chemical analysis to the amount in the synthesis mixture. d) BET surface area. e) Micropore volume, calculated using the *t*-plot method.

Although in most samples a large excess of potassium was added to the synthesis, less than 10% was recovered in the finalized materials. Moreover, the amount of potassium introduced in the material was found to not increase beyond around one potassium per four tin atoms in the structure (K/Sn = 0.26). This maximum was achieved using a nominal K/Sn ratio in the synthesis gel of ~7, yielding samples with high crystallinity (≥95%) and the expected characteristics of the pore systems mentioned above (high surface area and micropore volume). Increasing the amount of KOH in the synthesis gel beyond this nominal ratio hindered crystal growth leading to a decrease in both surface area (389 m^2/g) and micropore volume (0.15 mL/g), explaining the lower inclusion of potassium in

the finished material (Figure 4.1). That alkali can have detrimental effects on zeolite formation has previously been shown for similar Lewis acidic zeotypes; TS-1 and Ti-Beta.[22, 24, 86, 88]

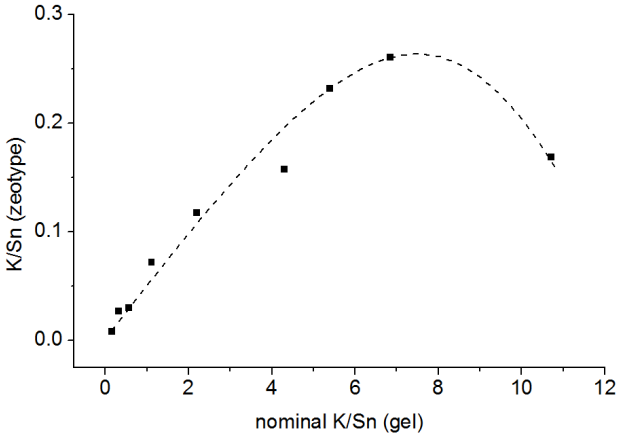

Figure 4.1. K/Sn ratio determined by elemental analysis in the finished Sn-Beta samples as a function of the nominal K/Sn ratio as present in the respective synthesis gel.

This maximum included potassium (K/Sn = 0.26) could originate from the incorporation of the cation on ion exchange positions present in the zeotype material. Unlike for the incorporation of trivalent aluminum, incorporating of tetravalent tin does not introduce a charge imbalance in the framework creating conventional ion exchange positions. Additionally, using the fluoride route synthesis ensures the formation of highly defect-free crystals, further limiting the number of Brønsted acid sites from imperfections in the structure. In line with the different theories on the nature of the active site of Sn-Beta, incorporation of tin could lead to the formation of small amounts of local defects in the near environment of tin.[59] Any residual alkali cations could therefore be present in the material exchanged with protons of hydroxyl groups as a result of the lack of conventional ion exchange sites present in the material.[46, 76, 86, 90, 162]

The difference in the *M*/Sn ratio observed for the different alkali and alkaline earth metals seen in Table 4.1 could be the result of a number of factors: the differences in ion-exchange capabilities of the mono- and divalent additives, the large difference in ionic size of these metals or from the changes in crystal growth as shown in **Chapter 3** by having these additives present during hydrothermal. Since the synthesis was not optimized for each individual alkali or alkaline earth

metal this could result in materials with both fewer or additional ion-exchange positions in the form of defects or hydrolyzed-open sites.

4.1.2 Catalytic activity of *M*-Sn-Beta

To investigate the impact of having alkali present in the material on the catalytic properties, the prepared samples were tested in the conversion of sucrose to ML (Figure 4.2). Sucrose has previously been shown to result in the highest yields of ML of any simple sugars.[16, 18] The cascade of reactions (as described in detail Section 1.5) involves the first the hydrolysis of sucrose, the retro-aldol reaction of the hexose sugars followed by dehydration and isomerization of the formed trioses to yield ML. A simplified overview can be seen in Scheme 4.1.

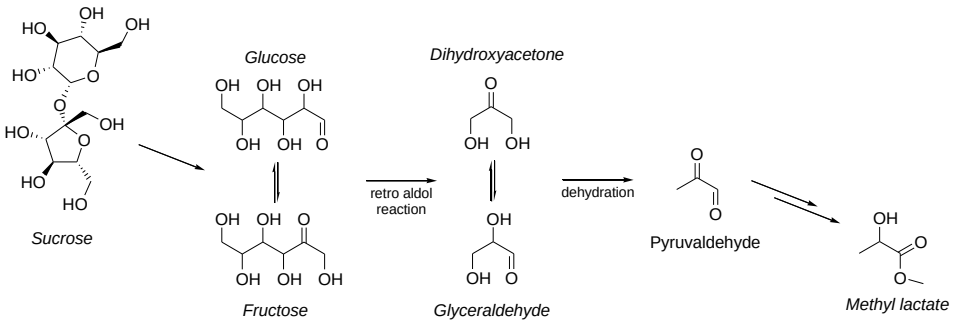

Scheme 4.1. Simplified schematic representation of the steps involved in the conversion of sucrose to methyl lactate.

When the alkali-free Sn-Beta catalyst was used, a low yield of only 29% ML was achieved. Similar low yields were achieved using the samples prepared in the presence of the alkaline earth metals (30-37%). For the samples modified using alkali metals, however, a more than two-fold increase in yield of ML was observed (up to 66%); a pronounced improvement in yield over the unmodified sample. The catalysts containing Li, K, Rb and Cs all led to ML yields of 60-66% (Figure 4.2). In the case of Na-Sn-Beta, the obtained yield was only around 50%, which might be due to the lower micropore volume and alkali content as described earlier.

Although all alkali-containing samples gave improved ML yields over the alkali-free variant, it is clear that the additional cation content was not optimized. To further investigate the dependence of the specific quantity of alkali on the catalytic outcome, we made use of the Sn-Beta series prepared with potassium included in the structure in varying amounts with a maximum K/Sn achieved of 0.26 (Figure 4.1). From Figure 4.3 the highest obtained ML yield (here ~60%) can

be seen to coincide with the maximum K/Sn achieved in the material. This further corroborates that the inclusion of alkali in the structure is linked to the catalytic properties of the material, hinting that potassium somehow modifies the active site of tin, as stated previously.

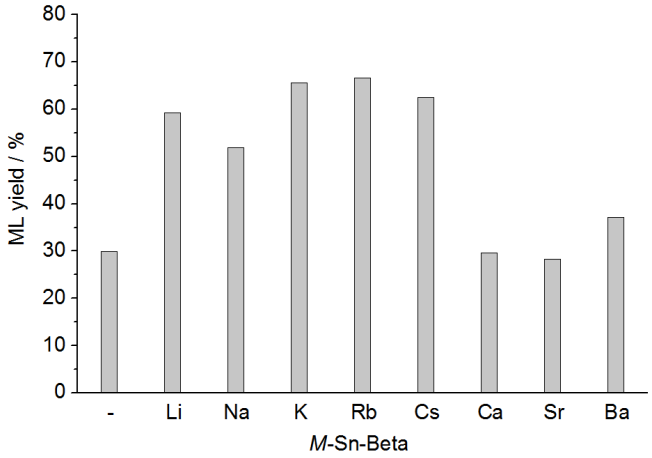

Figure 4.2. Methyl lactate yield obtained from sucrose using Sn-Beta zeolites (Si/Sn = 200) prepared with different alkali metals present (nominal *M*/Sn = 8). Physical properties in Table 4.1. Reaction conditions: 0.450 g sucrose, 0.150 g catalyst, 15 g methanol, 170 °C, 16 h.

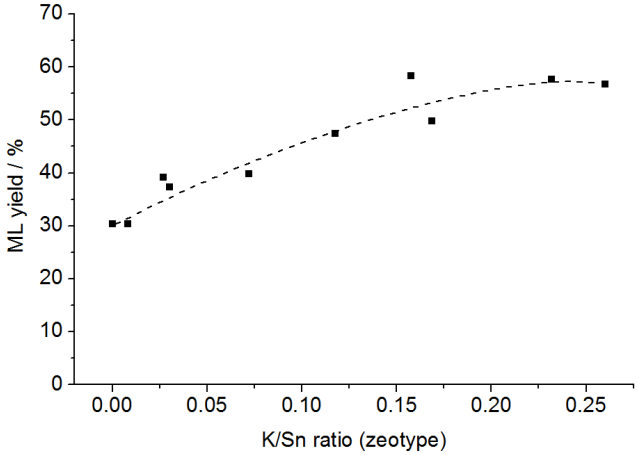

Figure 4.3. Yield of methyl lactate (ML) as a function of the K/Sn ratio included in the Sn-Beta sample as measured by elemental analysis. Reaction conditions: 0.450 g sucrose, 0.150 g catalyst, 15 g methanol, 160 °C, 16 h, performed in Parr autoclaves.

4.1.3 **Effect of alkali mobility**

Considering the potential mobility of the alkali ions during reaction,[90] meaning that they could leave the catalyst and migrate into the solution or vice versa, experiments were carried out, adding alkali ions directly to the reaction medium. Alkali metal salts were dissolved in the methanol solvent and used together with alkali-free Sn-Beta. Different concentrations of alkali chlorides (0-100 mM) were used and tested for any beneficial effects in the conversion of glucose to methyl lactate at 120 °C (Figure 4.4). The conversion of hexose sugars is similar to when sucrose is used as the starting substrate (Scheme 4.1 on p. 17). The reaction involves several of the same catalytic steps to obtain ML, but allows for lower temperatures (120 instead of 170 °C) as no initial hydrolysis step is required. This procedure was thus used for initial screening purposes. This however also results in lower achieved ML yields compared with sucrose with only ~9% ML obtained using an alkali-free Sn-Beta. For this reaction, a more than five-fold increase was achieved increasing the ML yield from 9% to ~55% with the introduction of alkali in solution. These yields are similar to what has been shown possible using a combination of Sn-MFI and MoO_3 at comparable temperatures from fructose and higher than what previously was obtained using Sn-Beta at even higher temperatures (160 °C).[18, 29]

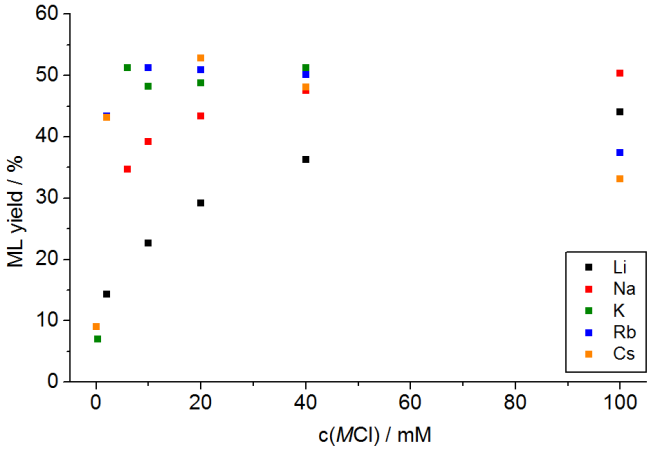

Figure 4.4. Yield of methyl lactate obtained in the conversion of glucose using Sn-Beta (200, HT) in the presence of different alkali chlorides. Reaction conditions: 0.250 g glucose, 0.100 g catalyst, 5 g of 0-100 mM *N*Cl dissolved in methanol (*N* = Li, Na, K, Rb, Cs), 120 °C, 19 h, 500 rpm stirring.

In Figure 4.5, the obtained ML yield can be seen when 0, 10 or 20 mM of the alkali chlorides were added during reaction. The effect of the added alkali appears

to improve moving down through the Group I elements, leading to significantly higher yields using cesium chloride (55%) than lithium chloride (23%) at comparable concentrations (10 mM). The trend seems to correlate with a fall in electronegativity and can be assume caused by an increase in ion exchange capabilities.

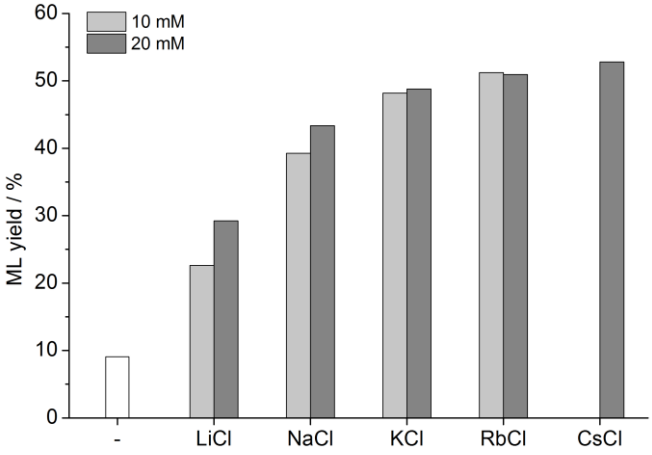

Figure 4.5. Yield of methyl lactate obtained in the conversion of glucose using Sn-Beta in 10 and 20 mM solutions of different alkali chlorides. The alkali-free experiment is marked in white. Reaction conditions: 0.250 g glucose, 0.100 g Sn-Beta (200, HT), 5 g of 0-20 mM *N*Cl dissolved in methanol (*N* = Li, Cl, Na, K, Rb and Cs), 120 °C, 19 h, 500 rpm stirring.

Following these results, the investigated salts were expanded to include a range of different sources, focusing solely on potassium as the cation. Although rubidium and cesium showed slightly higher yields than potassium (Figure 4.5), potassium was chosen for its greater natural abundance making a larger variety of chemicals available commercially for investigation. For the sources of alkali added to the solution, it was quickly found that the cosolutes divided into two groups, primarily depending on the basicity of the potassium source, see Figure 4.6.

The more basic sources of potassium including the carbonates, bicarbonates, acetates and lactates, all gave rise to a maximum yield of ~42% at low concentrations (0.6 mM) with a relatively narrow profile. At concentrations above this optimum, a steep decrease in ML yield was observed with little to no product formed above 3 mM. The causes for decrease in yield is the basic degradation of sugars clearly visible by a coloration of the reaction mixtures. The remaining more neutral salts gave yields of ML slowly increasing to ~50% at high concentrations (5-20 mM). This is similar to what was found for the Group I chlorides shown earlier (Figure 4.4). For these different potassium salts, no immediate decrease in

ML yield was observed for the concentrations tested for Figure 4.6. A decrease was however observed for the chlorides of rubidium and cesium at high concentrations (100 mM, Figure 4.4), hinting that a maximum yield likewise exists for the neutral salts. At these high concentration of salts, solubility in methanol becomes an issue for several of the tested cosolutes (including KCl, KNO_3, NaCl).[163] Potassium fluoride (KF, Figure 4.6) was found to not behave as the other halides, resulting instead in very low ML yields across the range of concentrations (≤5%). This is likely due to the reactivity of the fluoride ions and *in-situ* formation of small amounts of hydrofluoric acid in solution leading to detrimental effects on the zeolite structure at these concentrations.

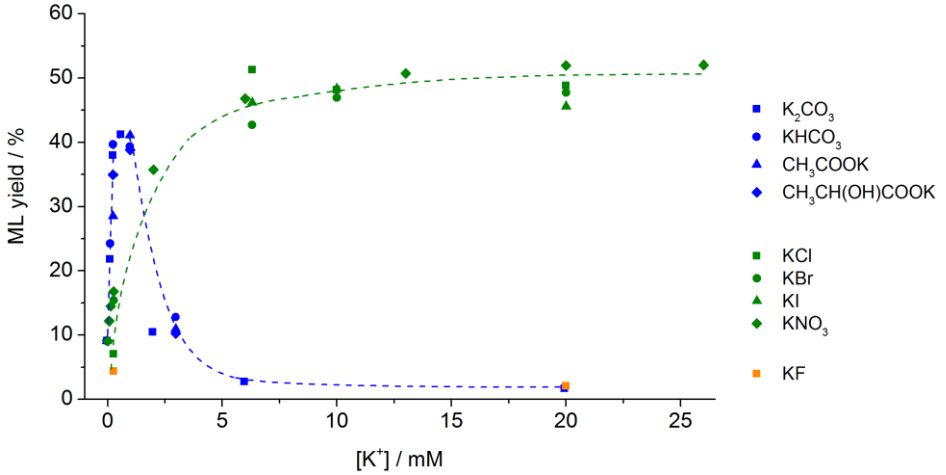

Figure 4.6. Yield of methyl lactate obtained in the conversion of glucose using different concentrations of a variety of potassium salts using Sn-Beta in methanol. Reaction conditions: 0.250 g glucose, 0.100 g Sn-Beta (200, HT), 120 °C, 19 h, 500 rpm stirring.

A similar concentration profile was found when changing the starting substrate from glucose to sucrose. For the conversion of this sugar substrate the reaction temperature was increased to 170 °C to ensure full conversion. As expected even greater ML yields were obtained from this disaccharide than from glucose, see Figure 4.7. Moreover, the obtained yields were significantly higher than what was achieved with the synthesized *M*-Sn-Beta series shown in Figure 4.2 on p. 75. By increasing the content of alkali in solution to a concentration of 0.065 mM, the ML yield increased from 29% to an unprecedented yield of 75%. Similar to what was found for the conversion of glucose, a relatively narrow concentration range of K_2CO_3 (0.05-0.07 mM) was found to produce the high yields of ML rapidly decreasing to 55-60% above the optimum. At alkali levels

below the optimum, the concentration of the cosolute is not high enough to fully neutralize the unwanted sites in the material and yield the highest the improvement of selectivity. Addition beyond the optimum results in excess base in the system leading to sugar degradation (seen by a darkening of the reaction liquid), a decrease in conversion and as a result a decrease in ML yield. [164]

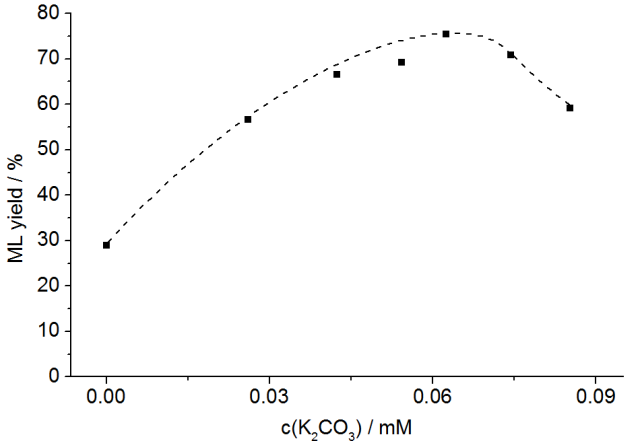

Figure 4.7. The methyl lactate yield obtained from sucrose using Sn-Beta versus the concentrations of K_2CO_3 in methanol. The line is a guide to the eye. Reaction conditions: 0.450 g sucrose, 0.150 g Sn-Beta (200, HT), 15 g solvent, 170 °C, 16 h.

From these results, it appears that the addition of an alkali salt indeed plays a crucial role in the conversion of sugars to ML and that very low yields are obtained in their absence. Although different effects are found for different chlorides of Group I showing that the effect is linked to the cation, it is here shown that the choice of counter ion likewise influences the reactivity of the reaction system. This seems to fit with previous reports on the epimerization of glucose to mannose, where different groups have shown correlating effects to both the presence of sodium and borate in the reaction.[90, 91, 103] For the conversion of glucose or sucrose to ML, following previous thoughts, the anion likely facilitates the deprotonation on the hydroxyl groups present in the zeolite materials, allowing for the ion exchange of alkali onto these sites. For the more basic sources of alkali, this is achieved at rather low concentrations (<0.2 mM), whereas for less basic cosolutes such as KCl or KNO_3, the optimum concentration is shifted to much higher concentrations. It is speculated that the effect of alkali can be explained as a titration of unwanted sites in the material, responsible for catalyzing other reactions than the retro-aldol cleavage and 1,2-hydride shift involved in formation of methyl lactate. This will be described in more detail in **Chapter 5**.

In order to further relate the effect of alkali to the active site of Sn-Beta, samples with varying amounts of tin were tested for the conversion of glucose in varying concentrations of KCl (up to 40 mM), see Figure 4.8. Here the results are compared on the basis of potassium relative to tin (K/Sn) in the reaction system. For this sample series, a similar trend was indeed found for the obtained yield in ML, although slightly lower yields were obtained with Sn-Beta (800, HT). It was shown in the previous chapter that tin incorporates unevenly in the prepared crystals, making it difficult to directly compare the accessible tin in the different zeotype samples. The coinciding profiles shown in Figure 4.8 does however indicate that the effect is correlated with the presence of tin in the structure and achieved by modifying some characteristics about the active site itself.

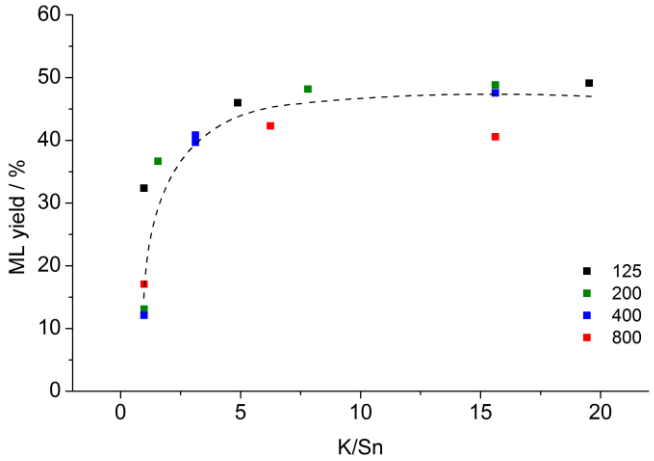

Figure 4.8. Yield of methyl lactate as a function of the K/Sn ratio present in solution using a combination of Sn-Beta and different concentrations of KCl. Reaction conditions: 0.250 g glucose, 0.100 g Sn-Beta (Si/Sn = 125-800), 5 g of up to 40 mM KCl dissolved in methanol, 120 °C, 19 h, 500 rpm stirring.

Although the effect of having alkali present was found to be most pronounced in methanol, an increase in lactate yield was likewise observed when the solvent was changed to both ethanol and butanol (Figure 4.9). In water almost no effect was observed. The tested concentration (2 mM) might be too low to achieve any effect in an aqueous solvent due to solvation effects. The group of Davis used a concentrated aqueous solution of NaCl (~3 M) to investigate and show the effect of alkali in water for isomerization/epimerization.[90] Higher concentrations in water will be investigated for the valorization of glycolaldehyde in **Chapter 6**.

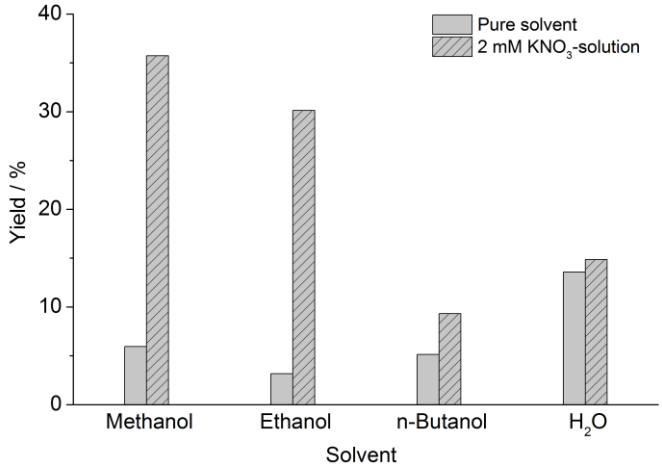

Figure 4.9. Yield of methyl, ethyl and butyl lactate or lactic acid obtained from glucose using Sn-Beta in methanol or a 2 mM KNO_3 solution. Reaction conditions: 0.250 g glucose, 0.100 g Sn-Beta (200, HT), 5 g of solvent, 120 °C, 19 h, 500 rpm stirring.

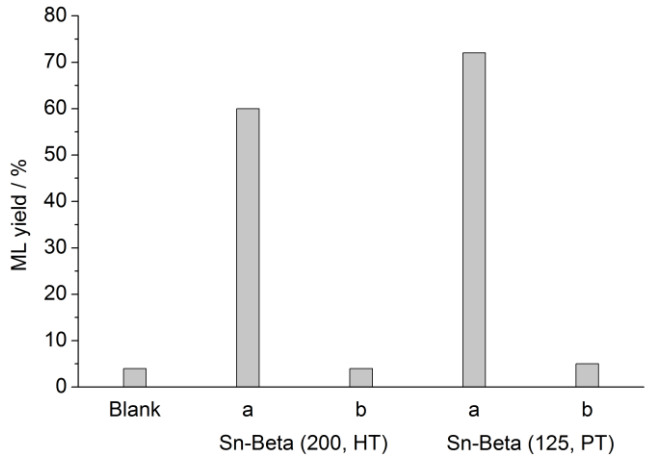

Figure 4.10. Comparison of the conversion of sucrose using a 0.17 mM K_2CO_3 solution in absence of Sn-Beta (Blank) or with a) the Sn-Beta catalyst or b) leaching experiment: Initially treating the catalyst in 15 g of 0.17 mM K_2CO_3 in methanol at 170 °C for 4 h, filtering off the catalyst and using this solution as the solvent for the reaction. Reaction conditions: 0.450 g sucrose, 15 g solvent, 170 °C, 16 h, 700 rpm.

To investigate any homogeneous catalytic contribution from leached tin from the catalysts used or the added alkali, control experiments were performed. Homogeneous tin salts have been shown to be active in the same reactions as Sn-Beta and retro-aldol reactions are known to also take place in basic media.[115, 118, 122] Any contribution from leached tin species was found to be negligible

under the used reaction conditions (170 °C, 16 hours in methanol), see Figure 4.10. Additionally, almost no ML was formed (~4%) when only the alkali metal ions were present during reaction in absence of the stannosilicate catalyst, see Table 4.2, entries 1-4. Similar low yields of ML were obtained from the reaction intermediates fructose and 1,3-dihydroxyacetone (DHA), Table 4.2, entries 5-8.[16] On the contrary, the alkali-containing solvent was found to hinder the formation of ML from DHA leading only to a yield of 3%, while 28% was formed in methanol. Using SnO_2-Beta or siliceous Beta (Table A.1 on p. 159) likewise gave no appreciable yield of ML, confirming that the obtained high yields are a result of the combined effect of alkali and the stannosilicate.

Table 4.2. The methyl lactate yield obtained in the absence of tin-containing catalyst using varying concentrations of K_2CO_3 in methanol starting from sucrose, fructose and 1,3-dihydroxyacetone (DHA).

Entry	Sugar	Concentration (K_2CO_3 in methanol) mM	ML %	Conversion %
1	Sucrose	0	4	N/A
2		0.065	3	N/A
3		0.17	3	N/A
4		0.25	3	N/A
5	Fructose	0	5	37
6		0.17	3	11
7	DHA	0	28	N/A
8		0.17	3	N/A

Reaction conditions: 1.31 mmol sugar substrate, 15 g solvent, 170 °C, 16 h, >700 rpm stirring.

4.1.4 Expanding the alkali effect

For the purpose of testing alternative stannosilicate materials, a post-synthesized Sn-Beta sample, Sn-Beta (125, PT), was prepared using the incipient wetness impregnation methodology and used for the conversion of sucrose, see Figure 4.11a.[51] Again, a narrow concentration optimum was observed for this material occurring at a concentration of 0.17 mM K_2CO_3 leading to a yield of 72% ML. Beyond this optimum, like for Sn-Beta (200, HT), lower yields were obtained, showing that the two materials indeed behave in a similar way in the presence of alkali, also resulting in comparable yields of ML.

The optimum concentration varies slightly between the two Sn-Beta materials. The optimum for the material prepared by hydrothermal synthesis, Sn-

Beta (200, HT), is found at 0.065 mM K_2CO_3 and for post-synthesized material, Sn-Beta (125, HT) at 0.17 mM. Although the effect of alkali is still not fully understood, if it is assumed that the effect is related to the active tin sites as discussed earlier, the difference can still not be explained only by the slightly larger content of tin in the post-treated material. The calculated K/Sn ratios present during reaction for the two catalysts are 0.20 and 0.32 for the samples prepared by hydrothermal synthesis and post-treatment, respectively. The additional alkali metal ions needed per tin atom for Sn-Beta (PT) could be ion-exchanged onto additional Brønsted acid sites formed from residual aluminum or from a higher number of defects.[58] Interestingly, the optimum K/Sn ratio to have in solution during reaction with Sn-Beta (200, HT) strongly resembles the maximum potassium successfully incorporated during the synthesis (K/Sn = 0.26) described earlier in Section 4.1.1. The latter was also linked to the highest ML yield, hinting that the modification of the sites in the material can either be achieved during synthesis or simply during reaction. As a consequence, however it appears that the alkali salt concentration requires optimization for the specific catalyst used to achieved the best results. Similar to what was found earlier in the conversion of glucose, much higher concentrations were required when KNO_3 or KCl was used as the alkali source and no clear optimum (Figure 4.11b-c).

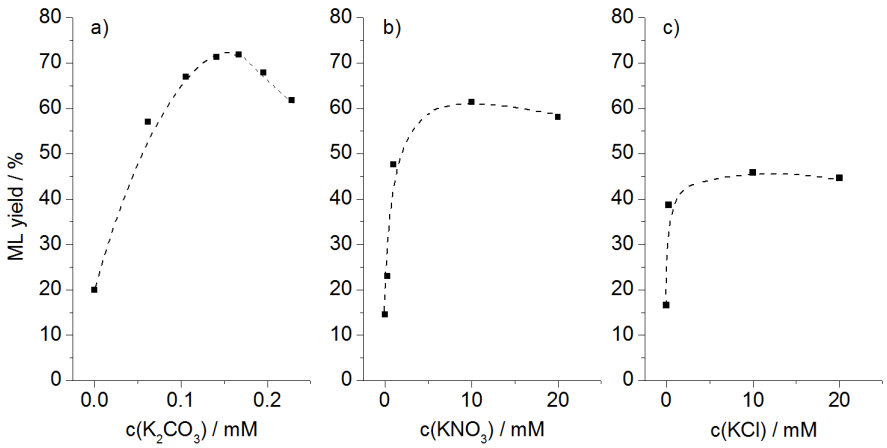

Figure 4.11. The methyl lactate yield obtained from sucrose using post-synthesized Sn-Beta (125, PT) versus the concentration of a) K_2CO_3, b) KNO_3 or c) KCl dissolved in methanol. The lines are a guide to the eye. Reaction conditions: 0.450 g sucrose, 0.150 g catalyst, 15 g solvent, 170 °C, 16 h.

As mentioned earlier, not only zeotype materials have proven relevant for the conversion of carbohydrates, also the mesoporous stannosilicates Sn-MCM-41 and Sn-SBA-15 have shown activity in the conversion of sugars.[13, 41, 119, 125]

The beneficial effect of alkali ions was found to also apply to this type of amorphous stannosilicate. The highest yield of ML obtained using Sn-MCM-41 of 58% at a K_2CO_3 concentration of 0.20 mM (Figure 4.12a) and only 20% ML was obtained in an alkali-free environment. For Sn-SBA-15, the optimum concentration (0.05 mM K_2CO_3 in methanol) resulted in an increase from 23 to 52% ML yield (Figure 4.12b). Since the insertion of tin in these amorphous materials is much more randomized, the improvement observed with these materials show that the effect is not exclusive to materials where tin is placed within a crystalline, rigid framework.

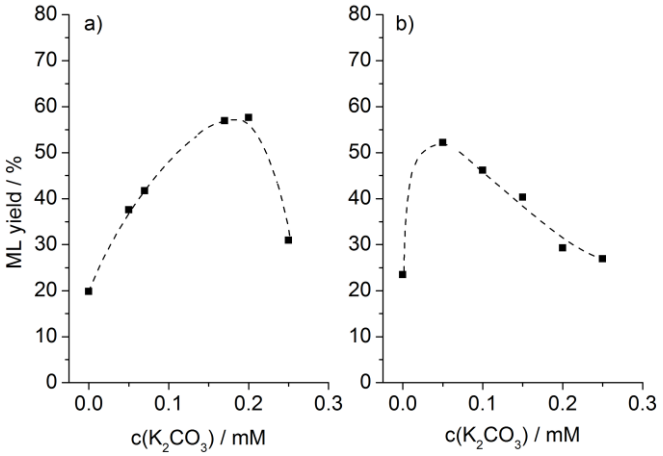

Figure 4.12. The methyl lactate yield obtained from sucrose using a) Sn-MCM-41 (Si/Sn = 200) and b) Sn-SBA-15 (Si/Sn = 200) versus the concentration of K_2CO_3 in methanol. The lines are a guide to the eye. Reaction conditions: 0.450 g sucrose, 0.150 g catalyst, 15 g solvent, 170 °C, 16 h. Adapted from ref. [56].

This shows that the already fairly complex reaction system can be tuned for high selectivity towards the retro-aldol product ML by using the appropriate concentration and source of alkali. Furthermore, the effect of adding alkali was found to extend to all simple monosaccharaides (Figure 4.13), enabling more flexibility in the choice of sugar.

Although it is still being investigated exactly how alkali salts improve the selectivity of the catalyst towards methyl lactate, as it was mentioned earlier, the alkali seems to be related to the tin in the material. This has also been corroborated by IR studies done by Otomo *et al.*[46] Alkali cations could modify the active tin site in the catalyst by exchanging onto adjacent Brønsted acid sites either as silanol group from a defect or a partially hydrolyzed site.[69, 90] Alkali could however also exchange onto other types of Brønsted acid sites formed from a defect-rich

structure or aluminum left in the framework in post-synthesized materials. Additionally, purely siliceous Beta has been shown to facilitate the hydrolysis of sucrose indicating that Brønsted acidic exchange positions could be present in highly defect-free materials.[18] For all these cases, the improvement in selectivity would arise from the neutralization of Brønsted acidity, limiting the formation of unwanted byproducts.

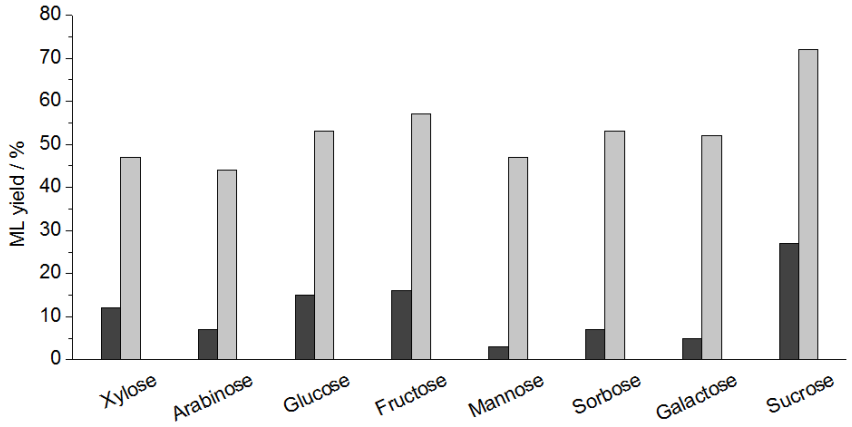

Figure 4.13. Yield of methyl lactate obtained in the conversion of various mono- and disaccharides using Sn-Beta (125, PT) in the absence (dark) and presence (light) of alkali during reactions. Reaction conditions: 0.150 g Sn-Beta (125, PT), 1.31 mmol sugar substrate, 15 g of methanol or a solution of 0.17 mM K_2CO_3 in methanol, 170 °C, 4 h, 700 rpm stirring.

4.2 **Conclusion**

It is shown here that the presence of alkali salts has a significant effect on the selectivity of tin-containing silicates catalysts for the conversion of sucrose to methyl lactate. The alkali salt can be added during the preparation of the catalyst, either by adding the metal compound directly to the template during synthesis through the hydrofluoric acid route, or by impregnating a post-treated Sn-Beta zeolite with the alkali metal. In both cases, the yield of methyl lactate increased more than twofold from 20-25% to 66-71%.

It was found that the positive effect of alkali salts on the ML yield can be obtained simply by adding the alkali salt directly to the reaction medium. Instead of depending on alkali to be included during preparation. The latter would result in high risk of leaching during continuous operation. By adding the appropriate amount of alkali directly to the reaction feed it was possible to achieve the same or greater positive effects on the ML yield. It was found that the concentration of alkali used was specific to the individual stannosilicates and that an optimum could

be found using K_2CO_3. Using this approach, it was possible to achieve ML yields in the range of 72-75% using both Sn-Beta prepared by hydrothermal synthesis and through post-synthesis methods. This is an important finding as it enables the use of more industrially feasible stannosilicate materials such as post-treated materials, which could lead to a faster industrialization of the process. Furthermore, it was shown that the beneficial effect of adding alkali can be extended to non-zeolite materials, here shown for Sn-MCM-41 and Sn-SBA-15.

From this it can be concluded that the total amount of alkali ions present in the reaction, both in the catalyst and in solution, is essential to reach a high ML yield. The amount of alkali has to be optimized for every salt and each specific catalyst.

5
Formation of Novel Biomonomers in the Absence of Alkali§

Chapter 4 has shown the optimization of the yield of a very promising biomonomer; methyl lactate (ML). It was found that the presence of alkali during reaction has a strong effect on product selectivity in the conversion of sugars using stannosilicates. The effect was furthermore found to be most pronounced for Sn-Beta leading to ML yields of up to 75%. The mechanism for this effect is however not yet fully understood. As a result, it is important to look at the reactions taking place and the products formed in the absence of any additives to better understand and further optimize this catalytic system.

The main objective of this chapter is to better understand the reaction pathways involved in the Lewis acid catalyzed conversion of carbohydrates. Using a combination of advanced NMR spectroscopy and gas chromatography, an entirely new pathway from sugars was discovered leading to a variety of interesting new products. As a result, it was possible to produce and identify several interesting new products from both pentose and hexose sugars using a variety of stannosilicate catalysts. These new products include highly functional α-hydroxy acid esters; *trans*-2,5-dihydroxy-3-pentenoic acid methyl ester (DPM) and *trans*-2,5,6-trihydroxy-3-hexenoic acid methyl ester (THM) were produced in acceptable yields (18-33%). Additionally, to investigate the potential of these new biomass-derived esters for polymer production, co-polymerization of DPM was performed.

§ This chapter is based on Tolborg *et al. Green Chem.,* **2016**, *18*, 3360 and Elliot *et al., RSC Adv.,* **2016**, *in press.*

5.1 Results and discussion

5.1.1 Identification of new α-hydroxy esters and lactones

The pronounced effect of alkali metal salts on the selectivity towards ML demands a further understanding of all the additional products formed from sugars. Especially intermediates and products formed in the absence of alkali metal salts using Lewis acid catalysts require further investigation. To target this catalytic system, reaction mixtures of either pentose or hexose sugars were converted using Sn-Beta and analyzed thoroughly by NMR spectroscopy and GC-MS. Reactions were performed at 160 °C in methanol with a reaction time of 6 hours for the hexoses and 2 hours for the pentoses. In both systems a Sn-Beta catalyst was used but for hexoses this was prepared by post-synthesis and for the pentoses by hydrothermal synthesis.

As expected, analysis of the conversion of both type of carbohydrates showed the presence of unconverted sugars, methoxylated sugars and substantial amounts of the well-known retro-aldol products formed from both hemicellulosic sugars. These products include ML, methyl vinyl glycolate (MVG), glycolaldehyde dimethyl acetal (GA-DMA) and methyl 4-methoxy-2-hydroxybutyrate (MMHB) as detailed in Section 1.5. In addition to these familiar products, several other major end-products were found in the mixture, a number of which were undescribed in this catalytic system. Although clear similarities in the formed products from the pentose and hexose sugars will be detailed in a later section, for simplicity the formed products will be first be discussed originating from the conversion of hexoses and then the conversion of pentoses. The chemical structures of all the identified products can be seen represented in Scheme 5.1 on p. 92 and a list of abbreviations used can be found in Table A.6 on p. 163.

From the conversion of the hexose sugars, several well-known and anticipated products were found. One of the most abundant products are the methyl glycosides, formed from the acetalization of the initial sugar substrate with the alcohol solvent. Quantification of these sugar derivatives were done by liquid chromatography with the combined yields verified by NMR. To differentiate the methyl glycosides originating from the hexoses from those obtained from the pentoses, these are henceforth denoted MG and MX, respectively. A large group of different furanic end-products were likewise observed from GC-MS. From hexoses these are denoted 'FUR_{C6}' and include 5-(hydroxymethyl)furfural (HMF) and 5-(methoxymethyl)furfural (MMF) as well as their corresponding acetals (HMF-DMA and MMF-DMA). Small amounts of furfural dimethyl acetal (F-

DMA) and methyl levulinate (MLA) were also found present in the reaction liquid. As these are expected to be derived from the furanic products, these are also included in the combined yield of FUR_{C6}. Trace amounts of formaldehyde dimethyl acetal were also observed but not quantified.

Aside from the products expected to form from the conversion of hexose sugars using Sn-Beta, three new products were identified by multidimensional NMR spectroscopy. These include the β,γ-unsaturated α-hydroxy acid; *trans*-2,5,6-trihydroxy-3-hexenoic acid methyl ester (THM), the 3-deoxy-*γ*-lactones (DGL) covering 3-deoxy-*γ*-gluconolactone and 3-deoxy-*γ*-mannonolactone as well as 3-deoxy-gluconic acid methyl ester (DGM), see Figure 5.1. Further identification of these products can be seen in the supporting information of ref. [119].

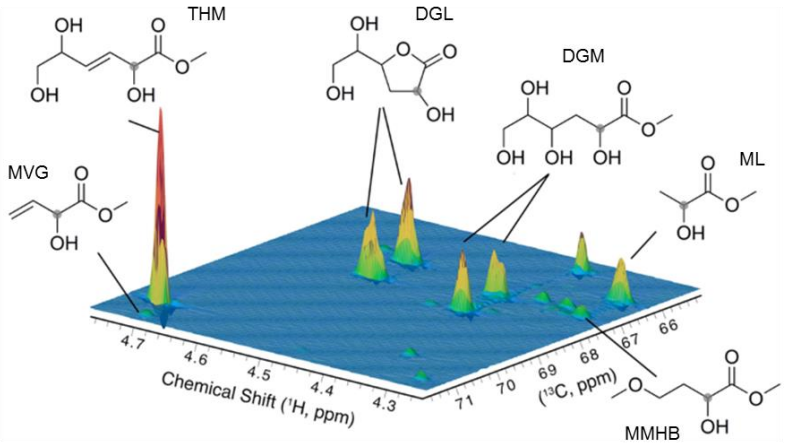

Figure 5.1. ^{1}H-^{13}C spectral region of secondary alcohol CH-groups (indicated by small spheres) of a reaction mixture produced by the catalytic conversion of glucose in methanol at 140 ºC. Figure prepared by Senior Researcher Sebastian Meier (DTU). Adapted from ref. [119].

From the pentose sugars, similar groups of products were observed. Again, a major product was the methyl glycosides (MX) and the formation of pentose-derived furanics such as furfural (F) and furfural dimethyl acetal (F-DMA), treated as one product denoted 'FUR_{C5}'. In addition to the anticipated products, several new compounds were observed, homologous to those identified from the hexoses. These new products include the α-hydroxy acid *trans*-2,5-dihydroxy-3-pentenoic acid methyl ester (DPM), the 3-deoxy-γ-pentonolactones (DPL) as well as 2,4,5-trihydroxypentanoic acid methyl ester (TPM) and 2,5-dihydroxy-4-methoxy pentanoic acid methyl ester (DMPM).

Out of these previously unidentified compounds, especially THM and DPM possess very interesting structures with multiple functionalities in addition to the

α-hydroxy acid core structure. Both compounds have previously been observed in minute amounts formed as their respective acids from the alkaline degradation of sugars in their acid form in low amounts (<1%).[165, 166] Very recently, the group of Román-Leshkov uncovered the same degradation pathway in water using tin-containing catalysts showing the formation of a number of analogous products including 2,5-dihydroxy-3-hexenoic acid (DPA).[167] Due to their high degree of functionality including both a vinyl group and one or more alcohol groups, many potential applications can be foreseen as a monomer or an additive in the synthesis of materials with improved properties.[164, 165] Implemented in a polymer these functional esters could be post-functionalized to yield materials with improved properties as it has been shown for comparable chemicals by the group of Sels.[116]

5.1.2 **Reaction pathway**

The reaction scheme for the conversion of both pentose and hexose sugars to the retro-aldol products has already been studied in much detail.[16, 18] This pathway has been proposed to involve a cascade of reactions as described in **Chapter 1** for the hexoses (Scheme 1.4 on p. 20). In brief, from hexoses this pathway involves an initial retro-aldol cleavage of fructose to yield the triose sugars. These smaller sugars then undergo β-dehydration to yield the 1,2-dione intermediate pyruvaldehyde, which can then react with the alcohol solvent and undergo 1,2-hydride shift to yield methyl lactate.[99] For the formation of MVG, this reaction undergoes the same sequence of reaction only with the retro-aldol cleavage taking place from the aldohexoses (glucose or mannose), and the formed 1,2-dione intermediate being the tetrose-derivative vinyl glyoxal.[18, 118] Both α-hydroxy esters ML and MVG are the products of an almost identical sequence of retro-aldol reaction, β-dehydrations and 1,2-hydride shifts. From these similarities, it is clear that tin efficiently catalyzes this type of transformations (β-dehydration to 1,2-dione and 1,2-hydride shift) independent of the type of sugars, and that this reactivity could extend to also include the larger pentose and hexose sugars. With this in mind and the products identified above, it is possible to propose a reaction pathway going through completely analogous 1,2-dione intermediates derived from either the pentose or hexose sugars. This pathway shows the key intermediates involved in the formation of the new biomonomers DPM and THM as well as the other newly reported co-products. An overview of the intermediates from sugars (C_3 to C_6) can be seen in Scheme A.1 on p. 157.

Scheme 5.1 (on p. 92) shows a simplified reaction schematic of the possible products formed when converting the hemicellulosic sugars. The scheme is

constructed to show the products starting from either the hexoses (top) and the pentoses (bottom) to emphasize the similarities between the conversion of the two sugars. Furthermore, the formed products are divided into three overall pathways: 1) the formation of methyl glycosides, 2) the formation of retro-aldol products shared for both pentoses and hexoses, and finally 3) the proposed formation of the newly identified products through a number of β-dehydration reactions.

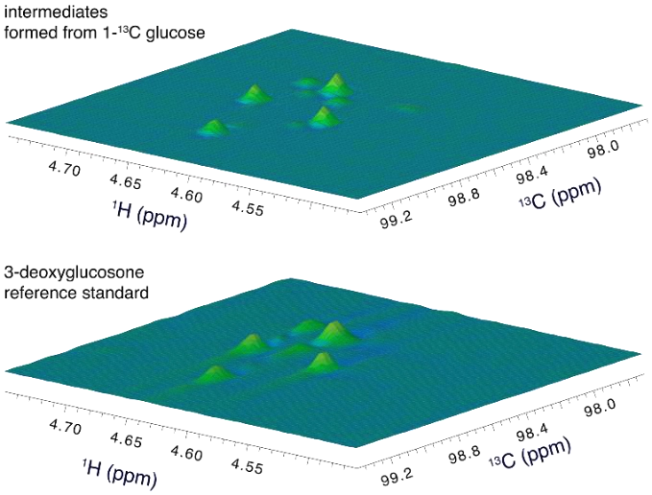

Figure 5.2. Identification of 3-deoxyglucosone (3DG) by comparison of the acetal region between a reaction mixture and a reference standard by 2D ^{1}H-^{13}C HSQC NMR spectroscopy. Figure prepared by senior researcher Sebastian Meier (DTU). Adapted from ref. [119].

For simplicity, I will initially focus on the β-dehydration pathway of the hexoses including the intermediates and products formed (top part of Scheme 5.1). In this case, the proposed 1,2-dione intermediate is 3-deoxyglucosone (3DG), a hexosone often reported as an intermediate in the Maillard and degradation reactions of carbohydrates.[168-171] For the conversion of glucose using Sn-Beta, this particular intermediate was indeed observed directly as the acetal of 3DG using ^{1}H-^{13}C HSQC NMR spectroscopy at low conversion. A visual comparison of the reference standard of 3DG and the observed intermediates can be seen on Figure 5.2 from the conversion of labeled 1-^{13}C glucose. The formation of this intermediate is believed to proceed by an analogous β-dehydration reaction mechanism as the one shown previously in Scheme 1.5 on p. 21 for the conversion of the trioses to the 1,2-dione intermediate pyruvaldehyde.[118, 119] The proposed mechanism can be seen in Scheme 5.2 on p. 93.

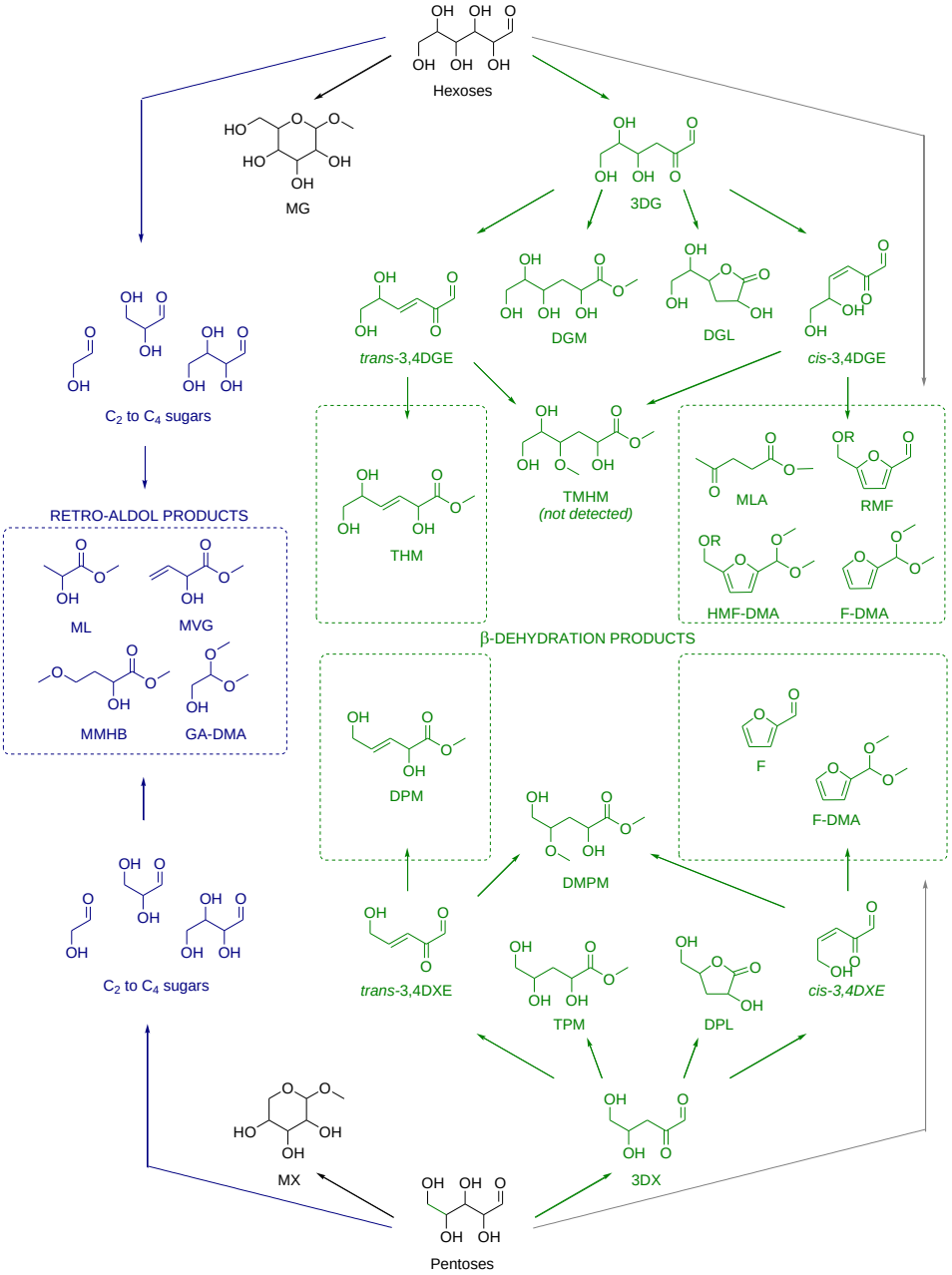

Scheme 5.1. Simplified overview of the reaction pathways leading to retro-aldol products (blue), dehydration products (green) and formation of methyl glycosides in the conversion of hexose and pentose sugars using tin-containing silicates in methanol. A detailed list of abbreviations used can be found in Table A.6 on p. 163.

The further conversion of 3DG can follow several routes. The cyclization and subsequent 1,2-hydrideshift of the 1,2-dione itself leads to the formation of the observed 3-deoxy-γ-lactones (DGL). 3-deoxy-gluconic acid methyl esters (DGM) were likewise observed, formed from the reaction between 3DG and the alcohol solvent. More importantly, however, 3DG can also undergo another β-elimination of water to yield another intermediate; 3,4-dideoxyglucosone-3-ene (3,4DGE), see Scheme 5.2. This is again entirely analogous to the intermediates 3-deoxytetrosone and vinyl glyoxal obtained from the tetroses described previously for Scheme 1.4 on p. 20.[118] Unlike 3DG, the intermediate 3,4DGE was not observed directly in the experiments, however it has been described to form from the dehydration of 3DG and is hypothesized to be an intermediate in the formation of furanic compounds such as HMF.[172-176] Moreover, it has been proposed that it is specifically the *cis*-isomer of 3,4DGE that can undergo cyclization and subsequent dehydration to yield HMF.[174] This pathway can be seen in Scheme 5.2.

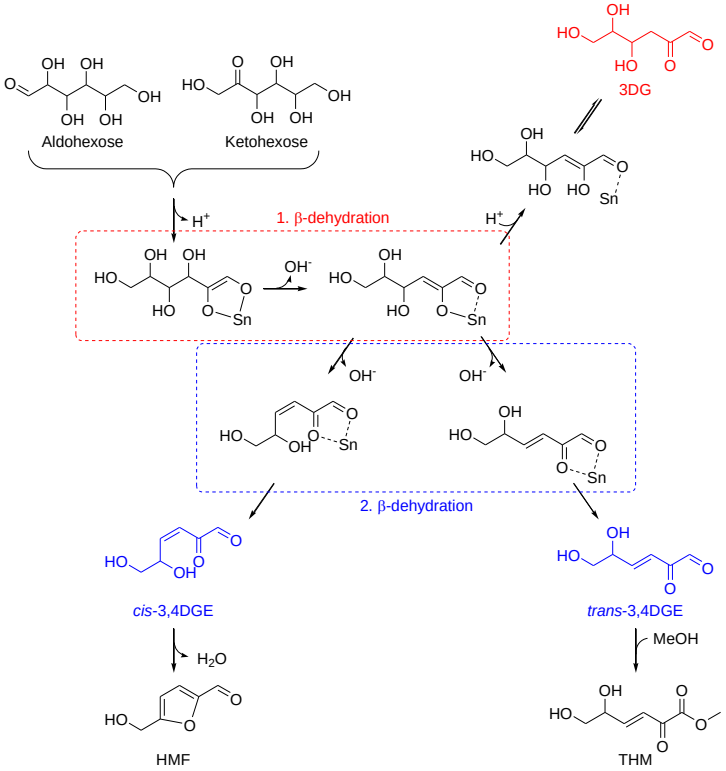

Scheme 5.2. Proposed reaction mechanism for the β-dehydrations of hexose sugars to the intermediates 3-DG (red) and *cis*/*trans*-3,4DGE (blue) showing how these intermediates relate to the products HMF and THM.[119]

The furanic end-products are known to readily form by Brønsted acid catalyzed dehydration of the fructose, also indicated on Scheme 5.1 by the grey arrow.[94, 177-179] Interestingly, Sn-Beta has previously been used in combination with different Brønsted acids to produce HMF from the glucose. In those studies, Sn-Beta was used solely for its ability to catalyze the isomerization of glucose to fructose, which could then undergo dehydration to HMF.[96, 104] Sn-Beta did not in itself comprise the strong Brønsted acidity required for the direct dehydration of the ketohexose, and as a result, groups employed the addition of a either HCl or an acidic Amberlyst resin to achieve acceptable yields by promoting this part of the reaction.[96, 104] This further corroborates the notion that furanic end-products here are formed instead by a Lewis acid catalyzed dehydration of glucose in the presence of Sn-Beta alone, as Sn-Beta simply does not possess the Brønsted acidity necessary to achieve any noticeable yields from fructose. Furthermore, only the *trans*-isomer of THM was detected in the reaction media leading to the speculation that this compound is likely formed by the conversion of the *trans*-isomer of 3,4DGE and that *cis*-3,4DGE here is converted into furanic end-products and presumably the main source of these in the absence of a strong Brønsted acid. Formation of the intermediates 3DG and 3,4DGE and their further transformation can be seen in Scheme 5.1.[174]

The conversion of 3,4DGE to THM is likewise analogous to what was described to occur for the tetrose sugars in Scheme 1.4 on p. 20. In brief, this transformation involves first reaction with the methanol on the aldehyde followed by a 1,2-hydrideshift to yield the α-hydroxy ester.[118] Addition of methanol to the unsaturation of 3,4DGE instead leads to 4-methoxy-2,5,6-trihydroxyhexanoic acid methyl ester (MTHM) following the subsequent steps as for THM. MTHM was not detected in any experiments, but is likely formed only in very small amounts as the equivalent xylose-derived compound; 2,5-dihydroxy-4-methoxypentanoic acids methyl ester (DMPM) was indeed detected.

To further support 3DG as the key intermediate in the formation of the aforementioned products, the tin-catalyzed conversion of a commercial source of 3DG was investigated. The products formed were indeed THM, a mixture of furanics and DGL, albeit with the lactones being the major components. Although this indeed shows that some of the found products including THM can be formed from 3DG, the distribution is contrary to what was obtained starting from the hexoses. In these reaction, the main products were instead THM and the combined furanics. This difference could however be explained by the complexity of the commercial sample of 3DG, which in methanol consists primarily of cyclic furanosides and pyranosides and only a small fraction found in

an acyclic form.[180] It is speculated that 3DG might have to be found in acyclic form to be reactive. 3DG formed during reaction could be kept in the acyclic form either by the confinement in the channels of Sn-Beta or while coordinated to the active site leading to THM and DGM. If this is the case, this interaction might not be reproduced with commercial 3DG leading to the different distribution. Interestingly, also small amounts of ML (1-2%) were found in the reaction mixture when 3DG was used as substrate. This indicates that 3DG could be an additional source of this retro-aldol product. It has indeed been reported that 3DG can convert into glyceraldehyde and the enol form of pyruvaldehyde.[181-183] Glyceraldehyde is readily converted into ML, and both are expected to be intermediates in the formation of ML from the larger sugars.[99, 106, 115, 184] The complex mixture found in the commercial sample of 3DG when dissolved in methanol makes it difficult however to evaluate the actual contribution of retro-aldol products through this intermediate.

Using the information gained from the hexose sugars, it is clear that the β-dehydration products obtained from the pentoses follow similar transformations involving corresponding intermediates as those shown in Scheme 5.2. From pentoses, the key 1,2-dione intermediate is 3-deoxyxylosone (3DX) which can either undergo 1,2-hydrideshift to yield 3-deoxy-γ-pentonolactones (DPL), react with the methanol solvent to yield 2,4,5-trihydroxypentanoic acid methyl ester (TPM), or further dehydrate to yield either the *trans*- or *cis*-form of 3,4-dideoxyxylosone-3-ene (3,4DXE), see Scheme 5.1. Along similar lines as for 3,4DGE, it is speculated that the *trans*-isomer of 3,4DXE leads either to the formation of the unsaturated α-hydroxy ester; *trans*-2,5-dihydroxy-3-hexenoic acid methyl ester (DPM) or 2,4-dihydroxy-4-methoxypentanoic acid methyl ester (DMPM). DPM was like THM only observed in its *trans*-configuration. DMPM is similar to DPM albeit with methanol added to the vinyl group. The formed furfural (F) and furfural dimethyl acetal (F-DMA) found in the reaction mixture is again assumed to form primarily from the *cis*-isomer of 3,4DXE.[173, 174] Like for the formation of HMF using Sn-Beta, addition of a Brønsted acid has likewise previously been found necessary to facilitate the dehydration of xylose to furfural.[185]

It is apparent that the two pathways shown in Scheme 5.1 leading from the hexoses or pentoses to either DPM or THM are very similar and involve the same sequence of reactions to form. Focusing solely on these two new products and the well-studied α-hydroxy esters ML and MVG, it is likewise clear that a family of chemicals is formed when tin-containing catalysts are used for the conversion of sugars of varying size (Figure 5.3). These products are the result of the same

overall mechanism through similar 1,2-dione intermediates leading to products with functionality increasing in step with the size of the converted sugar. The chemical structure of the α-hydroxy ester in ML forms the 'core-structure', which is then present in the structure of MVG extended with a β,γ-unsaturation and further extended in DPM and THM with either a primary or a primary and secondary alcohol groups.

The formation of these compounds both increase our understanding of the products formed in the conversion of sugars using Lewis acidic catalysts, but it also provides entirely new, highly functional chemicals.

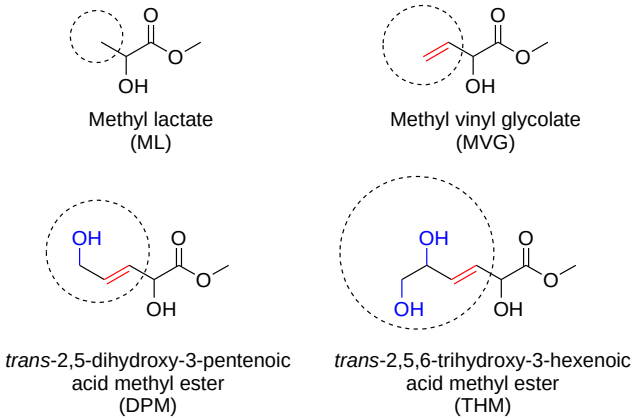

Figure 5.3. Representation of the similarities and functionalities of the α-hydroxy acid esters; methyl lactate (ML), methyl vinyl glycolate (MVG), trans-2,5-dihydroxy-3-pentenoic acid methyl ester (DPM) and trans-2,5,6-trihydroxy-3-hexenoic acid methyl ester (THM).

5.1.3 Effect of alkali on product distribution

It is clear that the conversion of sugars using tin-containing catalysts results in a range of different products, all results of a combination of retro-aldol reaction, β-dehydration or 1,2-hydride shifts. This simplifies the type of products that can form as described in the last section. The complexity of the product distribution arises from the retro-aldol/aldol reaction enabling the formation of a broad range of sugars (C_2-C_6) and thus significant increases the number of products formed, instead of simple transformations in which the carbon chain is maintained. The retro-aldol reaction has already been described in **Chapter 4** to be highly dependent on the concentration of cosolutes such as alkali metal salts in the reaction. In order to study the effect of alkali metal salts with the focus on these new products, solutions of glucose and xylose in methanol (9 wt%) were converted at 160 °C using Sn-Beta in the presence or absence of a cosolute, see

Figure 5.4. Like in **Chapter 4**, the employed alkali metal source was K_2CO_3, here used in a concentration range of 0-1.0 mM. The products shown in Figure 5.4 have been divided according to the three previously described pathways shown in Scheme 5.1 on p. 92; the methyl glycosides (MG, MX), the dehydration products (DPM, THM, etc.) and the retro-aldol products (ML, MVG, MMHB, etc.). Yields of some previously mentioned xylose-derived products such as TPM, MDPM and DPL were not quantified in these experiments. No unconverted sugars were observed under the chosen conditions.

In the absence of added alkali, it is evident that the β-dehydration products are dominant in both the conversion of glucose (Figure 5.4a, red colors) and xylose (Figure 5.4b, blue colors). Upon the addition of alkali an optimum concentration is found where the retro-aldol products instead dominate (Figure 5.4a-b, green colors), similar to what was shown for ML in **Chapter 4**.

For simplicity, I will again initially focus on the effect of alkali on the conversion of the hexoses and the impact on products formed. For these experiments a Sn-Beta zeolite prepared by post-synthesis, Sn-Beta (125, PT), was used. In the absence of alkali metal added to the reaction, a combination of dehydration products was obtained consisting of 14% THM, 6% DGL and 12% furanics (FUR_{C6}), resulting in a total carbon flux through this pathway of 32%. This number decreased significantly with the addition of alkali to a combined yield of 11% at 0.31 mM K_2CO_3. At these conditions all dehydration products decreased in yield; THM to 6%, DGL to 3% and furanic contribution to 2%. This further emphasizes that all three types of product are formed through the same intermediate species (3DG) and thus affected equally by the presence of alkali. In comparison, products formed by an initial retro-aldol reaction instead increased with the introduction of alkali. In absence, the combined yield of these products were 26% of the total carbon with ML and MVG accounting for 17% and 6%, respectively. The yield of these two ester increased to 48% (ML) and 18% (MVG) at the optimum concentration (0.31 mM). At this concentration, the total yield of retro-aldol products accounted for almost 70% of the total carbon. An increase in MMHB yield was also observed, however glycolaldehyde dimethyl acetal (GA-DMA) instead decreased slightly as the alkali content was increased. Above the optimum concentration, yields of all quantified products decreased due to alkaline degradation. From these experiments it thus becomes clear that having alkali present during reaction changes the product selectivity leading to the higher yields of ML and MVG at the expense of the dehydration products.

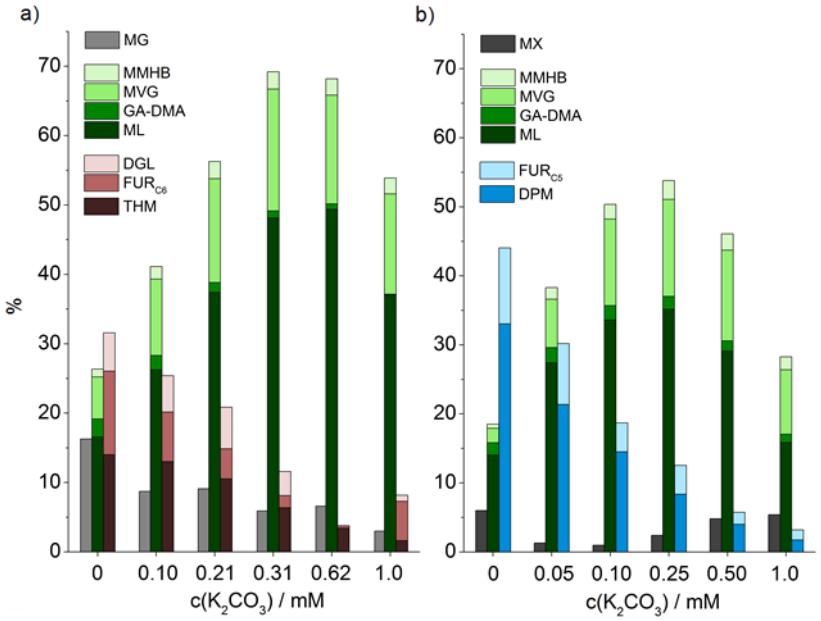

Figure 5.4. Product distribution for the conversion of glucose (a) and xylose (b) at different alkali concentrations using Sn-Beta. Reaction conditions: 0.360 g substrate, 0.180 g catalyst, 4.0 g solvent, 160 °C, reacted for a) 6 h and b) 2 h. The Sn-Beta catalyst used was in a) Sn-Beta (125, PT) and in b) Sn-Beta (150, HT).

As expected a similar influence of alkali on the product distribution was observed for the conversion of xylose. In these experiments a hydrothermally synthesized Sn-Beta zeotype, Sn-Beta (150, HT) was used. For this substrate, however, the formation of the dehydration products DPM and the furanics (FUR_{C5}) in the absence of alkali appeared even more favorable than what was found for glucose. A DPM yield of 33% was obtained as well as 11% furanics (FUR_{C5}). Under these conditions the sum of retro-aldol products was likewise lower than for glucose with a combined yield of 19% (14% ML, 2% MVG, 1% MMHB and 2% GA-DMA). At the optimum alkali concentration in this system at 0.25 mM K_2CO_3, this increased to 54% with ML and MVG making up 35% and 14%, respectively. The retro-aldol fraction even at the optimum was thus significantly lower for the conversion of xylose compared with glucose.

It is important to note, that the yields of the lactone DPL and TPM/DMPM have not been included in Figure 5.4b, while the equivalent hexose-derived compounds were included in Figure 5.4a as DGL/DGM. These additional dehydration products were only quantified using NMR in the absence of alkali and therefore not included in Figure 5.4b. Under these conditions a yield of 10%

DPL and 13% TPM/DMPM was observed (Table 5.2, entry 1 on p. 102). With these additional yields in mind, the resulting carbon flux through the 3DX pathway constitutes 68% of the total carbon when alkali is avoided. This shows that the pathway leading to the dehydration products is much more preferred for xylose than glucose. It is evident from the results shown here for both xylose and glucose that although selectivity to the retro-aldol and dehydration products can be tuned by adding or avoiding alkali, it is not possible to fully avoid either type of products. It is clear that with more control it would be possible to increase the yield of one group of products further by limiting formation of the other.

Surprisingly, it was found that even in reactions without added alkali, small amounts of sodium (~4 wt. ppm) were found to be present. In comparison, the optimum potassium content in the reaction involving glucose (0.31 mM) corresponds to roughly 30 wt. ppm. This 'background' alkali thus constitutes a small but potentially significant amount of alkali present even under 'alkali-free' conditions. This impurity was found in all investigated reactions and did not correlate to the amounts of alkali metal salts added. Instead it is likely that this contamination originates from either small levels of sodium present from preparation of the catalyst or from the reactor vessels used made from borosilicate glass. Washing the vessels prior to use with ample water or dilute nitric acid did not remove these impurities. It is therefore possible that the yields of this category of products could be increased slightly by removing also avoiding these impurities.

The effect of alkali metal salts on the reaction was furthermore evaluated for the conversion of glucose by performing a series of kinetic experiments at low reaction times using Sn-Beta (125, PT). Figure 5.5 clearly shows that the presence of alkali greatly influences the formation of products as all the investigated compounds (MG, ML, FUR and THM) were affected. A large difference was observed for the formation of methyl glucosides (MG) where the presence of alkali appeared to hinder reaction with the methanol solvent. In the absence of alkali, after only 10 min a majority of the initial hexose substrate (50%) was found in the form of MG. When alkali was added only 15% was formed. Although the formation of these by-products appeared to be somewhat reversible, shown here to decrease under both conditions, some isomers of MG are suspected to be highly stable and thus unable to undergo further conversion.[186-188] When commercially available methyl glycosides (Table 5.1, entries 1-3) were used as substrate only low conversion was achieved (3-15%) after 6 hours at 160 °C. An overview of the different isomers of the methyl glycosides can be found in Figure A.2 on p. 149.

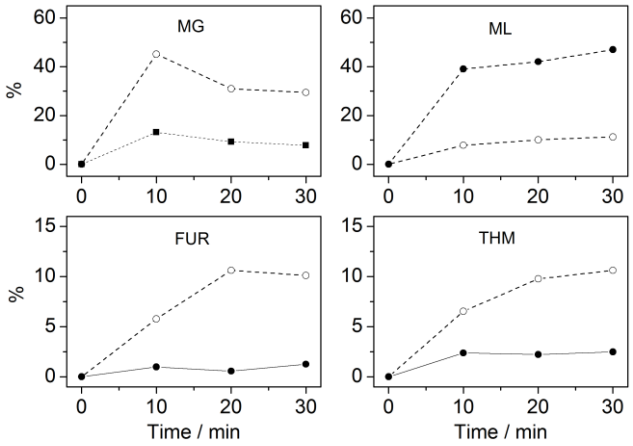

Figure 5.5. Kinetic experiment on the formation of MG, ML, FUR and THM at low conversion in the presence (*closed circle*) and absence (*open circle*) of added alkali. Reaction conditions: 0.180 g Sn-Beta (125, PT), 0.360 g glucose, 4.0 g of methanol (*open circle*) or 0.62 mM K_2CO_3/methanol (*closed circle*), 160 °C. Adapted from [119].

Table 5.1. Conversion of various commercially available methyl glycosides using Sn-Beta (125, PT), entries 1-3. Blank experiments done in the presence and absence of alkali, entries 4-5.

Entry	Catalyst	Substrate	Sugar	MG	ML	GA-DMA	MVG	MMHB	FUR	THM
			%							
1	Sn-Beta (125, PT)	Methyl *a*-D-glucopyranoside	-	85	1	<1	1	<1	<1	<1
2	Sn-Beta (125, PT)	Methyl *β*-D-glucopyranoside	-	82	1	<1	1	<1	<1	<1
3	Sn-Beta (125, PT)	Methyl *a*-D-mannopyranoside	-	97	2	<1	<1	<1	<1	<1
4	-	Glucose	78	18	<1	<1	<1	<1	1	<1
5[a]	-	Glucose	39	34	<1	<1	<1	<1	2	<1

a) Solvent used was 0.62 mM K_2CO_3/methanol. Abbreviations can be found in Table A.6 on p. 163. Reaction conditions: 160 °C, 360 mg substrate, 4 g methanol, 180 mg catalyst, 6 hours, 600 rpm stirring.

Even after 6 hours at 160 °C roughly 16% of the initial glucose is found as these potentially unreactive methyl glycosides in the absence of alkali (Figure 5.4a on p. 98). Hindering the formation of this unwanted by-product could therefore

lead to higher overall yields as more carbon is available for conversion to desirable products. In line with previous studies, no methyl furanosides were observed presumably due to their higher reactivity.[187]

Looking at the formation of ML compared with both FUR and THM in Figure 5.5, it is clear that where the yield of ML increases significantly in the presence of alkali metal salts, the opposite is true for FUR and THM. When alkali is avoided from the reaction, up to 11% of THM is obtained after 30 min compared with only a few percent when alkali is present. This again shows the influence of these cosolutes on the selectivity towards different products and highlights the fact that certain products appear to react similarly to the change in conditions.

5.1.1 Catalyst variations

Testing a range of different catalysts showed that the formation of DPM and THM from their respective sugars was more dependent on the incorporated metal (Sn, Ti, Zr or Al) rather than on the structure type of the catalyst (MFI, *BEA, etc.). The most important catalysts have been collected in Table 5.2 with additional results shown in Table A.4 and Table A.5 on p. 161-162, respectively. Significant yields (10-33%) of DPM or THM were obtained exclusively when tin was present in reaction. All tested stannosilicate materials (Table 5.2, entries 1-4, 8-10) were found to yield DPM from xylose, and all but Sn-MFI (Table 5.2, entry 11) likewise catalyzed the dehydration of glucose to THM. As can be seen from the difference in obtained yields from xylose and glucose, the intermediate 3DX again appears to form more readily from pentoses leading to significantly higher yields from this starting substrate. The highest achieved yields from the two sugars; 18% from glucose and 33% from xylose is in line with previous findings using Sn-Beta, where the yield of the formed α-hydroxy esters increase as the length of sugar decrease; 56% MVG was obtained from tetroses and >95% ML from trioses.[16, 99]

Although Sn-MFI was found able to convert the pentoses, yielding 11% DPM (Table 5.2, entry 3), less than 1% of THM was observed from glucose (Table 5.2, entry 10). This is likely a result of the smaller channels present in the MFI zeolite framework compared with those in *BEA. Although the pore channels are only slightly smaller, this difference in size has been shown (as mentioned in **Chapter 1**) to have a large impact on the conversion of the larger pentose and hexose sugars.[100, 117] Exploiting this difference in size for shape-selective catalysis is the main focus of **Chapter 6**.

Table 5.2. Conversion of xylose (entries 1-7) and glucose (entries 8-14) in the absence of alkali metal salts using a variety of catalysts. Adapted from ref. [119] and [128].

Entry	Catalyst	Sugars		Retro-aldol products					Dehydration products				
		Uncon.	MX	GA-DMA	ML	MVG	MMHB	Total	DPL	TPM/DMPM[a]	FUR_{C5}[b]	DPM	Total
		%		%					%				
1	Sn-Beta (150, HT)	n.d.	4	2	14	2	<1	19	10	13	11	33	68
2	Sn-Beta (125, PT)	n.d.	23	3	11	<1	<1	15	6	9	17	23	55
3	Sn-MCM-41 (150, HT)	n.d.	23	4	12	<1	<1	18	6	14	20	16	57
4	Sn-MFI (100, HT)	<1	30	6	17	1	<1	24	3	3	10	11	27
5	Ti-Beta (150, HT)	<1	48	7	11	3	<1	22	4	7	5	<1	16
6	Zr-Beta (150, HT)	<1	39	12	10	2	<1	25	2	2	4	<1	9
7	Al-Beta (150, HT)	6	82	n.d.	n.d.	n.d.	n.d.	<1	n.d.	n.d.	1	n.d.	1
	Catalyst	Uncon.	MG	GA-DMA	ML	MVG	MMHB	Total	DGL/DGM[c]		FUR_{C6}[d]	THM	Total
		%		%					%				
8	Sn-Beta (150, HT)	n.d.	8	1	24	8	1	34	N/A		9	17	25
9	Sn-Beta (125, PT)	n.d.	13	3	17	6	1	27	6		13	14	33
10	Sn-MCM-41 (200)	n.d.	16	3	26	5	3	37	N/A		13	18	31
11	Sn-MFI (400, HT)	n.d.	40	8	8	4	<1	20	N/A		<1	<1	<1
12	Ti-Beta (150, HT)	n.d.	14	3	28	6	1	38	N/A		3	3	6
13	Zr-Beta (150, HT)	n.d.	27	5	25	7	<1	37	N/A		2	3	5
14	Al-Beta (12.5, C)[e]	n.d.	32	<1	<1	<1	<1	<1	N/A		14	<1	14

Combined yields of a) TPM and DMPM, b) F and F-DMA, c) DGL and DGM, d) HMF and MMF and the acetal derivatives and MLA. e) commercial Al-Beta zeolite (Si/Al = 12.5, Zeolyst). n.d. = not detected, N/A = not available. Abbreviations are described in Table A.6 on p. 163. Reaction conditions: 160 °C, 0.360 g glucose (entries 1-7) or xylose (entries 8-14), 4 g methanol, 0.180 mg catalyst, 2 h (entries 1-7) or 6 h (entries 8-14), 600 rpm stirring.

The highest yield of DPM of 33% (Table 5.2, entry 1) was achieved using Sn-Beta (150, HT) as described earlier. The total products formed through the β-dehydration pathway accounted for 68% of the total carbon (leading aside from DPM to 10% DPL, 13% TPM/DMPM and 11% FUR_{C5}). With the dehydration pathway as the dominant route, only 19% of retro-aldol products were obtained with ML making up 14%. This gave a total mass balance of 91%, thereby accounting for almost all the carbon present during reaction. Using a similar hydrothermally synthesized Sn-Beta catalyst for glucose (Table 5.2, entry 8) yielded 16% THM as well as 9% FUR_{C6}. The yield of DGL/DGM was not quantified for this catalyst, making the total accounted carbon from the dehydration pathway only 25%. From glucose, DGL/DGM was only quantified for the post-synthesized catalyst Sn-Beta (125, PT) resulting in a combined yield of only 6%. These two products are thus not expected to substantially increase the total carbon from the dehydration pathway.

The highest yields of THM were obtained using Sn-Beta prepared by hydrothermal synthesis yielding 17% and Sn-MCM-41 (150, HT) giving 18%. The latter yielded comparable contributions from both the retro-aldol (37%) and dehydration (31% excluding DGL/DGM) pathways. Sn-MCM-41 has previously shown to possess similar catalytic properties to Sn-Beta both in the presence and absence of alkali (see **Chapter 4**).[13, 40, 56, 117]

Using a Sn-Beta catalyst instead prepared by the post-synthesis protocol lead to a small decrease in THM yield (14%) and a significant decrease in yield of DPM (23%), see Table 5.2, entries 2 and 9. A similar decrease in yield of retro-aldol products was observed. Instead, formation of methyl glycosides (both MG and MX) as well as the yield of furanics increased for both substrates. Both types of products are readily formed by Brønsted acid catalyzed dehydration and are here likely formed as a result of residual aluminum still present in small amounts after dealumination or from the presence of defects known to be more pronounced in this type of material.[187, 188] The difference in activity could, however, also originate from fundamental difference in the environment surrounding the active site as has recently described recently by the groups of Sels and Hermans.[59, 78, 81]

Ti-Beta and Zr-Beta, likewise solid Lewis acids, are known to catalyze the many of same type of reactions as Sn-Beta as exemplified in **Chapter 1**.[16, 31, 37, 189] Changing the incorporated metal for the conversion of xylose and glucose, however, lead to almost no β-dehydration products. Very low yields of DPM (<1%) and THM (3%) were obtained and the formation of furanics ranging from 2-5% (Table 5.2, entries 5-6 and 12-13). This shows that the pathway leading

to the different dehydration products indeed is exclusively catalyzed with tin as the active site. The substantial decrease in yield of both product groups (DPM/THM and the corresponding furanics) again corroborates the formation of these compounds through similar pathways through 3DX/3DG. Compared with Sn-Beta, the retro-aldol product distribution and yields were found to be largely unaffected by the change in element. Only GA-DMA gave significantly higher yields using Ti- and Zr-Beta (up to 7%). Concurrently, the amounts of sugar found as methyl glycosides were significantly higher using these catalysts with for instance up to 48% MX obtained for Ti-Beta (200, HT). These findings seem to indicate that the dehydration pathway and thereby the formation of either 3DX or 3DG are much more dependent on the Lewis acidic element than the fragmentation. Furthermore, despite being found to achieve similar yields of ML and MVG compared with Sn-Beta in the absence of alkali, no effect of adding K_2CO_3 was found using Zr-Beta (not shown), hindering the high yields of retro-aldol products obtained in **Chapter 4**.[119] This also indicates that only the local environment of the tin site is affected by the alkali effect, further underlining that some degree of ion-exchange can take place either directly on the tin site or in the near vicinity as also speculated in **Chapter 4**.[56] To further corroborate the importance of the strength of the active site, the conversion of xylose and glucose was followed using Beta zeotype materials prepared either without an active metal, Si-Beta (HT), (Table A.4, entry 11 and Table A.5, entry 12 on p. 161-162) or using nanosized SnO_2 particles as the tin source instead of $SnCl_4 \cdot 5H_2O$ yielding SnO_2-Beta (200, HT) (Table A.4, entry 10 and Table A.5, entry 11).[119] For both catalysts, no formation of DPM or THM was observed. The same was found from blank experiments (Table A.4, entry 12 and Table A.5, entry 4).

It was speculated in Section 5.1.2 that the dehydration through the 1,2-dione intermediates 3DX/3DG were likely not catalyzed by conventional strong Brønsted acid catalysts. To confirm this aluminum-containing Beta catalysts were prepared by hydrothermal synthesis and acquired commercially. The commercial zeolite was also tested after having underwent dealumination, as this was parent material used for the preparation of Sn-Beta (125, PT). For all tested aluminosilicates, no DPM/THM was formed from either sugar substrate (Table A.4, entries 7, 14 and Table A.5, entries 9-10). Instead high degrees of degradation and methyl glycosides were observed as well as some degrees of furanics (up to 14%). The current findings seem to indicate that tin sites present in both crystalline and amorphous silicates are fully capable of catalyzing the dehydration reaction required for the formation of DPM and THM and that an increase in

strong Brønsted sites (as is the case for residual aluminum present in post-synthesized Sn-Beta) instead leads to furanics.

This shows that using a variety of tin-containing catalysts it is possible to obtained acceptable yields of entirely new products directly in a 'one-pot' reaction from xylose and glucose. Still, more work is required to improve these yields in order to develop industrially relevant processes for these chemicals.

5.1.2 **Polymerization of DPM**

Both DPM and THM are highly functional molecules containing several alcohol groups (both primary and secondary) and a vinyl group in the backbone. To investigate the polymerization potential of these new α-hydroxy ester it was decided to focus exclusively on DPM due in part to the higher achieved yields (up to 33%) and the slightly lower functionality of this monomer compared with THM. It was estimated that polymerization of this ester would be more selective due to the fewer alcohol groups. The approach chosen for testing DPM as a building block follows the work done by Dusselier *et al.* on the polymerization of MVG.[116] In this work, vinyl glycolic acid (VGA, obtained by hydrolysis of MVG) was co-polymerized with lactic acid (LA) as conceptual proof. Poly(lactic acid) as mentioned previously is an already utilized bio-derived plastic, but the polymer has a number of drawbacks including high hydrophobicity and the lack of functional side groups available for post-functionalization.[190-192] Dusselier *et al.* showed that these limitations of the polymer could be improved by incorporating small amounts of VGA (up to 12%) into the structure. The unsaturation present in VGA thus afforded pendant vinyl groups in the polymer, allowing for further functionalization.[116, 193-195] Recently, using metathesis reaction, MVG was converted into dimethyl 2,5-dihydroxy-3-hexenedioate and likewise co-polymerized with LA.[120, 121] The same approach was also used for diethyl 2-methylene-4-oxopentanedioate (an itaconic acid ester analogue).[196, 197] Both of these products, resemble somewhat DPM/THM in terms of functional groups.

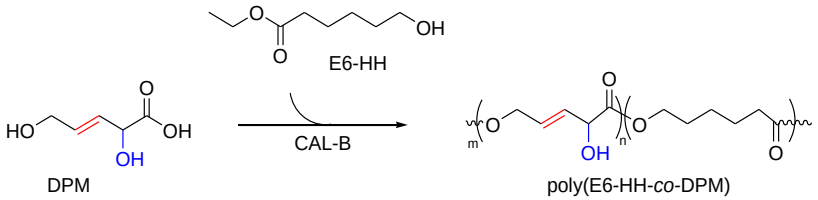

Scheme 5.3. Schematic of the desired product obtained when co-polymerizing ethyl 6-hydroxyhexanoate (E6-HH) with trans-2,5-dihydroxy-3-pentenoic acid methyl ester (DPM) using *Candida Antarctica* Lipase B (CAL-B).

Due to the increased functionality of DPM it was not possible to directly follow the experimental procedure described for the polymerization of VGA.[116] The tin-based polymerization catalysts used in that study were unfortunately not suitable here due to a low control of selectivity from the additional alcohol present in DPM. Instead, it was chosen to perform a conceptual proof by exploiting the added control of selectivity from enzymatic polymerization using *Candida Antarctica* Lipase B (CAL-B).[198, 199] Co-polymerization was done using ethyl 6-hydroxyhexanoate (E6-HH).[200] E6-HH is obtained from hydrolysis of ε-caprolactone. Polymerization was performed by mixing E6-HH with DPM in a molar ratio (MR) of 0.22 using the enzyme CAL-B under vacuum at 60 °C for 18 h. Ideally, this would lead to the formation of a linear polymer with a 1,5-linkage and both the secondary and the vinyl group available for post-functionalization. This co-polymer is denoted poly(E6-HH-*co*-DPM), see Scheme 5.3. That the polymerization was indeed successful was verified by both NMR and FT-IR spectroscopy. Using these techniques the presence of the vinyl group (^{1}H NMR, C-11 and -12 in Figure 5.6) was confirmed as well as the alcohol, alkane and ester groups observed from characteristic bands in IR at 3496 cm^{-1} (O-H stretch), 1721 cm^{-1} (C=O stretch) and 1159 and 1045 cm^{-1} (C-O stretch), see Figure A.11. The vinyl group was likewise observed in the IR spectrum as a shoulder on the C=O stretch and a strong C=C bend signal at 961 cm^{-1}.

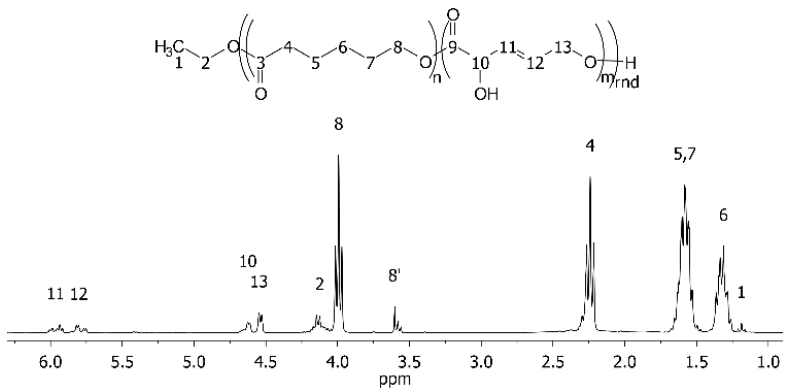

Figure 5.6. ^{1}H NMR assignment of poly(E6-HH-*co*-DPM). Figure prepared by Research Assistant Christian Andersen (DTU) for ref. [128].

Although a MR of 0.22 was targeted in the preparation of the polymer, only roughly half of the DPM was found to co-polymerize and incorporate in the polymer. This instead lead to an obtained MR of 0.12 (Table 5.3, entry 1). Increasing the reaction time from 18 to 72 h, led to an increase in the

incorporation of DPM up to 0.17 (Table 5.3, entries 1-3), *i.e.* to a degree of incorporation of ~78%. This increase in MR resulted in an increase in the molecular weight of the polymer (M_w, from 10,050 to 12,350 g/mol) but also in a less uniform polymer as the dispersity likewise increased (*Đ*, from 2.1 to 2.5). Dispersity is defined as the molecular weight of the polymer (M_w) over the number-average molar mass (M_n). For both prepared polymers, the values of *Đ* are comparable to those found in similar systems for the polymerization of monomers with both primary and secondary alcohol groups.[198, 199] Increasing the target MR led to a higher degree of insertion of DPM (up to 0.66), but simultaneously led to a significant decrease in the molecular weight of the formed polymers (down to 3,700 g/mol, Table 5.3, entries 4-5). This could indicate that an optimum MR exists for the incorporation of DPM, as it was likewise not possible to form a homopolymer using the ester.

Table 5.3. Properties and characterization of poly(E6-HH-*co*-DPM) products obtained from enzymatic co-polymerization of E6-HH and DPM using CAL-B. Table prepared by Research Assistant Christian Andersen (DTU) for ref. [128].

Entry	Time	Feed	Product	T_g[c]	T_m[c]	M_n[d]	M_w[d]	*Đ*[d]
	h	MR[a]	MR[a,b]	°C		g/mol		
1	18	0.22	0.12	-47.8	42.5	5,150	10,050	2.1
2	42	0.22	0.14	-47.3	42.5	4,490	10,750	2.4
3	72	0.22	0.17	-48.0	34.6	5,000	12,350	2.5
4	72	0.44	0.44	-55.5	15.2	1,900	4,500	2.4
5	72	0.66	0.66	-52.0	7.5	1,760	3,700	2.1
6[e]	18	0	0	-61.4	48.9	3,600	4,700	1.3

a) Molar ratio (MR) listed as DPM/E6-HH (mol/mol). b) Determined by ^{1}H NMR. c) Determined by DSC. d) Dispersity (*Đ* = M_w/M_n) determined by SEC in THF using PS standards. e) Using only E6-HH as monomer. Reaction conditions: 60 °C, pressure held at 200 mbar for 2 h then reduced to 5 mbar.

The thermal properties of the prepared polymers were investigated using differential scanning calorimetry (DSC), see Table 5.3. The highly flexible properties of these co-polymers were confirmed by the measured glass transition temperature (T_g) ranging from -49 °C to -56 °C. The inclusion of DPM in the E6-HH polymer strongly influenced the melting temperature (T_m) of the material decreasing from ~49 °C for the homopolomer of E6-HH to as low as 7.5 °C at a MR of 0.66. For incorporation of DPM lower than 0.15 the temperature was still above 42 °C. Additionally, further post-functionalization was done on the

prepared polymer and included in ref. [128], indeed showing the high functionality of the formed materials. Although more work is required to fully illuminate the use of these newly discovered α-hydroxy esters as monomers, the work presented here shows proof of high molecular weight polymers prepared from the co-polymerization of DPM.

5.2 **Conclusion**

In this chapter it was shown that aside from the retro-aldol cleavage of sugars, leading to the formation of a variety of retro-aldol products, a secondary reaction pathway exists involving the Lewis acid catalyzed β-dehydration of the sugars. The investigation of this new pathway led to the identification of several new products obtainable directly from pentose and hexose sugars including the DPM and THM and the lactones DGL and DPL. By avoiding the presence of alkali metal salts during reaction of the sugars with the tin-containing catalysts, it was possible to obtain DPM and THM in acceptable yields of 18-33%. The dependence on cosolutes in the reaction media showed that it was possible to tune the reaction leading either to the formation of high yields of retro-aldol products (as was also touched upon in **Chapter 4**) or to the so-called dehydration products. Further work is still required to fully unveil how alkali modified the stannosilicate selectivity. Additionally, alkali salts were found to reduce the formation of methyl glycosides resulting in more free sugar available for conversion than in the absence of alkali. This pathway was found to be primarily catalyzed by tin and could be formed with a wide variety of tin-containing catalysts with acceptable yields achieved for using both Sn-Beta and Sn-MCM-41.

The identified β-dehydration pathway was found to be analogous in the conversion of both the pentose and hexose sugars. Both reactions involved the formation of a 1,2-dione intermediate; 3DG (from hexoses) or 3DX (from pentose). The intermediates were either converted directly into products or underwent another β-dehydration to yield 3,4DGE or 3,4DXE, respectively. Depending on the *cis*/*trans*-isomerism of the intermediate either THM/DPM (*trans*) were formed or furanic end-products (*cis*). Additionally, DPM was used for the co-polymerization with E6-HH using enzymatic polymerization, leading to highly functional polyesters with a 0.17 to 0.66 molar ratio content of DPM.

This shows that new, highly functional α-hydroxy acid ester can be formed in the presence of a variety of stannosilicates from both pentose and hexose sugars when alkali metal salts are avoided during reaction. With further optimization and better understanding of the role of the interaction between the alkali salt and the stannosilicate, I believe that the yields of these products can be further improved.

6
Shape-selective Valorization of Glycolaldehyde**

The two-carbon sugar glycolaldehyde (GA) has potential to become a valuable biomass-derived platform chemical. It is currently obtained in high yields in supercritical water or as a main component in bio-oil, and other processes are presently being developed to efficiently transform sugars to GA in high yields.[201-203] GA can be catalytically converted into many interesting chemicals. For instance, ethylene diamine or ethanolamine, with application in polymer production and pharmaceuticals, can be produced by direct amination.[204] Glyoxal, glycolic acid or glyoxylic acid can be obtained by oxidation whereas ethylene glycol can be produced by hydrogenation. Alternatively, the aldehyde functionality can be employed in C-C bond formation, such as aldol condensations.[205] Selective aldol condensation of GA is the focus of this chapter.

The self-condensation of GA leading to the formation of tetrose sugars permits the production of uncommon and expensive sugars. The tetroses currently have limited potential uses, for example within pharmaceutical treatments,[206] but increased availability could provide a new platform for biomass-derived products. Especially products that are otherwise difficult to access from the cheaper pentose and hexose sugars are attractive. The sweetener erythritol for instance is currently obtained by fermentation of glucose and sucrose, but could be obtained through hydrogenation of the tetrose sugars.[207]

** This chapter was adapted from Tolborg *et al. ChemSusChem* **2016**, *9*, 3054-3061.

Under hydrothermal alkaline conditions, lactic acid has also been obtained by way of aldol condensation and subsequent conversion of GA.[208, 209]

One of the major advantages of zeolite catalysis is the ability to control product selectivity by choosing materials with suitable pore sizes.[9] Zeolites have previously been used with some success to control the condensation of formaldehyde to selectively form the triose 1,3-dihydroxyacetone.[210, 211] Recently, solid Lewis acid catalysts have been shown to achieve high selectivity in the aldol and cross-aldol reactions for the formation of a range of chemicals including the pharmaceutical precursor α-hydroxy-γ-butyrolactone (HBL).[116, 196, 205, 212-214] As mentioned in **Chapter 1**, the choice of zeolite framework has proven important in many reactions including the conversion of carbohydrates.[23, 100, 215] In brief, the large channels in Sn-Beta could easily facilitate the conversion of all monosaccharides, whereas the slightly smaller channels of the MFI framework were only adequate for the isomerization of the triose sugars.[100, 215] Exploiting this difference in size is the objective of this study, showing the influence of catalyst framework on the product selectivity in water at moderate temperatures. Here it is shown that the medium pore zeolite Sn-MFI is able to catalyze the formation of tetrose sugars and vinyl glycolic acid with high selectivity (up to 98%) resulting in a combined yield of C_4 products of up to 80% (at 90% conversion), while avoiding the formation of hexoses (<2%). Due to the mild reaction conditions (80 °C), the catalyst showed good reusability over several cycles.

6.1 Results and Discussion

6.1.1 Lewis acidic aldol condensation of glycolaldehyde

The condensation of GA with small oxygenates such as formaldehyde (FA) has long been considered a plausible pathway in the abiotic synthesis of sugars.[216-218] The most common catalysts used in this reaction include bases,[219] amino acids,[220, 221] and peptides.[222, 223] Inorganic hydroxides as well as various minerals such as borates,[224, 225] silicates,[226] and phosphates have also been studied.[217] A combined yield of tetrose derivatives of 86% was obtained using GA and borates at moderate temperatures (65 °C).[225] In the catalytic self-condensation of GA, the challenge is to control the selectivity towards tetrose sugars while avoiding the formation of hexoses.

The Lewis acid catalyzed condensation of GA was first reported by Holm *et al.* using Sn-Beta in methanol yielding the C_4-products; methyl vinyl glycolate (MVG) and methyl 4-methoxy-2-hydroxybutanoate (MMHB) as well as methyl

lactate (ML). [18] The reaction mechanism was later investigated in more detail by the group of Sels using homogeneous tin catalysts.[116] In both studies, GA underwent condensation to yield the tetrose sugars that were then immediately converted to MVG or MMHB following a cascade of reactions identical to those described in Section 1.5. In brief, the conversion of formed tetroses involved the two β-dehydration reactions yielding first the 1,2-dione 3-deoxytetrosone and then vinyl glyoxal followed by esterification and isomerization.[116, 118]

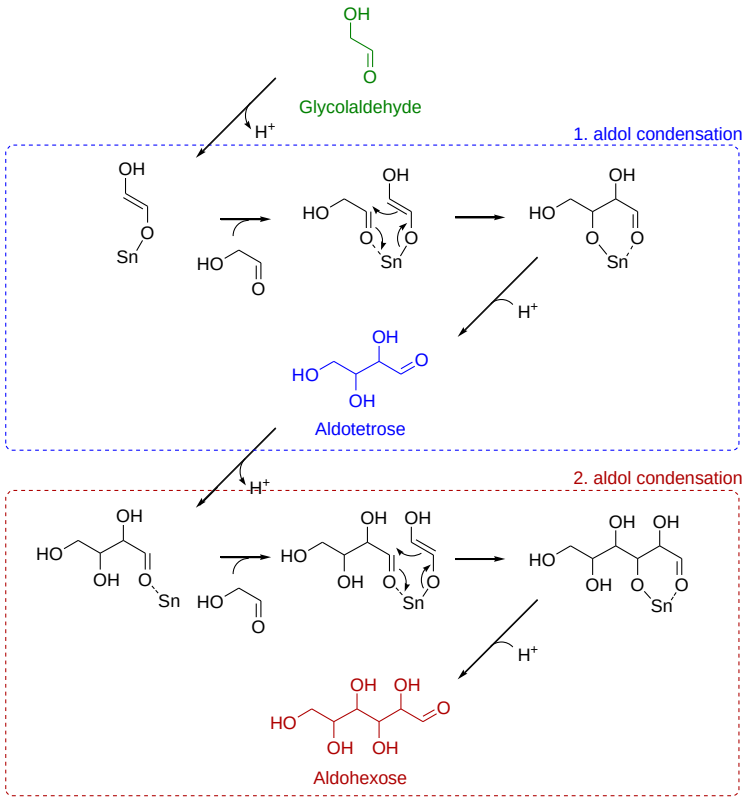

Scheme 6.1. Proposed mechanism for the Lewis acid catalyzed of the C_2 sugar glycolaldehyde (green) followed by aldol condensation to the tetrose sugars (blue) and subsequent aldol condensation to hexoses (red).

Although GA in water is known to exists in a number of forms depending on the substrate, the proposed reaction mechanism is believed to proceed through the 1,2-enol of glycolaldehyde formed upon interaction with the tin site, see Scheme 6.1. The coordination with tin is thus analogous to the proposed mechanism for the retro-aldol reaction (shown Scheme 1.3 on p. 19), facilitating the fragmentation of larger sugars at higher temperatures (>120 °C) as

investigated in **Chapters 4 and 5**. The C-C bond forming reaction then proceeds through condensation of the enol-form with another GA molecule (Scheme 6.1) yielding the aldotetroses; erythrose (ERY) and threose (THR). However, due to the ability of the solid Lewis acids to catalyze the isomerization of sugars as described earlier, a mixture of ERU, THR and the ketotetrose; erythrulose (ERU) are obtained. As mentioned above and shown on Scheme 6.1, GA can also react with the formed aldotetroses to yield even larger hexose sugars. The challenge in maintaining a high selectivity is therefore to avoid this second condensation step from taking place.

6.1.2 Catalyst preparation and characterization

To investigate whether this second condensation step could be hindered by the shape and size of the channels of the catalyst, stannosilicates with varying channel diameters were prepared and tested. The materials include Sn-MFI (pore opening of 5.5 Å), Sn-Beta (6.5 Å), Sn-MCM-41 (~30 Å) and Sn-SBA-15 (~40 Å).[23] For this chapter Sn-Beta was prepared exclusively using the fluoride route. Sn-MFI was prepared following two different approaches: 1) utilizing hydroxide ions as mineralizing agents yielding the catalyst designated Sn-MFI (100, OH^-) or 2) using fluoride ions yielding Sn-MFI (400, F^-).[61] The large difference in the nominal Si/Sn ratios was due to limitations in the preparation methods.

The structure and physical properties of the micro- and mesoporous materials were confirmed by X-ray diffraction and N_2-adsorption/desorption measurements (Table 6.1, and Figure A.3 Figure A.4 on p. 150-151). The prepared Beta and MFI zeotypes all showed high crystallinity (Figure A.3a-c). As expected, the morphology and size of the prepared Sn-MFI catalyst crystals were highly influenced by the preparation method. As mentioned in **Chapter 3**, the differences between using fluoride and hydroxide ions are caused by a difference in the supersaturation during crystallization. In fluoride-containing media, this leads to highly defect-free crystals but large in size. Scanning electron microscopy revealed that the hydroxide route resulted in the formation of small (0.5-1.5 μm), spherical crystals, whereas the fluoride route yielded much larger, prism-shaped crystals, see Figure 6.1a-b. This also explains the differences in textural properties seen in Table 6.1, entries 1-2. The capped square bipyramidal morphology of the Sn-Beta crystals with an approximate size of 5-10 μm can be seen in Figure 6.1c.[44] For both Sn-MCM-41 and Sn-SBA-15 no discernible morphology was found.[13]

Table 6.1. Structure and physical properties of the catalysts. Adapted from [117].

Entry	Catalyst	Elemental analysis	Surface area		Pore volume	
		Si/Sn[a]	S_{BET}[b]	S_{micro}	V_{total}	V_{micro}[c]
			m^2/g		mL/g	
1	Sn-MFI (100, OH^-)	82	404	273	0.25	0.14
2	Sn-MFI (400, F^-)	383	377	337	0.20	0.13
3	Sn-Beta (150, HT)	186	492	395	0.28	0.21
4	Sn-MCM-41 (150)	148	857	-	1.09	-
5	Sn-SBA-15 (200)	271	918	111	1.09	0.06

a) Determined by ICP analysis. b. BET surface area. c. Micropore volume calculated using the *t*-plot method.

Low angle X-ray diffraction (0-5° 2θ) of the ordered amorphous materials (MCM-41 and SBA-15) showed the characteristic (100), (110) and (200) reflections appearing as a consequence of diffraction from the hexagonally ordered structure (Figure A.3d-e on p. 150).[13, 41] The measured angles correspond to d_{100} spacings of ~40 and ~100 Å for Sn-MCM-41 and Sn-SBA-15, respectively. The large pore volume and surface area anticipated for these two types of materials was confirmed with N_2-adsorption/desorption showing total surface areas of ~900 m^2/g and a pore volumes of ~1.2 mL/g for both materials (Table 6.1).

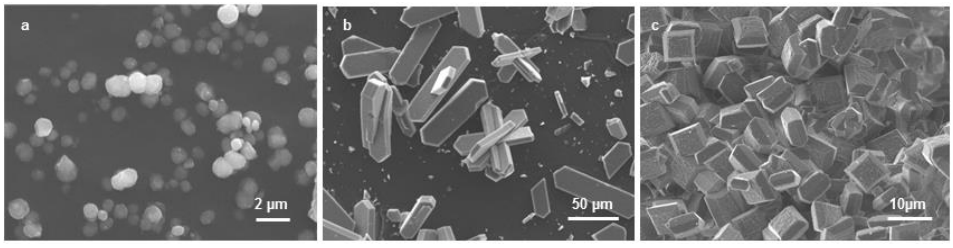

Figure 6.1. Electron micrographs of a) Sn-MFI (100, OH^-), b) Sn-MFI (400, F^-) and c) Sn-Beta (150, HT).

6.1.3 Condensation of glycolaldehyde with different catalysts

As expected in consecutive reactions where products can undergo further conversion, selectivity here was highly dependent on the degree of conversion. Furthermore, due to the difference in amount of tin incorporated in the different stannosilicate catalysts, the intrinsic activity of the individual catalysts was found to vary greatly (Figure 6.2). To allow for the comparison of the different catalysts under comparable conditions, catalysts are from this point related on the basis of conversion rather than as a function of time as is shown on Figure 6.2 for the different tin-containing catalysts.

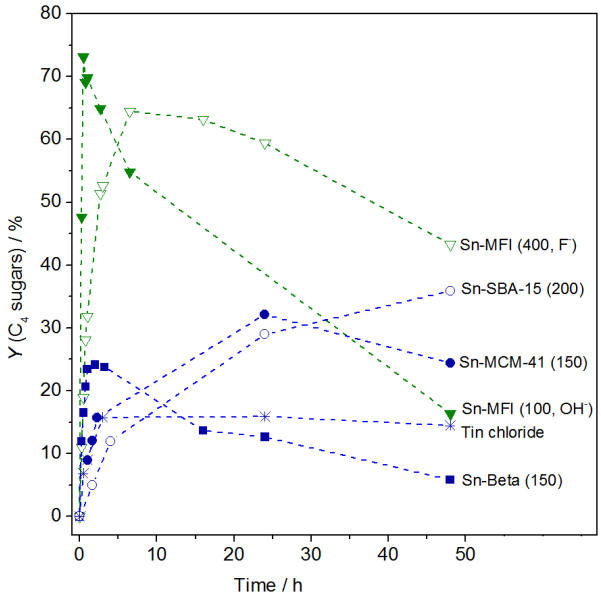

Figure 6.2. Yield of tetrose sugars obtained with different tin-containing catalysts from glycolaldehyde as a function of time. Reaction conditions: 0.125 g glycolaldehyde (dimer), 0.075 g of catalyst, 2.5 g of water, 80 °C, reaction times 1-48 h, 600 rpm. Adapted from [117].

Figure 6.3 shows the combined yield of tetrose sugars as a function of conversion for several Lewis acid and base catalysts. Apart from the stannosilicates, materials without a defined pore structure (zirconia, Amberlyst A21) and a homogeneous tin catalyst such as $SnCl_4 \cdot 5H_2O$ were used to probe the effect of the pore structure. A weak base resin, Amberlyst A21, containing dimethyl amino functional groups was used as a reference for base-catalyzed aldol-condensation.

The tested catalysts were found to fall into two different groups in terms of product yield (Figure 6.3). For the group marked in blue including Sn-Beta, Sn-MCM-41 and Sn-SBA-15, only low yields of the tetroses were obtained (up to 38%) as the formed sugars instead underwent further condensation or transformations (touched upon later). Although only low yields of tetroses were obtained using Sn-MCM-41 and Sn-SBA-15, both the stannosilicates and zirconia were found to reach high selectivity towards the C_4 sugars albeit only at a conversion below 20%.

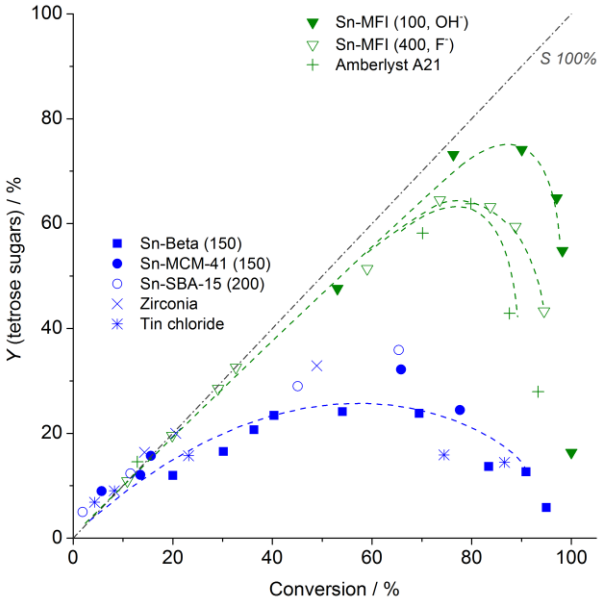

Figure 6.3. Yield of tetrose sugars obtained with different catalysts from glycolaldehyde as a function of conversion. The grey dotted line represents a selectivity of 100%. Reaction conditions: 80 °C, 5 wt% glycolaldehyde (dimer) in water, 0.075 g of catalyst, 2.5 g of water, reaction times 1-48 h. Adapted from [117].

The other group (marked in green on Figure 6.3) including both Sn-MFI zeotypes and the Amberlyst resin, all resulted in high maintained selectivity (up to 96%) towards the tetroses. All three catalysts were found to almost selectively form the tetroses up to a degree of conversion of 70-80%, where after a significant decrease in the obtained yield was observed. This drop in selectivity can be explained by the lower concentration of GA left in the reaction media. At high conversion, the probability for two molecules of GA to interact and undergo aldol condensation decreases and instead alternative reaction pathways are preferred

such as the further transformation of the formed tetroses causing the yield to drop. These additional reactions will be discussed in a later section.

From Figure 6.3 it is clear that Sn-MFI (100, OH^-) maintains a high selectivity for tetrose sugar formation to higher conversion values than all the other selective catalysts tested, resulting in a yield of 74% of tetrose sugar at 76% conversion. This yield of tetroses was furthermore obtained after only 30 min (Figure 6.2). Testing the reaction temperature in the interval from 40 °C to 100 °C was found to have little influence on the selectivity for tetrose formation when Sn-MFI (100, OH^-) was used, see Figure 6.4.

As expected, no tetrose formation was observed using purely siliceous Beta or Sn-Beta prepared using SnO_2 as the tin source (as described in **Chapter 3**). From this it can be concluded that tin incorporated in the zeolite must be the active sites for the aldol condensation as neither tin nor the silicious framework show any activity in the reaction.[16, 44]

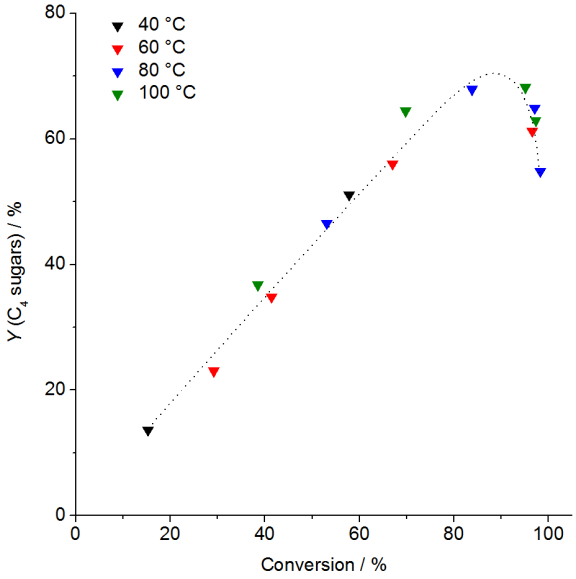

Figure 6.4. Yields of tetrose sugars obtained using Sn-MFI (100, OH^-) varying the reaction temperature. Reaction conditions: 5 wt% glycolaldehyde, 0.075 g Sn-MFI (100, OH^-), 40-100 °C, 0.08-24 h, 600 rpm stirring.

As described in **Chapter 1**, all stannosilicate materials tested here (Sn-MFI, Sn-Beta, Sn-MCM-41, and Sn-SBA-15) have been reported to also catalyze the 1,2-hydride shift enabling the isomerization of sugars, this naturally includes the tetrose sugars.[13, 18] As a result, although the aldotetroses threose (THR) and erythrose (ERY) are the product of the aldol condensation of GA, the distribution

of isomers changes over time as the ketotetrose erythrulose (ERU) is formed, see Figure 6.5a-d.[227] A different distribution of tetroses is observed for the basic Amberlyst A21 resin (Figure 6.5e) primarily THR is observed at full conversion as hardly any isomerization takes place.

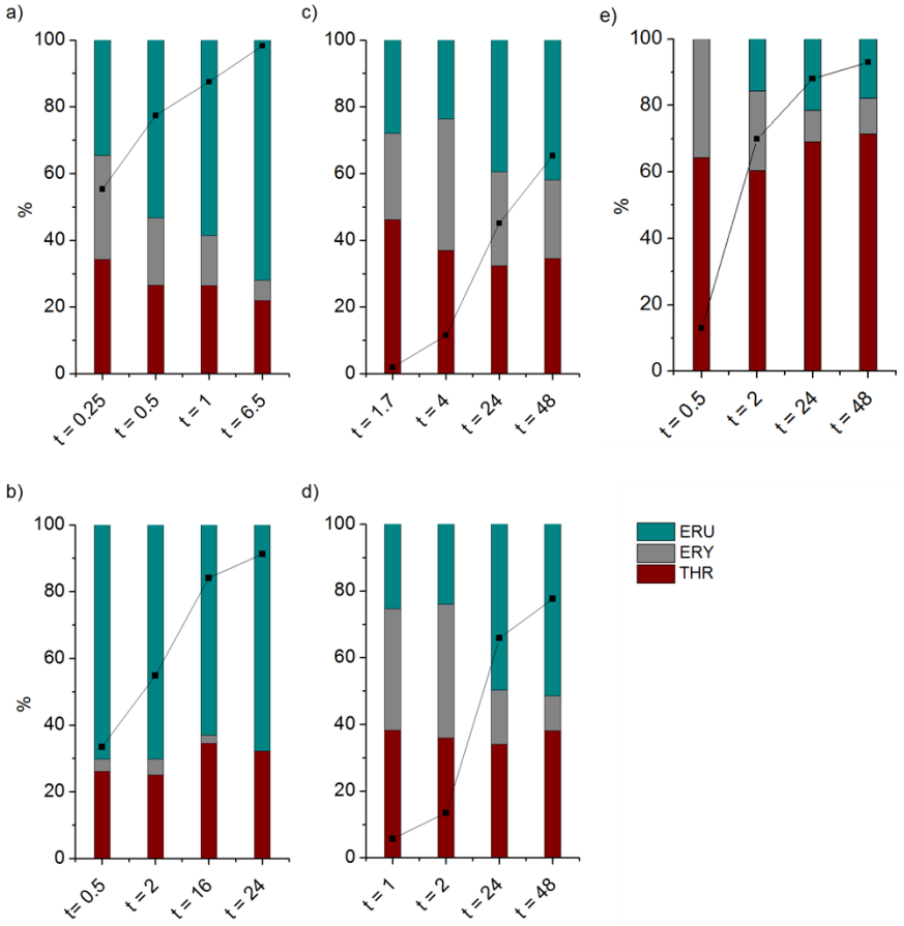

Figure 6.5. Normalized distribution of tetrose sugars obtained at 80 °C in water at different times (in hours) using a) Sn-MFI (100, OH^-), b) Sn-Beta (150, HT), c) Sn-SBA-15 (150, HT), d) Sn-MCM-41 (150, HT) and e) Amberlyst A21. The black points show conversion at each point in time. Reaction conditions: 0.125 g glycolaldehyde (dimer), 0.075 g of catalyst, 2.5 g of water, 80 °C, reaction times 0.25-48 h, 600 rpm stirring. ERU: Erythrulose, ERY: Erythrose and THR: Threose.

6.1.4 **Catalyst stability**

One of the many benefits of using zeolites is their reusability, significantly reducing catalyst cost in an industrial process. As it is well-known that reactions taking place in water can be detrimental to the structural integrity of silicates, it was important to investigate the stability of these selective zeotype catalysts.[62, 228] Additionally, Amberlyst A21 is normally used for its anion exchange capabilities and the stability of the resin under the reaction conditions used here likewise requires investigation. For this purpose, Sn-MFI (100, OH^-) and Amberlyst A21 was tested in five consecutive experiments at 80 °C. Both catalysts were washed thoroughly with water and dried overnight in-between experiments.

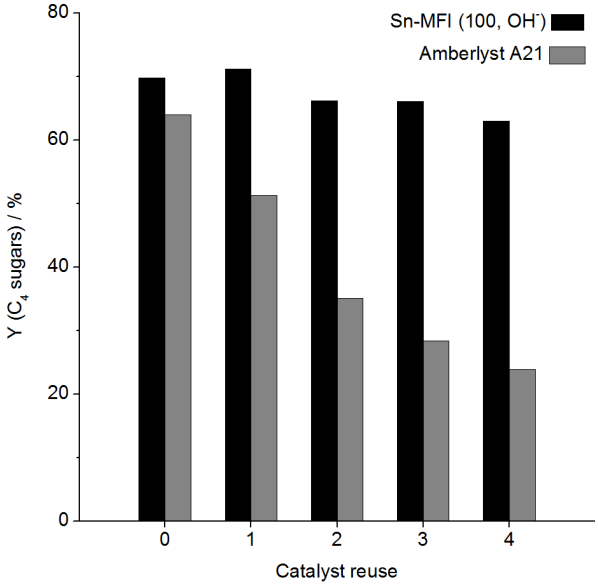

Figure 6.6. Yields of tetrose sugars obtained from glycolaldehyde when reusing Sn-MFI (100, OH^-) or Amberlyst A21. The catalysts were washed repeatedly with water and dried over night at 80 °C between runs. Reaction conditions: 80 °C, 5 wt% glycolaldehyde in water, substrate-to-catalyst ratio of 1.7, 2 h, 600 rpm stirring. Adapted from ref. [117].

Significant differences in stability were observed when comparing the two materials, see Figure 6.6. For Sn-MFI (100, OH^-) reusing the catalyst over several consecutive cycles was found to only result in a small decrease in tetrose yield from 69% to 65%, showing the high stability of this type of catalyst. Using the same conditions and treatments for Amberlyst A21 instead resulted in a step-wise

decrease in yield from 64% to 25% over the five repetitions, thus showing poor reusability under the chosen conditions.

It is important to note, that both materials normally require regeneration in-between uses to recover activity (Sn-MFI) or their ion-exchange capabilities (Amberlyst). Zeolites used for catalysis are often thermally treated at temperatures above 500 °C in order to remove any carbonaceous species confined within the pores and channels of the material.[229] Amberlyst A21 is normally regenerated by treating the resin in a flow of aqueous base. From Figure 6.6, it is evident that thorough washing of the Sn-MFI catalyst with water in-between experiments was sufficient in regenerating the catalyst. This was also confirmed when a washed sample of spent Sn-MFI catalyst was investigated using thermograviometric analysis (TG/DSC). This measurement indeed showed that little to no residual carbon remained in the washed zeotype as only a negligible mass loss (2.9 wt%) was observed upon heating the sample to 1,000 °C, see Figure 6.7.

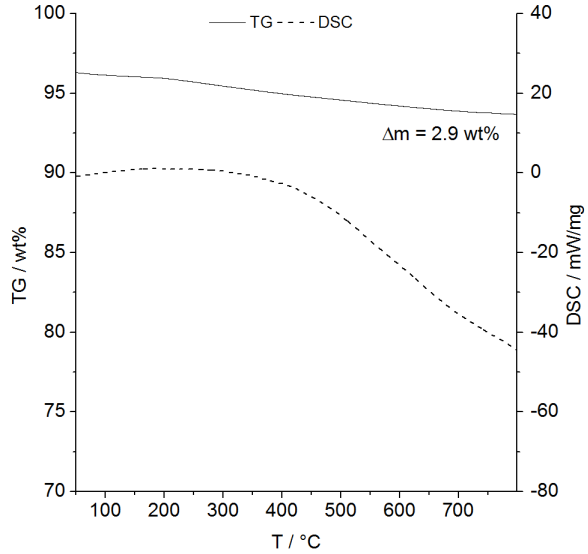

Figure 6.7. Thermogravimetric analysis (TG/DSC) of spent Sn-MFI (100, OH^-) after being washed three times with demineralized water and then dried overnight at 80 °C. The preceding reaction was performed using 0.360 g glycolaldehyde (dimer), 0.225 g catalyst, 80 °C, 2 h, 600 rpm stirring. No mass loss was observed above 800 °C. Initial mass loss caused by drying prior to shown analysis. Adapted from [117].

Regeneration of Amberlyst A21 was done by exposing the resin to an aqueous solution of NH_4OH (2 and 7 M), a method adapted from the procedure provided by the supplier (DOW). The resin was stirred in the basic media for one hour and followed by thorough washing in water to remove any excess base. Unfortunately

a large decrease in the achieved tetrose yield was still observed for both the treated Amberlyst samples, see Figure 6.8. Moreover, the decrease in yield was even more pronounced than when the sample was simply washed. Although these experiments show a lower stability of this material, more dedicated studies are still required to thoroughly investigate both alternative regeneration procedures or to confirm that the integrity of the material is indeed irreversibly deactivated during reactions.

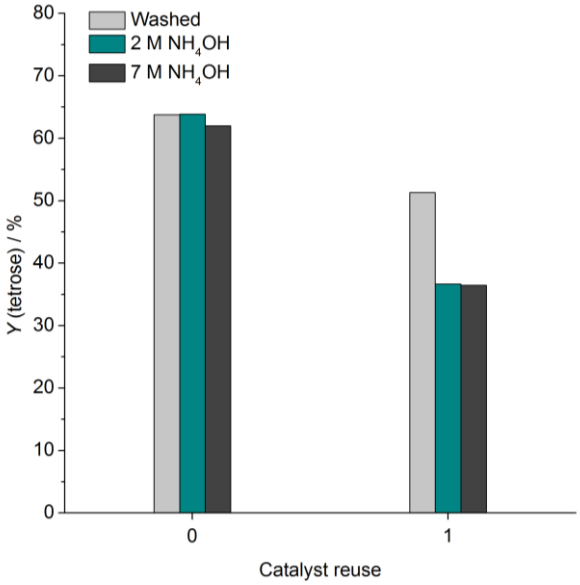

Figure 6.8. Yields of tetrose sugars obtained from glycolaldehyde when reusing Amberlyst A21. The resin was either washed three times and dried (80 °C) overnight or stirred in a solution of NH_4OH for 1 h, washed (three times) and dried overnight. Reaction conditions: Amounts were adjusted for every cycle based on the catalyst recovery. First catalyst use was performed using 0.360 g glycolaldehyde (dimer), 0.225 g catalyst, 80 °C, 2 h, 600 rpm stirring. Adapted from [117].

6.1.1 By-product formation

One of the main reasons for the lower obtained yields of the targeted tetroses was that the formed sugars were converted into other products. The primary by-products observed here were the larger hexose sugars, the α-hydroxy acid vinyl glycolic acid (VGA) as well as α-hydroxy-γ-butyrolactone (HBL). These additional products were either the result of additional aldol condensation reactions taking place between the formed tetroses and GA (shown in Scheme 6.1 on p. 111) or formed from the transformation of the tetroses to other C_4 products. Both VGA

and HBL can be assumed to be formed through a similar β-dehydration pathway as described in **Chapter 5**. In brief, this involves an initial β-dehydration of the tetrose to yield the 1,2-dione intermediate 3-deoxytetrosone which can then either cyclize to yield HBL or undergo an additional β-dehydration and subsequent 1,2-hydride shift to form VGA.[18, 118]

The product distribution for the tested catalysts is shown at comparable levels of conversion (70±6%) in Table 6.2. From these results, the very high selectivity (96%) of Sn-MFI (100, OH^-) can again be seen resulting in 19% THR, 15% ERY and 39% ERU giving a combined tetrose yield of 74% and a mass balance of 99% (Table 6.2, entry 1). A similar distribution of the tetrose isomers and are found for Sn-MFI (400, F^-) with only a slightly lower mass balance (95%) (Table 6.2, entry 2).

Table 6.2. Comparison of product distribution using different catalysts at comparable conversion levels (70±6%). Adapted from [117].

Entry	Catalyst	Time	Conversion[a]	Product distribution					Selectivity[b]	Total
				THR	ERY	ERU	VGA/ HBL	Hexoses		
		h	%							
1	Sn-MFI (100, OH^-)	0.5	76	19	15	39	1	1	96	99
2	Sn-MFI (400, F^-)	6.5	74	19	16	30	2	1	88	95
3	Sn-MCM-41 (150, HT)	24	66	11	5	16	3	7	48	76
4	Sn-SBA-15 (200, HT)	48	65	12	8	15	-	6	54	78
5	Sn-Beta (150, HT)	3	69	6	1	16	16	5	33	75
6	$SnCl_4 \cdot 5H_2O$[c]	24	74	9	4	3	-	3	22	45
7	Amberlyst A21	2	70	35	14	9	-	4	83	92

a) Conversion of GA, b) selectivity towards the tetroses (THR, ERY, ERU) c) 0.025 g of catalyst used. Reaction conditions: 0.125 mg glycolaldehyde dimer, 0.075 g catalyst, 2.5 g demineralized water, 80 °C, 600 rpm, 0.25-48 h.

All the catalysts tested were found to form varying amounts of hexose sugars. Comparing the formation of these larger sugars as a function of conversion (Figure 6.9), it is again evident that the investigated catalysts divide into two groups indicated here by the blue and green dashed lines. One group contains the two Sn-MFI zeotypes (green line) and the other group includes all other catalysts both Lewis acidic and basic (blue line).

The catalysts in the second group were all found to continuously form hexoses even at low conversion. At close to full conversion, this lead to the formation of up to 10% hexoses. Although Amberlyst A21 achieved a high selectivity towards the tetrose sugars (83%, Table 6.2, entry 7), the resin likewise formed the highest quantities of hexoses of all the tested catalysts reaching 10% approaching full conversion, see Figure 6.9.

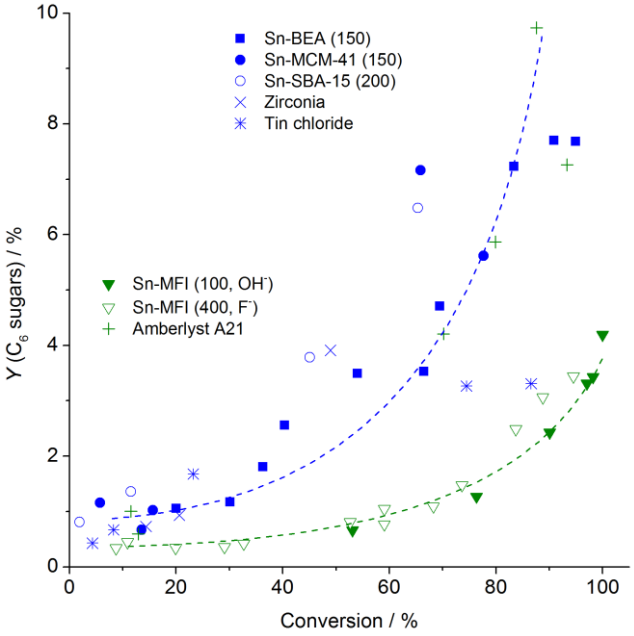

Figure 6.9. Yield of C_6 sugars obtained with different catalysts from pure glycolaldehyde as a function of conversion. Reaction conditions: 80 °C, 5 wt% glycolaldehyde (dimer) in water, 0.075 g of catalyst, 2.5 g of water, reaction times 0.25-48 h. Adapted from [117].

As expected, no VGA or HBL was observed for this catalyst. The ordered amorphous stannosilicates (Sn-MCM-41 and Sn-SBA-15) were likewise found to continuously form hexose sugars (up to 7%, Figure 6.9) as well as low yields of VGA (up to 4%). Additionally, a much lower mass balance of 76-78% was found for these materials (Table 6.2, entries 3-4). Sn-Beta shown in **Chapter 4 and 5** to efficiently catalyze retro-aldol and β-dehydration reactions, was found to facilitate both the aldol condensation of tetrose to larger sugars (~8% at high conversion, Figure 6.9) and the cascade of reactions leading to VGA and HBL in a combined yield of 16% at 74% conversion (Table 6.2, entry 5). As a result of this high activity in the consecutive reactions, the selectivity of Sn-Beta towards tetrose selectivity is highest at low conversion (60% at 20% conversion, Figure 6.9) decreasing

continuously with the increase in conversion (33% selectivity at 69% conversion, Table 6.2, entry 5). Using dissolved tin chloride in the conversion of GA, only 16% of tetrose sugars were formed at 74% conversion, see Table 6.2, entry 6. Several volatile unidentified products with high boiling points were observed on GC not observed for any of the other stannosilicates, explaining the low mass balance of 45%. The different reactivity of tin chloride when compared with the other tin-containing catalysts could be explained by the precipitation of tin (hydr)oxide species in the aqueous solvent.[116]

In Figure 6.9, the other group (green dashed line) comprised only the two Sn-MFI zeotypes (OH^- and F^-). For this type of catalyst very low formation of hexoses was observed (<1%) and maintained until a conversion of 75% was reached, after which the yield of hexoses increased to ~4%. This clearly indicates that hexose formation is hindered when this type of catalyst is used, presumably from the narrow channels and pore openings found in the MFI framework. This is further corroborated by the similar product distribution observed for the two Sn-MFI catalysts, see Table 6.2, entries 1-2. The two different preparation methods (OH^- and F^-) yielded Sn-MFI catalysts possessing very different physical characteristics as shown earlier. Large differences in crystal size (0.5-1 versus 50-100 μm crystals, Figure 6.1 on p. 113) were observed as well as differences in surface area and pore volume (Table 6.1 on p. 113). As described in **Chapter 3**, zeotypes prepared in fluoride media generally result in highly defect-free crystals, making the materials more hydrophobic. Despite these many differences, the two catalysts still performed comparably in terms of product formation (Table 6.2, entries 1-2). This indeed suggests that the high selectivity towards the tetrose sugars is not caused by limitations brought on by the physical properties of the materials, but instead is a result of the restricted tin sites within the narrow channels of the MFI framework.[23] This type of 'restricted transition-state' shape-selectivity was visualized in Figure 1.1 on p. 3 and occurs when formation of certain intermediary states (here the coordination between tetrose and GA as shown in Scheme 6.1) is hindered by the confined environment around the active site. This is further supported by the different product distribution obtained with Sn-MFI and Sn-Beta. As mentioned earlier, Sn-Beta formed the larger hexoses in comparable yields (~8%) to both the mesoporous stannosilicates and Amberlyst catalysts (7-10%, Figure 6.9) having very large or no pore structure. From this it is clear that the 12-membered ring pores found in the framework of Sn-Beta does not restrict the formation of larger products, whereas the 10-ring pores in MFI does. This limitations of the channels size in Sn-MFI is in line with previous reports targeting the conversion of the larger pentose and hexose sugars. Where

Sn-Beta was fully capable of converting the hexose sugars, very poor activity was found for Sn-MFI, hinting that hexoses are too large to enter the narrower channels of this pore system.[100] Additionally, it can also be ruled out that larger products are formed but trapped within cavities in the MFI crystals as almost no carbonaceous species were left in the material after washing the catalyst in water (Figure 6.7). As a result, it can be concluded that the high selectivity achieved with Sn-MFI is likely a consequence of shape selectivity.[8]

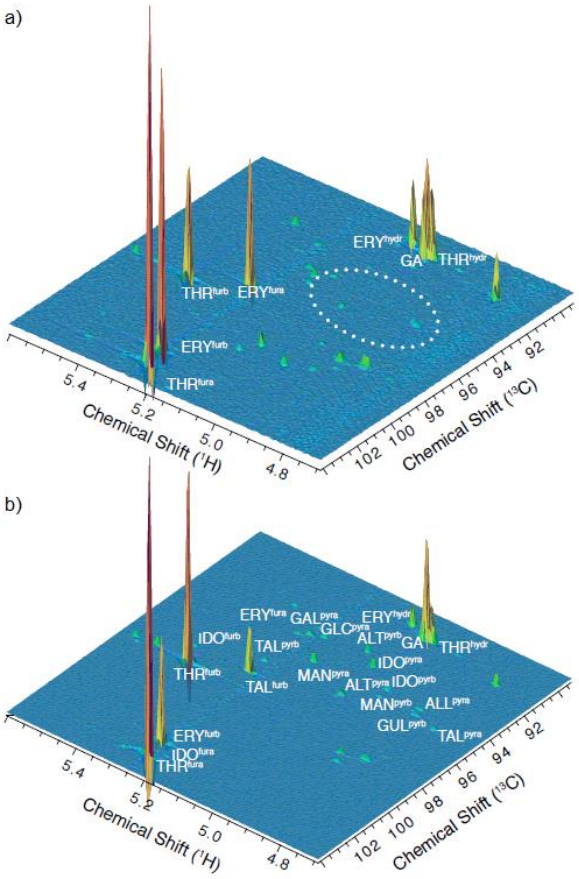

Figure 6.10. ^{1}H–^{13}C HSQC spectra of hemiacetal groups formed from the catalytic conversion of glycolaldehyde at ~85% conversion (80 °C, D_2O) using a) Sn-MFI (100, OH-) and b) Amberlyst A21. Figure prepared by Senior Researcher Sebastian Meier (DTU). Information on abbreviations used can be found in Scheme A.2. Adapted from [117].

To validate the formation of hexoses, multidimensional NMR analyses of the reaction mixtures were carried out.[230, 231] Figure 6.10 shows the anomeric

region using Sn-MFI (100, OH^-) (Figure 6.10a) and Amberlyst A21 (Figure 6.10b) for the conversion of GA in D_2O at ~85% conversion. The abbreviations and corresponding compounds identified in Figure 6.10 are shown in Scheme A.2 on p. 158. As expected, both catalysts form large quantities of the aldotetroses ERY and THR found in their respective furanose forms (α and β) as well as in the hydrated open-chain forms. For Amberlyst A21 earlier shown to result in high formation of hexoses, all eight aldohexose isomers (allose, altrose, glucose, gulose, idose mannose, and talose) were observed (Figure 6.10b). In contrast, only minor amounts of mannose, glucose and gulose were detected for Sn-MFI (Figure 6.10a). These findings confirm that all stereoisomers of the hexose sugars can be formed from consecutive aldol reactions at high conversion and confirms the lower formation of hexoses for Sn-MFI.

In addition to the formation of larger sugars, the formed tetroses can undergo dehydration and 1,2-hydride shift to yield the α-hydroxyacid vinyl glycolic acid (VGA).[18, 118] As mentioned earlier, VGA has been successfully co-polymerized with lactic acid and shown to form interesting, functional polyesters and polyamides through condensation or metathesis reactions.[116, 121, 232] In a previous study by the group of Sels, several ester analogues of VGA were formed using $SnCl_4 \cdot 5H_2O$ in alcohol solvents. Under these conditions, methyl-4-methoxy-2-hydroxybutanoate (MMHB) was the main product with a maximum yield of 55%.[116] This molecule does not contain the vinyl group characteristic for VGA. As mentioned in **Chapter 5** when co-polymerized with LA, it is these pendant vinyl group that gives the polymer its improved properties.

From the data presented in Table 6.2 on p. 121, it is clear that not all the catalysts tested form HBL and VGA in significant amounts. The most active catalysts for HBL and VGA formation are Sn-Beta and Sn-MFI. The yield of VGA as a function of conversion can be seen for the different stannosilicates in Figure 6.11. It is interesting to note that Sn-Beta readily produces VGA from tetroses, even at low conversion where GA is still available in solution, while Sn-MFI only starts transforming the tetroses at close to full conversion.

The results also suggest that the selectivity towards the different co-products is not only affected by the type of catalyst, but also by the concentration of GA in the medium. At the beginning of the reaction, the reaction medium is rich in GA and the possibility for two molecules of GA reacting with each other is high. With diminishing GA substrate and tetrose sugar formation, reactions can progress by formation of hexose sugars or further conversion to VGA becomes more likely. This effect was also observed when the starting concentration of GA was changed (Figure A.12). At low GA concentrations, VGA is formed in higher

relative yields (10% vs 3%, for initial concentrations of GA of 2% and 8%, respectively, after 2 h, using the same amount of catalyst). Bearing this difference in selectivity in mind, we tried to optimize the reaction conditions for the production of VGA.

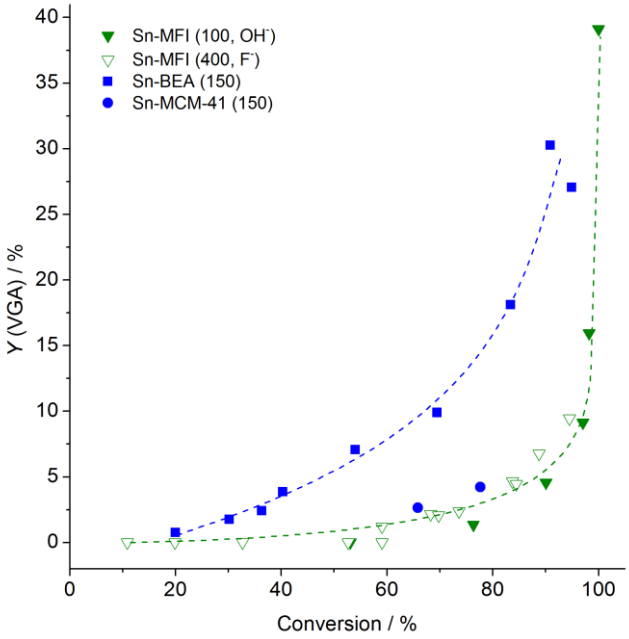

Figure 6.11. Yield of vinyl glycolic acid (VGA) as a function of conversion using different stannosilicates. Reaction conditions: 0.125 g glycolaldehyde (dimer), 0.075 g of catalyst, 2.5 g of water, 80 °C, reaction times 0.25-48 h, 600 rpm stirring.

Sn-Beta and Sn-MFI were found to form significant amounts of VGA in water, leading to yields of 39% using Sn-MFI (100, OH^-) and 30% using Sn-Beta (150, HT) after 48 h (Figure 6.12). When the amount of Sn-MFI catalyst and temperature was increased, the β-dehydration reaction was favored and the yield of VGA reached 44% (Table A.2 on p. 159) at 100 °C after 4.5 hours. This is the highest VGA yield reported in water so far. In the case of Sn-Beta, similar conditions lead to the formation of up to 33% HBL and 27% VGA after 48 h at 80 °C to give a combined yield of ~60% (Figure 6.12).

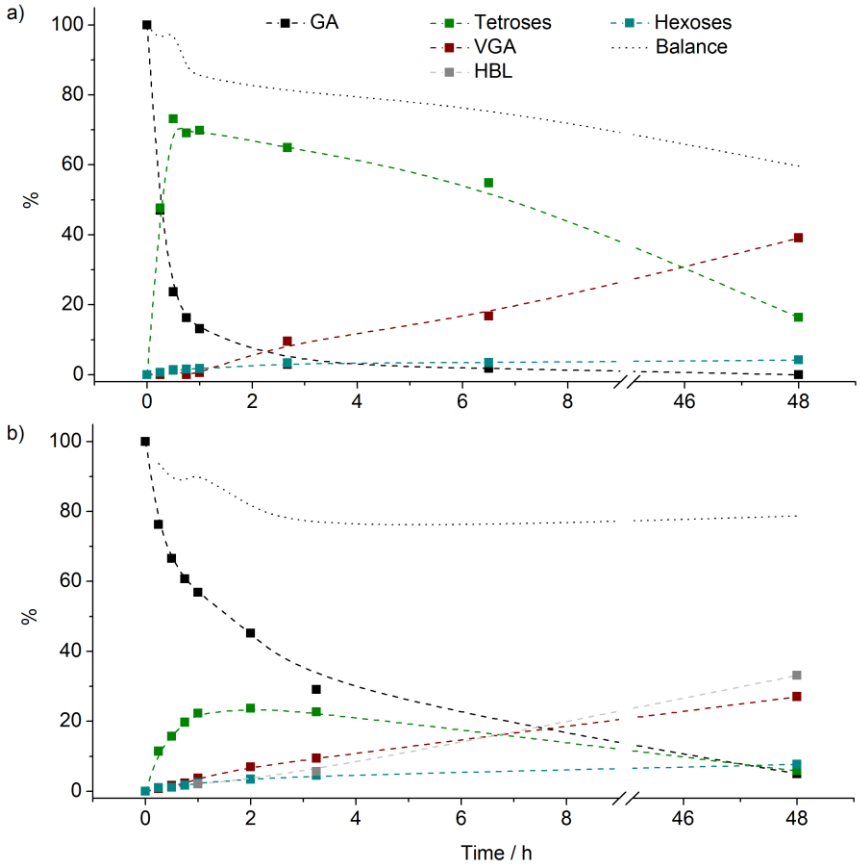

Figure 6.12. Yields of the different products as a function of time using a) Sn-MFI (100, OH^-) and b) Sn-Beta (150). Reaction conditions: 80 °C, 5 wt% glycolaldehyde in water, 0.075 g of catalyst, 2.5 g of water, 0-48 h.

6.1.2 Effect of alkali metal salts on the product distribution

It was shown in **Chapters 4 and 5** that the presence of small amounts of alkali metal salts had a pronounced effect on the product distribution when converting the pentose and hexose sugars using stannosilicates. Alkali was found to modify the reaction pathway leading in the absence of alkali to β-dehydration products, and to retro-aldol products when alkali salts were present. Analogous to the study in **Chapter 5**, the conversion of GA can likewise be divided into two reaction similar pathways. One pathway involves the aldol condensation of GA to tetroses and hexoses following a similar mechanism as that in the retro-aldol reaction, only in reverse. The other pathway, involves the conversion of the

formed tetroses to VGA and HBL requiring β-dehydration and subsequent 1,2-hydride shift or cyclization to form. Since these were precisely the type of reactions that alkali was shown to influence at higher temperatures, it was important to investigate the impact of alkali on the product distribution starting from GA. Aside from the higher temperatures employed in the previous chapters (>140 °C), another main difference is the methanol solvent used. The group of Davis recently showed that the effect of adding an alkali metal cosolute could be applied to an aqueous solvent albeit at much higher salt concentrations (saturation of NaCl) compared with the ppm levels used in methanol.[90] As a result, high concentrations of KNO_3 were used to test the effect in the reactions here.

To ensure a broad product distribution, Sn-Beta was used as the catalyst at high temperatures (100 °C) in order to better distinguish any effect brought on by the added cosolute. It is well-known that bases such as K_2CO_3 can facilitate aldol condensation, instead KNO_3 was chosen as the source of alkali to avoid any contribution from basicity of the additive. From blank experiments, it was indeed confirmed that the small amount of condensation products (tetroses and hexoses) formed in the presence of KNO_3 alone (Table A.3, entries 6-7 on p. 160) was comparable to that of a blank experiment performed in pure water (Table A.3, entry 5).

In Figure 6.13, the preliminary findings can be seen when adding KNO_3 to the aqueous solution of GA in increasing amounts (0-2.6 M). As it can be seen in the absence of alkali, equal amounts of HBL (13%) and VGA (13%) were formed with most of the carbon being unaccounted for at these conditions. For this sample, almost no GA, tetrose or hexose sugars were observed in the reaction mixture. With the introduction and increase in KNO_3 in the reaction, the combined yield of HBL and VGA decreased slightly (to a total of 13%), while an even larger increase in sugar content was observed resulting in an improved carbon balance of 79%. This meant both an increase in the yield of tetroses (4% to 29%) and hexoses (3% to 21%), but also a simultaneous decrease in conversion of GA from 2 to 16%. Although the increase in condensation products cannot be explained entirely from the decrease in HBL and VGA yield, the conditions used here did appear to favor aldol condensation, and several unknown products were suppressed by the introduction alkali, affording the increase in accounted carbon in the reaction. Alkali thereby also appears to have a large impact on product distribution from GA. Similar to retro-aldol reaction being favored in the presence of alkali at higher temperatures in methanol, aldol condensation was favored in water at lower temperatures. More experiments are however required to

investigate this in more detail in order to determine whether the effect observed here is indeed linked to what was discussed in **Chapters 4 and 5**.

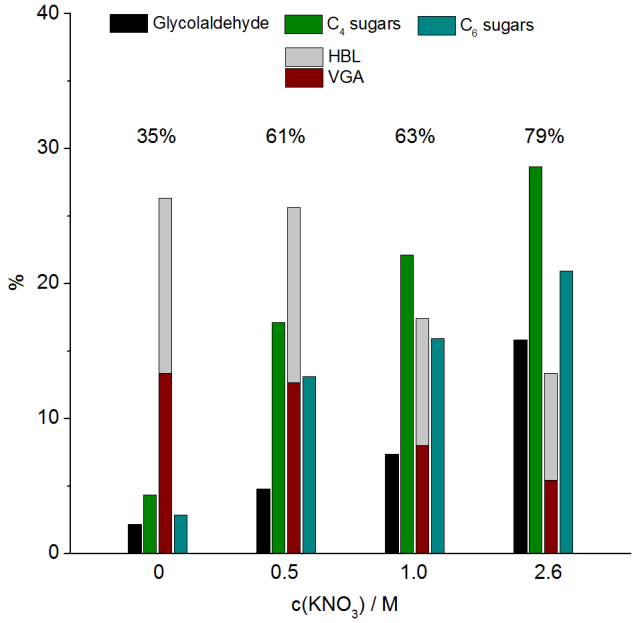

Figure 6.13. Product distribution obtained in the presence or absence of alkali during conversion of glycolaldehyde using Sn-Beta. Reaction conditions: 0.075 g Sn-Beta (150, HT), 5 wt% glycolaldehyde (dimer), 3 mL of 0-2.6 M KNO_3 in H_2O, 100 °C, 6 h. Data can be found in Table A.3, entries 1-4 on p. 160.

6.2 Conclusion

Valorization of biomass-derived GA using tin-containing zeotypes in water has potential for establishing a platform for tetrose-derived products. By exploiting the shape-selectivity of the zeolite frameworks with different pore sizes, a high selectivity towards C_4 products could be achieved in water at moderate temperatures (80 °C). The main products of the reaction of GA in water using Sn-MFI as catalyst were a mixture of the tetrose sugars; erythrose, threose and erythrulose. A combined yield of 74% of these rare sugars were obtained with Sn-MFI at a selectivity of 96%. Sn-MFI was likewise found to retain most of its activity after consecutive uses and could be regenerated by thoroughly washing the catalyst in-between uses.

High selectivity towards the tetroses (83%) was likewise found using the basic resin Amberlyst A21 but this catalyst was found difficult to regenerate and lead to the simultaneous formation of hexoses (up to 10%).

It was found that consecutive aldol condensation reactions leading to the unwanted hexose sugars could be significantly minimized with by using a Lewis acidic catalyst with the MFI framework. The narrow channels in this zeotype (10-membered ring pores) were unable to accommodate for this second aldol condensation reaction. This restriction was not found when Sn-Beta was employed having only slightly larger channels (12-membered ring pores).

It was furthermore observed that both Sn-MFI and Sn-Beta catalyzed the additional transformation of tetrose sugars into VGA and HBL. By varying the reaction conditions, the product distribution could be tuned to not only result in the high yield of tetrose sugars, but also to achieve good yields of VGA of up to 44%. Moreover, it was found from very preliminary experiments that alkali likewise influenced the product distribution obtained from GA, as more aldol condensation products (both tetrose and hexose sugars) were obtained with Sn-Beta in the presence of alkali.

A natural next step following the work presented here is the investigation of this process in a continuous reaction in order to facilitate later scale up.

7
Conclusion

Throughout this dissertation the versatility and usability of a variety of stannosilicates have continuously been shown for the conversion of a broad range of carbohydrates. All the prepared stannosilicate materials from the zeotypes Sn-Beta and Sn-MFI to the ordered amorphous materials Sn-MCM-41 and Sn-SBA-15 were found to form desirable, (potential) high-value products from sugars such as methyl lactate, methyl vinyl glycolate and previously unknown α-hydroxy β,γ-unsaturated esters. These reactions and catalysts are very promising in the context in the conversion of carbohydrates into chemicals.

Conclusion summarizing all results and findings in the individual chapters can be found on p. 66 (**Chapter 3**), p. 85 (**Chapter 4**), p. 108 (**Chapter 5**), and p. 129 (**Chapter 6**). In this final conclusion, I will try to list the most key findings across all chapters:

The dissertation compiles four results chapters, which can be divided into preparation (**Chapter 3**) or catalytic investigation (**Chapters 4 to 6**) of the stannosilicates. Here, **Chapter 3** focuses primarily on the synthesis and understanding of the zeotype Sn-Beta. The following chapters describe the optimization of the retro-aldol product methyl lactate (**Chapter 4**), the different reaction pathways and formed products taking place when tin-containing catalysts are used (**Chapter 5**), and the use of shape selectivity to upgrade glycolaldehyde to valuable products (**Chapter 6**).

The following key findings across all chapters of this dissertation will likewise be split into a preparative and a catalytic part.

The main findings when investigating the preparation of Sn-Beta:

- Tin was found to have a pronounced influence on morphology and crystal growth and composition in the preparation of Sn-Beta. This translates to a change in morphology from truncated to almost plate-like square bipyramidal crystals containing an enriched outer shell of tin with crystallization times varying from 2 to 60 days. Addition of small amounts of alkali metal salts could counter this effect leading to Sn-Beta zeolite of higher tin content (up to 3%) at the expense of high crystallinity.

The main findings regarding catalytic conversion of sugars:

- It was found that the versatility of these tin-containing catalysts in the conversion of carbohydrates could be expressed as being the result of only **a few, very similar types of reactions**, all involving coordination of tin with the alcohol and aldehyde moiety on the sugars. All products formed could be explained by sequence of retro-aldol/aldol reactions, one or more β-dehydration or 1,2-hydride shifts, all catalyzed by tin. This was particularly shown for glucose were different combinations of these reactions lead to either ML or THM. Depending on the starting substrate, the only influences on the product distribution were temperature, solvent, type of catalyst and additives. In regards, to the latter it was found that the presence of small amounts of alkali would enable especially reaction involving retro-aldol/aldol reactions, whereas the absence led to pronounced formation of products obtained by β-dehydration.
- In the absence of any added alkali during conversion of the pentose and hexose sugars, several **new and highly functional products** were obtained including DPM or THM and other previously unknown lactones and sugar derivatives. DPM and THM were formed directly from the most abundant sugars under relatively mild reaction conditions in acceptable yields (18-33%) with a large potential for optimization and as potential high-value products for polymerization
- **Confinement effects** found to hinder the formation of larger byproducts were likewise found to add versatility to the choice of catalyst. By selecting the smaller MFI framework as opposed to slightly or much larger *BEA framework or mesoporous network MCM-41/SBA-15, it was shown that glycolaldehyde could undergo shape selective aldol condensation to achieve high yields of the rare tetrose sugars.

8
References

1. Zhou, Q.-L., Transition-Metal Catalysis and Organocatalysis: Where Can Progress Be Expected? *Angew. Chem. Int. Ed.* **2016**, *55* (18), 5352-5353.
2. Taarning, E.; Osmundsen, C. M.; Yang, X.; Voss, B.; Andersen, S. I.; Christensen, C. H., Zeolite-catalyzed biomass conversion to fuels and chemicals. *Energy Environ. Sci.* **2011**, *4* (3), 793-804.
3. Vennestrøm, P. N. R.; Osmundsen, C. M.; Christensen, C. H.; Taarning, E., Beyond Petrochemicals: The Renewable Chemicals Industry. *Angew. Chem., Int. Ed.* **2011**, *50* (45), 10502-10509.
4. Corma, A., State of the Art and Future Challenges of Zeolites as Catalysts. *J. Catal.* **2003**, *216* (1–2), 298-312.
5. Broach, R. W.; Jan, D.-Y.; Lesch, D. A.; Kulprathipanja, S.; Roland, E.; Kleinschmit, P., Zeolites. In *Ullmann's Encyclopedia of Industrial Chemistry*, Wiley-VCH Verlag GmbH & Co. KGaA: 2000.
6. Tanabe, K.; Hölderich, W. F., Industrial Application of Solid Acid–base Catalysts. *Appl. Catal. A-Gen* **1999**, *181* (2), 399-434.
7. Yilmaz, B.; Müller, U., Catalytic Applications of Zeolites in Chemical Industry. *Topics in Catalysis* **2009**, *52* (6), 888-895.
8. Weisz, P. B., Molecular Shape Selective Catalysis. *Pure Appl. Chem.* **1980**, *52*, 2091-2103.
9. Csicsery, S. M., Shape-selective Catalysis in Zeolites. *Zeolites* **1984**, *4* (3), 202-213.
10. Bermejo-Deval, R.; Assary, R. S.; Nikolla, E.; Moliner, M.; Román-Leshkov, Y.; Hwang, S.-J.; Palsdottira, A.; Silverman, D.; Lobo, R. F.; Curtiss, L. A.; Davis, M. E., Metalloenzyme-like Catalyzed Isomerizations of Sugars by Lewis Acid Zeolites. *Proc. Natl. Acad. Sci.* **2012**, *109* (25), 9727-9732.
11. Guo, Q.; Fan, F.; Pidko, E. A.; van der Graaff, W. N. P.; Feng, Z.; Li, C.; Hensen, E. J. M., Highly Active and Recyclable Sn-MWW Zeolite Catalyst for Sugar Conversion to Methyl Lactate and Lactic Acid. *ChemSusChem* **2013**, *6* (8), 1352-1356.
12. Yang, X.; Wu, L.; Wang, Z.; Bian, J.; Lu, T.; Zhou, L.; Chen, C.; Xu, J., Conversion of Dihydroxyacetone to Methyl Lactate Catalyzed by Highly Active Hierarchical Sn-USY at Room Temperature. *Catal. Sci. Technol.* **2016**, *6*, 1757-1763.
13. Osmundsen, C. M.; Holm, M. S.; Dahl, S.; Taarning, E., Tin-containing Silicates: Structure-activity Relations. *Proc. R. Soc. A* **2012**, *468* (2143), 2000-2016.

14. Corma, A.; Nemeth, L. T.; Renz, M.; Valencia, S., Sn-zeolite Beta as a Heterogeneous Chemoselective Catalyst for Baeyer-Villiger Oxidations. *Nature* **2001**, *412* (6845), 423-425.
15. Corma, A.; Domine, M. E.; Nemeth, L.; Valencia, S., Al-Free Sn-Beta Zeolite as a Catalyst for the Selective Reduction of Carbonyl Compounds (Meerwein-Ponndorf-Verley Reaction). *J. Am. Chem. Soc.* **2002**, *124* (13), 3194-3195.
16. Holm, M. S.; Saravanamurugan, S.; Taarning, E., Conversion of Sugars to Lactic Acid Derivatives Using Heterogeneous Zeotype Catalysts. *Science* **2010**, *328* (5978), 602-605.
17. Moliner, M.; Román-Leshkov, Y.; Davis, M. E., Tin-containing Zeolites are Highly Active Catalysts for the Isomerization of Glucose in Water. *Proc. Natl. Acad. Sci.* **2010**, *107* (14), 6164-6168.
18. Holm, M. S.; Pagán-Torres, Y. J.; Saravanamurugan, S.; Riisager, A.; Dumesic, J. A.; Taarning, E., Sn-Beta Catalyzed Conversion of Hemicellulosic Sugars. *Green Chem.* **2012**, *14* (3), 702-706.
19. Taramasso, M. P., G.; Notari, B. Preparation of Porous Crystalline Synthetic Material Comprised of Silicon and Titanium Oxides. US 4410501 A, 1983.
20. Notari, B., Titanium silicalites. *Catal. Today* **1993**, *18* (2), 163-72.
21. Camblor, M. A.; Corma, A.; Pérez-Pariente, J., Synthesis of Titanoaluminosilicates Isomorphous to Zeolite Beta, Active as Oxidation Catalysts. *Zeolites* **1993**, *13* (2), 82-87.
22. Blasco, T.; Camblor, M. A.; Corma, A.; Esteve, P.; Guil, J. M.; Martinez, A.; Perdigon-Melon, J. A.; Valencia, S., Direct Synthesis and Characterization of Hydrophobic Aluminum-Free Ti-Beta Zeolite. *J. Phys. Chem. B* **1998**, *102* (1), 75-88.
23. De Clercq, R.; Dusselier, M.; Christiaens, C.; Dijkmans, J.; Iacobescu, R. I.; Pontikes, Y.; Sels, B. F., Confinement Effects in Lewis Acid-Catalyzed Sugar Conversion: Steering Toward Functional Polyester Building Blocks. *ACS Catal.* **2015**, *5* (10), 5803-5811.
24. Corma, A.; Camblor, M. A.; Esteve, P.; Martinez, A.; Pérez-Pariente, J., Activity of Ti-Beta Catalyst for the Selective Oxidation of Alkenes and Alkanes. *J. Catal.* **1994**, *145* (1), 151-158.
25. van der Waal, J. C.; Rigutto, M. S.; van Bekkum, H., Zeolite Titanium Beta as a Selective Catalyst in the Epoxidation of Bulky Alkenes. *Appl. Catal., A* **1998**, *167* (2), 331-342.
26. Mal, N. K.; Ramaswamy, V.; Ganapathy, S.; Ramaswamy, A. V., Synthesis and Characterization of Crystalline, Tin-silicate Molecular Sieves with MFI Structure. *J. Chem. Soc., Chem. Commun.* **1994**, (17), 1933-1934.
27. Luo, H. Y.; Bui, L.; Gunther, W. R.; Min, E.; Román-Leshkov, Y., Synthesis and Catalytic Activity of Sn-MFI Nanosheets for the Baeyer–Villiger Oxidation of Cyclic Ketones. *ACS Catal.* **2012**, *2* (12), 2695-2699.
28. Dapsens, P. Y.; Mondelli, C.; Jagielski, J.; Hauert, R.; Perez-Ramirez, J., Hierarchical Sn-MFI Zeolites Prepared by Facile Top-down Methods for Sugar Isomerisation. *Catal. Sci. Technol.* **2014**, *4* (8), 2302-2311.

29. Orazov, M.; Davis, M. E., Tandem Catalysis for the Production of Alkyl Lactates from Ketohexoses at Moderate Temperatures. *Proc. Natl. Acad. Sci.* **2015**, *112* (38), 11777-11782.
30. Mal, N. K.; Ramaswamy, A. V., Oxidation of Ethylbenzene over Ti-, V- and Sn-containing Silicalites with MFI Structure. *Appl. Catal. A-Gen* **1996**, *143* (1), 75-85.
31. Renz, M.; Blasco, T.; Corma, A.; Fornes, V.; Jensen, R.; Nemeth, L., Selective and Shape-selective Baeyer-Villiger Oxidations of Aromatic Aldehydes and Cyclic Ketones with Sn-Beta Zeolites and H_2O_2. *Chem. - Eur. J.* **2002**, *8* (20), 4708-4717.
32. Mal, N. K.; Ramaswamy, A. V., Synthesis and Catalytic Properties of Large-pore Sn-β and Al-free Sn-β Molecular Sieves. *Chem. Commun.* **1997**, (5), 425-426.
33. Corma, A.; Renz, M., Sn-Beta zeolite as Diastereoselective Water-resistant Heterogeneous Lewis-acid Catalyst for Carbon-carbon Bond Formation in the Intramolecular Carbonyl-ene Reaction. *Chem. Commun.* **2004**, (5), 550-551.
34. Boronat, M.; Corma, A.; Renz, M.; Viruela, P. M., Predicting the Activity of Single Isolated Lewis Acid Sites in Solid Catalysts. *Chem. - Eur. J.* **2006**, *12* (27), 7067-7077.
35. Zhu, Y.; Chuah, G.; Jaenicke, S., Chemo- and Regioselective Meerwein–Ponndorf–Verley and Oppenauer Reactions Catalyzed by Al-free Zr-zeolite Beta. *J. Catal.* **2004**, *227* (1), 1-10.
36. Sushkevich, V. L.; Ivanova, I. I.; Tolborg, S.; Taarning, E., Meerwein–Ponndorf–Verley–Oppenauer Reaction of Crotonaldehyde with Ethanol over Zr-containing Catalysts. *J. Catal.* **2014**, *316*, 121-129.
37. Wolf, P.; Hammond, C.; Conrad, S.; Hermans, I., Post-synthetic Preparation of Sn-, Ti- and Zr-Beta: A Facile Route to Water Tolerant, Highly Active Lewis Acidic Zeolites. *Dalton T.* **2014**, *43* (11), 4514-4519.
38. Zhu, Y.; Chuah, G.-K.; Jaenicke, S., Selective Meerwein–Ponndorf–Verley Reduction of α,β-Unsaturated Aldehydes over Zr-zeolite Beta. *J. Catal.* **2006**, *241* (1), 25-33.
39. Kholdeeva, O. A., Recent Developments in Liquid-phase Selective Oxidation using Environmentally Benign Oxidants and Mesoporous Metal Silicates. *Catal. Sci. Technol.* **2014**, *4* (7), 1869-1889.
40. Corma, A.; Iborra, S.; Mifsud, M.; Renz, M., Mesoporous Molecular Sieve Sn-MCM-41 as Baeyer-Villiger Oxidation Catalyst for Sterically Demanding Aromatic and α,β-Unsaturated Aldehydes. *Arkivoc* **2005**, *IX*, 124-132.
41. Li, L.; Stroobants, C.; Lin, K.; Jacobs, P. A.; Sels, B. F.; Pescarmona, P. P., Selective Conversion of Trioses to Lactates over Lewis Acid Heterogeneous Catalysts. *Green Chem.* **2011**, *13* (5), 1175-1181.
42. Corma, A.; Renz, M., Water-resistant Lewis-acid Sites: Carbonyl-ene Reactions Catalyzed by Tin-containing, Hydrophobic Molecular Sieves *Arkivoc* **2007**, *VIII*, 40-48.
43. Chang, C.-C.; Wang, Z.; Dornath, P.; Cho, H. J.; Fan, W., Rapid synthesis of Sn-Beta for the isomerization of cellulosic sugars. *RSC Adv.* **2012**, *2* (28), 10475-10477.

44. Tolborg, S.; Katerinopoulou, A.; Falcone, D. D.; Sádaba, I.; Osmundsen, C. M.; Davis, R. J.; Taarning, E.; Fristrup, P.; Holm, M. S., Incorporation of Tin Affects Crystallization, Morphology, and Crystal Composition of Sn-Beta. *J. Mater. Chem. A* **2014**, *2* (47), 20252-20262.
45. Yakimov, A. V.; Kolyagin, Y. G.; Tolborg, S.; Vennestrom, P. N. R.; Ivanova, I. I., Accelerated Synthesis of Sn-BEA in Fluoride Media: Effect of H_2O Content in the Gel. *New J. Chem.* **2016**, *40* (5), 4367-4374.
46. Otomo, R.; Kosugi, R.; Kamiya, Y.; Tatsumi, T.; Yokoi, T., Modification of Sn-Beta Zeolite: Characterization of Acidic/basic Properties and Catalytic Performance in Baeyer-Villiger Oxidation. *Catal. Sci. Technol.* **2016**, *6* (8), 2787-2795.
47. Kang, Z.; Zhang, X.; Liu, H.; Qiu, J.; Yeung, K. L., A Rapid Synthesis Route for Sn-Beta Zeolites by Steam-assisted Conversion and Their Catalytic Performance in Baeyer–Villiger Oxidation. *Chem. Eng. J.* **2013**, *218*, 425-432.
48. Kang, Z.; Zhang, X.; Liu, H.; Qiu, J.; Han, W.; Yeung, K. L., Factors Affecting the Formation of Sn-Beta Zeolites by Steam-assisted Conversion Method. *Mater. Chem. Phys.* **2013**, *141* (1), 519-529.
49. Chang, C.-C.; Cho, H. J.; Wang, Z.; Wang, X.; Fan, W., Fluoride-free Synthesis of a Sn-BEA Catalyst by Dry Gel Conversion. *Green Chem.* **2015**, *17* (5), 2943-2951.
50. Li, P.; Liu, G.; Wu, H.; Liu, Y.; Jiang, J.-g.; Wu, P., Postsynthesis and Selective Oxidation Properties of Nanosized Sn-Beta Zeolite. *J. Phys. Chem. C* **2011**, *115* (9), 3663-3670.
51. Dijkmans, J.; Demol, J.; Houthoofd, K.; Huang, S.; Pontikes, Y.; Sels, B., Post-synthesis Snβ: An Exploration of Synthesis Parameters and Catalysis. *J. Catal.* **2015**, *330*, 545-557.
52. van der Graaff, W. N. P.; Li, G.; Mezari, B.; Pidko, E. A.; Hensen, E. J. M., Synthesis of Sn-Beta with Exclusive and High Framework Sn Content. *ChemCatChem* **2015**, *7* (7), 1152-1160.
53. Hammond, C.; Conrad, S.; Hermans, I., Simple and Scalable Preparation of Highly Active Lewis Acidic Sn-β. *Angew. Chem., Int. Ed.* **2012**, *51* (47), 11736-11739.
54. Tang, B.; Dai, W.; Wu, G.; Guan, N.; Li, L.; Hunger, M., Improved Postsynthesis Strategy to Sn-Beta Zeolites as Lewis Acid Catalysts for the Ring-Opening Hydration of Epoxides. *ACS Catal.* **2014**, *4* (8), 2801-2810.
55. Kang, Z.; Liu, H. o.; Zhang, X., Preparation and Characterization of Sn-β Zeolites by a Two-Step Postsynthesis Method and Their Catalytic Performance for Baeyer-Villiger Oxidation of Cyclohexanone. *Chin. J. Catal.* **2012**, *33* (5), 898-904.
56. Tolborg, S.; Sádaba, I.; Osmundsen, C. M.; Fristrup, P.; Holm, M. S.; Taarning, E., Tin-containing Silicates: Alkali Salts Improve Methyl Lactate Yield from Sugars. *ChemSusChem* **2015**, *8* (4), 613-617.
57. Dijkmans, J.; Gabriels, D.; Dusselier, M.; de Clippel, F.; Vanelderen, P.; Houthoofd, K.; Malfliet, A.; Pontikes, Y.; Sels, B. F., Productive Sugar Isomerization with Highly Active Sn in Dealuminated β Zeolites. *Green Chem.* **2013**, *15* (10), 2777-2785.

58. Conrad, S.; Wolf, P.; Mueller, P.; Orsted, H.; Hermans, I., Influence of Hydrophilicity on the Snβ-Catalyzed Baeyer-Villiger Oxidation of Cyclohexanone with Aqueous Hydrogen Peroxide. *ChemCatChem* **2016**, *in press*. (DOI: 10.1002/cctc.201600893)
59. Wolf, P.; Valla, M.; Núñez-Zarur, F.; Comas-Vives, A.; Rossini, A. J.; Firth, C.; Kallas, H.; Lesage, A.; Emsley, L.; Copéret, C.; Hermans, I., Correlating Synthetic Methods, Morphology, Atomic-Level Structure, and Catalytic Activity of Sn-β Catalysts. *ACS Catal.* **2016**, *6* (7), 4047-4063.
60. Hammond, C.; Padovan, D.; Al-Nayili, A.; Wells, P. P.; Gibson, E. K.; Dimitratos, N., Identification of Active and Spectator Sn Sites in Sn-β Following Solid-State Stannation, and Consequences for Lewis Acid Catalysis. *ChemCatChem* **2015**, *7* (20), 3322-3331.
61. Mal, N. K.; Ramaswamy, V.; Rajamohanan, P. R.; Ramaswamy, A. V., Sn-MFI Molecular Sieves: Synthesis Methods, ^{29}Si Liquid and Solid MAS-NMR, ^{119}Sn Static and MAS NMR Studies. *Microporous Mater.* **1997**, *12* (4–6), 331-340.
62. Lari, G. M.; Dapsens, P. Y.; Scholz, D.; Mitchell, S.; Mondelli, C.; Perez-Ramirez, J., Deactivation Mechanisms of Tin-zeolites in Biomass Conversions. *Green Chem.* **2016**, *18* (5), 1249-1260.
63. Dapsens, P. Y.; Mondelli, C.; Perez-Ramirez, J., Design of Lewis-acid Centres in Zeolitic Matrices for the Conversion of Renewables. *Chem. Soc. Rev.* **2015**, *44* (20), 7025-7043.
64. Boronat, M.; Concepcion, P.; Corma, A.; Renz, M.; Valencia, S., Determination of the Catalytically Active Oxidation Lewis Acid Sites in Sn-Beta Zeolites, and Their Optimization by the Combination of Theoretical and Experimental Studies. *J. Catal.* **2005**, *234* (1), 111-118.
65. Courtney, T. D.; Chang, C.-C.; Gorte, R. J.; Lobo, R. F.; Fan, W.; Nikolakis, V., Effect of Water Treatment on Sn-BEA Zeolite: Origin of 960 cm^{-1} FTIR Peak. *Microporous Mesoporous Mater.* **2015**, *210*, 69-76.
66. Gunther, W. R.; Michaelis, V. K.; Caporini, M. A.; Griffin, R. G.; Román-Leshkov, Y., Dynamic Nuclear Polarization NMR Enables the Analysis of Sn-Beta Zeolite Prepared with Natural Abundance ^{119}Sn Precursors. *J. Am. Chem. Soc.* **2014**, *136* (17), 6219-22.
67. Wolf, P.; Valla, M.; Rossini, A. J.; Comas-Vives, A.; Núñez-Zarur, F.; Malaman, B.; Lesage, A.; Emsley, L.; Copéret, C.; Hermans, I., NMR Signatures of the Active Sites in Sn-β Zeolite. *Angew. Chem., Int. Ed.* **2014**, *53* (38), 10179-10183.
68. Kolyagin, Y. G.; Yakimov, A. V.; Tolborg, S.; Vennestrøm, P. N. R.; Ivanova, I. I., Application of ^{119}Sn CPMG MAS NMR for Fast Characterization of Sn Sites in Zeolites with Natural ^{119}Sn Isotope Abundance. *J. Phys. Chem. C* **2016**, *7* (7), 1249-1253.
69. Rai, N.; Caratzoulas, S.; Vlachos, D. G., Role of Silanol Group in Sn-Beta Zeolite for Glucose Isomerization and Epimerization Reactions. *ACS Catal.* **2013**, *3* (10), 2294-2298.
70. Li, G.; Pidko, E. A.; Hensen, E. J. M., Synergy Between Lewis Acid Sites and Hydroxyl Groups for the Isomerization of Glucose to Fructose over Sn-containing Zeolites: A Theoretical Perspective. *Catal. Sci. Technol.* **2014**, *4* (8), 2241-2250.

71. Roy, S.; Bakhmutsky, K.; Mahmoud, E.; Lobo, R. F.; Gorte, R. J., Probing Lewis Acid Sites in Sn-Beta Zeolite. *ACS Catal.* **2013**, *3* (4), 573-580.
72. Gunther, W. R.; Michaelis, V. K.; Griffin, R. G.; Roman-Leshkov, Y., Interrogating the Lewis Acidity of Metal Sites in Beta Zeolites with ^{15}N Pyridine Adsorption Coupled with MAS NMR Spectroscopy. *J. Phys. Chem. C* **2016**, *in press* (DOI: 10.1021/acs.jpcc.6b07811).
73. Harris, J. W.; Cordon, M. J.; Di Iorio, J. R.; Vega-Vila, J. C.; Ribeiro, F. H.; Gounder, R., Titration and Quantification of Open and Closed Lewis Acid Sites in Sn-Beta Zeolites that Catalyze Glucose Isomerization. *J. Catal.* **2016**, *335*, 141-154.
74. Yakimov, A. V.; Kolyagin, Y. G.; Tolborg, S.; Vennestrøm, P. N. R.; Ivanova, I. I., ^{119}Sn MAS NMR Study of Probe Molecules Interaction with Sn-BEA: The Origin of Penta- and Hexacoordinated Tin Formation. *J. Phys. Chem. C* **2016**, *in press* (DOI: 10.1021/acs.jpcc.6b09999).
75. Bellussi, G.; Carati, A.; Clerici, M. G.; Maddinelli, G.; Millini, R., Reactions of Titanium Silicalite with Protic Molecules and Hydrogen Peroxide. *J. Catal.* **1992**, *133* (1), 220-230.
76. Ogura, M.; Nakata, S. I.; Kikuchi, E.; Matsukata, M., Effect of NH_4^+ Exchange on Hydrophobicity and Catalytic Properties of Al-Free Ti-Si-beta Zeolite. *J. Catal.* **2001**, *199* (1), 41-47.
77. Goa, Y.; Wu, P.; Tatsumi, T., Catalytic Performance of [Ti,Al]-Beta in the Alkene Epoxidation Controlled by the Postsynthetic Ion Exchange. *The Journal of Physical Chemistry B* **2004**, *108* (24), 8401-8411.
78. Dijkmans, J.; Dusselier, M.; Janssens, W.; Trekels, M.; Vantomme, A.; Breynaert, E.; Kirschhock, C.; Sels, B. F., An Inner-/Outer-Sphere Stabilized Sn Active Site in β-Zeolite: Spectroscopic Evidence and Kinetic Consequences. *ACS Catal.* **2016**, *6* (1), 31-46.
79. Boronat, M.; Corma, A.; Renz, M., Chapter 38 Catalysis by Lewis Acids: Basic Principles for Highly Stereoselective Heterogeneously Catalyzed Cyclization Reactions. In *Turning Points in Solid-State, Materials and Surface Science: A Book in Celebration of the Life and Work of Sir John Meurig Thomas*, The Royal Society of Chemistry: 2008; pp 639-650.
80. Hwang, S.-J.; Gounder, R.; Bhawe, Y.; Orazov, M.; Bermejo-Deval, R.; Davis, M. E., Solid State NMR Characterization of Sn-Beta Zeolites that Catalyze Glucose Isomerization and Epimerization. *Top. Catal.* **2015**, *58* (7), 435-440.
81. Wolf, P.; Liao, W.-C.; Ong, T.-C.; Valla, M.; Harris, J. W.; Gounder, R.; van der Graaff, W. N. P.; Pidko, E. A.; Hensen, E. J. M.; Ferrini, P.; Dijkmans, J.; Sels, B.; Hermans, I.; Copèret, C., Identifying Sn Site Heterogeneities Prevalent among Sn-Beta Zeolites. *Helv. Chim. Acta* **2016**, *99* (12), 916-927.
82. Lobo, R. F.; Zones, S. I.; Davis, M. E., Structure-direction in Zeolite Synthesis. *J. Inclusion Phenom. Mol. Recognit. Chem.* **1995**, *21* (1-4), 47-78.
83. Shetti, V. N.; Srinivas, D.; Ratnasamy, P., Enhancement of Chemoselectivity in Epoxidation Reactions Over TS-1 Catalysts by Alkali and Alkaline Metal Ions. *J. Mol. Catal. A: Chem.* **2004**, *210* (1-2), 171-178.

84. Garcia Vargas, N.; Stevenson, S.; Shantz, D. F., Synthesis and Characterization of Tin(IV) MFI: Sodium Inhibits the Synthesis of Phase Pure Materials. *Microporous Mesoporous Mater.* **2012**, *152*, 37-49.
85. Kuwahara, Y.; Nishizawa, K.; Nakajima, T.; Kamegawa, T.; Mori, K.; Yamashita, H., Enhanced Catalytic Activity on Titanosilicate Molecular Sieves Controlled by Cation-π Interactions. *J. Am. Chem. Soc.* **2011**, *133* (32), 12462-12465.
86. Tatsumi, T.; Koyano, K. A.; Shimizu, Y., Effect of Potassium on the Catalytic Activity of TS-1. *Appl. Catal., A* **2000**, *200* (1-2), 125-134.
87. Khouw, C. B.; Davis, M. E., Catalytic Activity of Titanium Silicates Synthesized in the Presence of Alkali Metal and Alkaline Earth Ions. *J. Catal.* **1995**, *151* (1), 77-86.
88. Notari, B., Titanium Silicalite: A New Selective Oxidation Catalyst. *Stud. Surf. Sci. Catal.* **1991**, *67*, 243-256.
89. Blasco, T.; Camblor, M. A.; Corma, A.; Pérez-Pariente, J., The State of Ti in Titanoaluminosilicates Isomorphous with Zeolite β. *J. Am. Chem. Soc.* **1993**, *115* (25), 11806-11813.
90. Bermejo-Deval, R.; Orazov, M.; Gounder, R.; Hwang, S.-J.; Davis, M. E., Active Sites in Sn-Beta for Glucose Isomerization to Fructose and Epimerization to Mannose. *ACS Catal.* **2014**, *4* (7), 2288-2297.
91. Gunther, W. R.; Wang, Y.; Ji, Y.; Michaelis, V. K.; Hunt, S. T.; Griffin, R. G.; Román-Leshkov, Y., Sn-Beta Zeolites with Borate Salts Catalyze the Epimerization of Carbohydrates via an Intramolecular Carbon Shift. *Nat. Commun.* **2012**, *3*, 1109.
92. Corma, A.; Iborra, S.; Velty, A., Chemical Routes for the Transformation of Biomass into Chemicals. *Chem. Rev.* **2007**, *107* (6), 2411-2502.
93. Christensen, C. H.; Rass-Hansen, J.; Marsden, C. C.; Taarning, E.; Egeblad, K., The Renewable Chemicals Industry. *ChemSusChem* **2008**, *1* (4), 283-289.
94. Román-Leshkov, Y.; Chheda, J. N.; Dumesic, J. A., Phase Modifiers Promote Efficient Production of Hydroxymethylfurfural from Fructose. *Science* **2006**, *312* (5782), 1933-1937.
95. Ji, N.; Zhang, T.; Zheng, M.; Wang, A.; Wang, H.; Wang, X.; Chen, J. G., Direct Catalytic Conversion of Cellulose into Ethylene Glycol Using Nickel-Promoted Tungsten Carbide Catalysts. *Angew. Chem.* **2008**, *120* (44), 8638-8641.
96. Nikolla, E.; Román-Leshkov, Y.; Moliner, M.; Davis, M. E., "One-Pot" Synthesis of 5-(Hydroxymethyl)furfural from Carbohydrates using Tin-Beta Zeolite. *ACS Catal.* **2011**, *1* (4), 408-410.
97. Liu, Y.; Luo, C.; Liu, H., Tungsten Trioxide Promoted Selective Conversion of Cellulose into Propylene Glycol and Ethylene Glycol on a Ruthenium Catalyst. *Angew. Chem.* **2012**, *124* (13), 3303-3307.
98. Saravanamurugan, S.; Riisager, A., Zeolite Catalyzed Transformation of Carbohydrates to Alkyl Levulinates. *ChemCatChem* **2013**, *5* (7), 1754-1757.
99. Taarning, E.; Saravanamurugan, S.; Spangsberg, H. M.; Xiong, J.; West, R. M.; Christensen, C. H., Zeolite-Catalyzed Isomerization of Triose Sugars. *ChemSusChem* **2009**, *2* (7), 625-627.

100. Lew, C. M.; Rajabbeigi, N.; Tsapatsis, M., Tin-containing Zeolite for the Isomerization of Cellulosic Sugars. *Microporous Mesoporous Mater.* **2012**, *153*, 55-58.
101. Román-Leshkov, Y.; Moliner, M.; Labinger, J. A.; Davis, M. E., Mechanism of Glucose Isomerization using a Solid Lewis Acid Catalyst in Water. *Angew. Chem. Int. Ed.* **2010**, *49* (47), 8954-8957.
102. Christianson, J. R.; Caratzoulas, S.; Vlachos, D. G., Computational Insight into the Effect of Sn-Beta Na Exchange and Solvent on Glucose Isomerization and Epimerization. *ACS Catal.* **2015**, *5* (9), 5256-5263.
103. Gunther, W. R.; Duong, Q.; Román-Leshkov, Y., Catalytic Consequences of Borate Complexation and pH on the Epimerization of L-arabinose to L-ribose in Water Catalyzed by Sn-Beta Zeolite with Borate Salts. *J. Mol. Catal. A: Chem.* **2013**, *379*, 294-302.
104. Lew, C. M.; Rajabbeigi, N.; Tsapatsis, M., One-Pot Synthesis of 5-(Ethoxymethyl)furfural from Glucose using Sn-BEA and Amberlyst Catalysts. *Ind. Eng. Chem. Res.* **2012**, *51* (14), 5364-5366.
105. Schutyser, W.; Van den Bosch, S.; Dijkmans, J.; Turner, S.; Meledina, M.; Van Tendeloo, G.; Debecker, D. P.; Sels, B. F., Selective Nickel-Catalyzed Conversion of Model and Lignin-Derived Phenolic Compounds to Cyclohexanone-Based Polymer Building Blocks. *ChemSusChem* **2015**, *8* (10), 1805-1818.
106. Pescarmona, P. P.; Janssen, K. P. F.; Delaet, C.; Stroobants, C.; Houthoofd, K.; Philippaerts, A.; De Jonghe, C.; Paul, J. S.; Jacobs, P. A.; Sels, B. F., Zeolite-catalysed Conversion of C_3 Sugars to Alkyl Lactates. *Green Chem.* **2010**, *12* (6), 1083-1089.
107. Dusselier, M.; Van Wouwe, P.; Dewaele, A.; Makshina, E.; Sels, B. F., Lactic Acid as a Platform Chemical in the Biobased Economy: The Role of Chemocatalysis. *Energ. Environ. Sci.* **2013**, *6* (5), 1415-1442.
108. Datta, R.; Henry, M., Lactic Acid: Recent Advances in Products, Processes and Technologies - a Review. *J. Chem. Techn. Biotechn.* **2006**, *81* (7), 1119-1129.
109. Lunt, J., Large-scale Production, Properties and Commercial Applications of Polylactic Acid Polymers. *Polym. Degrad. Stabil.* **1998**, *59* (1–3), 145-152.
110. Vink, E. T. H.; Rábago, K. R.; Glassner, D. A.; Gruber, P. R., Applications of Life Cycle Assessment to NatureWorks™ Polylactide (PLA) Production. *Polym. Degrad. Stabil.* **2003**, *80* (3), 403-419.
111. Venus, J., Utilization of Renewables for Lactic Acid Fermentation. *Biotechnol. J.* **2006**, *1* (12), 1428-1432.
112. Li, L.; Shen, F.; Smith, R. L.; Qi, X., Quantitative Chemocatalytic Production of Lactic Acid from Glucose under Anaerobic Conditions at Room Temperature. *Green Chemistry* **2016**.
113. Dusselier, M.; Sels, B. F., Selective Catalysis for Cellulose Conversion to Lactic Acid and Other α-Hydroxy Acids. In *Selective Catalysis for Renewable Feedstocks and Chemicals*, Nicholas, K. M., Ed. Springer International Publishing: Cham, 2014; pp 85-125.
114. Lobo, R. F., Synthetic Glycolysis. *ChemSusChem* **2010**, *3* (11), 1237-1240.

115. Hayashi, Y.; Sasaki, Y., Tin-catalyzed Conversion of Trioses to Alkyl Lactates in Alcohol Solution. *Chem. Commun.* **2005**, (21), 2716-2718.
116. Dusselier, M.; Van Wouwe, P.; De Smet, S.; De Clercq, R.; Verbelen, L.; Van Puyvelde, P.; Du Prez, F. E.; Sels, B. F., Toward Functional Polyester Building Blocks from Renewable Glycolaldehyde with Sn Cascade Catalysis. *ACS Catal.* **2013**, *3* (8), 1786-1800.
117. Tolborg, S.; Meier, S.; Saravanamurugan, S.; Fristrup, P.; Taarning, E.; Sádaba, I., Shape-selective Valorization of Biomass-derived Glycolaldehyde using Tin-containing Zeolites. *ChemSusChem* **2016**, *9* (21), 3054-3061.
118. Dusselier, M.; Van Wouwe, P.; de Clippel, F.; Dijkmans, J.; Gammon, D. W.; Sels, B. F., Mechanistic Insight into the Conversion of Tetrose Sugars to Novel α-Hydroxy Acid Platform Molecules. *ChemCatChem* **2013**, *5* (2), 569-575.
119. Tolborg, S.; Meier, S.; Sadaba, I.; Elliot, S. G.; Kristensen, S. K.; Saravanamurugan, S.; Riisager, A.; Fristrup, P.; Skrydstrup, T.; Taarning, E., Tin-containing Silicates: Identification of a Glycolytic Pathway via 3-Deoxyglucosone. *Green Chem.* **2016**, *18* (11), 3360-3369.
120. Sølvhøj, A.; Taarning, E.; Madsen, R., Methyl Vinyl Glycolate as a Diverse Platform Molecule. *Green Chem.* **2016**, *18*, 5448-5455.
121. Dewaele, A.; Meerten, L.; Verbelen, L.; Eyley, S.; Thielemans, W.; Van Puyvelde, P.; Dusselier, M.; Sels, B., Synthesis of Novel Renewable Polyesters and Polyamides with Olefin Metathesis. *ACS Sustain. Chem. Eng.* **2016**, *4* (11), 5943-5952.
122. Dusselier, M.; De Clercq, R.; Cornelis, R.; Sels, B. F., Tin Triflate-catalyzed Conversion of Cellulose to Valuable (α-Hydroxy-)esters. *Catalysis Today* **2017**, *279, Part 2*, 339-344.
123. Capello, C.; Fischer, U.; Hungerbuhler, K., What is a Green Solvent? A Comprehensive Framework for the Environmental Assessment of Solvents. *Green Chem.* **2007**, *9* (9), 927-934.
124. Larlus, O.; Valtchev, V., Synthesis of All-silica BEA-type Material in Basic Media. *Microporous Mesoporous Mater.* **2006**, *93* (1-3), 55-61.
125. Ramaswamy, V.; Shah, P.; Lazar, K.; Ramaswamy, A. V., Synthesis, Characterization and Catalytic Activity of Sn-SBA-15 Mesoporous Molecular Sieves. *Catal. Surv. Asia* **2008**, *12* (4), 283-309.
126. Scarlett, N. V. Y.; Madsen, I. C., Quantification of Phases with Partial or No Known Crystal Structures. *Powder Diffr.* **2006**, *21* (4), 278-284.
127. Saravanamurugan, S.; Riisager, A.; Taarning, E.; Meier, S., Mechanism and Stereoselectivity of Zeolite-catalysed Sugar Isomerisation in Alcohols. *Chem. Commun.* **2016**, *52* (86), 12773-12776.
128. Elliot, S. G.; Andersen, C.; Tolborg, S.; Meier, S.; Sádaba, I.; Daugaard, A. E.; Taarning, E., Synthesis of a Novel Polyester Building Block from Pentoses by Tin-containing Silicates. *RSC Adv.* **2016**, *in press*.
129. Pérez-Pariente, J.; A. Martens, J.; A. Jacobs, P., Crystallization Mechanism of Zeolite Beta from $(TEA)_2O$, Na_2O and K_2O Containing Aluminosilicate Gels. *Appl. Catal.* **1987**, *31* (1), 35-64.

130. Pérez-Pariente, J.; Martens, J. A.; Jacobs, P. A., Factors Affecting the Synthesis Efficiency of Zeolite Beta from Aluminosilicate Gels Containing Alkali and Tetraethylammonium Ions. *Zeolites* **1988**, *8* (1), 46-53.
131. Camblor, M. A.; Mifsud, A.; Pérez-Pariente, J., Influence of the Synthesis Conditions on the Crystallization of Zeolite Beta. *Zeolites* **1991**, *11* (8), 792-797.
132. Camblor, M. A.; Pérez-Pariente, J., Crystallization of Zeolite Beta: Effect of Na and K Ions. *Zeolites* **1991**, *11* (3), 202-210.
133. Eapen, M. J.; Reddy, K. S. N.; Shiralkar, V. P., Hydrothermal Crystallization of Zeolite Beta using Tetraethylammonium Bromide. *Zeolites* **1994**, *14* (4), 295-302.
134. Yu, J., Chapter 3 Synthesis of Zeolites. In *Studies in Surface Science and Catalysis*, Čejka, J.; Bekkum, H. v.; Corma, A.; Schüth, F., Eds. Elsevier: 2007; Vol. Volume 168, pp 39-103.
135. Camblor, M. A.; Corma, A.; Valencia, S., Spontaneous Nucleation and Growth of Pure Silica Zeolite-β Free of Connectivity Defects. *Chem. Commun.* **1996**, (20), 2365-2366.
136. Cubillas, P.; Anderson, M. W., *Chapter 1 Synthesis Mechanism: Crystal Growth and Nucleation*. Wiley-VCH Verlag GmbH & Co. KGaA: 2010; p 1-55.
137. Valencia, S.; Corma, A. Stannosilicate Molecular Sieves. US6306364 B1, 1999.
138. Larlus, O.; Valtchev, V. P., Control of the Morphology of All-Silica BEA-type Zeolite Synthesized in Basic Media. *Chem. Mater.* **2005**, *17* (4), 881-886.
139. Serrano, D. P.; Van Grieken, R.; Sánchez, P.; Sanz, R.; Rodríguez, L., Crystallization Mechanism of All-silica Zeolite Beta in Fluoride Medium. *Microporous Mesoporous Mater.* **2001**, *46* (1), 35-46.
140. Chen, Y.; Zhu, G.; Peng, Y.; Yao, X.; Qiu, S., Synthesis and Characterization of (*h0l*) Oriented High-silica Zeolite Beta Membrane. *Microporous Mesoporous Mater.* **2009**, *124* (1–3), 8-14.
141. Voorhees, P. W., The Theory of Ostwald Ripening. *J. Stat. Phys.* **1985**, *38* (1-2), 231-252.
142. Schubert, U.; Hüsing, N., *Synthesis of Inorganic Materials*. Second, Revised and Updated Edition ed.; Wiley-VCH: Weinheim, 2005.
143. Teketel, S.; Lundegaard, L. F.; Skistad, W.; Chavan, S. M.; Olsbye, U.; Lillerud, K. P.; Beato, P.; Svelle, S., Morphology-induced Shape Selectivity in Zeolite Catalysis. *J. Catal.* **2015**, *327*, 22-32.
144. Hay, D. G.; Jaeger, H.; Wilshier, K. G., Systematic Intergrowth in Crystals of ZSM-5 Zeolite. *Zeolites* **1990**, *10* (6), 571-576.
145. Sun, J.; Zhu, G.; Chen, Y.; Li, J.; Wang, L.; Peng, Y.; Li, H.; Qiu, S., Synthesis, Surface and Crystal Structure Investigation of the Large Zeolite Beta Crystal. *Microporous Mesoporous Mater.* **2007**, *102* (1–3), 242-248.
146. von Ballmoos, R.; Meier, W. M., Zoned Aluminium Distribution in Synthetic Zeolite ZSM-5. *Nature* **1981**, *289* (5800), 782-783.
147. Derouane, E. G.; Determmerie, S.; Gabelica, Z.; Blom, N., Synthesis and Characterization of ZSM-5 Type Zeolites I. Physico-chemical Properties of Precursors and Intermediates. *Appl. Catal.* **1981**, *1* (3), 201-224.

148. Danilina, N.; Krumeich, F.; Castelanelli, S. A.; van Bokhoven, J. A., Where Are the Active Sites in Zeolites? Origin of Aluminum Zoning in ZSM-5. *J. Phys. Chem. C* **2010**, *114* (14), 6640-6645.
149. Cundy, C. S.; Cox, P. A., The Hydrothermal Synthesis of Zeolites: Precursors, Intermediates and Reaction Mechanism. *Microporous Mesoporous Mater.* **2005**, *82* (1–2), 1-78.
150. Larlus, O.; Valtchev, V.; Delmotte, L.; Kessler, H., Size and Morphological Control of All-silica Zeolite Beta. *Stud. Surf. Sci. Catal.* **2004**, *154A*, 725-730.
151. Althoff, R.; Schulz-Dobrick, B.; Schüth, F.; Unger, K., Controlling the Spatial Distribution of Aluminum in ZSM-5 Crystals. *Microporous Mater.* **1993**, *1* (3), 207-218.
152. Nemeth, L.; Bare, S. R., Chapter One - Science and Technology of Framework Metal-Containing Zeotype Catalysts. In *Advances in Catalysis*, Friederike, C. J., Ed. Academic Press: 2014; Vol. Volume 57, pp 1-97.
153. Groen, J. C.; Moulijn, J. A.; Perez-Ramirez, J., Desilication: On the Controlled Generation of Mesoporosity in MFI Zeolites. *J. Mater. Chem.* **2006**, *16* (22), 2121-2131.
154. Fan, W.; Fan, B.; Shen, X.; Li, J.; Wu, P.; Kubota, Y.; Tatsumi, T., Effect of Ammonium Salts on the Synthesis and Catalytic Properties of TS-1. *Microporous Mesoporous Mater.* **2009**, *122* (1–3), 301-308.
155. Abdel-Rahman, M. A.; Tashiro, Y.; Sonomoto, K., Recent Advances in Lactic Acid Production by Microbial Fermentation Processes. *Biotechnol. Adv.* **2013**, *31* (6), 877-902.
156. Wang, F.-F.; Liu, C.-L.; Dong, W.-S., Highly Efficient Production of Lactic Acid from Cellulose using Lanthanide Triflate Catalysts. *Green Chem.* **2013**, *15* (8), 2091-2095.
157. Lei, X.; Wang, F.-F.; Liu, C.-L.; Yang, R.-Z.; Dong, W.-S., One-pot Catalytic Conversion of Carbohydrate Biomass to Lactic Acid using an $ErCl_3$ Catalyst. *Appl. Catal. A-Gen* **2014**, *482*, 78-83.
158. Zhou, L.; Wu, L.; Li, H.; Yang, X.; Su, Y.; Lu, T.; Xu, J., A Facile and Efficient Method to Improve the Selectivity of Methyl Lactate in the Chemocatalytic Conversion of Glucose Catalyzed by Homogeneous Lewis Acid. *J. Mol. Catal. A: Chem.* **2014**, *388–389*, 74-80.
159. Zhou, X.; Bi, R. Method for Synthesis of Lactic Acid and Its Derivatives. US20140058130A1, 2014.
160. Zhao, D.; Szostak, R.; Kevan, L., Role of alkali-metal cations and seeds in the synthesis of silica-rich heulandite-type zeolites. *Journal of Materials Chemistry* **1998**, *8* (1), 233-239.
161. Hould, N. D.; Foster, A.; Lobo, R. F., Zeolite Beta Mechanisms of Nucleation and Growth. *Microporous Mesoporous Mater.* **2011**, *142* (1), 104-115.
162. Tatsumi, T.; Watanabe, Y.; Koyano, K. A., Synthesis of Dimethyl Carbonate from Ethylene Carbonate and Methanol using TS-1 as Solid Base Catalyst. *Chem. Commun.* **1996**, (19), 2281-2282.
163. Pinho, S. P.; Macedo, E. A., Solubility of NaCl, NaBr, and KCl in Water, Methanol, Ethanol, and Their Mixed Solvents. *J. Chem. Eng. Data* **2005**, *50* (1), 29-32.

164. Niemela, K.; Sjostrom, E., Alkaline Degradation of Mannan. *Holzforschung* **1986**, *40* (1), 9-14.
165. Löwendahl, L.; Samuelson, O., Influence of Iron and Cobalt Compounds upon Oxygen-alkali Treatment of Cellulose. *Sven. Papperstidn.* **1974**, *77* (16), 593-602.
166. Löwendahl, L.; Lindström, L.-Å.; Samuelson, O., Nonoxidative and Oxidative Alkaline Degradation of Mannan. *Acta Chem. Scand., Ser. B* **1980**, *B34* (9), 623-8.
167. Chen, H.-S.; Wang, A.; Sorek, H.; Lewis, J. D.; Román-Leshkov, Y.; Bell, A. T., Production of Hydroxyl–rich Acids from Xylose and Glucose Using Sn-BEA Zeolite. *ChemistrySelect* **2016**, *1* (14), 4167-4172.
168. Anet, E. F. L. J., Degradation of Carbohydrates. III. Unsaturated Hexosones. *Aust. J. Chem.* **1962**, *15*, 503-9.
169. Anet, E. F. L. J., 3-Deoxyglycosuloses (3-Deoxyglycosones) and the Degradation of Carbohydrates. *Advan. Carbohydr. Chem.* **1964**, *19*, 181-218.
170. Sugisawa, H.; Sudo, K., The Thermal Degradation of Sugars. The Initial Products of Browning Reaction in Glucose Caramel. *Can. Inst. Food Technol. J.* **1969**, *2* (2), 94-97.
171. El-Dash, A. A.; Hodge, J. E., Determination of 3-Deoxy-D-erythro-hexosulose (3-Deoxy-D-glucosone) and other Degradation Products of Sugars by Borohydride Reduction and Gas-liquid Chromatography. *Carbohyd. Res.* **1971**, *18* (2), 259-267.
172. Feather, M. S.; Harris, J. F., Mechanism of Conversion of Hexoses into 5-(Hydroxymethyl)-2-furaldehyde and Metasaccharinic Acid. *Carbohyd. Res.* **1970**, *15* (2), 304-9.
173. Usui, T.; Yanagisawa, S.; Ohguchi, M.; Yoshino, M.; Kawabata, R.; Kishimoto, J.; Arai, Y.; Aida, K.; Watanabe, H.; Hayase, F., Identification and Determination of α-Dicarbonyl Compounds Formed in the Degradation of Sugars. *Biosci. Biotechnol. Biochem.* **2007**, *71* (10), 2465-2472.
174. Hellwig, M.; Degen, J.; Henle, T., 3-Deoxygalactosone, a "New" 1,2-Dicarbonyl Compound in Milk Products. *J. Agr. Food. Chem.* **2010**, *58* (19), 10752-10760.
175. Jadhav, H.; Pedersen, C. M.; Solling, T.; Bols, M., 3-Deoxy-glucosone is an Intermediate in the Formation of Furfurals from D-glucose. *ChemSusChem* **2011**, *4* (8), 1049-51.
176. Hellwig, M.; Nobis, A.; Witte, S.; Henle, T., Occurrence of (Z)-3,4-Dideoxyglucoson-3-ene in Different Types of Beer and Malt Beer as a Result of 3-Deoxyhexosone Interconversion. *J. Agr. Food. Chem.* **2016**, *64* (13), 2746-2753.
177. Moreau, C.; Durand, R.; Razigade, S.; Duhamet, J.; Faugeras, P.; Rivalier, P.; Ros, P.; Avignon, G., Dehydration of Fructose to 5-Hydroxymethylfurfural over H-mordenites. *Appl. Catal., A* **1996**, *145* (1), 211-224.
178. Yong, G.; Zhang, Y.; Ying, J. Y., Efficient Catalytic System for the Selective Production of 5-Hydroxymethylfurfural from Glucose and Fructose. *Angew. Chem. Int. Ed.* **2008**, *47* (48), 9345-9348.
179. Tao, F.; Song, H.; Chou, L., Dehydration of fructose into 5-hydroxymethylfurfural in acidic ionic liquids. *RSC Adv.* **2011**, *1* (4), 672-676.

180. Weenen, H.; Tjan, S. B., Analysis, Structure, and Reactivity of 3-Deoxyglucosone. In *Flavor Precursors*, American Chemical Society: 1992; Vol. 490, pp 217-231.
181. Thornalley, P. J.; Langborg, A.; Minhas, H. S., Formation of Glyoxal, Methylglyoxal and 3-Deoxyglucosone in the Glycation of Proteins by Glucose. *Biochem. J.* **1999**, *344* (Pt 1), 109-116.
182. Fiedler, T.; Moritz, T.; Kroh, L., Influence of α-Dicarbonyl Compounds to the Molecular Weight Distribution of Melanoidins in Sucrose Solutions: Part 1. *Eur. Food Res. Technol.* **2006**, *223* (6), 837-842.
183. Pfeifer, Y. V.; Haase, P. T.; Kroh, L. W., Reactivity of Thermally Treated α-Dicarbonyl Compounds. *J. Agric. Food Chem.* **2013**, *61* (12), 3090-3096.
184. Rasrendra, C. B.; Fachri, B. A.; Makertihartha, I. G. B. N.; Adisasmito, S.; Heeres, H. J., Catalytic Conversion of Dihydroxyacetone to Lactic Acid Using Metal Salts in Water. *ChemSusChem* **2011**, *4* (6), 768-777.
185. Choudhary, V.; Pinar, A. B.; Sandler, S. I.; Vlachos, D. G.; Lobo, R. F., Xylose Isomerization to Xylulose and its Dehydration to Furfural in Aqueous Media. *ACS Catal.* **2011**, *1* (12), 1724-1728.
186. Saravanamurugan, S.; Riisager, A., Solid Acid Catalysed Formation of Ethyl Levulinate and Ethyl Glucopyranoside from Mono- and Disaccharides. *Catal. Commun.* **2012**, *17*, 71-75.
187. Saravanamurugan, S.; Paniagua, M.; Melero, J. A.; Riisager, A., Efficient Isomerization of Glucose to Fructose over Zeolites in Consecutive Reactions in Alcohol and Aqueous Media. *J. Am. Chem. Soc.* **2013**, *135* (14), 5246-5249.
188. Saravanamurugan, S.; Riisager, A.; Taarning, E.; Meier, S., Combined Function of Brønsted and Lewis Acidity in the Zeolite-Catalyzed Isomerization of Glucose to Fructose in Alcohols. *ChemCatChem* **2016**, *8* (19), 3107-3111.
189. Boronat, M.; Corma, A.; Renz, M., Mechanism of the Meerwein-Ponndorf-Verley-Oppenauer (MPVO) Redox Equilibrium on Sn- and Zr-Beta Zeolite Catalysts. *J. Phys. Chem. B* **2006**, *110* (42), 21168-21174.
190. Rasal, R. M.; Janorkar, A. V.; Hirt, D. E., Poly(lactic acid) Modifications. *Prog. Polym. Sci.* **2010**, *35* (3), 338-356.
191. Van Wouwe, P.; Dusselier, M.; Vanleeuw, E.; Sels, B., Lactide Synthesis and Chirality Control for Polylactic acid Production. *ChemSusChem* **2016**, *9* (9), 907-921.
192. Södergård, A.; Stolt, M., Properties of Lactic Acid Based Polymers and their Correlation with Composition. *Prog. Polym. Sci.* **2002**, *27* (6), 1123-1163.
193. Jing, F.; Smith, M. R.; Baker, G. L., Cyclohexyl-Substituted Polyglycolides with High Glass Transition Temperatures. *Macromolecules* **2007**, *40* (26), 9304-9312.
194. Liu, T.; Simmons, T. L.; Bohnsack, D. A.; Mackay, M. E.; Smith, M. R.; Baker, G. L., Synthesis of Polymandelide: A Degradable Polylactide Derivative with Polystyrene-like Properties. *Macromolecules* **2007**, *40* (17), 6040-6047.
195. Yin, M.; Baker, G. L., Preparation and Characterization of Substituted Polylactides. *Macromolecules* **1999**, *32* (23), 7711-7718.
196. Wang, Y.; Lewis, J. D.; Román-Leshkov, Y., Synthesis of Itaconic Acid Ester Analogues via Self-Aldol Condensation of Ethyl Pyruvate Catalyzed by Hafnium BEA Zeolites. *ACS Catal.* **2016**, *6* (5), 2739-2744.

197. Okuda, T.; Ishimoto, K.; Ohara, H.; Kobayashi, S., Renewable Biobased Polymeric Materials: Facile Synthesis of Itaconic Anhydride-Based Copolymers with Poly(l-lactic acid) Grafts. *Macromolecules* **2012**, *45* (10), 4166-4174.
198. Kline, B. J.; Beckman, E. J.; Russell, A. J., One-Step Biocatalytic Synthesis of Linear Polyesters with Pendant Hydroxyl Groups. *J. Am. Chem. Soc.* **1998**, *120* (37), 9475-9480.
199. Kulshrestha, A. S.; Gao, W.; Gross, R. A., Glycerol Copolyesters: Control of Branching and Molecular Weight Using a Lipase Catalyst. *Macromolecules* **2005**, *38* (8), 3193-3204.
200. Dong, H.; Wang, H.-d.; Cao, S.-g.; Shen, J.-c., Lipase-catalyzed Polymerization of Lactones and Linear Hydroxyesters. *Biotechnol. Lett.* **1998**, *20* (10), 905-908.
201. Sasaki, M.; Goto, K.; Tajima, K.; Adschiri, T.; Arai, K., Rapid and Selective Retro-aldol Condensation of Glucose to Glycolaldehyde in Supercritical Water. *Green Chem.* **2002**, *4* (3), 285-287.
202. Mohan, D.; Pittman, C. U.; Steele, P. H., Pyrolysis of Wood/Biomass for Bio-oil: A Critical Review. *Energy Fuels* **2006**, *20* (3), 848-889.
203. Vinu, R.; Broadbelt, L. J., A Mechanistic Model of Fast Pyrolysis of Glucose-based Carbohydrates to Predict Bio-oil Composition. *Energy Environ. Sci.* **2012**, *5* (12), 9808-9826.
204. Mägerlein, W.; Melder, J. P.; Pastre, J.; Eberhardt, J.; Krug, T.; Kreitschmann, M. Reaction of Glycolaldehyde with an Aminating Agent. US20120271068 A1, 2012.
205. Van de Vyver, S.; Román-Leshkov, Y., Metalloenzyme-Like Zeolites as Lewis Acid Catalysts for C-C Bond Formation. *Angew. Chem. Int. Ed.* **2015**, *54* (43), 12554-12561.
206. Jariwalla, R. J. Methods and Compositions for Selective Cancer Chemotherapy. US 20040092549 A1, 2001.
207. Ooms, R.; Dusselier, M.; Geboers, J. A.; Op de Beeck, B.; Verhaeven, R.; Gobechiya, E.; Martens, J. A.; Redl, A.; Sels, B. F., Conversion of Sugars to Ethylene Glycol with Nickel Tungsten Carbide in a Fed-batch Reactor: High Productivity and Reaction Network Elucidation. *Green Chem.* **2014**, *16* (2), 695-707.
208. Kishida, H.; Jin, F.; Yan, X.; Moriya, T.; Enomoto, H., Formation of Lactic Acid from Glycolaldehyde by Alkaline Hydrothermal Reaction. *Carbohyd. Res.* **2006**, *341* (15), 2619-2623.
209. Yan, X.; Jin, F.; Tohji, K.; Kishita, A.; Enomoto, H., Hydrothermal Conversion of Carbohydrate Biomass to Lactic Acid. *AIChE J.* **2010**, *56* (10), 2727-2733.
210. Trigerman, S.; Biron, E.; Weiss, A. H., Formaldehyde Base Catalysis by NaX zeolite. *React. Kinet. Catal. Lett.* **1977**, *6* (3), 269-274.
211. Tajima, H.; Tabata, K.; Niitsu, T.; Inoue, H., The Formose Reaction on a Synthetic Zeolite Impregnated with Thiazolium Catalyst. *J. Chem. Eng. Jpn.* **2002**, *35* (6), 564-568.
212. Yamaguchi, S.; Matsuo, T.; Motokura, K.; Sakamoto, Y.; Miyaji, A.; Baba, T., Mechanistic Studies on the Cascade Conversion of 1,3-Dihydroxyacetone and Formaldehyde into α-Hydroxy-γ-butyrolactone. *ChemSusChem* **2015**, *8* (5), 853-860.

213. Yamaguchi, S.; Matsuo, T.; Motokura, K.; Miyaji, A.; Baba, T., Influence of the Interaction between a Tin Catalyst and an Accelerator on the Formose-Inspired Synthesis of α-Hydroxy-γ-butyrolactone. *ChemCatChem* **2016**, *8* (7), 1386-1391.
214. Lewis, J. D.; Van de Vyver, S.; Román-Leshkov, Y., Acid–Base Pairs in Lewis Acidic Zeolites Promote Direct Aldol Reactions by Soft Enolization. *Angew. Chem., Int. Ed.* **2015**, *54* (34), 9835-9838.
215. Jae, J.; Tompsett, G. A.; Foster, A. J.; Hammond, K. D.; Auerbach, S. M.; Lobo, R. F.; Huber, G. W., Investigation into the shape selectivity of zeolite catalysts for biomass conversion. *J. Catal.* **2011**, *279* (2), 257-268.
216. Simonov, A. N.; Matvienko, L. G.; Pestunova, O. P.; Parmon, V. N.; Komandrova, N. A.; Denisenko, V. A.; Vas'kovskii, V. E., Selective Synthesis of Erythrulose and 3-Pentulose from Formaldehyde and Dihydroxyacetone Catalyzed by Phosphates in a Neutral Aqueous Medium. *Kinet. Catal.* **2007**, *48* (4), 550-555.
217. Simonov, A. N.; Pestunova, O. P.; Matvienko, L. G.; Snytnikov, V. N.; Snytnikova, O. A.; Tsentalovich, Y. P.; Parmon, V. N., Possible Prebiotic Synthesis of Monosaccharides from Formaldehyde in Presence of Phosphates. *Adv. Space Res.* **2007**, *40* (11), 1634-1640.
218. Delidovich, I.; Simonov, A.; Pestunova, O.; Parmon, V., Catalytic Condensation of Glycolaldehyde and Glyceraldehyde with Formaldehyde in Neutral and Weakly Alkaline Aqueous Media: Kinetics and Mechanism. *Kinet. Catal.* **2009**, *50* (2), 297-303.
219. Matsumoto, T.; Inoue, S., Formose Reactions. Part 3. Selective Formose Reaction Catalyzed by Organic Bases. *J. Chem. Soc., Perkin Trans. 1* **1982**, (0), 1975-1979.
220. Córdova, A.; Ibrahem, I.; Casas, J.; Sundén, H.; Engqvist, M.; Reyes, E., Amino Acid Catalyzed Neogenesis of Carbohydrates: A Plausible Ancient Transformation. *Chem. Eur. J.* **2005**, *11* (16), 4772-4784.
221. Kofoed, J.; Reymond, J.-L.; Darbre, T., Prebiotic Carbohydrate Synthesis: Zinc-proline Catalyzes Direct Aqueous Aldol Reactions of α-Hydroxy Aldehydes and Ketones. *Org. Biomol. Chem.* **2005**, *3* (10), 1850-1855.
222. Pizzarello, S.; Weber, A. L., Prebiotic Amino Acids as Asymmetric Catalysts. *Science* **2004**, *303* (5661), 1151.
223. Weber, A. L.; Pizzarello, S., The Peptide-catalyzed Stereospecific Synthesis of Tetroses: A Possible Model for Prebiotic Molecular Evolution. *Proc. Natl. Acad. Sci.* **2006**, *103* (34), 12713-12717.
224. Ricardo, A.; Carrigan, M. A.; Olcott, A. N.; Benner, S. A., Borate Minerals Stabilize Ribose. *Science* **2004**, *303* (5655), 196.
225. Kim, H.-J.; Ricardo, A.; Illangkoon, H. I.; Kim, M. J.; Carrigan, M. A.; Frye, F.; Benner, S. A., Synthesis of Carbohydrates in Mineral-Guided Prebiotic Cycles. *J. Am. Chem. Soc.* **2011**, *133* (24), 9457-9468.
226. Lambert, J. B.; Gurusamy-Thangavelu, S. A.; Ma, K., The Silicate-Mediated Formose Reaction: Bottom-Up Synthesis of Sugar Silicates. *Science* **2010**, *327* (5968), 984-986.
227. Saravanamurugan, S.; Riisager, A., Zeolite-catalyzed Isomerization of Tetroses in Aqueous Medium. *Catal. Sci. Technol.* **2014**, *4* (9), 3186-3190.

228. Sádaba, I.; Lopez Granados, M.; Riisager, A.; Taarning, E., Deactivation of Solid Catalysts in Liquid Media: The Case of Leaching of Active Sites in Biomass Conversion Reactions. *Green Chem.* **2015**, *17* (8), 4133-4145.
229. Jong, S.-J.; Pradhan, A. R.; Wu, J.-F.; Tsai, T.-C.; Liu, S.-B., On the Regeneration of Coked H-ZSM-5 Catalysts. *J. Catal.* **1998**, *174* (2), 210-218.
230. Bøjstrup, M.; Petersen, B. O.; Beeren, S. R.; Hindsgaul, O.; Meier, S., Fast and Accurate Quantitation of Glucans in Complex Mixtures by Optimized Heteronuclear NMR Spectroscopy. *Anal. Chem.* **2013**, *85* (18), 8802-8808.
231. Petersen, B. O.; Hindsgaul, O.; Meier, S., Profiling of Carbohydrate Mixtures at Unprecedented Resolution using High-precision ^{1}H-^{13}C Chemical Shift Measurements and a Reference Library. *Analyst* **2014**, *139* (2), 401-406.
232. Dusselier, M.; Van Wouwe, P.; Dewaele, A.; Jacobs, P. A.; Sels, B. F., Shape-selective Zeolite Catalysis for Bioplastics Production. *Science* **2015**, *349* (6243), 78-80.

Appendix A
Supporting Information

Figures

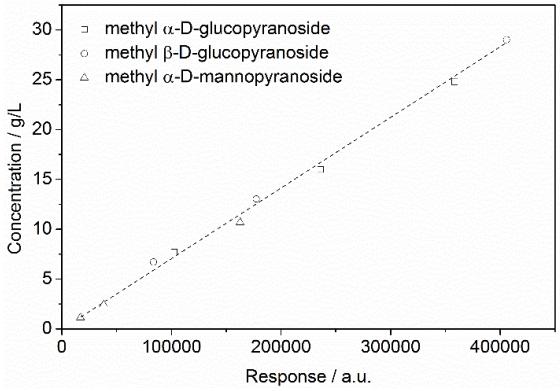

Figure A.1. Concentration as a function of response for the three commercially available methyl glycosides; methyl α-D-glucopyranoside, methyl β-D-glucopyranoside and methyl α-D-mannopyranoside measured Carbohydrate (Zorbax) column running an eluent of 60 wt% acetonitrile/water at 0.5 mL/min with a column temperature at 30 °C.

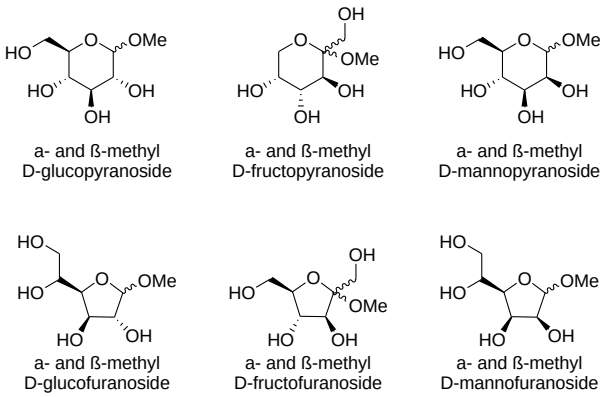

Figure A.2. Representation of the different isomers of methyl glycosides obtained from glucose, fructose and mannose.[127]

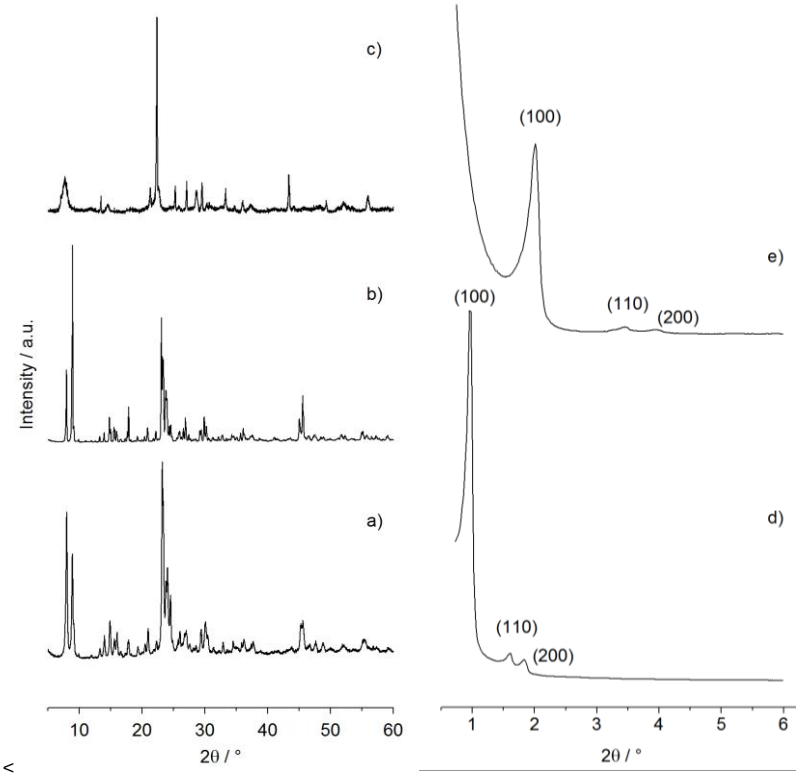

Figure A.3 Normalized X-ray diffraction patterns (5° – 60° 2θ) of a) Sn-MFI (100, OH^-), b) Sn-MFI (400, F^-), and c) Sn-Beta (150, HT) and Low-angle X-ray diffraction (0.7° – 6° 2θ) of d) Sn-SBA-15 (200, HT), and e) Sn-MCM-41 (150, HT).

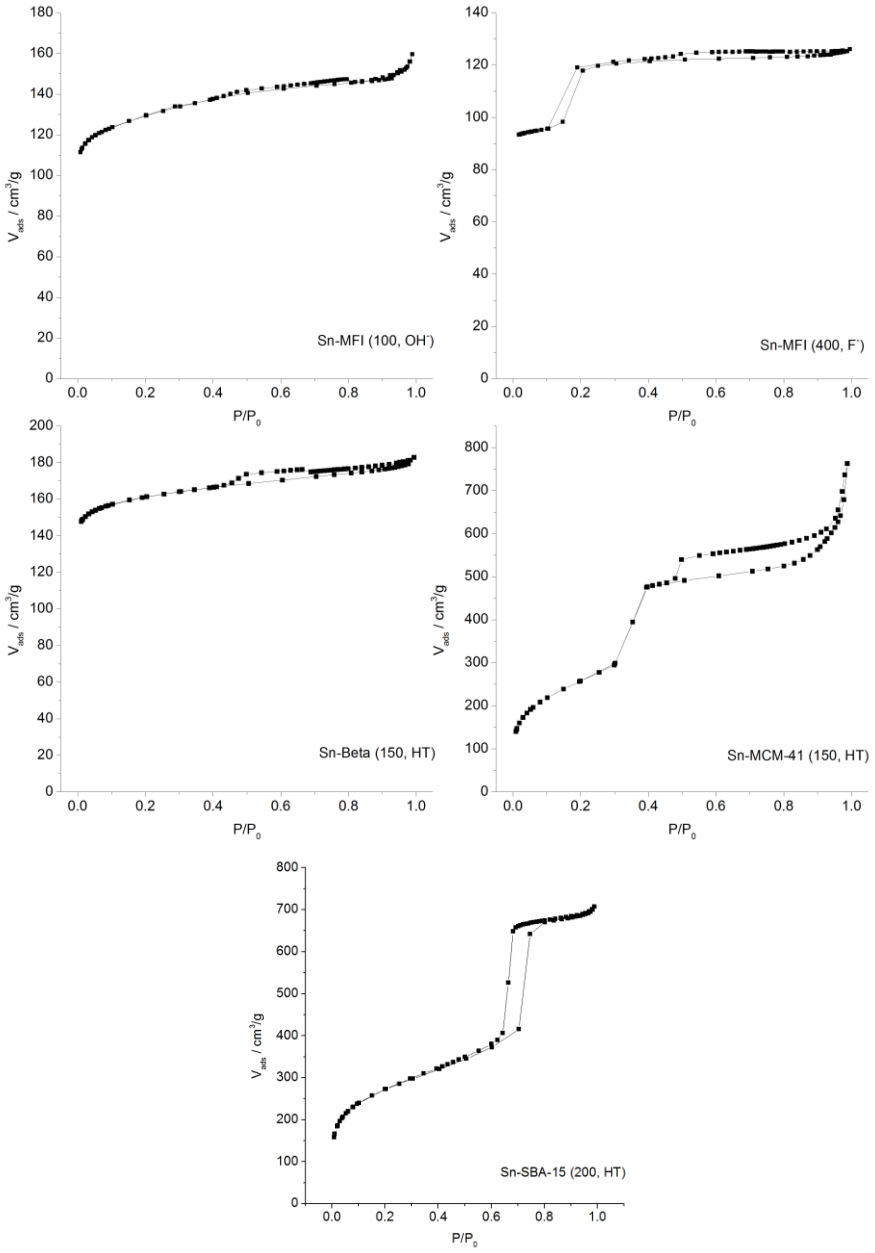

Figure A.4. N_2-adsorption/desorption isotherms for Sn-MFI (100, OH-), Sn-MFI (400, F-), Sn-Beta (150, HT), Sn-MCM-41, (150, HT) and Sn-SBA-15 (200, HT) used for the determination of total and micropore surface area as well as total and micropore volume showed in Table 6.1 on p. 113.

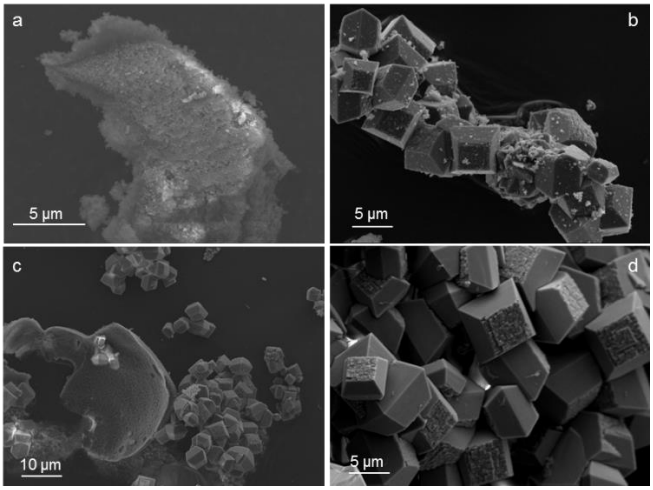

Figure A.5. Micrographs of Sn-Beta sample with Si/Sn = 200 synthesized under hydrothermal conditions for a) 2 days, b) 4 days, c) 7 days and d) 14 days.

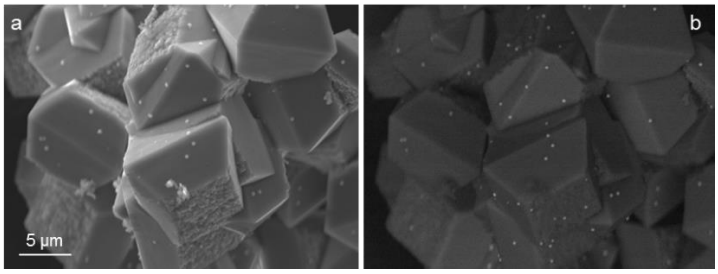

Figure A.6. a) Secondary electron and b) back-scattered electron images of Sn-Beta (Si/Sn = 200) synthesized for 7 days with SnO_2 particles visible on the surface.

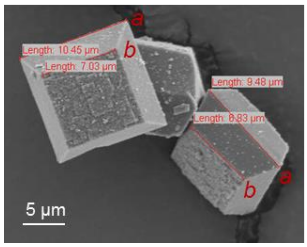

Figure A.7. SEM image of Sn-Beta sample with Si/Sn = 150 synthesized for 14 days with measurements of *a* and *b*.

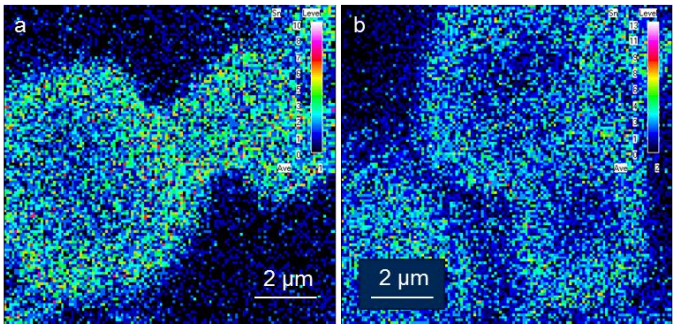

Figure A.8. SEM-WDS measurements showing the tin distribution in transverse sections of Sn-Beta zeolite (Si/Sn = 200, synthesized for 7 days). The measurements are done a) before and b) after thermal removal of the organic template at 550 °C for 6 h.

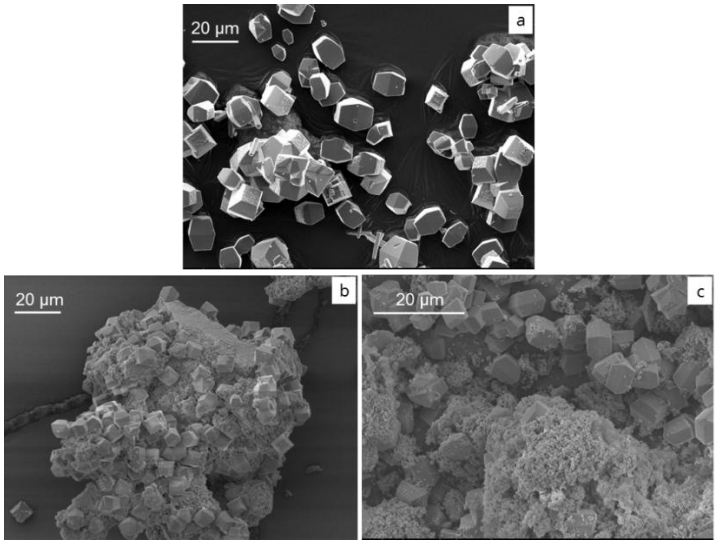

Figure A.9. Micrographs of purely siliceous Beta samples synthesized varying the TEA/SiO2 ratio in the gel from 0.55 to a) 0.44, b) 0.66 and c) 0.71 and allowing them to crystallize for 7 days at 140 °C.

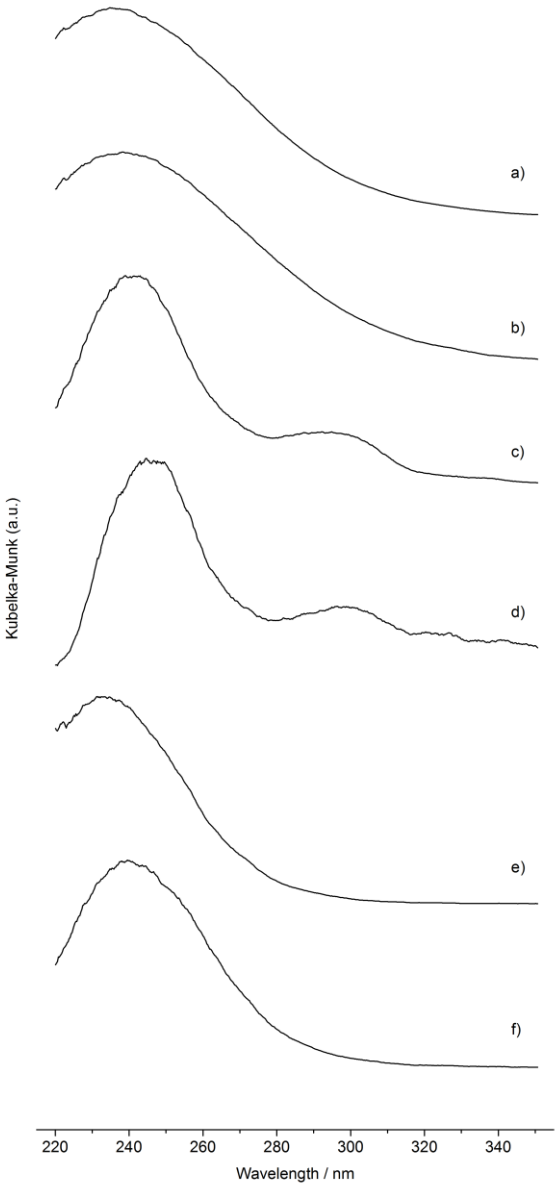

Figure A.10. Ultraviolet-visible (UV-Vis) reflectance spectra measurements of Sn-Beta zeolites samples (Si/Sn = 200) prepared a) without alkali, Sn-Beta (200, HT), in the synthesis gel and with alkali yielding; b) Li-Sn-Beta (200, HT), c) Na-Sn-Beta (200, HT), d) K-Sn-Beta (200, HT), e) Rb-Sn-Beta (200, HT) and f) Cs-Sn-Beta (200, HT).

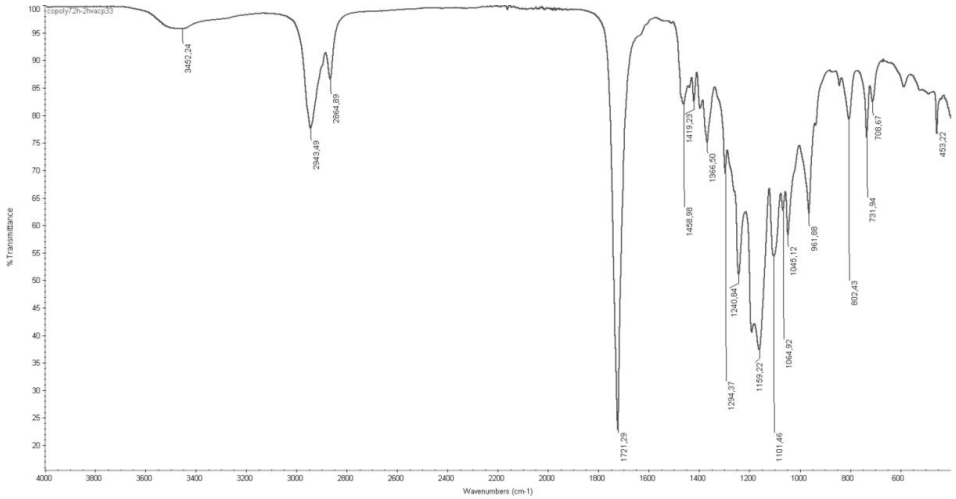

Figure A.11. FT-IR spectrum of poly(E6-HH-co-DPM) showing a broad signal at 3496 cm-1 arising from the O-H stretch as well as a characteristic C=O stretch at 1721 cm-1 and C-O stretch at 1159 and 1045 cm-1 from the ester functionality. A weak signal from the C=C stretch is visible on the shoulder of the C=O stretch and a strong C=C out-of-plane bend signal is visible at 961 cm-1. Figure prepared by Ph.D. Student Christian Anders. Adapted from ref. [49].

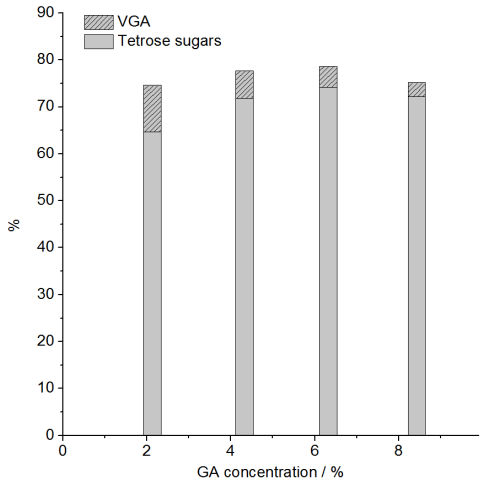

Figure A.12. Yields of tetrose sugars and vinyl glycolic acid (VGA) obtained using Sn-MFI (100, OH^-) varying the glycolaldehyde concentration. Reaction conditions: 0.060-0.250 g glycolaldehyde (dimer), 0.075 g Sn-MFI (100, OH^-), 80 °C, 2 h, 600 rpm stirring. Adapted from [117].

Schemes

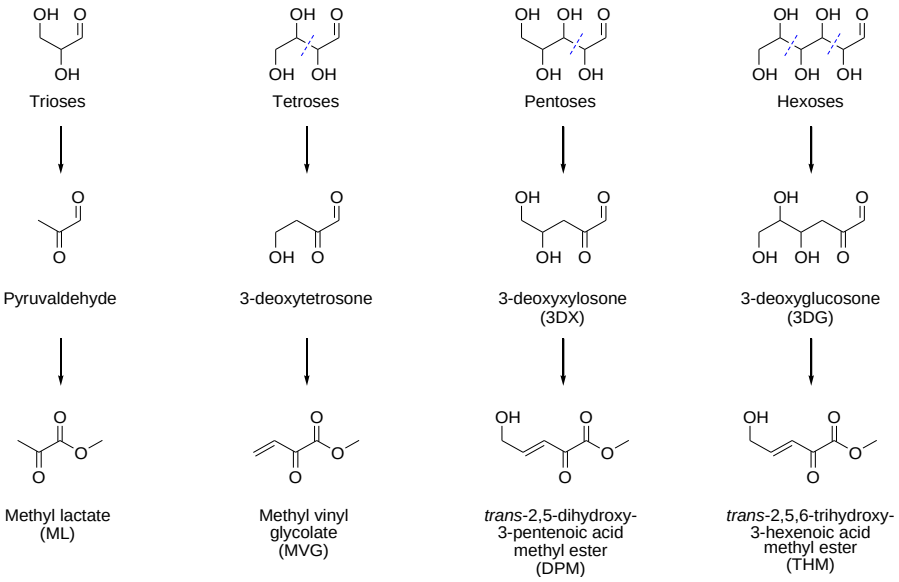

Scheme A.1. Overview of the different 1,2-dione intermediates formed in the tin catalyzed conversion of different sugars (trioses to hexoses) to their corresponding α-hydroxy acid esters.

C_2 sugar

Glycolaldehyde
(GA)

C_4 sugars

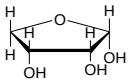

a-D-erythrofuranose
(ERY^{fura})

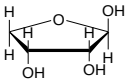

ß-D-erythrofuranose
(ERY^{furb})

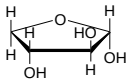

a-D-threofuranose
(THR^{fura})

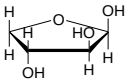

ß-D-threofuranose
(THR^{furb})

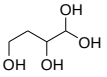

C_4 sugar hydrate
(ERY/THR^{hyd})

C_6 sugars

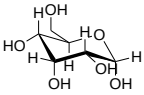

a-D-allopyranose
(ALL^{pyra})

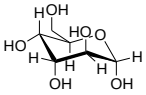

a-D-altopyranose
(ALT^{pyra})

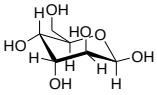

ß-D-altropyranose
(ALT^{pyrb})

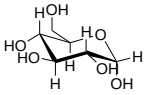

a-D-glucopyranose
(GLC^{pyra})

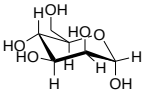

a-D-mannopyranose
(MAN^{pyra})

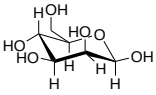

ß-D-mannopyranose
(MAN^{pyrb})

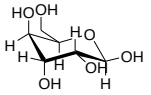

ß-D-gulopyranose
(Gul^{pyrb})

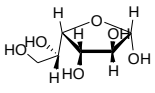

a-D-idofuranose
(IDO^{fura})

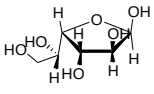

ß-D-idofuranose
(IDO^{furb})

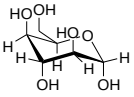

a-D-idopyranose
(IDO^{pyra})

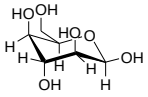

ß-D-idopyranose
(IDO^{pyrb})

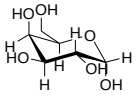

a-D-galactopyranose
(GAL^{pyra})

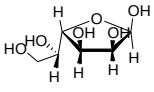

a-D-talofuranose
(Tal^{fura})

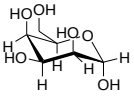

a-D-talopyranose
(Tal^{pyra})

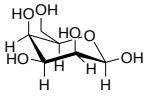

ß-D-talopyranose
(Tal^{pyrb})

Scheme A.2. Names, structures and abbreviations of glycolaldehyde and the tetrose and hexose sugar isomers identified by high-field NMR spectroscopy shown in Figure 6.10 on p. 124. Adapted from [117].

Tables

Table A.1. The methyl lactate yield obtained in the absence and presence of a variety of catalysts.

Catalyst	ML yield
	%
Blank	3
Si-Beta	4
SnO_2-Beta	3
SnO_2[a]	<1
Sn-Beta (200, HT)	60

a) For this experiment, 50 mg of catalyst was used. Reaction conditions: 0.150 g catalyst, 0.450 g sucrose (1.31 mmol), 15 g 0.17 mM K_2CO_3 in methanol, 170 °C, 16 h.

Table A.2. Conversion of glycolaldehyde dimer at low substrate-to-catalyst ratios using Sn-MFI (100, OH^-)

Entry	Glycolaldehyde concentration	Substrate-to-catalyst ratio (wt/wt)	Time	VGA
	%	-	h	%
1	2	0.27	4	44
2	2	0.28	20	43
3	1	0.14	20	37

Reaction conditions: 0.031-0.062 g glycolaldehyde dimer, 0.230 g Sn-MFI (100, OH^-), 2.5 g water, 100°C, 4-20 h, 600 rpm.

Table A.3. Conversion of glycolaldehyde in the presence or absence of alkali added to the reaction media. Entries 1-4 were performed using Sn-Beta (150, HT) while entries 5-7 were done with done without added catalyst.

Entry	Catalyst	c(KNO_3)	GA	Tetroses	Hexoses	VGA	HBL	Total
		M			%			
1	Sn-Beta (150, HT)	0.2	2	4	3	13	13	36
2	Sn-Beta (150, HT)	0.5	5	17	13	13	13	61
3	Sn-Beta (150, HT)	1.0	7	22	16	8	9	63
4	Sn-Beta (150, HT)	2.6	16	29	21	5	8	79
5	-	-	93	5	2			100
6	-	1.1	89	6	2			97
7	-	3.3	87	7	1			95

Reaction conditions: 0.075 g Sn-Beta (150, HT), 5 wt% glycolaldehyde (dimer), 0-3.3 M KNO_3 in H_2O, 100 °C, 6 h.

Table A.4. Conversion of pentose sugars in the absence of alkali. Adapted from ref. [128].

Entry	Catalyst	Substrate	T	Sugars		Retro-aldol products					Dehydration products				
				Uncon.	MX	GA-DMA	ML	MVG	MMHB	Total	DPL	TPM/ DMPM[a]	FUR_{C5}[b]	DPM	Total
			°C	%		%					%				
1	Sn-Beta (150, HT)	Xylose	140	n.d.	4	3	11	1	<1	16	10	14	17	31	72
2	Sn-Beta (150, HT)	Xylose	150	n.d.	3	2	15	2	<1	19	10	12	13	32	68
3	Sn-Beta (150, HT)	Xylose	170	n.d.	3	1	18	4	1	25	10	10	9	34	63
4	Sn-Beta (150, HT)	Xylose	180	n.d.	3	<1	18	4	1	24	10	9	8	32	59
5	Sn-Beta (150, HT)	Ribose	160	n.d.	3	2	12	2	<1	17	10	10	12	30	63
6	Sn-Beta (150, HT)	Lyxose	160	n.d.	3	2	15	2	<1	20	12	13	11	31	66
7	Sn-Beta (150, HT)	Xylose[c]	160	<1	6	<1	14	2	<1	17	11	13	9	34	68
8	Sn-Beta (150, HT)	Xylose[d]	160	n.d.	6	2	13	2	<1	17	11	13	11	32	67
9	Sn-SBA-15 (150, HT)	Xylose	160	<1	32	6	11	<1	<1	18	3	10	18	12	42
10	SnO_2-Beta (150, HT)	Xylose	160	53	42	2	<1	<1	<1	3	1	2	1	<1	6
11	Si-Beta (HT)	Xylose	160	13	42	5	2	<1	<1	8	2	3	3	<1	8
12	-	Xylose	160	75	10	<1	<1	<1	<1	1	n.d.	n.d.	<1	n.d.	1

a) combined yields of 2,4,5-trihydroxy-3-pentanoic acid methyl ester and 2,5-dihydroxy-4-methoxypentanoic acid methyl ester. b) Combined yields of furfural and furfural dimethyl acetal. c) 15 wt% xylose. d) 23 wt% xylose. n.d. = not detected. Abbreviations can be found in Table A.6 on p. 163. Reaction conditions: 160 °C, 0.360 g xylose, 4 g methanol, 0.180 g catalyst, 2 h, 600 rpm stirring.

Table A.5. Conversion of a variety of hexose sugars in the absence of alkali. Adapted from ref. [119].

Entry	Catalyst	Substrate	Sugars		Retro-aldol products					Dehydration products		
			T	MG	GA-DMA	ML	MVG	MMHB	Total	FUR_{CC}[a]	THM	Total[b]
			°C	%	%					%		
1	Sn-Beta (125, PT)	Glucose	120	44	1	3	1	<1	4	10	8	18
2	Sn-Beta (125, PT)	Glucose	140	21	2	10	3	1	16	16	12	28
3	Sn-Beta (125, PT)	Glucose	180	5	2	26	11	1	40	10	8	18
4	Sn-Beta (125, PT)	Fructose	160	9	2	19	7	1	29	14	18	32
5	Sn-Beta (125, PT)	Mannose	160	12	2	20	8	1	31	12	15	27
6	Sn-Beta (125, PT)	Sorbose	160	13	3	15	9	2	29	14	17	31
7	Sn-Beta (125, PT)	Galactose	160	26	2	10	6	1	19	13	12	25
8	Sn-Beta (125, PT)	Sucrose	160	10	2	22	8	2	34	13	15	28
9	deAl-Beta	Glucose	160	86	<1	<1	<1	<1	1	<1	<1	1
10	deAl-Beta	Fructose	160	51	<1	<1	<1	<1	1	14	<1	14
11	SnO_2-Beta (200, HT)	Glucose	160	37	1	<1	<1	<1	1	2	<1	2
12	Si-Beta (HT)	Glucose	160	46	3	2	1	<1	6	3	<1	3

a) combined yields of 5-(hydroxymethyl)furfural (HMF) and 5-(methoxymethyl)furfural (MMF) and the acetal derivatives. b) total dehydration products excluding 3-deoxy-γ-gluconolactones (DGL) and 3-deoxy-gluconic acid methyl ester (DGM), not quantified for these samples. Abbreviations are found in Table A.6 on p. 163. Reaction conditions: 160 °C, 0.360 g glucose, 4 g methanol, 0.180 g catalyst, 6 h, 600 rpm stirring. No unconverted sugars were observed.

Table A.6. Overview of abbreviations, names and structures of substrates, reaction intermediates and product relevant for this dissertation.

Abbreviation	Name; *IUPAC name*	Structure
3DG	3-Deoxyglucosone, *4,5,6-Trihydroxy-2-oxohexanal*	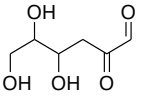
3DT	3-Deoxytetrosone; *4-Hydroxy-2-oxobutanal*	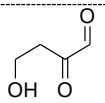
3DX	3-Deoxyxylosone; *4,5-Dihydroxy-2-oxopentanal*	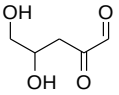
(Trans/cis)-3,4DGE	(*Trans/cis*)-3,4-dideoxyglucosone-3-ene; *(Trans/cis)-5,6-dihydroxy-2-oxo-3-hexenal*	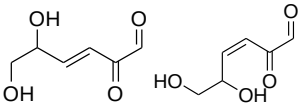
(Trans/cis)-3,4DXE	(*Trans/cis*)-3,4-Dideoxyxylosone-3-ene; *(Trans/cis)-5-hydroxy-2-oxo-3-pentenal*	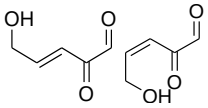
DGL	3-Deoxy-γ-lactones	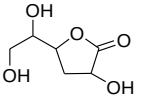
DGM	3-Deoxyhexonic acid methyl ester; *Methyl 2,4,5,6-tetrahydroxyhexanoate*	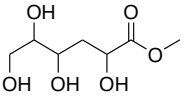
DHA	1,3-Dihydroxyacetone; *1,3-Dihydroxypropanone*	
DMPM	2,4-Dihydroxy-4-methoxy-pentanoic acid methyl ester; *Methyl 2,4-dihydroxy-4-methoxy pentanoate*	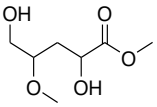
DPL	3-Deoxy-γ-pentonolactones	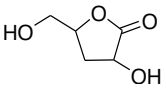

DPM	*Trans*-2,5-dihydroxy-3-pentenoic acid methyl ester; *Methyl 2,5-dihydroxy-3-pentenoate*	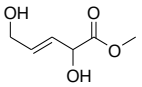
E6-HH	Ethyl 6-hydroxyhexanoate *Ethyl 6-hydroxyhexanoate*	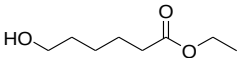
ERU	Erythrulose; *(2R,3R)-2,3,4-Trihydroxybutanal*	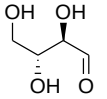
ERY	Erythrose; *(R)-1,3,4-Trihydroxybutan-2-one*	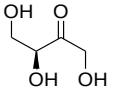
F(-DMA)	Furfural (dimethyl acetal); *Furan-2-carbaldehyde (dimethyl acetal)*	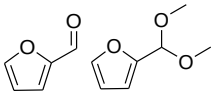
GA(-DMA)	Glycolaldehyde (dimethyl acetal); *2-Hydroxyacetaldehyde (dimethyl acetal)*	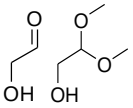
GLA	Glyceraldehyde; *2,3-Dihydroxypropanal*	
HBL	α-Hydroxy-γ-butyrolactone; *4,5-Dihydro-3-hydroxy-2(3H)-furanone*	
HMF(-DMA)	5-(hydroxymethyl)furfural (dimethyl acetal); *5-(Hydroxymethyl)-2-furaldehyde (dimethyl acetal)*	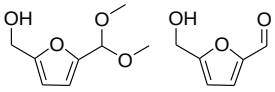
MG	Methyl glycosides obtained from hexoses	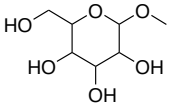
MMHB	Methyl 4-methoxy-2-hydroxybutanoate; *Methyl 2-hydroxy-4-methoxybutanoate*	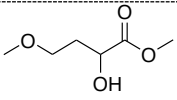
ML	Methyl lactate; *Methyl 2-hydroxypropanoate*	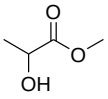

MLA	Methyl levulinate; *Methyl 4-oxo-pentanoate*	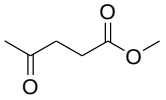
MMF(-DMA)	5-(methoxymethyl)furfural (dimethyl acetal); *5-(Methoxymethyl)-2-furaldehyde (dimethyl acetal)*	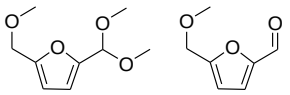
MVG	Methyl vinyl glycolate; *Methyl 2-hydroxy-3-butenoate*	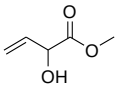
MX	Methyl glycosides obtained from pentoses	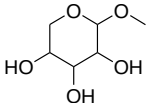
PA	Pyruvaldehyde; *2-Oxopropanal*	
TMHM	2,5,6-trihydroxy-4-methoxy hexanoic acid methyl ester; *Methyl 2,5,6-trihydroxy-4-methoxyhexanoate*	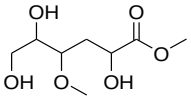
THM	*Trans*-2,5,6-trihydroxy-3-hexenoic acid methyl ester; *Methyl trans-2,5,6-trihydroxy-3-hexenoate*	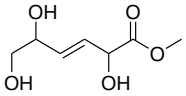
TPM	2,4,5-trihydroxypentanoic acid methyl ester; *Methyl 2,4,5-trihydroxypentanoate*	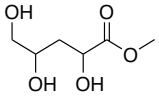
THR	Threose; *(2S,3R)-2,3,4-Trihydroxybutanal*	
VG	Vinyl glyoxal; *2-oxo-3-butenal*	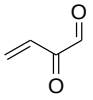
VGA	Vinyl glycolic acid; *2-hydroxy-3-butenoic acid*	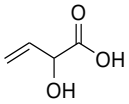

Table A.7. List of general abbreviations used throughout the dissertation.

1D	1-dimensional	DNP	Dynamic nuclear polarization
2D	2-dimensional	DSC	Differential scanning calorimetry
Al-Beta	Aluminum-containing zeotype with the *BEA framework	FID	Flame ionization detector
ATR	Attenuated total reflection	FTIR	Fourier transformed infrared
*BEA	The zeolite framework of the Beta zeolite	GC	Gas chromatography
BET	Brunauer–Emmett–Teller	ICP-OES	Inductively coupled plasma optical emission spectroscopy
BSE	Backscattered electron	HMBC	Heteronuclear multiple bond correlation
BV	Baeyer-Villiger	HPLC	High-performance liquid chromatography
CAL-B	*Candida arctica* Lipase B	HSQC	Heteronuclear single quantum coherence
COSY	Correlation spectroscopy	HT	Hydrothermal
CPMG	Carr−Purcell−Meiboom−Gill	MCM	Mobil Composition of Matter
CSBP	Capped square bipyramidal	MFI	The zeolite framework of the MFI zeolite
CTABr	Hexadecyltrimethyl ammonium bromide	Mn	Number-average molar mass
DAD	Diode array detector	MPV	Meerwein-Ponndorf-Verley
DFT	Density function theory	MPVO	Meerwein-Ponndorf-Verley-Oppenauer

Mw	Molecular weight	Ti-Beta	Titanium-containing zeotype with the *BEA framework
NMR	Nuclear magnetic resonance	Tg	Glass transitions temperature
PLA	Poly(lactic acid)	TG	Thermogravimetric
PONCKS	Partial or no known crystal structure	Tm	Melting temperature
PT	Post-treatment/post-synthesis	TMAS	Tetraethylammonium silicate
RI	Refractive index	TOCSY	Total correlation spectroscopy
SBA	Santa Barbara Amorphous	TPA	Tetrapropylammonium
SDA	Structure directing agent	TPABr	Tetrapropylammonium bromide
SE	Secondary electron	TPAOH	Tetrapropylammonium hydroxide
SEC	Size exclusion chromatography	TS-1	Titanium silicate-1 (titanium-containing zeotype with the MFI framework)
SEM	Scanning electron microscopy	UV	Ultraviolet
Sn-Beta	Tin-containing zeotype with the *BEA framework	UV-Vis	Ultraviolet-visible
Sn-MFI	Tin-containing zeotype with the MFI framework	WDS	Wavelength dispersive spectroscopy
TEA	Tetraethylammonium	XRD	X-ray diffraction
TEAOH	Tetraethylammonium hydroxide	ZAF	Atomic number, absorbance and fluorescence
TEOS	Tetraethyl orthosilicate	Zr-Beta	Zirconium-containing zeotype with the *BEA framework

Appendix B
List of Publications

Publications relevant for the dissertation

Peer-reviewed articles:

Elliot, S. G., Andersen, C., Tolborg, S., Meier, S., Sádaba, I., Daugaard, A. E., and Taarning, E. Synthesis of a Novel Polyester Building Block from Pentoses by Tin-containing Silicates. *RSC Adv.,* **2016**, *in press*. Ref. [128].

Tolborg, S., Meier, S., Saravanamurugan, S., Fristrup, P., Taarning, E., and Sádaba, I. Shape-selective Valorization of Biomass-derived Glycolaldehyde using Tin-containing silicates. *ChemSusChem*, 2016, *9*, 3054-3061. Ref. [117].

Tolborg, S., Meier, S., Sádaba, I., Elliot, S. G., Kristensen, S. K., Saravanamurugan, S., Riisager, A., Fristrup, P., Skrydstrup, T., and Taarning, E. Tin-containing Silicates: Identification of a Glycolytic Pathway via 3-Deoxyglucosone. *Green. Chem.*, 2016, *18*, 3360-3369. Ref. [119].

Tolborg, S., Sádaba, I., Osmundsen, C. M., Fristrup, P., Holm, M. S., and Taarning, E. Tin-containing Silicates: Alkali Metal Salts Improve Methyl Lactate Yield from Sugars. *ChemSusChem*, **2015**, *8*, 613-617. Ref. [56].

Tolborg, S., Katerinopoulou, A., Falcone, D. D., Sádaba, I., Osmundsen, C. M., Davis, R. J., Taarning, E., Fristrup, P., and Holm, M. S. The Incorporation of Tin Affects Crystallization, Morphology and Crystal Composition of Sn-Beta. *J. Mater. Chem. A*, **2014**, *2* (47), 20252-20262. Ref. [44].

Magazine article:

Tolborg, S., Taarning, E., and Holm, M. S. Discovery and Perspectives of Zeotype Sn-Beta. *The Catalyst Review* **2013**, *26* (11), 6-12.

Patent:

Holm, M. S., Sádaba, I., Tolborg, S., Osmundsen, C. M., and Taarning, E. Metallosilicates and a Process for the Conversion of Sugars to Esters of Lactic Acid, 2-hydroxy-3-butenoic Acid and Lactic Acid Itself Comprising a Metallosilicate and a Metal Ion. **2013**, WO 2015024875 A1.

Other publications:

Yakimov, A. V., Kolyagina, Y. G., Tolborg, S., Vennestrøm, P. N. R. and Ivanova, I. I. Probing Tin Sites in Sn-BEA by ^{119}Sn MAS NMR of Adsorbed Probe Molecules. *J. Phys. Chem. C* **2016**, *in press*. (DOI: 10.1021/acs.jpcc.6b09999) Ref. [74].

Yakimov, A. V., Kolyagina, Y. G., Tolborg, S., Vennestrøm, P. N. R., and Ivanova, I. I. Accelerated Synthesis of Sn-BEA in Fluoride Media: Effect of H_2O Content in the Gel. *New J. Chem.*, **2016**, *40*, 4367-4374. Ref. [45].

Kolyagina, Y. G., Yakimov, A. V., Tolborg, S., Vennestrøm, P. N. R., and Ivanova, I. I. Application of ^{119}Sn CPMG MAS NMR for Fast Characterization of Sn Sites in Zeolites with Natural ^{119}Sn Isotope Abundance. *J. Phys. Chem. Lett.*, **2016**, *7*, 1249-1253. Ref. [68].

Sushkevich, V. L., Ivanova, I. I., Tolborg, S., and Taarning, E. Meerwein–Ponndorf–Verley-Oppenauer Reaction of Crotonaldehyde with Ethanol over Zr-containing Catalysts. *J. Catal.*, **2014**, *316*, 121-129. Ref. [36]

Journal of Catalysis 316 (2014) 121–129

Contents lists available at ScienceDirect

Journal of Catalysis

journal homepage: www.elsevier.com/locate/jcat

Meerwein–Ponndorf–Verley–Oppenauer reaction of crotonaldehyde with ethanol over Zr-containing catalysts

Vitaly L. Sushkevich [a], Irina I. Ivanova [a,b,*], Søren Tolborg [c], Esben Taarning [c]

[a] Department of Chemistry, Lomonosov Moscow State University, Leninskye Gory 1, bld. 3, 119991 Moscow, Russia
[b] A.V. Topchiev Institute of Petrochemical Synthesis, Russian Academy of Science, Leninskiy prospect, 29, 119991 Moscow, Russia
[c] Haldor Topsøe A/S, Nymoellevej 55, 2800 Kgs. Lyngby, Denmark

ARTICLE INFO

Article history:
Received 23 December 2013
Revised 19 April 2014
Accepted 27 April 2014

Keywords:
MPVO reaction between crotonaldehyde and ethanol
Zr-BEA
Supported zirconia
Zr-MCM-41
Lewis acid sites

ABSTRACT

A series of Zr-containing catalysts including bulk ZrO_2, ZrO_2 supported on silica, titania and ceria, Zr-BEA zeolite and Zr-MCM-41 mesoporous material was prepared and characterized by X-ray diffraction, nitrogen adsorption-desorption, X-ray photoelectron spectroscopy, ^{29}Si MAS NMR, TPD NH_3, and FTIR of adsorbed CO. The catalytic materials were tested in the MPVO reaction of crotonaldehyde and ethanol in the temperature range of 473–573 K. The results showed that the activity of Zr-based catalysts in the MPVO reduction of crotonaldehyde correlates with the amount of Zr^{4+} Lewis acid sites in the catalysts. Tetrahedral Zr atom sites isolated within the crystalline structure of zeolite BEA were found to be the most efficient. The best catalyst performance in terms of selectivity was observed over ZrBEA: 72% selectivity to crotyl alcohol was achieved at crotonaldehyde conversion of 15%.

1. Introduction

Meerwein–Ponndorf–Verley–Oppenauer (MPVO) reaction between crotonaldehyde and ethanol is one of the key intermediate steps of ethanol conversion into butadiene-1,3 [1–3], an important monomer for the production of polybutadiene, styrene–butadiene rubber, styrene–butadiene latex, and other polymers. Nowadays, the necessity in this catalytic route of butadiene synthesis is growing, due to the shortage of butadiene production from steam cracking of oil fractions and therefore the lack of this product on the market. Therefore this process has attracted much attention during the last years [4–7].

Ethanol conversion into butadiene is a complex process involving at least four consecutive reaction steps [1–3,5]: (1) ethanol dehydrogenation into acetaldehyde; (2) aldol condensation of acetaldehyde leading to crotonaldehyde; (3) MPVO reaction between crotonaldehyde and ethanol yielding crotyl alcohol and acetaldehyde, and (4) dehydration of crotyl alcohol into butadiene. The complexity of the reaction network requires the detailed information on each reaction step for the design of the optimal multifunctional catalyst of the overall process. While ethanol dehydrogenation into acetaldehyde [8–10] and aldol condensation of acetaldehyde [11–13] have been repeatedly addressed in the literature, no information on MPVO reaction between crotonaldehyde and ethanol over solid catalysts is available as yet.

MPVO reaction has been reported for various alkyl- and aryl-substituted ketones [14–22], and cyclohexanones [23–26], as well as for some α,β-unsaturated carbonyl compounds [16,17,27–33]. The reductant is usually an easily oxidazable secondary alcohol, such as 2-propanol or 2-butanol. The reaction can be carried out in liquid phase [14–26] or in vapor phase [27–33] with the dilution by solvent or inert gas correspondingly.

The traditional homogeneous catalysts of MPVO reactions are aluminum or titanium alkoxides [35]. The reaction mechanism involves a cyclic six-membered transition state, in which both the reducing alcohol and the carbonyl compound are coordinated to the same metal center. The reaction proceeds by a hydride transfer from the alcohol, bound to the metal center as an alkoxide, to the carbonyl group. The main drawbacks of homogenously catalyzed MPVO reaction are related to the necessity of stoichiometric amounts of catalyst, the moisture sensitivity and the problems with catalyst separation.

The solid catalysts studied so far in MPVO reaction include metal oxides [19,20,27–33], hydrotalcites [21,22], zeolites [14,16,17,23–26,34], and immobilized metal alkoxides [18]. Ivanov et al. [36] have compared the MPVO reaction of acetone with ethanol over various metal oxides with different acid-base properties: magnesium oxide,

* Corresponding author at: A.V. Topchiev Institute of Petrochemical Synthesis, Russian Academy of Science, Leninskiy prospect, 29, 119991 Moscow, Russia. Fax: +7 (495)939 3570.
E-mail address: iivanova@phys.chem.msu.ru (I.I. Ivanova).

http://dx.doi.org/10.1016/j.jcat.2014.04.019
0021-9517/

Journal of Materials Chemistry A

PAPER

View Article Online
View Journal | View Issue

Cite this: J. Mater. Chem. A, 2014, 2, 20252

Incorporation of tin affects crystallization, morphology, and crystal composition of Sn-Beta†

S. Tolborg,[ab] A. Katerinopoulou,[b] D. D. Falcone,[c] I. Sádaba,[b] C. M. Osmundsen,[b] R. J. Davis,[c] E. Taarning,*[b] P. Fristrup[a] and M. S. Holm[b]

Received 26th September 2014
Accepted 23rd October 2014

DOI: 10.1039/c4ta05119j

www.rsc.org/MaterialsA

The crystallization of Sn-Beta in fluoride medium is greatly influenced by the amount and type of tin source present in the synthesis gel. By varying the amount of tin in the form of tin(IV) chloride pentahydrate, the time required for crystallization was studied. It was found that tin not only drastically affects the time required for crystallization, but also that the presence of tin changes the morphology of the formed Sn-Beta crystals. For low amounts of tin (Si/Sn = 400) crystallization occurs within four days and the Sn-Beta crystals are capped bipyramidal in shape, whereas for high amounts of tin (Si/Sn = 100) it takes about sixty days to reach full crystallinity and the resulting crystals are highly truncated, almost plate-like in shape. Using SEM-WDS to investigate the tin distribution along transverse sections of the Sn-Beta crystals, a gradient distribution of tin was found in all cases. It was observed that the tin density in the outer parts of the Sn-Beta crystals is roughly twice as high as in the tin depleted core of the crystals. Sn-Beta was found to obtain its maximum catalytic activity for the conversion of dihydroxyacetone to methyl lactate close to the minimum time required for obtaining full crystallinity. At excessive crystallization times, the catalytic activity decreased, presumably due to Ostwald ripening.

1 Introduction

Sn-Beta is a zeotype material containing tin incorporated in the zeolite framework. The crystalline material has strong Lewis acidic properties, attributable to discrete tin sites, as well as a microporous network characteristic of a zeolite system. These two features combined with sufficiently large pores have made this material a promising catalyst for a range of industrially relevant reactions. Sn-Beta has been shown to be an active catalyst for Meerwein–Ponndorf–Verley–Oppenauer redox reactions as well as for Baeyer–Villiger oxidations where the use of hydrogen peroxide with Sn-Beta makes it possible to avoid the use of expensive peracids.[1,2] In recent years other interesting potential uses of Sn-Beta have been explored within the emerging area of biomass conversion.[3,4] The catalytic synthesis of lactates from sugars is one such example where Sn-Beta has been found to be a useful catalyst.[3,5–7] The production of this biodegradable plastic monomer is otherwise restricted to base catalyzed conversion of sugars and fermentation.[8–10] Apart from this reaction, Sn-Beta also catalyzes the isomerization of monosaccharides *e.g.* glucose to fructose.[4,6,11]

Fundamental studies have revealed the presence of two or more configurations of the framework tin site.[11–13] This was achieved using a combination of computational studies with advanced techniques such as cross polarization nuclear magnetic resonance, infrared spectroscopy, and thermogravimetric measurements using a variety of probe molecules.[11–16]

In spite of the interest in Sn-Beta, fundamental aspects of the effect of tin during the preparation of the catalyst are still not fully understood. It is well-known from preparation of other zeolite structures that even small variations in the composition of the gel during synthesis can have great impact on the resulting material. For instance, changing pH, silica-source, structure directing agent (SDA), water content, and the use of agitation during the synthesis have all been shown to affect the crystallization behavior for other zeolites.[17–21]

The traditional procedure for synthesizing Sn-Beta involves fluoride media at near neutral pH as described by Corma,[1,3,11] but it has also been prepared in hydroxide media.[22] The role of the mineralizing agent is to dissolve and transport silica species during the formation of the zeolite framework.[23] Due to the strong interaction between the fluor and the silica-species, fluoride ions can advantageously be used as the mineralizing agent.[1,24,25] The fluoride route produces largely defect-free and hydrophobic materials as well as larger crystals, in the order of several μm, compared to the hydroxide counterparts where crystals of only a few hundred nanometers in diameter are

[a]Technical University of Denmark, Department of Chemistry, Kemitorvet, 2800-Kgs. Lyngby, Denmark
[b]Haldor Topsøe A/S, New Business R&D, Nymøllevej 55, 2800-Kgs. Lyngby, Denmark. E-mail: esta@topsoe.dk; Tel: +45 22754291
[c]University of Virginia, Department of Chemical Engineering, 102 Engineer's Way, PO Box 400741, Charlottesville, VA 22904, USA

† Electronic supplementary information (ESI) available: Further details are given in Tables S1, S2 and Fig. S1–S5 as well as additional SE images and SEM-WDS measurements. See DOI: 10.1039/c4ta05119j

ChemPubSoc Europe

DOI: 10.1002/cssc.201403057

CHEMSUSCHEM Communications

Tin-containing Silicates: Alkali Salts Improve Methyl Lactate Yield from Sugars

Søren Tolborg,[a, b] Irantzu Sádaba,[a] Christian M. Osmundsen,[a] Peter Fristrup,[b] Martin S. Holm,[a] and Esben Taarning*[a]

This study focuses on increasing the selectivity to methyl lactate from sugars using stannosilicates as heterogeneous catalyst. All group I ions are found to have a promoting effect on the resulting methyl lactate yield. Besides, the alkali ions can be added both during the preparation of the catalyst or directly to the solvent mixture to achieve the highest reported yield of methyl lactate (ca. 75%) from sucrose at 170 °C in methanol. The beneficial effect of adding alkali to the reaction media applies not only to highly defect-free Sn-Beta prepared through the fluoride route, but also to materials prepared by post-treatment of dealuminated commercial Beta zeolites, as well as ordered mesoporous stannosilicates, in this case Sn-MCM-41 and Sn-SBA-15. These findings open the door to the possibility of using other preparation methods or different Sn-containing silicates with equally high methyl lactate yields as Sn-Beta.

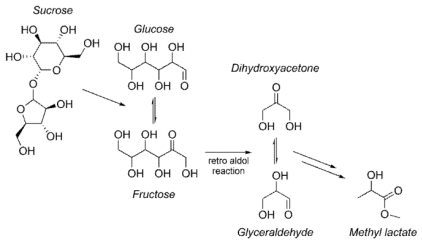

Figure 1. Proposed reaction pathway for the conversion of sucrose to methyl lactate.[1a]

Tin-containing silicates are very promising heterogeneous catalysts for sugar conversion[1] and other important reactions such as Baeyer–Villiger oxidations and Meerwein–Ponndorf–Verley–Oppenauer redox reactions.[2] At low temperatures (40–100 °C), Sn-Beta selectively converts the C_3-sugars 1,3-dihydroxyacetone (DHA) and glyceraldehyde (GLA) into lactic acid (LA) derivatives.[3] At mild reaction conditions (80–110 °C), Sn-Beta is also capable of catalyzing the isomerization of monosaccharide sugars, such as glucose into fructose.[1b,4] At yet higher reaction temperatures (> 150 °C), Sn-Beta catalyzes the retro-aldol reaction of monosaccharides, resulting in the formation of C_3 sugars which are further converted into lactic acid derivatives (Figure 1).[1a,e] This catalytic pathway could become useful as an alternative to fermentation for the production of LA, which is an important bio-based commodity chemical.[5] Another alternative to fermentation is the oxidation of glycerol to DHA and the subsequent conversion to LA. Glycerol is readily available as a byproduct from the production of biodiesel.[6]

In the conversion of sugars to lactic acid, it is important to improve the selectivity towards lactates if the catalytic pathway is to compete with state-of-the-art fermentative processes, which yield up to 95% lactic acid from sugars.[7] Therefore, the focus of this study is on the optimization of the catalyst synthesis and reaction conditions in order to increase the selectivity to lactic acid derivatives from sugars using Sn-Beta.

Alkali ions are known to be of great importance in the preparation of a variety of zeolites. For high-silica metallosilicate zeolites such as TS-1, Ti-Beta, and Sn-MFI the presence of alkali metals during synthesis has been reported to hinder successful crystallization[8] and negatively influence the catalytic activity.[9] As a result, several works have studied the post-synthetic removal of alkali metal impurities to obtain catalytically active materials.[9,10] On the other hand, other studies have reported that small amounts of alkali metal ions can improve the activity of titanium-containing silicates for the epoxidation of allyl alcohol and the oxidation of cyclohexene and styrene.[8c,11]

Recent studies have shown that alkaline conditions and the presence of salts can also affect the catalytic conversion of monosaccharides.[1f,12] For example, the addition of sodium chloride was found to change the reaction pathway for the isomerization of glucose using Sn-Beta. In this case, Sn-Beta treated with sodium ions catalyzes the epimerization to mannose through a 1,2-carbon shift instead of isomerization via a 1,2-hydride shift to form fructose.[1f] In another case, tin(IV) chloride was used as catalyst in the formation of methyl lactate (ML) from glucose.[13] Here, the addition of alkali hydroxide (KOH and NaOH) or alkali metal chlorides increased the yield of ML from 25 to 45%.

[a] S. Tolborg, Dr. I. Sádaba, Dr. C. M. Osmundsen, Dr. M. S. Holm, Dr. E. Taarning
Haldor Topsøe A/S, New Business R&D
Nymøllevej 55, 2800, Kgs. Lyngby (Denmark)
E-mail: esta@topsoe.dk

[b] S. Tolborg, Dr. P. Fristrup
Technical University of Denmark
Department of Chemistry
Kemitorvet, 2800, Kgs. Lyngby (Denmark)

Supporting Information for this article is available on the WWW under http://dx.doi.org/10.1002/cssc.201403057.

Green Chemistry

PAPER

View Article Online
View Journal | View Issue

Cite this: *Green Chem.*, 2016, **18**, 3360

Tin-containing silicates: identification of a glycolytic pathway *via* 3-deoxyglucosone†

S. Tolborg,[a,b] S. Meier,[a] I. Sádaba,[b] S. G. Elliot,[a,b] S. K. Kristensen,[c] S. Saravanamurugan,[a] A. Riisager,[a] P. Fristrup,[a] T. Skrydstrup[c] and E. Taarning*[b]

Inorganic glycolytic systems, capable of transforming glucose through a cascade of catalytic steps, can lead to efficient chemical processes utilising carbohydrates as feedstock. Tin-containing silicates, such as Sn-Beta, are showing potential for the production of lactates from sugars through a cascade of four to five sequential steps. Currently, there is a limited understanding of the competing glycolytic pathways within these systems. Here we identify dehydration of glucose to 3-deoxyglucosone as an important pathway that occurs in addition to retro-aldol reaction of hexoses when using tin-containing silicates. It is possible to influence the relative carbon flux through these pathways by controlling the amount of alkali metal salts present in the reaction mixture. In the absence of added potassium carbonate, at least 15–30% carbon flux *via* 3-deoxyglucosone is observed. Addition of just a few ppm of potassium carbonate makes retro-aldol pathways dominant and responsible for about 60–70% of the overall carbon flux. The 3-deoxyglucosone pathway results in new types of chemical products accessible directly from glucose. Furthermore, it is argued that 3-deoxyglucosone is a contributing source of some of the methyl lactate formed from hexoses using tin-containing silicates in the presence of alkali metal salts. Further catalyst design and system tuning will permit even better control between these two different glycolytic pathways and will enable highly selective catalytic transformations of glucose to a variety of chemical products using tin-containing silicates.

Received 27th November 2015,
Accepted 24th February 2016
DOI: 10.1039/c5gc02840j
www.rsc.org/greenchem

Introduction

Processes, in which glucose is directly converted to useful chemical products, have a high potential for industrial implementation.[1] Inorganic catalytic systems, although with limited examples of industrial implementation, have potential advantages over enzymatic and fermentative systems in terms of scalability, tolerance to a broad range of harsh reaction conditions and tolerance to cytotoxic intermediates or products.[2] So far, direct industrial conversion of glucose with inorganic catalytic systems has been limited to the production of sorbitol and gluconic acid, but several other chemicals have been reported as being accessible directly from glucose in high yields. These include fructose, ethylene glycol, propylene glycol, levulinic acid, 5-(hydroxymethyl)furfural (HMF) and lactic acid derivatives.[3–9]

The use of tin-containing silicates for the conversion of sugars to lactates has received considerable attention. The first report from 2009 described the isomerisation of triose sugars to lactic acid and methyl lactate (ML) in near quantitative yields using Sn-Beta at low temperatures.[10] The scope was expanded the following year with a report that also hexoses can be converted to ML at higher temperatures (160 °C) in 68% yield, with formation of small amounts of methyl vinyl glycolate (MVG).[4] At the same time, Sn-Beta was reported to be an active catalyst for the isomerisation of glucose to fructose and mannose in water at moderate temperatures (100 °C).[3]

This dependence on temperature enables some degree of versatility in the use of Sn-Beta as a catalyst. At moderate temperatures the Lewis acidic tin sites primarily catalyse a 1,2-hydride shift leading to isomerisation. At higher temperatures a C–C bond cleaving retro-aldol reaction is catalysed resulting in the fragmentation of monosaccharides to either the aforementioned triose sugars, which subsequently lead to ML (in methanol) or to C_2- and C_4-sugar fragments (glycolaldehyde and tetrose sugars) that form MVG (and glycolaldehyde dimethyl acetal, GA-DMA).[11,12] Additionally, Sn-based catalysts have also been used to catalyse the C–C bond formation to

[a]*Technical University of Denmark, Department of Chemistry, Kemitorvet, 2800-Kgs. Lyngby, Denmark*
[b]*Haldor Topsøe A/S, Haldor Topsøes Allé 1, 2800-Kgs. Lyngby, Denmark. E-mail: esta@topsoe.dk*
[c]*Aarhus University, Carbon Dioxide Activation Center, Interdisciplinary Nanoscience Center, Department of Chemistry, Gustav Wieds Vej 14, 8000-Aarhus C, Denmark*
†Electronic supplementary information (ESI) available. See DOI: 10.1039/c5gc02840j

NJC

PAPER

View Article Online
View Journal | View Issue

Cite this: *New J. Chem.*, 2016, 40, 4367

Accelerated synthesis of Sn-BEA in fluoride media: effect of H_2O content in the gel†

Alexander V. Yakimov,[a] Yury G. Kolyagin,[ab] Søren Tolborg,[cd] Peter N. R. Vennestrøm[c] and Irina I. Ivanova*[ab]

Received (in Montpellier, France) 4th February 2016,
Accepted 25th March 2016

DOI: 10.1039/c6nj00394j

www.rsc.org/njc

Tin-containing zeotypes, particularly Sn-BEA, are promising heterogeneous catalysts for a number of important industrially relevant reactions. However, the direct hydrothermal synthesis of these materials requires unfavourably long times, which is an obstacle for their industrial application. In the present study we show that up to 4-fold reduction of the crystallization time can be achieved by a decrease of the H_2O/SiO_2 ratio in the synthesis gel from 7.5 to 5.6. The crystallization kinetics has been studied for five series of gels containing $1.0SiO_2 : 0.27TEA_2O : xSnO_2 : 0.54HF : yH_2O$, for which y was fixed to 5.6, 6.8 and 7.5 at x = 0.005 and to 5.6 and 6.8 at x = 0.010. The crystallization time was varied within 0.5–60 days. The intermediate and final products obtained were investigated using XRD, FTIR, XRF, SEM, UV-Vis, MAS NMR spectroscopy and nitrogen adsorption–desorption techniques. The products obtained with lower water content are shown to have the same structure, textural properties and morphology as materials synthesized with higher water content. Although the size of the crystals is found to decrease with water content in the gel, it does not affect the Sn coordination and environment as confirmed by ^{119}Sn MAS NMR.

1. Introduction

Tin-containing zeolites and zeotypes, particularly Sn-BEA, have been demonstrated to be promising heterogeneous catalysts for many important industrially relevant reactions including the conversion of sugars into methyl lactate,[1,2] the isomerization of glucose into fructose,[3–5] Baeyer–Villiger oxidation reactions,[6] Meerwein–Ponndorf–Verley–Oppenauer redox reactions[7] and ring-opening hydration of epoxides.[8] In general there are a large number of examples of the widespread applicability of Sn-BEA zeolites as catalysts in biomass-derived processes.[9]

The outstanding catalytic properties of Sn-BEA are considered to be due to high Lewis acidity attributed to isolated Sn atoms in the zeolite lattice and the hydrophobic environment associated with a defect-free siliceous surface.[10,11] The latter feature is a consequence of the fluoride route used for the hydrothermal synthesis of Sn-BEA materials.[10] Fluoride ions facilitate the mineralization of silica sources and compensate the positive charges associated with organic structure directing agents, resulting in highly crystalline materials with a low amount of structural defects compared to materials synthesized using hydroxide ions.[12] However, the application of fluoride ions is accompanied by a number of drawbacks, including complicated handling measures of the fluoride source *e.g.* HF and formation of large zeolite crystals. Furthermore, the increase of Sn content in the reaction mixture, required for the creation of higher amount of Lewis sites results in long crystallization times.[1] As an result, in the case of low amounts of Sn (Si/Sn = 400) crystallization occurs within 4 days, whereas the synthesis of Sn-BEA with Si/Sn = 100 requires up to 60 days of synthesis.[1]

To reduce the crystallization time and the crystal size several approaches have been proposed. These include extensive seeding,[13–15] steam-assisted conversion[13] and post-synthesis modification.[8,16–21] Significant efforts have been made for shortening the crystallization time by seeded growth methods.[22–24] Although noticeable reduction of crystallization time was achieved, the induced nucleation severely affected the crystal morphology, resulting in intergrown zeolite crystals forming large agglomerates.[22,24,25] An interesting method was proposed by Chang *et al.*,[23] who demonstrated that Sn-BEA can be synthesized in non-fluoride media *via* dry gel conversion using a seeded growth procedure. However, this approach yielded materials with a hydrophilic surface and a different distribution and location of Sn sites, as revealed by FTIR of adsorbed CD_3CN, which resulted in lower catalytic activity in glucose isomerization. Several approaches have been proposed for the

[a] *Department of Chemistry, Lomonosov Moscow State University, Leninskie gory 1, Moscow, Russia. E-mail: IIIvanova@phys.chem.msu.ru*
[b] *A.V. Topchiev Institute of Petrochemical Synthesis RAS, Moscow, Russia*
[c] *Haldor Topsøe A/S, Haldor Topsøes Allé 1, DK-2800 Kgs. Lyngby, Denmark*
[d] *Technical University of Denmark, Department of Chemistry, Kemitorvet, DK-2800 Kgs. Lyngby, Denmark*

† Electronic supplementary information (ESI) available: XRD, UV-Vis and adsorption data. See DOI: 10.1039/c6nj00394j

THE JOURNAL OF PHYSICAL CHEMISTRY Letters

Letter

pubs.acs.org/JPCL

Application of ^{119}Sn CPMG MAS NMR for Fast Characterization of Sn Sites in Zeolites with Natural ^{119}Sn Isotope Abundance

Yury G. Kolyagin,[†,‡] Alexander V. Yakimov,[†] Søren Tolborg,[§,∥] Peter N. R. Vennestrøm,[§] and Irina I. Ivanova*[,†,‡]

[†]Department of Chemistry, Lomonosov Moscow State University, Leninskie gory 1, 119991, Moscow, Russia

[‡]A.V. Topchiev Institute of Petrochemical Synthesis RAS, Leninskiy prospect 29, 119992, Moscow, Russia

[§]Haldor Topsøe A/S, Haldor Topsøes Allé 1, DK-2800 Kongens Lyngby, Denmark

[∥]Department of Chemistry, Technical University of Denmark, Kemitorvet, DK-2800 Kongens Lyngby, Denmark

Supporting Information

ABSTRACT: ^{119}Sn CPMG MAS NMR is demonstrated to be a fast and efficient method for characterization of Sn-sites in Sn-containing zeolites. Tuning of the CPMG echo-train sequence decreases the experimental time by a factor of 5−40 in the case of as-synthesized and hydrated Sn-BEA samples and by 3 orders of magnitude in the case of dehydrated Sn-BEA samples as compared to conventional methods. In the latter case, the reconstruction of the quantitative spectrum without the loss of sensitivity is shown to be possible. The method proposed allows obtaining ^{119}Sn MAS NMR spectra with improved resolution for Sn-BEA zeolites with natural ^{119}Sn isotope abundance using conventional MAS NMR equipment.

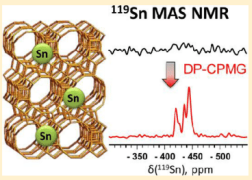

Tin-containing zeolites have received considerable attention over the last years due to their profound catalytic properties. These materials show high activity and selectivity in many important reactions such as Baeyer−Villiger oxidation,[1,2] Meerwein−Ponndorf−Verley and Oppenauer reaction,[2−4] ring-opening in epoxides,[5] and in the different processes of sugar conversion.[6−13]

The information about the state, location, and coordination of tin atoms in these materials is critical for the optimization and the development of novel Sn-containing zeolite catalysts for various industrial applications. Among the broad range of analytical methods (EXAFS,[14] ^{119}Sn Mössbauer spectroscopy,[15,16] UV−vis,[17] IR of adsorbed probe molecules[18,19]) which were used for characterization of Sn-zeolites, ^{119}Sn MAS NMR spectroscopy is considered to be the most appropriate as it provides reliable information on the state of tin, its environment and coordination.[20−25]

One of the largest limitations in using ^{119}Sn MAS NMR is its low sensitivity arising from both low tin content in the zeolite framework (up to 2 wt %),[26,27] and low natural abundance of the NMR active nucleus ^{119}Sn (8.59%). Furthermore, due to the high relaxation time (T_1) of ^{119}Sn, it is not possible to compensate the low isotope content by an increase in the number of scans to obtain higher sensitivity.[28] Therefore, the measurement of ^{119}Sn MAS NMR spectra by standard protocols with reasonable detection time is possible only for samples enriched in ^{119}Sn isotope.

To overcome this restriction, a method involving dynamic nuclear polarization (DNP-SENS NMR) was adapted by the groups of Román-Leshkov[29] and Copéret.[30] Its application makes the detection of framework incorporated Sn-sites possible without isotopic enrichment. However, this technique requires state-of-the art equipment (high-power microwave source, low-temperature DNP MAS probe, etc.) available only in a limited number of laboratories. Additionally, it requires the modification of the samples with specially selected biradical compounds and conducting the experiment at low temperature (usually 100 K), which limits its application for adsorption and in situ catalytic studies.

Herein we report on the application of Carr−Purcell−Meiboom−Gill (CPMG) echo-train acquisition for the registration of ^{119}Sn MAS NMR spectra with improved signal-to-noise ratio over Sn-containing zeolites with natural ^{119}Sn isotope abundance using conventional solid-state NMR equipment.

Sn-BEA zeolites containing 0.98 wt % of Sn (Si/Sn = 200) with natural isotope abundance (^{na}Sn-BEA) or enriched with ^{119}Sn (^{119}Sn-BEA) were synthesized under hydrothermal conditions in fluorine media.[26] The samples prepared were characterized by XRD, SEM, ^{29}Si and ^{19}F MAS NMR spectroscopy. The results presented in the Supporting Information (Figures S1−S6) point to the same structure, composition, and morphology of labeled and unlabeled samples.

Since it is well-established that the interaction with water and other substrates drastically changes the state of the tin in zeolites, the samples were studied in as-synthesized form, containing the structure directing agent (denoted as Sn-

Received: February 4, 2016
Accepted: March 15, 2016
Published: March 15, 2016

DOI: 10.1021/acs.jpclett.6b00249
J. Phys. Chem. Lett. 2016, 7, 1249−1253

ChemPubSoc Europe

DOI: 10.1002/cssc.201600757

CHEMSUSCHEM Full Papers

VIP *Very Important Paper*

Shape-selective Valorization of Biomass-derived Glycolaldehyde using Tin-containing Zeolites

Søren Tolborg,[a, b] Sebastian Meier,[a] Shunmugavel Saravanamurugan,[a] Peter Fristrup,[a] Esben Taarning,[b] and Irantzu Sádaba*[b]

A highly selective self-condensation of glycolaldehyde to different C_4 molecules has been achieved using Lewis acidic stannosilicate catalysts in water at moderate temperatures (40–100 °C). The medium-sized zeolite pores (10-membered ring framework) in Sn-MFI facilitate the formation of tetrose sugars while hindering consecutive aldol reactions leading to hexose sugars. High yields of tetrose sugars (74%) with minor amounts of vinyl glycolic acid (VGA), an α-hydroxyacid, are obtained using Sn-MFI with selectivities towards C_4 products reaching 97%. Tin catalysts having large pores or no pore structure (Sn-Beta, Sn-MCM-41, Sn-SBA-15, tin chloride) led to lower selectivities for C_4 sugars due to formation of hexose sugars. In the case of Sn-Beta, VGA is the main product (30%), illustrating differences in selectivity of the Sn sites in the different frameworks. Under optimized conditions, GA can undergo further conversion, leading to yields of up to 44% of VGA using Sn-MFI in water. The use of Sn-MFI offers multiple possibilities for valorization of biomass-derived GA in water under mild conditions selectively producing C_4 molecules.

Introduction

Glycolaldehyde (GA), a two-carbon monosaccharide, has the potential to become a valuable biomass-derived platform chemical. It is currently obtained in high yields in supercritical water or as a main component of bio-oil, and other processes to efficiently transform sugars to GA in high yields are currently being developed.[1]

GA can be catalytically converted into many interesting chemicals. For example, ethylene diamine or ethanolamine, with applications in polymer production and pharmaceuticals, can be produced by direct amination.[2] Glyoxal, glycolic acid, or glyoxylic acid can be obtained by oxidation, whereas ethylene glycol can be produced by reduction (hydrogenation). Alternatively, the aldehyde functionality can be employed in C–C bond formations, such as aldol condensations.[3] The self-condensation of GA, leading to the formation of tetrose sugars, permits the production of uncommon and expensive sugars. The tetroses currently have limited potential uses, for example within pharmaceutical treatments,[4] but increased availability could provide a new platform for biomass-derived products. Especially products that are otherwise difficult to access from cheaper pentose and hexose sugars are attractive. The sweetener erythritol, for example, is currently obtained by fermentation of glucose and sucrose, but could be obtained through hydrogenation of the tetrose sugars.[5] Under hydrothermal alkaline conditions the monomer lactic acid has also been obtained, by way of aldol condensation and subsequent conversion of GA.[6] Similarly, several interesting products have been obtained by employing Lewis-acid catalysts, including the α-hydroxyacids lactic acid/methyl lactate (LA/ML), methyl vinyl glycolate (MVG), and methyl 4-methoxy-2-hydroxy-3-butenoate (MMHB).[7] In addition to these, the formation of the pharmaceutical precursor α-hydroxy-γ-butyrolactone (HBL) from smaller sugars (C_1 to C_3) has been reported.[3,7b,8]

The condensation of GA with small oxygenates such as formaldehyde (FA) has long been considered a plausible pathway in the abiotic synthesis of sugars.[9] In the catalytic self-condensation of GA, the challenge is to control the selectivity towards tetrose sugars while avoiding the formation of hexoses (Scheme 1). Various strategies have been utilized to control the aldol condensation of smaller sugars towards the desired condensation products. The most common catalysts used in this reaction include bases,[10] amino acids,[11] and peptides.[12] Inorganic hydroxides such as calcium hydroxide have been extensively studied, alongside various minerals such as borates,[13] silicates,[14] and phosphates.[9b] A combined yield of tetrose derivatives of 86% was obtained using GA and borates at moderate temperatures (65 °C).[13b]

One of the major advantages of zeolite catalysis is the ability to control product selectivity by choosing materials with suitable pore sizes.[15] Zeolites have previously been used with

[a] S. Tolborg, Dr. S. Meier, Dr. S. Saravanamurugan,[+] Dr. P. Fristrup
Department of Chemistry
Technical University of Denmark
Kemitorvet, 2800-Kgs. Lyngby (Denmark)

[b] S. Tolborg, Dr. E. Taarning, Dr. I. Sádaba
New Business R&D
Haldor Topsøe A/S
Haldor Topsøes Allé 1, 2800-Kgs. Lyngby (Denmark)
E-mail: irsz@topsoe.dk

[+] Current address:
Center of Innovative and Applied Bioprocessing (CIAB)
Mohali, 160071-Punjab (India)

Supporting Information and the ORCID identification numbers for the authors of this article can be found under http://dx.doi.org/10.1002/cssc.201600757.

Appendix C
ChemSusChem (21/2016)

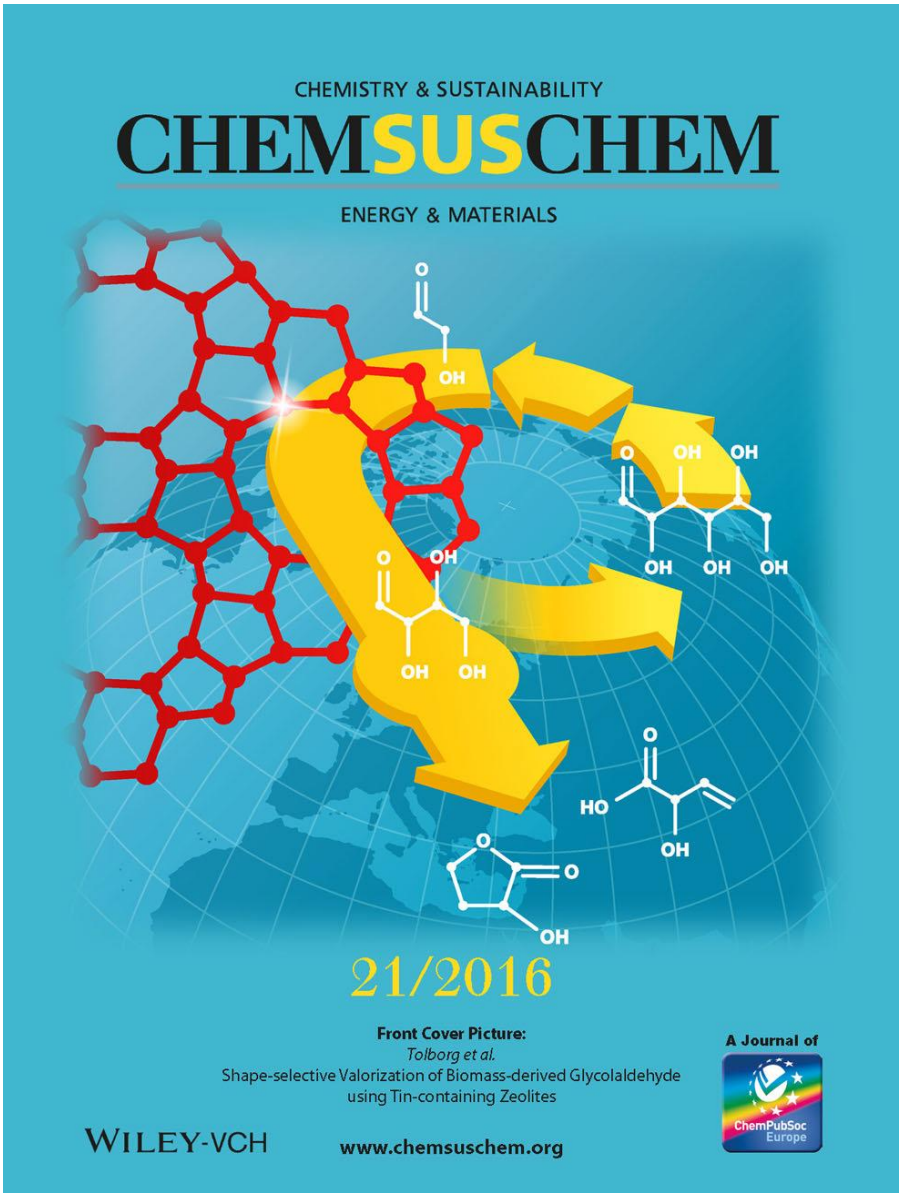

Appendix D
Conference Proceedings

Sep. 2014 Poster and poster workshop presentation at the 6th International conference of the Federation of European Zeolite Associations (FEZA) titled *"New Insights into the Synthesis of Sn-Beta Catalyst"*. Leipzig, Germany (September 8th – 11th, 2014)

May 2015 Oral presentation (10 min) at the 3rd International Symposium on Green Chemistry (ISGC) titled *"Stannosilicates for Catalytic Conversion of Sugar: Alkali Ions Boost the Yield"*. La Rochelle, France (May 3rd – 7th, 2015).

Sep. 2015 Oral presentation (20 min) at the 12th European Congress on Catalysis (EuropaCat) titled *"New Insights in the Catalytic Conversion of Sugars with Sn-Beta"*. Kazan, Russia (August 30th – September 4th, 2015).

- Awarded the EuropaCat XII Ph.D. Student Award (p. 185)

Jun. 2016 Oral presentation (20 min) at the 18th International Zeolite Conference (IZC) titled "*Shape-selectivity in Biomass Conversion: Zeotype-catalyzed Formation of C_4 Sugars*". Rio de Janeiro, Brazil (June 19th – 24th, 2016).

2013 – 2016 Oral presentations internally at Haldor Topsøe A/S.

2013 – 2016 Oral presentations on two occasions at the Annual Ph.D. symposium organized by Technical University of Denmark.

2013 – 2016 Oral presentations on two occasions at the Annual BioValue meeting.

Appendix E
Curriculum Vitae

Name: Søren Tolborg
Date of birth: November 24th 1986
Place of birth: Vejle, Denmark
Nationality: Danish

Education

Sep. 2013 – Dec. 2016	Ph.D. under the supervision of first Associate Professor Peter Fristrup and then Professor Anders Riisager, Technical University of Denmark, Department of Chemistry, Kgs. Lyngby (Denmark) with Irantzu Sádaba, Haldor Topsøe A/S, Kgs. Lyngby (Denmark) as co-supervisor.
Nov. 2012 – Sep. 2013	Research Assistant at Haldor Topsøe A/S, New Business R&D, Kgs. Lyngby (Denmark)
Aug. 2010 – Nov. 2012	M.Sc. Eng. In Chemical Sciences at Aarhus University, Aarhus (Denmark)
Mar. 2012 – Nov. 2012	Research internship, Haldor Topsøe A/S, New Business R&D, Kgs. Lyngby (Denmark).
Sep. 2011 – Feb. 2012	Research internship, Fritz-Haber-Institute of the Max-Planck Society, Department of Inorganic Chemistry, Berlin (Germany)
Aug. 2010 – Dec. 2010	External stay, University of Calgary, Calgary (Canada)
Aug. 2007 – Aug. 2010	B.Sc. in Chemical Sciences at Aarhus University, Aarhus (Denmark)

Appendix F
Ph.D. Student award EuropaCat XIII

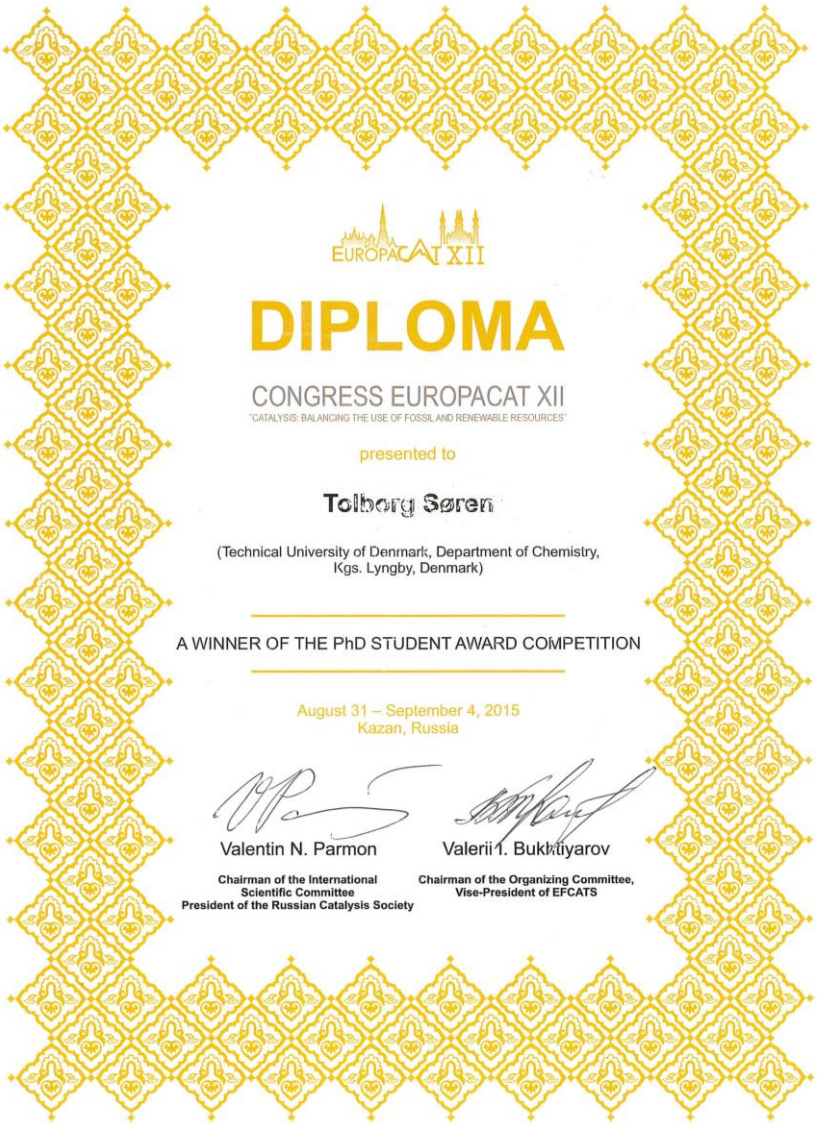

EUROPACAT XII

DIPLOMA

CONGRESS EUROPACAT XII

"CATALYSIS: BALANCING THE USE OF FOSSIL AND RENEWABLE RESOURCES"

presented to

Tolborg Søren

(Technical University of Denmark, Department of Chemistry, Kgs. Lyngby, Denmark)

A WINNER OF THE PhD STUDENT AWARD COMPETITION

August 31 – September 4, 2015
Kazan, Russia

Valentin N. Parmon
Chairman of the International Scientific Committee
President of the Russian Catalysis Society

Valerii I. Bukhtiyarov
Chairman of the Organizing Committee,
Vise-President of EFCATS